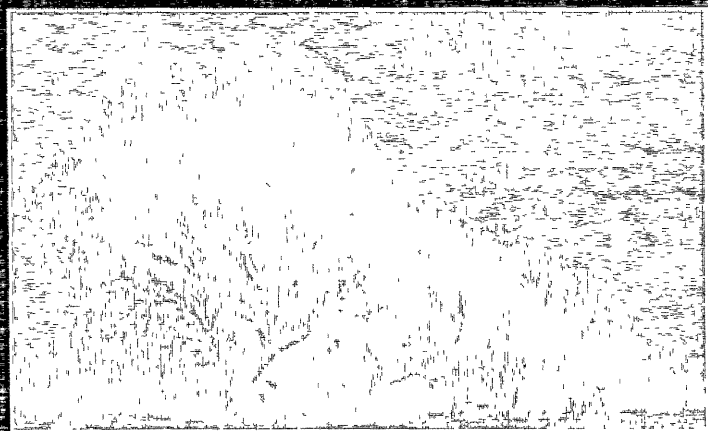


RELAXATION PHENOMENA IN  
DENSE GAS SEPARATION MEMBRANES



MATTHIAS WESSLING

25



**RELAXATION PHENOMENA  
IN DENSE  
GAS SEPARATION MEMBRANES**





**RELAXATION PHENOMENA  
IN DENSE  
GAS SEPARATION MEMBRANES**

**PROEFSCHRIFT**

ter verkrijging van  
de graad van doctor aan de Universiteit Twente,  
op gezag van de rector magnificus,  
prof. dr. Th.J.A. Popma,  
volgens besluit van het College van Dekanen  
in het openbaar te verdedigen  
op vrijdag 5 maart 1993 te 16.45 uur

door

**Matthias Wessling**  
geboren op 10 maart 1963  
te Ahaus

Dit proefschrift is goedgekeurd door de promotor prof. dr. C.A. Smolders en de  
assistent-promotor dr. ing. Th. van den Boomgaard.

---

## Preface

Four years Twente; four years joy and fun. Looking back and asking myself "why has it been such a good time?" generates a huge number of impressions. Some of them, like the daily working together and social events such as bicycle tours, barbecues, sporting and excursions, express a unique team spirit in the Membrane Technology group.

This encouraging spirit has influenced the work of a number of people who contributed tremendously to this thesis: Steven Groot-Wassink, Sacha Schoeman, Eric Boxma, Wim Veneman, Mariska van der Linden, Ingmar Huisman and Hans Beukers. Thank you all for your input.

Furthermore, I would like to express my special thanks to Kees Smolders and Thonie van den Boomgaard; I appreciate your always positive and constructive guidance. Your support has had an invaluable impact on this thesis.

Marcel Mulder, Ingo Blume and Ingo Pinnau; the long, relaxed conversations about the fun of membranes, people around membranes and everything else will last in my mind and will certainly find continuation.

Zandrie Borneman; thank you for your ideas, assistance and your continuous contribution to the spirit of the group.

Geert-Henk Koops; finding a friend (who also knows how to make membranes) is more I could wish.

Thanks also to my room mates Herry, Hyan-Chae, Shuguang, Christel, Geert-Henk and Richard, to our always helpful secretaries Bartie, Annemieke and Gret, the members of the "gas separation membranes cluster" Edwin, Evert and Jean-Marc and finally to the whole research group.

Some of the work was carried out outside the group and, although "stranger", I experienced always all the support I needed. My thanks therefore to Albert Bos, Henri Karrenbelt and, especially, to Wim Briels.

Eine solche Arbeit kann man nur erfolgreich abschließen, wenn man sich auch im privaten Bereich ausgeglichen und zufrieden fühlt. Ich danke meiner ganzen Familie und allen Freunden, die in den letzten vier Jahren dafür Sorge getragen haben.

Mein ganz besonderer Dank gilt Marion, für Ihre Geduld und unermüdliche Unterstützung.

Thanks to all of you,

*Matthias*

---

---

CIP-GEGEVENS KONINKLIJKE BIBLIOTHEEK, DEN HAAG

Wessling, Matthias

Relaxation phenomena in dense gas separation membranes/

Matthias Wessling. - [S.l. : s.n.]

Thesis Enschede.

ISBN 90-9005884-2

Subject headings: polymerphysics / membranes.

© Matthias Wessling, Enschede, The Netherlands, 1992

All rights reserved.

---

---

# CONTENTS

## CHAPTER 1 INTRODUCTION

1.1.	Membrane Separations	1
1.2.	Solution-Diffusion Membranes	3
1.3.	Structure of this Thesis	7

## CHAPTER 2 MASS TRANSPORT IN SOLUTION-DIFFUSION MEMBRANES

2.1.	Introduction	11
2.2.	Diffusion	13
2.3.	Sorption and Dilation	19
2.4.	Structure of Amorphous Polymers	30

## CHAPTER 3 EXPERIMENTAL METHODS

3.1.	Introduction	39
3.2.	Polymer Synthesis and Characterization	40
3.3.	Permeation	42
3.4.	Sorption	45
3.5.	Comparison of Diffusion Coefficients obtained from different Experimental Methods	50
3.6.	Dilation	52

## CHAPTER 4 SORPTION AND DILATION OF POLYMER-CARBON DIOXIDE SYSTEMS

4.1.	Introduction	63
4.2.	The Glass Transition Temperature Depression based Model of Vrentas and Vrentas	64
4.3.	The Dual Mode Sorption Model and the Partial Molar Volume of Gases in Polymeric Glasses	67

---

---

4.4.	The Partial Molar Volume of Carbon Dioxide in Rubbery and Glassy Polymers	71
4.5.	The Elastic Strain Corrected Flory-Huggins Model of Bitter	75
4.6	Conclusions	84
	Appendix A Partial Molar Volumes of CO <sub>2</sub> -Polymer Systems	86
	Appendix B Fitted Model Parameters for the Model of Bitter	87

## **CHAPTER 5 RELAXATION PHENOMENA IN DENSE GAS SEPARATION MEMBRANES**

5.1.	Introduction	91
5.2.	Relaxational Permeation	91
5.3.	Relaxational Dilation	99
5.4.	Qualitative Model for the Description of Relaxational Dilation Phenomena	113
5.5.	Swelling Related Phenomena occurring in Separation Processes making use of Solution-Diffusion Membranes	118
5.6.	Conclusions	124

## **CHAPTER 6 A MOLECULAR DYNAMICS STUDY ON THE AMORPHOUS STATE OF POLY(ETHYLENE TEREPHTHALATE) AND POLY(ETHYLENE ISO-PHTHALATE)**

6.1.	Introduction	127
6.2.	Details of the Molecular Dynamics Simulation	128
6.3.	Methods to Analyze the Amorphous State of Glassy Polymers	131
6.4	Choice of the Polymeric System	135
6.5.	Results and Discussion	138
6.5.1.	General Considerations	138
6.5.2.	The Total Radial Distribution Function of PET	141
6.5.3.	Pair Radial Distribution Functions	145
6.5.4.	On the Morphology of Poly(ethylene terephthalate) and Poly(ethylene isophthalate)	147
6.6.	Conclusions	151
	Appendix A Pair Radial Distribution Functions	153
	Appendix B Pair Radial Distribution Functions	154

---

---

**CHAPTER 7 CARBON DIOXIDE FOAMING OF GLASSY  
POLYMERS**

7.1.	Introduction	155
7.2.	Mass and Heat Transport Phenomena occurring during the Foaming Process of Polycarbonate	156
7.3.	Sorption induced Glass Transition Temperature Depression of the Polyimide 6FDA-3PDA	165
7.4.	Tracing the Glassy State of Polysulfone by Nucleation of Bubbles	169
7.5.	Conclusions	172

**APPENDIX I MODELLING THE PERMEABILITY OF POLYMERS  
A NEURAL NETWORK APPROACH**

I.1.	Introduction	175
I.2.	Neural Networks	176
I.3.	Infrared Spectroscopy	178
I.4.	Set of Polymers	179
I.5.	Results and Discussion	180

**APPENDIX II PHASE INVERSION PROCESSES IN TERNARY  
POLYMER SYSTEMS RESULTING IN FRACTAL  
PATTERNS** 183

**SUMMARY** 185

**SAMENVATTING** 189

**ZUSAMMENFASSUNG** 193

**LIST OF PUBLICATIONS** 196

**CURRICULUM VITAE** 197

---





# Chapter 1

## Introduction

### 1.1. Membrane Separations

Chemical processes, in general, can be regarded as a sequence of a pretreatment step, a reaction step and a separation step, transforming the incoming raw materials (input) into the desired products (output). This transformation requires energy. Besides the desired product, often undesired by- or waste-products will also be produced. Engineering of chemical processes is more and more carried out in the framework of the minimization of energy consumption and waste disposal.

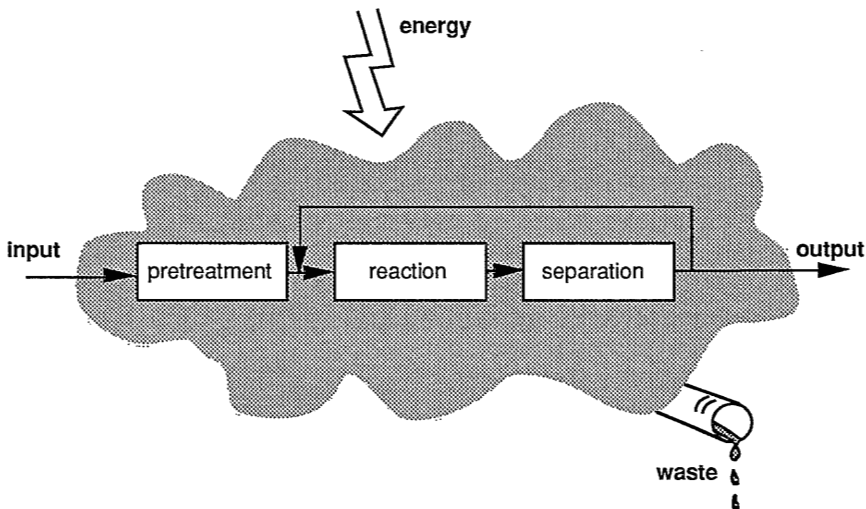


*Figure 1. Schematic representation of a chemical process*

To fulfil the tasks of diminishing energy consumption and minimization of waste, modular, energy efficient and highly selective separation techniques are required. In the past 20 years, membrane processes have demonstrated to possess these required characteristics.

In a membrane process, a membrane acts as a selective interphase between two bulk phases. By means of a driving force, some of the species from a multi-component

mixture are transported through the membrane into the other bulk phase while other components are retained by the membrane. Selective mass transport has occurred. Often, a sufficiently high selectivity is accompanied by low transmembrane fluxes and vice versa, making a highly selective membrane process too expensive. Future financial rejudgement of charges for waste disposal may favour highly selective separation processes like membrane processes which minimize waste streams and even offer a possibility to recycle valuable species from the effluent streams. Besides applications in chemical engineering, membranes are often used in medical applications. In fact, membrane sales are having the largest turnover in the artificial kidney business.

Because of the future prospective, especially in environmental engineering, membrane technology attracts a considerable amount of research interest. The research carried out in membrane technology can be roughly divided into two groups. The first group, the membrane process group, uses membranes with certain specified characteristics as a black box and studies its behaviour under certain process conditions as a singular process or, more often, as a hybrid process in combination with other unit operations. The other group is interested in material science aspects of membranes, *e.g.*, the morphology of membranes, and how this morphology relates to the mass transport characteristics. Depending on the morphology, the applications for a given membrane can be very different.

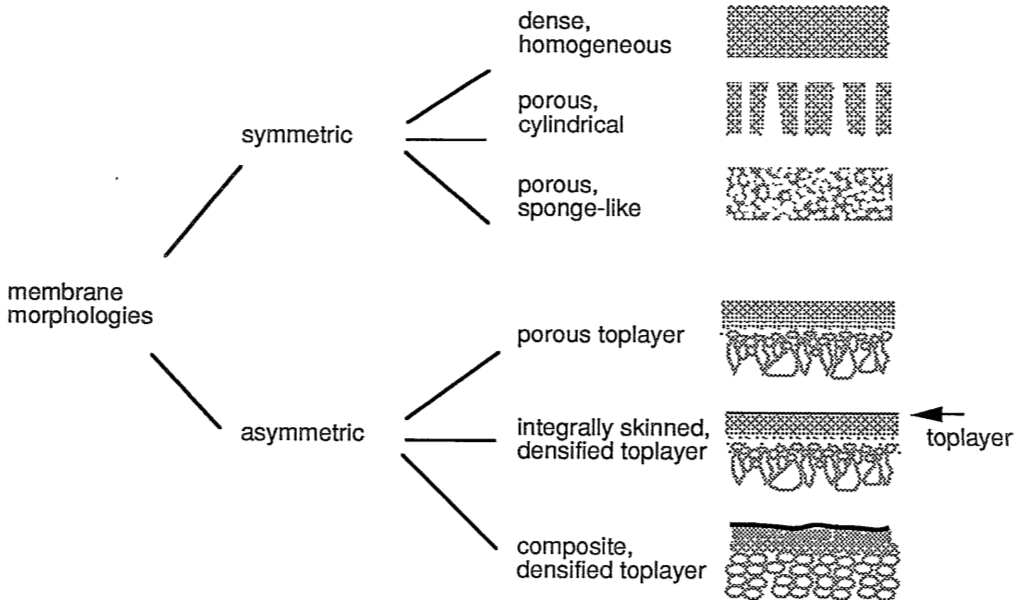


Figure 2. Schematic representation of different membrane morphologies, after Mulder [1]

In general, two classes of membrane morphologies can be distinguished [1]: symmetric and asymmetric membranes. The first class can be subdivided into three groups of membranes:

- homogeneous, dense membranes with an active layer thickness of more than 10  $\mu\text{m}$ ; these membranes are often used for the study of polymer material science aspects in gas separation and pervaporation;
- cylindrical porous membranes which are normally used in small size laboratory experiments like enzyme and DNA separations from dilute solutions;
- sponge-like porous membranes; these membranes have normally an average pore size of 0.2 - 5  $\mu\text{m}$  and find application in the field of microfiltration.

The second class, the class of asymmetric membranes can be subdivided into three groups:

- porous membranes; here, the membrane does not have the same pore size over the whole membrane thickness but a pore size gradient;
- porous membranes having a top layer; these membranes have normally, atop an open porous support layer, a second layer with much smaller pores (5-500 nm). Membranes of this type, *i.e.*, integrally skinned asymmetric membranes are generally used in ultrafiltration applications. In gas separation applications, the porous top layer separates gases by a Knudsen diffusion or Poiseuille mechanism. Alternatively, the top layer may be dense, which means that this layer is a continuous polymer phase. Then, solid particles can not at all and fluids only hardly penetrate through the film.
- composite membranes; a homogeneous layer is placed in a second production step on top of a support membrane. Integrally-skinned and composite membranes for the separation of gases and liquids (pervaporation) have selective layers thinner than 1  $\mu\text{m}$ .

## 1.2. Solution-Diffusion Membranes

In this thesis only dense membranes which can be used for gas separation as well as for pervaporation will be considered. Since the active layers of these membranes are dense, they do not separate species on the basis of an ordinary sieving mechanism. The separation mechanism for dense membranes is the so-called solution-diffusion mechanism.

At the feed side, molecules of component  $i$  dissolve in the polymer phase and thermodynamic equilibrium exists between the penetrants sorbed in the membrane

phase and the penetrants in the feed or permeate side compartment. The chemical potential of component  $i$  at the downstream side is lower than that at the feed side, which means that the concentration of  $i$  at the membrane downstream side is also lower. This driving force causes a continuous diffusional mass transport of the species  $i$  through the membrane. The feed may be a mixture of gases, vapours or liquids. The sorption and diffusional processes are determined by the characteristics of the permeant and the polymeric membrane material.

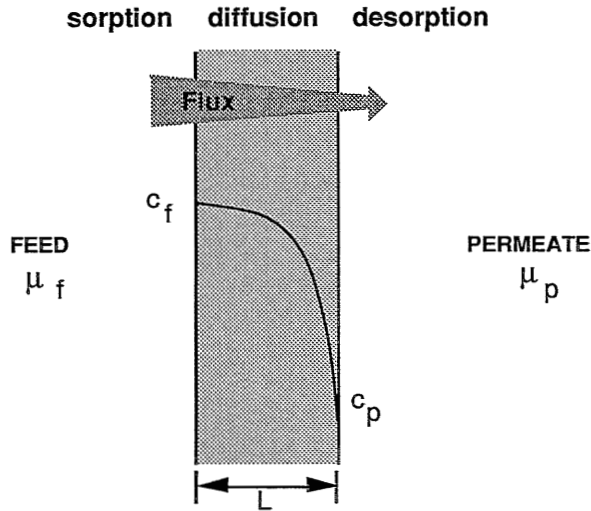


*Figure 3. Schematic representation of mass transport phenomena occurring in a solution-diffusion membrane*

A quantitative measure of the amount of mass transported through the polymeric membrane is given by the “permeability”  $P$ . It is, in fact, the flux  $J$  normalized for the driving force (in gas separation given by the pressure difference  $\Delta p$ ) and for the membrane thickness  $L$ . According to the solution-diffusion model, the permeability is a product of diffusivity and solubility [2]. The solubility  $S$  is defined as the equilibrium concentration solved in the polymer phase divided by the applied pressure.

$$J = P \frac{\Delta p}{L} \quad (1a)$$

$$P = D * S \quad (1b)$$

$$S = \frac{c}{p} \quad (1c)$$

The permeability of gases through polymers can vary up to 4 orders of magnitude,

which results from differences in solubility or diffusivity. Figure 4 shows the diffusivity of penetrant molecules of different size in water, natural rubber and the glassy polymer polystyrene.

In water, the diffusion coefficient decreases slightly with increasing molecular weight of the diffusing species. The decrease is much more pronounced in natural rubber and polystyrene. Natural rubber, the polymer with the larger chain flexibility, shows a less dramatic decrease compared to polystyrene. The polymer chains in natural rubber can move apart much easier to open up a diffusional pathway allowing mass transport into the direction of the gradient in chemical potential.

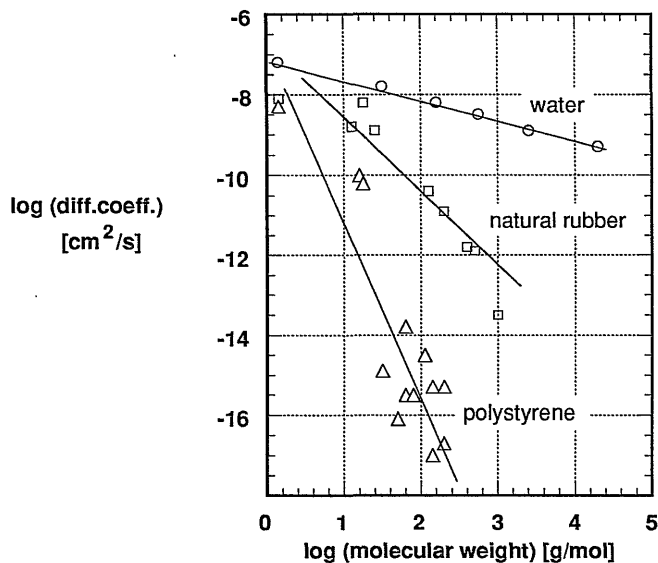


Figure 4. Diffusion coefficients of penetrant molecules with different molecular weights in water, natural rubber and polystyrene, after Strathmann [3]

A feed mixture containing species of different size but same chemical nature will be separated in gas separation and pervaporation processes during diffusion by a *molecular sieving* mechanism. On the other hand, the sorption and desorption process is thermodynamic in nature and the solubility is mainly determined by the affinity between penetrant and polymer. Chemically different species in the feed mixture will have a different affinity and, therefore, the polymer membrane shows also a sorption selectivity (see figure 5) besides the diffusion selectivity. Both together result in the permselectivity of the polymer.

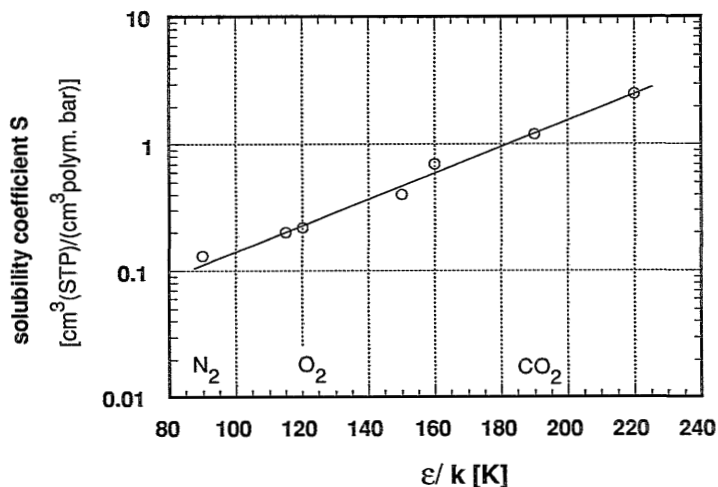


Figure 5. Solubility coefficients of different gases in silicone rubber as a function of the Lennard-Jones potential well depth, after Koros [4]

In the ideal case, the permselectivity for a pair of components  $i$  and  $j$  is a material characteristic and can be calculated from the permeabilities of the pure components.

$$\alpha_{\text{ideal}} = \frac{P_i}{P_j} \quad (2)$$

In pervaporation, however, the permselectivity can seldom be predicted from permeation experiments carried out with pure components. Similar results have been found for the selective properties of cellulose acetate membranes separating a gaseous mixture of carbon dioxide and methane [5]. In a BRITE research project on the development of new membranes for the treatment of sour gases [6], similar problems were observed: highly selective polymers (polyimides) lost their outstanding low pressure separation characteristics for the treatment of CO<sub>2</sub>-containing natural gas in high pressure applications as shown in figure 6.

This loss in selectivity is generally interpreted as *plasticization*; a weakening effect on the polymer introduced by the strongly sorbing carbon dioxide. The CO<sub>2</sub> swells the polymer and the swollen polymer loses therefore its selective properties. However, it remains the open question what plasticization or swelling means; whether it is measurable in the case of gases and to what extent it occurs. Aim of this thesis is to explore and understand the physical meaning of the "plasticization" phenomena occurring in polymer-penetrant systems.

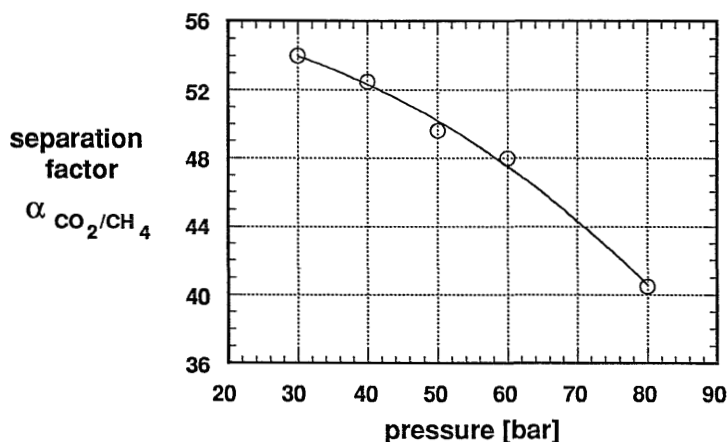


Figure 6. Separation factor of a 6FDA-4PDA polyimide membrane for a 20/80 vol% gas mixture of  $CO_2/CH_4$  at different upstream pressures and  $T=25^\circ C$  [6,7]

### 1.3. Structure of this Thesis

Mass transport behaviour through polymeric membranes has been thoroughly investigated experimentally and theoretically in the past 40 years. Nowadays, almost every month a new publication or patent appears where new polymers have been synthesized and gas permeabilities, diffusivities and solubilities have been determined. The essence of all relevant literature information will be presented in *chapter 2*. First, different *diffusion* models are presented and compared with experimental results. In a second part, models describing the *sorption* behaviour of polymers will be summarized; strong and weak points will be elaborated. Since in some of the models, the physical background is related to the morphology of the amorphous polymer matrix, a rather compact overview will be given on the amorphous state of polymers.

*Chapter 3* describes in detail the experimental tools, like sorption and permeation set-ups, developed for the determination of mass transport behaviour of polymers. A new technique allowing the measurement of swelling *kinetics* of polymers in a gaseous atmosphere will be presented. Briefly, the synthesis of various polyimides and their physical properties will be described.

In *chapter 4*, the sorption and dilation behaviour of polyimides will be discussed with regard to the sorption models described in chapter 2. A final choice for an elastic strain corrected Flory-Huggins model developed by Bitter [8] will be made.

This model will be used, furthermore, for the analysis of the sorption behaviour of CO<sub>2</sub> in 70 different polymers. An experimental relation between the solubility coefficient obtained from this analysis to the glass transition temperature of the polymers will be presented. Considering the glass transition temperature as a measure for the chain flexibility, the experimental relation is in accordance with the theoretical prediction derived from Bitter's model: the logarithmic solubility coefficient is linearly related to the inverse of a polymer chain flexibility parameter.

Time-dependent morphology alterations in the membrane due to swelling stresses exerted by sorbed penetrant molecules on the glassy polymer matrix will be described in *chapter 5*. In the first part, permeation experiments at high pressures will be analyzed and a new term "aging time" will be introduced in order to understand and interpret certain time-dependent phenomena. In a second part, time-dependent phenomena occurring during sorption and dilation will be presented. A physical picture will be developed that discriminates between "Fickian" sorption sites, which are instantaneously available for sorption, and sorption sites which will be produced due to swelling stresses. The creation of these "relaxational" sorption sites is slow and can easily be distinguished from the Fickian ones during dilation kinetics. Having this picture in mind, a number of unsolved phenomena in pervaporation and gas separation will be presented and explained.

The unique relation found in chapter 4 between the solubility of a penetrant in a polymer and the glass transition temperature of a polymer is based on the elastic strain corrected Flory-Huggins model. In this model, the assumption of local ordering was made in order to derive this model. In the last part of chapter 2, a compact overview on local ordering phenomena in amorphous polymers was given. (The nodular structure of outer, dense layers in carbon dioxide foamed glassy polymers, described later on in chapter 7, may be interpreted as aggregates of local orderings). In *chapter 6*, molecular dynamics simulations have been used to get some insight on the term "local ordering". The study was carried out with poly(ethylene terephthalate) as a model polymer because sufficient experimental data were available to compare the simulation results with experimental results. For the first time, it could be shown from the comparison of experimental and simulated X-ray diffraction patterns that the modelled structure and that of the bulk of the polymer compare well. It can also be concluded that local ordering is present in PET, but it is generally difficult to detect this in experimental X-ray patterns. Secondly, the simulated structure of PET which contains the benzene ring in the para position in the polymer backbone, is compared with poly(ethylene isophthalate). This polymer contains the benzene ring in the meta position in the polymer backbone. Free volume distributions are calculated for these two different structures showing that the meta substituted polymer has a lower content of larger volumes elements compared to the para isomer of PET.



The “plasticizing” effect of carbon dioxide on glassy polymers is discussed in *chapter 7*. Glassy polymers saturated with nitrogen form a foam if they are quickly heated above their glass transition temperature due to the thermally induced supersaturation of the polymer matrix. If the polymer, however, is saturated with carbon dioxide, foams can be produced at much lower temperature indicating a depressed glass transition temperature. This phenomenon is used to develop an easy-to-use experimental technique to determine the extent of glass transition temperature depression depending on the pressure at which the polymer sample was saturated. Non-porous toplayers on the samples are reported and their occurrence and thickness can completely be explained and predicted. Albeit “dense”, the toplayer does not consist of a homogeneous polymer network but is build up by nodular entities. Two interpretations will be presented, namely the disentanglement of the polymer matrix or the aggregation of areas of local ordering into “super-nodules”, but no final decision for one or the other physical picture can be made.

In *Appendix A* of this thesis a completely new approach to the prediction of the permeability of a gas through a polymer film will be presented. It is assumed that an infrared spectrum of a polymer contains most of the necessary information to characterize the polymer and its mass transport behaviour. However, the complexity of the spectrum makes a linkage to mass transport properties difficult. A neural network capable of doing such a complex task will be used to correlate the infrared spectrum of a polymer to the permeability of carbon dioxide through this polymer. The potential of this approach will be demonstrated and a satisfactory relation between experimental and predicted permeabilities will be presented. It is reasonable to expect that an extension of the trainings set of polymers will increase the quality of the relation considerably.

## References

- (1) M.H.V. Mulder, *Basic Principles of Membrane Technology*, Kluwer Academic Publisher, 1991
- (2) S. vonWroblewski, *Wied. Ann. Phys.* 8 (1879) 29
- (3) H. Strathmann, *Trennung von molekularen Mischungen mit Hilfe synthetischer Membranen*, Steinkopf Verlag, Darmstadt, 1979
- (4) W.J. Koros, M.W. Hellums, *Transport properties*, in: *Encyclopedia of polymer science and engineering*, Supplement, J.Wiley & Sons, 1989
- (5) H. Finken, *Asymmetric membranes for gas separation*, in: *Material Science of Synthetic Membranes*, ACS Symp. Ser. 269, American Chemical Society,

- Washington, 1984
- (6) BRITE Project RI/B-0098/NL, Membrane separation of CO<sub>2</sub> and H<sub>2</sub>S from mixtures with gaseous hydrocarbons, in: Future industrial aspects of membrane processes, L. Cecille, J.-C. Toussaint (Ed.), Elsevier Appl. Sci., 1989
  - (7) M. Wessling, S. Schoeman, Th. v.d.Boomgaard, C.A. Smolders, Plasticization of gas separation membranes, *Gas Sep.&Purif.*, 5 (1991) 222
  - (8) J.G.A. Bitter, Transport mechanisms in membrane separation processes, Plenum Press, New York, 1991

## Chapter 2

# Mass Transport in Solution-Diffusion Membranes

### 2.1. Introduction

Classical techniques for the separation of gas-gas, gas-liquid, and liquid-liquid mixtures are adsorption and absorption, distillation, crystallization and extraction. Membrane separation processes have occasionally been able to replace classical techniques in cases where the separation task was hard to achieve and the membrane process was economically competitive. Examples are the separation of azeotropic alcohol-water mixtures by pervaporation and the recovery of hydrogen from a purge gas stream in ammonia synthesis processes by gas separation membranes. Membrane technology, however, is not a break-through technology. Progress has been made in the past gradually and it was learned that classical separation techniques cannot be replaced from one day to the other.

Future applications of membranes are most likely expected to be in the environmental field where continuously intensified governmental restrictions require the need for specific and highly selective separation techniques. The removal of organic vapours from air streams, the removal of trace organics from water, the recovery of  $\text{CO}_2$  and  $\text{CH}_4$  from landfills and the recovery of  $\text{CO}_2$  and  $\text{SO}_2$  from natural gas and flue gas stand for these separation tasks. Membranes which can be used for these applications are so-called solution-diffusion type membranes. Mass transport through a dense, selective polymeric membrane occurs according to a solution (sorption) step at the upstream side of the membrane, diffusion through the membrane and a desorption step on the downstream side. The total amount of mass transported through the membrane is characterized by the permeability. It is a characteristic value for a specific polymer-penetrant system and quantifies a certain amount of mass per time unit permeating through the membrane normalized for the film thickness, the driving force and the surface area through which permeation takes place.

Permeability is the product of diffusivity and solubility:

$$P = D * S \quad (1)$$

The capability of solution-diffusion membranes to *separate* multi-component mixtures is based on specific thermodynamic interactions of the membrane material with the different components in the mixture, and, furthermore on the selective, diffusive mass transport through a dense homogeneous layer of the membrane. The selective diffusion of the penetrant molecules through a layer of a dense polymer is mainly influenced by the molecular structure of the polymer itself. Short range motions in the polymer chains, like chain bending, bond rotation and phenyl ring flips, which of course depend on this molecular structure, allow penetrant molecules to proceed into the direction of the driving force [1,2].

Two dissertations [3,4] have been published at the University of Twente in the past two years dealing with specific chemical modifications in the polymer main chain in order to investigate the influence of the polymer molecular structure on the diffusion of penetrant molecules through the polymeric matrix. Based on experimental results obtained with two different polymer families, *i.e.*, polyimides and polytriazoles, a molecular picture of diffusional jumps of the penetrant molecule has been developed. This jumping mechanism can be confirmed by Computer Aided Molecular Modelling. We will start with briefly summarizing these results in paragraph 2.2. It will be the basis for a review on models describing diffusion through a polymeric membrane.

Besides the diffusivity of a penetrant molecule, the thermodynamic interaction between polymer and penetrant contributes to the overall mass transport properties of a polymer. In a third part of this chapter (paragraph 2.3.), the substantial body of experimental results and theoretical models on the sorption behaviour of polymers, especially glassy polymers, will be reviewed. The diffusion of penetrant molecules into a polymer matrix causes a volumetric change of the polymer. Penetrant induced swelling stresses might alter the structure of the matrix and can be observed as relaxational alterations of physical characteristics and morphology of the polymer. In order to understand and interpret these phenomena properly, a detailed physical picture of the morphology of an amorphous polymer is required. Previous concepts developed on the structure of amorphous polymeric matter will be reviewed in 2.4. In this whole chapter we will provide a framework of relevant experimental and theoretical results dealing with mass transport phenomena in solution-diffusion membranes.

## 2.2. Diffusion

In molecular models describing the diffusion of penetrant molecules through a polymer matrix it is commonly assumed that microcavities of different sizes are formed and destroyed continuously in the polymer. Small, dissolved molecules trapped in these locations are able to move into the direction of a driving force by cooperative motion of adjacent polymer chains [2]. Meares [5] developed a model in which the trapped molecules jump from one cavity to another one and the energy required for this jump, the activation energy of diffusion, is correlated with the jump length  $\lambda$ , the cross section of the penetrant molecule  $\sigma^2$ , and the energy required to disrupt neighbouring polymer chains, hence the cohesive energy density (C.E.D.).

$$E_D = \pi/4 \sigma^2 \lambda N_A \text{ (C.E.D.)} \quad (2)$$

$N_A$  is Avogadro's constant. More sophisticated models like the one of Brandt [6], DiBenedetto [7] and Pace and Datyner [8] incorporate in their theoretical description of the activation energy of diffusion basically terms describing the overcoming of attractive forces between the chains and the energy required for bending of polymer chains. However, molecular models deal with the prediction of the *energy* required for a diffusional jump. They do not predict beforehand absolute values of diffusion coefficients.

In contrast, free-volume models based on the ideas of Cohen and Turnbull [9] and further developed by Fujita [10] describe the absolute velocity of the penetrant molecule in the polymer matrix. A simple relation elaborated by Lee [11] correlates the diffusion coefficient to the polymer free-volume as given by equation (3)

$$D = A^* \exp\{-B/v_f\} \quad (3)$$

with  $v_f = v - v_0$ .  $v$  is the specific volume of the polymer which can be obtained by a density measurement and  $v_0$  is the specific occupied volume of the polymer chains, which can be estimated using group contribution methods. The total free-volume is accessible for diffusion.  $A^*$  and  $B$  are empirical constants equal for all polymers. Vrentas and Duda [12] developed an extended model in which more detailed molecular aspects are considered. Here, the absolute value of the diffusivity of a penetrant in a polymer can be described as follows:

$$D = D_0 \exp\left\{-\frac{E_D}{RT}\right\} \exp\left\{-\frac{\gamma \xi V_2^*}{V_{FH2}}\right\} \quad (4)$$

where  $V_{FH2}$  is the average hole free-volume per gram polymer. Furthermore the following molecular parameters are incorporated:  $E_D$  which is the energy required per mole of penetrant to overcome attractive forces between polymer and penetrant,  $V_2^*$ , which is the specific critical hole free-volume for a jump,  $\xi$ , which is the ratio of the critical molar volume of the solvent jumping unit to the critical molar volume of the polymer jumping unit, and  $\gamma$ , which is an overlap factor since the same free-volume may be available to more than one approaching molecule. The average hole free-volume is only a part of the total free-volume. It can be redistributed without an increase in energy. The remainder free-volume is the interstitial free-volume which is distributed uniformly in the polymer matrix but which is not accessible for diffusion. The disadvantage of this model is certainly that it needs a number of different parameters which are difficult to obtain experimentally.

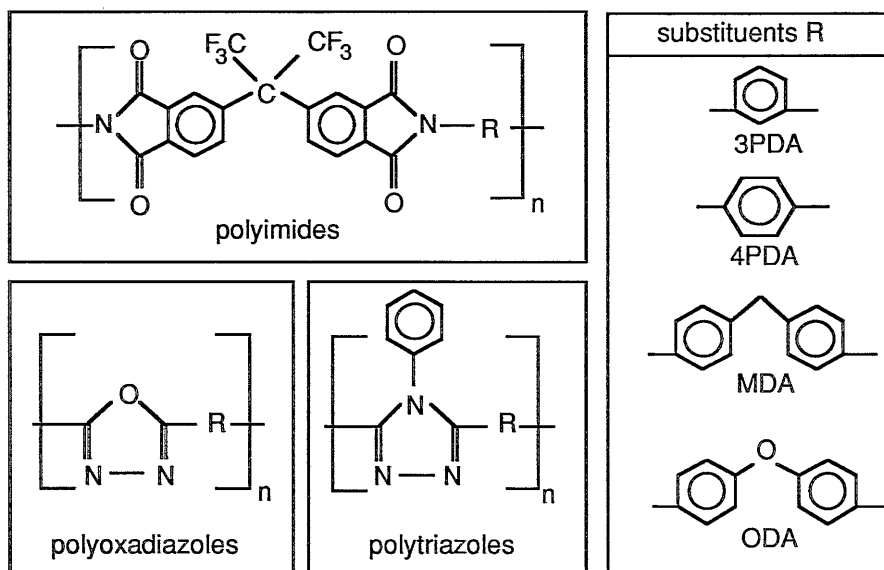


**Figure 1.** Basic chemical structures of polyimides, polyoxadiazoles and polytriazoles listed with a selection of substituents [3,4]

In the research work by Smit and Hensema three different polymer families, *i.e.*, polyimides (PI) [3] and polytriazoles (PT), polyoxadiazoles (POD) [4] have been synthesized to elucidate the influence of polymer structure on the mechanism of diffusion. General structures of the polymers are shown in figure 1. Film preparation and experimental procedures are described elsewhere [3,4,13]. Since the investigations were carried out as parts of projects dealing with the treatment of sour gases by means of a membrane separation process, the gases used for the

characterization of mass transport parameters where generally  $\text{CO}_2$  and  $\text{CH}_4$ .

Substituting equation (3) into (1) results in

$$\ln P = \ln S + \ln A^* - B/v_f \quad (5)$$

Assuming that  $\log S$  varies only little with respect to  $\log D$  a plot of  $\log(P)$  versus  $(1/v_f)$  should result in a linear relationship [11]. Figure 2 compares the relation found by Lee for conventional polymers with data obtained for a large variety of specifically synthesized polymers.

A considerable deviation between earlier results obtained by Lee [11] and the results obtained with polyimides, polyoxadiazoles and polytriazoles can be observed. Furthermore, a remarkable contradiction to the simple free-volume relation is illustrated by analyzing the mass transport behaviour of polymers which differ only in their meta or para position of the phenylring moiety in the main chain.

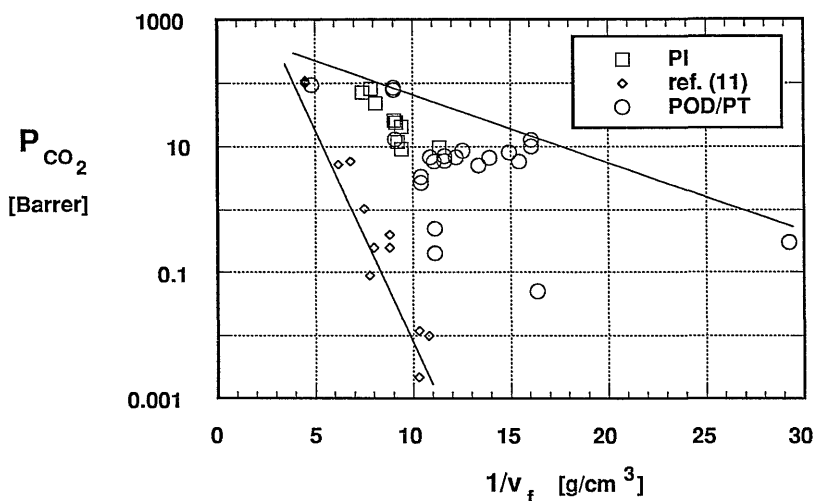


Figure 2.  $\text{CO}_2$ -permeability as a function of free-volume for different polymers, replotted from [4]

In figure 3, the permeability of  $\text{CO}_2$  through polytriazoles with different meta/para-phenylene contents is plotted versus the free-volume. Polymers presented were synthesized in such a way that the phenylene moieties occur randomly or in an alternating fashion in the polymer backbone. With increasing para-phenylene

content the free-volume of the polymer decreases, but the permeability increases. Time-lag experiments carried out with gases like oxygen and nitrogen [4] emphasized that this increase in permeability was mainly caused by an increase in diffusivity. Several authors [14-16] have observed the drastic decrease in diffusivity for meta substituted polymers before, but none of the reports show this distinct contradiction to the free-volume approach. Similar results have been obtained with 6FDA-based polyimides. These observations lead to the conclusion that not only the *absolute value* of the free-volume calculated from density measurements is of importance but that the *distribution* of the free-volume is also important. However, the free-volume distribution is hardly to detect experimentally.

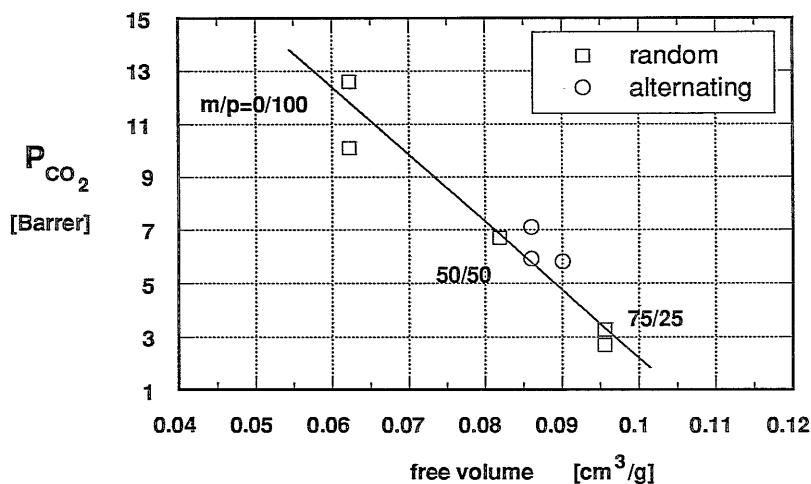


Figure 3.  $\text{CO}_2$ -permeability for polytriazoles with different amounts of meta/para substituted phenylring moieties; data were taken from [4]

From the foregoing discussion one can also conclude that the problems correlating the permeability with the free-volume of a polymer might have their origin in the difficulty to find a precise definition of the free-volume.

In a different approach to correlate gas transport through polymers with their molecular structure, extensive synthesis work on a series of 6FDA-based polyimides led to an experimental relation between the diffusivity of a penetrant molecule and the jump in heat capacity at the glass transition temperature as shown in figure 4.



Smit [3,13] developed a molecular picture based on the ideas of Meares and Brandt. Mass transport through the polymer is determined by the ability of the polymer chains to open up tunnels so that molecules trapped in a microcavity can move into a neighbouring one. With an already published experimental relation between the jump in the heat capacity of the polymer at the glass transition temperature and the cohesive energy density (C.E.D.) [17]

$$\Delta c_p = 1.25 (\text{C.E.D.}) + 2.17 \text{ [cal/(mol K)]} \quad (6)$$

and the relation of Meares for the activation energy of diffusion, a relation between the diffusion coefficient and the jump in the heat capacity at  $T_g$  was proposed.

$$\log D \sim \lambda \text{ C.E.D.} \sim \lambda \Delta c_p \quad (7)$$

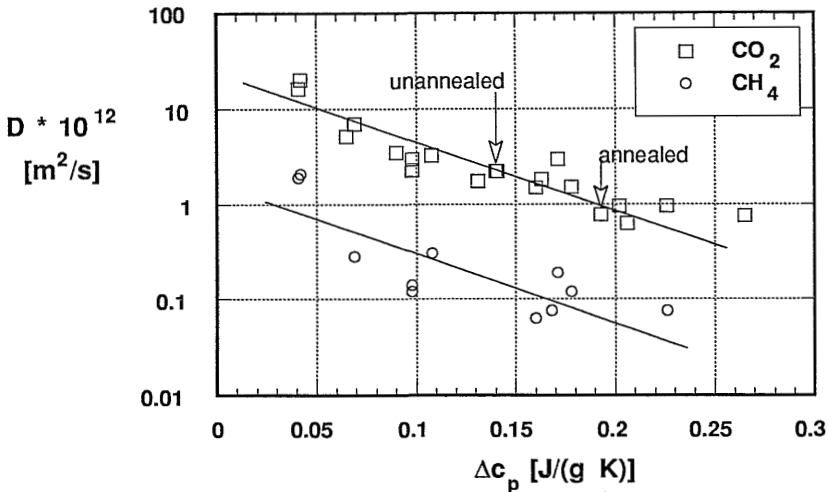


Figure 4. Diffusion coefficients of CO<sub>2</sub> and CH<sub>4</sub> in different polyimides as a function of the jump in the heat capacity at the glass transition temperature; arrows indicate the effect of annealing; data were taken from [3]

Besides studying variations in the polymer backbone, additional experiments were carried out by annealing the polymers. Annealing resulted in an increased  $\Delta c_p$  since the polymer matrix is more tightly packed. As a result the energy required to separate neighbouring chains will increase. This higher  $\Delta c_p$  could indeed be correlated with a decreased diffusivity (see arrows in figure 4).

Hensema [18] explained the experimental relation found in figure 4 on the basis of a hole theory approach given by Wunderlich [19]. The free-volume definition used by Hensema is based on the Hirai-Eyring rate theory [20] describing the equilibrium occurrence of "holes" in a liquid.

Wunderlich correlates the jump in the heat capacity at the glass transition temperature  $\Delta c_p$  to the energy  $\epsilon_h$  required to form holes of a certain molar volume  $V_h$ .

$$\Delta c_p = R \frac{V_0}{V_h} \left( \frac{\epsilon_h}{R T_g} \right)^2 \exp \left\{ - \frac{\epsilon_h}{R T_g} \right\} \quad (8)$$

In equation (8),  $T_g$  is the glass transition temperature,  $R$  the universal gas constant and  $V_0$  the molar hard core volume of the polymer. Wrasidlo [21] has shown that  $\epsilon_h/T_g$  is constant for all polymers. Hence the molar volume of the holes  $V_h$  is directly correlated with the jump in the heat capacity at the glass transition temperature. On cooling of the rubbery polymer towards the glass transition temperature, the number of holes decreases by a loss of polymer chain mobility. At lower temperatures than the  $T_g$ , the number of holes is constant and corresponds to the equilibrium value at the glass transition zone. From equation (8) it is clear that the jump in heat capacity is proportional to the reciprocal molar hole volume. In combination with equation (2) Hensema suggests that an increasing  $\Delta c_p$  should result in a decreasing diffusivity as shown in figure 4. The interpretations of both Smit and Hensema seem to be reasonable but need further refinement.

### *Molecular Dynamics*

A diffusion coefficient is a macroscopic property of a polymer-penetrant system that does not give particular, detailed information about molecular motions of parts of the polymer chains during the diffusional process. However, the above described models, molecular and free-volume models, assume local cooperative polymer chain motions. It would be of general interest to have more detailed molecular information on the diffusion mechanism. Computer Aided Molecular Modelling is a simulation technique in which the motion of every atom can be followed as time evolves. For the simulations, the GROMOS package was used [22] to model an amorphous polymer matrix built from a polyimide [23]. The package makes use of a force field consisting of a sum of bonded and non-bonded interactions between atoms in the system. For the simulations described below, 10 molecules of CO<sub>2</sub> were placed into such an amorphous polymer matrix. The position of one of the molecules in time is

shown in figure 5.

During the first 100 picoseconds of the simulation the penetrant molecule is bouncing inside a cavity. Then, it moves within a very short time over a distance of approximately 10 Å into another cavity. Unfortunately, simulations longer than 200 ps are extremely high in computer time consumption so that such simulations could not be carried out. In order to estimate a realistic value of the diffusion coefficient and an average jump length, the observation of more jumps would be necessary. The calculations do confirm, however, that in this complex system diffusion of a penetrant molecule occurs by a jumping mechanism.

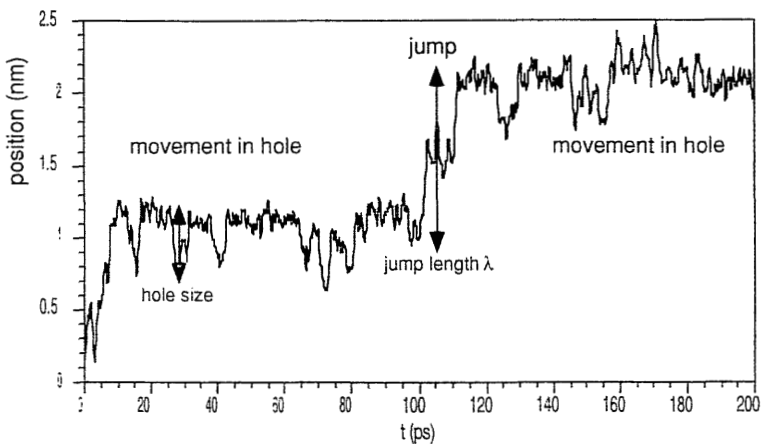


Figure 5. Motion of a  $\text{CO}_2$  molecule in a 6FDA-4PDA polymer matrix [3]

### 2.3. Sorption and Dilation

The affinity of a penetrant molecule for a polymer has a considerable influence on the mass transport behaviour of this polymer. Equation (1) shows that diffusion and solubility are equally important for the overall mass transport described by the value of the permeability. The solubility of a penetrant in a polymer matrix is described by the sorption isotherm. It correlates, at a constant temperature, the amount of sorbed penetrant to the activity of the phase around the polymer. Depending on the nature of the polymer-penetrant system, sorption isotherms may show considerable differences in shape. For the sorption of simple gases in rubbery polymers the relation of the sorbed penetrant to the activity is linear (see figure 6) and obeys

Henry's law

$$c = k_D p \quad (9)$$

where  $c$  is the volumetric concentration of penetrant at standard temperature and pressure per volume of polymer,  $k_D$  is Henry's law constant and  $p$  is the applied pressure. For high penetrant concentrations the sorption isotherm turns upwards into a convex shaped curve. This isotherm, often found for vapours in rubbery polymers, is well represented by the Flory-Huggins theory [13].

$$\ln \left( \frac{p}{p^0} \right) = \ln (1 - \phi_p) + \phi_p + \chi \phi_p^2 \quad (10)$$

$p$  is the applied pressure or vapor pressure,  $p^0$  is the saturation pressure,  $\phi_p$  is the polymer volume fraction and  $\chi$  the Flory-Huggins interaction parameter.

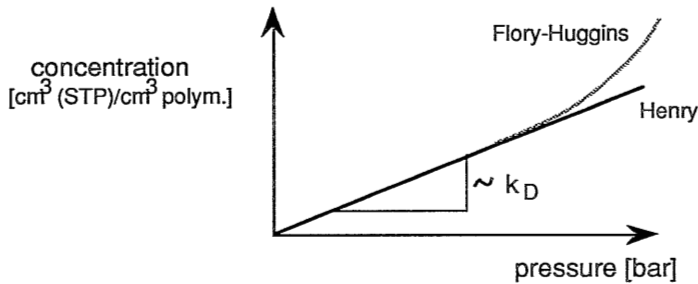


Figure 6. Schematic representation of sorption isotherms in rubbery polymers

The sorption behaviour of glassy polymers is rather different. Glassy polymers typically show concave shaped sorption isotherms [24] for the sorption of gases and vapours as shown in figure 7. As for rubbery polymers, the sorption isotherms for polymers sorbing large amounts of penetrant might turn into a convex curve deviating from the concave part [25-27].

The physical meaning of the inflection point of the sorption isotherm is the following: the concentration  $c_g$  represents that concentration of penetrant molecules at which the glass transition temperature of the polymer-penetrant system is equal to the experimental temperature. Above this concentration the Flory-Huggins regime (equation (10)) is valid again. In the past a number of models have been developed to describe the concave shape (first part) of the sorption isotherm in more

detail. These models will be reviewed briefly below.

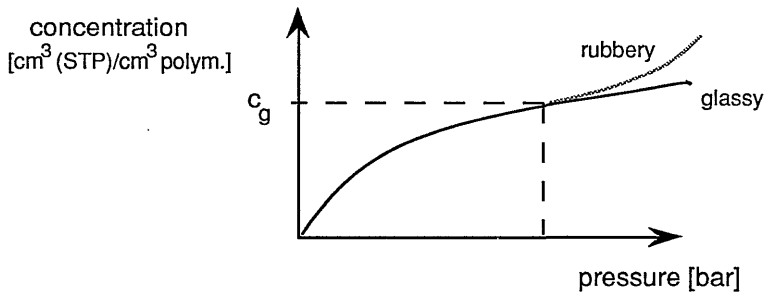


Figure 7. Schematic representation of sorption isotherms in glassy polymers

### Dual Mode Sorption

Cooling a liquid-like rubbery polymer from temperatures above  $T_g$  through the glass transition temperature causes an abrupt change in thermal expansivity. The ability of polymer chains in the rubbery state to instantaneously adjust their conformation upon any kind of perturbation is lost at the glass transition temperature. Long-chain motions are frozen-in and most of the chain dynamics below the glass transition temperature is believed to be of torsional nature. Figure 8 shows the specific volume of a polymer depending on the temperature [1].

The total polymer volume is the sum of the occupied van der Waals volume and the free-volume (see above). The van-der-Waals volume varies only a little with decreasing temperature coming from the rubbery region. However, the total specific volume decreases significantly with decreasing temperature due to a decreasing frequency and amplitude of rotational, torsional and vibrational polymer chain motions. At the glass transition these motions are frozen-in and so are molecular volume fluctuations related to these motions.

The difference between the hypothetically extrapolated rubbery specific volume and the actual specific volume of the glass is often called the unrelaxed free-volume. Because of the non-equilibrium state of the polymeric glass, volumetric changes can be observed [28] indicating a relaxational densification of the unrelaxed free-volume. These relaxation phenomena can also be monitored by mechanical and dielectrical experiments.

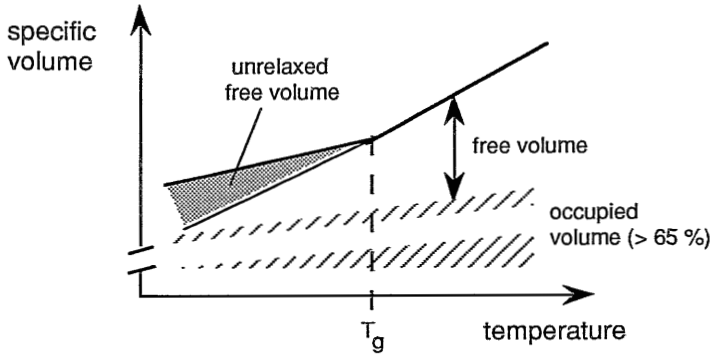


Figure 8. Temperature dependence of the specific volume of a polymer

In the dual-mode sorption model the glassy polymer is considered to consist of a homogeneously densified matrix in which a small amount of microcavities are embedded. The volumes of these microcavities sum up to the total unrelaxed free-volume. The sorption behaviour depends on the location where a penetrant molecule is sorbed [29]. In the homogeneously densified matrix, the sorption is assumed to occur as ordinary dissolution described by Henry's law (equation (9)). In the microcavities, however, the sorption behaviour obeys an *adsorption*-type of isotherm, namely a Langmuir isotherm.

$$c_H = \frac{c'_H b p}{(1 + b p)} \quad (11)$$

The parameters  $c'_H$  and  $b$  are the Langmuir capacity and affinity factor, respectively. Adding both equations results in the Dual-Mode Sorption model.

$$c = k_D p + \frac{c'_H b p}{(1 + b p)} \quad (12)$$

With its three fitting parameters, equation (12) represents experimental sorption data well for different gases as well as for different temperatures.

Linked to these two distinct populations, two distinct diffusion coefficients are assumed, one describing diffusion in the dense matrix ( $D_D$ ) and the other one describing the diffusion in the holes ( $D_H$ ). A *decreasing* permeability with *increasing* upstream pressure could be described by the assumption of these two penetrant mobilities. Petropoulos derives a pressure dependent permeability [30] based on a

chemical potential approach shown in equation (13).

$$P = k_D D_D + \frac{c'_H D_H}{P} \ln(1 + b p) \quad (13)$$

Koros and Paul [31], in their approach based on a concentration difference as the driving forces, derived equation (14).

$$P = k_D D_D \left( 1 + \frac{c'_H b}{k_D} \frac{D_H}{D_D} \frac{1}{1 + b p} \right) \quad (14)$$

The sorption capacity of glassy polymers is often correlated with an average interchain distance obtained from wide angle diffraction experiments (WAXD) [32]. Such an experiment gives as a result the scattering intensity depending on the scattering angle  $2\theta$  as shown in figure 9. For amorphous polymers the X-ray pattern is diffuse and no distinct Bragg reflection peaks can be observed.

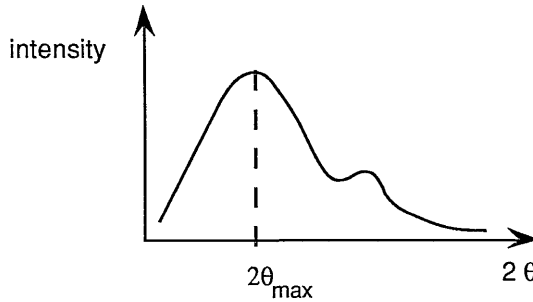


Figure 9. X-ray diffraction pattern of an amorphous polymer showing the scattering intensity versus the scattering angle  $2\theta$

Assuming the validity of Braggs law

$$n \lambda^* = 2 d \sin \theta \quad (15)$$

with  $n$  as the order of reflection,  $\lambda^*$  the wavelength of the X-rays and  $d$  the distance of reflecting planes, a so-called “d-spacing” can be calculated from the angle at which the maximum in the scattering intensity curve can be observed. However, the d-spacing value must be used with caution [33]. Most of the amorphous polymers investigated show a maximum in the range of 4 to 7 Å [3,4,32]. In fact, this is the range of distances where considerable *intramolecular* scattering occurs as will be shown later in chapter 6.

The validity of the Dual Mode Sorption model is supported by the fact that the Langmuir capacity factor  $c_H'$  approaches zero as the experimental temperature for sorption experiments approaches the glass transition temperature as depicted in figure 10. This represents the fact that the unrelaxed free-volume decreases with increasing temperature [34,35].

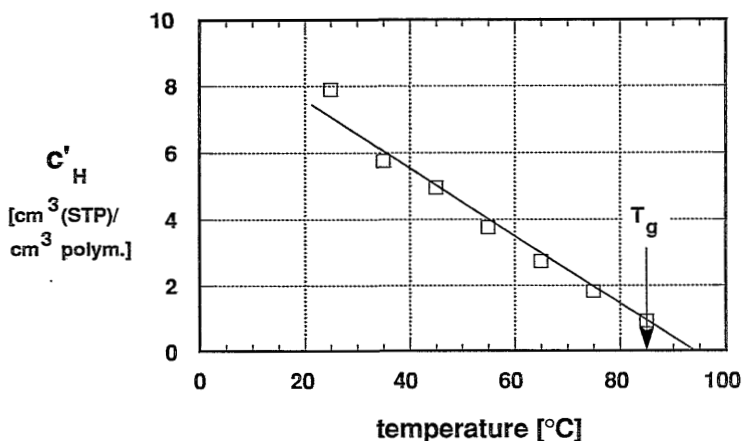


Figure 10. Langmuir capacity factor depending on the temperature for the system PET/CO<sub>2</sub>

A second verification of the model is believed to be found in the experimental observation regarding the volumetric behaviour of the polymer-penetrant system. Because the Langmuir sorption corresponds to a hole filling process, this population should not participate in the dilation of a polymer sample. Only that fraction of sorbed penetrant which is sorbed in the Henry mode should swell the polymer resulting in a linear relation of the sample dilation with increasing applied pressure. This is actually found for three different polycarbonates by Fleming and Koros [36,37] as schematically shown in figure 11.

Kamiya *et al.* [38] and Funke [39], however, did not find this *clear* evidence. Instead, they found for the systems PMMA/CO<sub>2</sub>, PMMA/propane [40] and cellulose triacetate/CO<sub>2</sub> the same shape in the dilation isotherm as the sorption isotherm (see later also chapter 4). Kamiya omitted this contradiction by introducing a fourth fitting parameter in the Dual Mode Sorption model; a fitting factor  $f$  which describes to what extent the Langmuir species dilate the microcavities. A factor of



zero represents the case of no dilation of the microcavities while a factor of 1 represents the fact that microcavities are dilated to the same extent as the homogeneously densified polymer matrix. For a number of glassy polymers, a factor  $f > 0.5$  can be observed which actually weakens considerably the support for the Dual Mode Sorption model believed to be found in the dilation experiments .

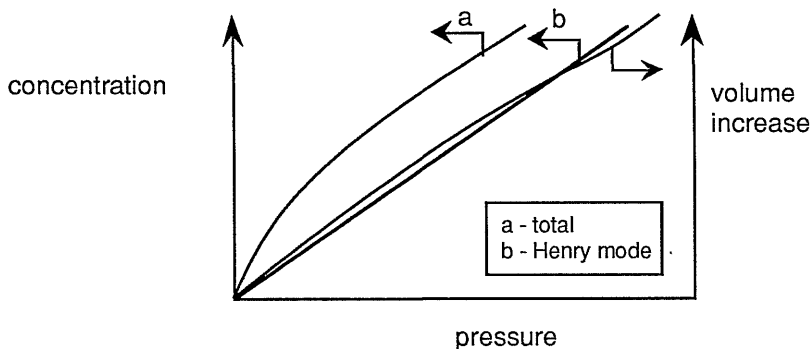


Figure 11. Comparison of sorption and dilation isotherms for the  $\text{CO}_2$  sorption in polycarbonate at  $T=35^\circ\text{C}$

Because none of the polyimides investigated in chapter 4 shows the same behaviour as the polycarbonates ( $f=0$ ), we refrain later in our work from an interpretation of the obtained data in terms of the Dual Mode Sorption model.

For completeness, a further development of the Dual Mode Sorption model should also be mentioned at this place. From equation (11) it is clear that there exists only one population of microcavities with one specific microcavity size. Recently, Weiss *et al.* [41] stated that the assumption of condensation and localization of penetrant molecules in microcavities of *one* size suffer physical origin. Instead, they suggest a model in which gas molecules interact with density fluctuations. The model is also phenomenological like the Dual Mode Sorption model and it is based on a single, continuous *distribution* of Langmuir isotherms in terms of a distribution  $\rho(\lambda_{\text{aff}})$  of the affinity parameter  $\lambda_{\text{aff}}$ . The equilibrium concentration sorbed in the polymer can then be expressed by the integral relation

$$c = c_{\text{sat}} p \int_0^{\infty} \frac{\rho(\lambda_{\text{aff}}) \lambda_{\text{aff}}}{1 + \lambda_{\text{aff}} p} d\lambda_{\text{aff}} \quad (18)$$

Assumptions of different mathematical forms for the distribution of Langmuir sites  $\rho(\lambda_{\text{aff}})$  result in different final, mathematical relations which fit sorption data well.

### *Modified Flory-Huggins equations*

Vrentas and Vrentas [42,43] developed on the basis of thermodynamic considerations of the polymer-penetrant system above and below the glass transition temperature a predictive, as they state, rather than a correlative theory (Dual Mode Sorption). This treatment incorporates the free energy of mixing as formulated in the Flory-Huggins theory. Key point of their theoretical treatment is the depression of the glass transition temperature when penetrant molecules are sorbed into the polymer matrix (see chapter 7). Here, two different mathematical descriptions can be found.

- First a linear relation, which relates the glass transition temperature of the polymer-penetrant system  $T_{\text{gm}}$  linearly to the weight fraction  $\omega_1$  of the sorbed penetrant, obeying equation (19)

$$T_{\text{gm}} = T_{\text{go}} - A \omega_1 \quad (19)$$

$A$  is an empirical plasticization constant (hence not predictive as claimed) depending on the nature of the polymer-penetrant system [44] and  $T_{\text{go}}$  is the glass transition temperature of the pure polymer. The constant  $A$  may be determined experimentally as described in chapter 7.

- Secondly, an equation developed by Chow [45] which is actually predictive

$$\ln\left(\frac{T_{\text{gm}}}{T_{\text{go}}}\right) = \beta \left[ (1-\theta) \ln(1-\theta) + \theta \ln\theta \right] \quad (20)$$

with

$$\beta = \frac{z R}{M_p \Delta c_p} \quad (21)$$

and

$$\theta = \frac{M_p \omega_1}{z M_1 (1 - \omega_1)} \quad (22)$$

$M_p$  is the molecular weight of the polymer repeating unit,  $\Delta c_p$  the jump in the heat capacity at  $T_g$  and  $z$  is the lattice coordination number. Equation (23) shows the final equation relating the applied pressure  $p$  to the penetrant volume fraction  $\phi_1$  in the polymer matrix.

$$\frac{p}{p^0} = \phi_1 \exp \left\{ (1 - \phi_1) + \chi (1 - \phi_1)^2 \right\} \exp \{ F \} \quad (23)$$

with

$$F = \frac{M_1 \omega_2^2 \Delta c_p \frac{d T_{gm}}{d \omega_1}}{R T} \left( 1 - \frac{T}{T_{gm}} \right) \quad (24)$$

$p^0$  is the vapour pressure of the pure liquid penetrant,  $M_1$  the molecular weight of the penetrant,  $T$  the experimental temperature and  $\chi$  the Flory-Huggins interaction parameter. Vrentas *et al.* state that the interaction parameter  $\chi$  can be estimated using a solubility parameter approach. As can be seen from equation (24), the prediction of the isotherm depends on the relation chosen for the glass transition temperature depression. For low mass fractions equation (19) and (20) describing the concentration dependence of the  $T_g$  do not differ very much. However, at higher mass fractions differences are considerable.

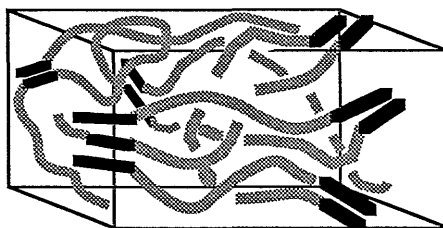


Figure 12. Schematic representation of semicrystalline polymers

Another model based on a Flory-Huggins approach has been developed by Bitter [46,47]. It is originally based on the physical picture of polymer chains which are aligned in crystalline or semi-crystalline regions and which leave this region into amorphous matter but finally aligning again in another crystalline region. Sorption only takes place in the amorphous phase, not in the crystalline regions. Polymer chains are stretched as penetrant molecules are sorbed into the amorphous phase and the resulting strain is included in the derivation of the entropy of mixing. Hence

crystallites act as local constraints fixing the chains in a three dimensional network. This model is schematically depicted in figure 12. A very similar model has been published later on [48] which also states that the concave curvature of the isotherms of polymeric glasses is due to the thermodynamics of solid deformation.

Following the lattice approach of Flory and Huggins and embodying the elastic strain induced by the penetrant, Bitter developed a final equation (25) in its most general form.

$$\ln a_i = \ln\left(\frac{Z_i}{Z_{av}} \phi_i\right) + 1 - \frac{V_i}{V_{av}} \frac{Z_i}{Z_{av}} \phi_s + \frac{V_i}{c_L} \phi_a^{2/3} + \frac{\Delta H_i^{\text{mix}}}{R T} \quad (25)$$

Here,  $Z_i$  is the coordination number of the pure component  $i$ ,  $Z_{av}$  the coordination number of the swollen polymer phase,  $V_i$  the partial molar volume of permeant  $i$ ,  $V_{av}$  the average partial molar volume of the permeant mixture,  $\phi_i$  the volume fraction of the component  $i$ ,  $\phi_s$  the total volume fraction of all dissolved components in the amorphous phase,  $\phi_a$  the volume fraction of amorphous polymer in the unswollen polymer phase,  $\Delta H_i^{\text{mix}}$  the partial molar enthalpy of mixing of the component  $i$  and  $c_L$  an elastic strain factor.  $c_L$  is related, for the sorption of a single component, to a number of characteristics of the topological model by equation (26)

$$c_L = 3 v f(s) \quad (26)$$

with

$$f(s) = \frac{L_{av} - s_0}{s_0} \frac{y}{y-1} \quad (27)$$

Here,  $L_{av}$  is the average chain length between two topological constraints,  $s_0$  the average distance between ends of an amorphous polymer chain in an unswollen polymer system,  $v$  the molar volume of a segment site and  $y$  the flexibility of a polymer segment in the unswollen state. Therefore,  $f(s)$  is purely a parameter describing the conformation of the polymer chain.

By making a number of assumptions, a mathematical relation giving the equilibrium concentration  $c_i$  sorbed in the polymer as a function of the applied fugacity  $f_i$  was developed shown as equation (28).

$$c_i = \frac{H_i^\infty f_i}{1 - \phi_s} \exp\{B_i \phi_i\} \quad (28)$$

$H_i^\infty$  is the Henry's law constant at infinitely low fugacity,  $\phi_s$  the sum of all penetrant volume fractions  $\phi_i$  of components  $i$ , and  $B_i$  a constant expressing the nonideal behaviour of the polymer-penetrant system. Since  $\phi_s$  is the sum over all penetrant volume fractions, equation (28) holds also for the sorption of mixtures. The expression for  $B_i$  is:

$$B_i = \left\{ \frac{V_i}{9v} \frac{2f(s) - 1}{f(s)^2} + 2 \frac{V_i}{RT} \delta_{ip}^2 + \frac{V_i}{V_{av}} \frac{Z_i}{Z_{av}} \right\} \quad (29)$$

$\delta_{ip}$  is a binary mixture parameter which approximates the partial molar heat of mixing  $\Delta H_i^{\text{mix}}$ . Bitter shows that equation (28) perfectly fits sorption isotherms of gases in glassy polymers with one fit parameter less than the Dual Mode Sorption model. Also the sorption behaviour of a gas mixture is well represented.

In its mathematical form equation (28) is very similar to the equation of the gas-polymer matrix model developed by Sefcik and Raucher [49]. In fact, fitting equation (28) or fitting equation (30) gives *nearly* the same solubility coefficients  $\sigma_0$  or Henry coefficient  $H_i^\infty$ , respectively.

$$c = \sigma_0 \exp(-\alpha c) p \quad (30)$$

However, this model is stated to be rather correlative and the link of model parameters to physical polymer properties remains difficult [50].

Two major drawbacks of the model of Bitter must be mentioned: first the difficulty to correlate physical polymer characteristics obtained from experiments to the model parameters and secondly, the assumption of crystallites in amorphous polymers although it is well known for a lot of polymers that they are amorphous in the sense that they do not show any distinct Bragg peaks in their wide angle X-ray diffraction (WAXD) pattern. Hence, Bitter argues that the local constraints do not have to be necessarily crystallites but may be semi-crystalline regions or regions of local order without *clarifying* this picture. Because experimental sorption and dilation data presented in chapter 4 are interpreted using Bitter's modified Flory Huggins model, it seems necessary to shed some light on technical terms like "regions of enhanced local order".

## 2.4. Structure of Amorphous Polymers

Polymers which are regarded as amorphous do not show any Bragg reflection peaks in their X-ray pattern and, furthermore, they do not show any first order melting transition. A pot of spaghetti in which entangled spaghetti strands build up a three dimensional random network is the most simple and popular picture about the bulk state of amorphous polymers [3,4,51]. In terms of physical pictures, two different approaches can be distinguished. Mark [52] and, later, Flory [53] proposed that bulk material which is homogeneous in structure consists of randomly coiled polymer chains (see figure 12). The conformation of a chain in the melt or in a glass are the same as that of an unperturbed polymer chain in solution. This model is supported by the experimental finding that the radii of gyration of a polymer chain is the same for the bulk as in a  $\theta$ -solvent [54].

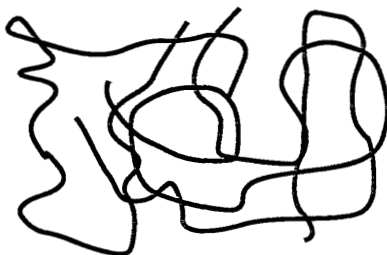


*Figure 12. Schematic representation of the random coil model*

The second group of models are so-called bundle models. The polymer matrix is considered as a continuous network of dimensionally small ordered regions showing strong, narrow distance correlations which are surrounded by disordered regions showing very broad distance correlations [55]. The development of this physical picture was basically initiated by the observations of nodular structures in homogeneous polymer films. Polymer films which showed "liquid-like" diffuse diffraction (X-ray or electron) patterns consisted of distinct domains of 30-100 Å diameter as indicated by transmission electron photomicrographs. Yeh suggested [56,57] that there exists within these domains local ordering or alignment of neighbouring segments and developed from these observations the folded-chain fringed-micellar grain model as schematically depicted in figure 13.

Hence the polymer consists of two phases: an ordered domain which is typically 30-100 Å in diameter and an intergrain region. The transition region from the ordered to non-ordered phase is the grain boundary. The intergrain region is a truly disordered state and might include chain ends, segments of polymer molecules going from one grain to another and also low molecular weight molecules. At this

point the similarity with the physical picture of Bitter on sorption in amorphous polymers must be pointed out.

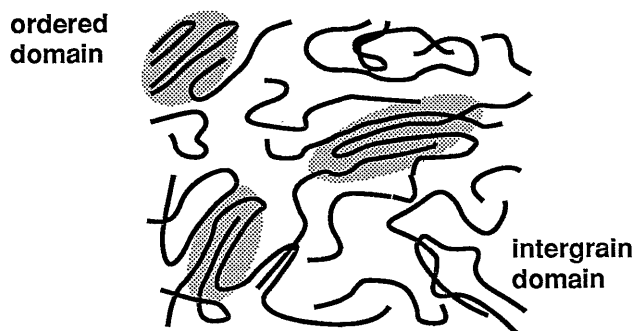


Figure 13. Schematic representation of the folded-chain fringed-micellar grain model

The existence of nodules in various amorphous polymers [58] like amorphous poly(ethylene terephthalate) [59], polycarbonate [60] and atactic polystyrene [61] is subject of much debate. Two symposia were dedicated to the order-disorder argument in amorphous polymer matter [62,63]. Here, even the question was risen whether these small nodules are not just simply artefacts. However, the existence of larger nodular structures, which are experimentally easier to determine due to their increased size, cannot be ignored. Neki and Geil present nodules of the size of 500 to 700 Å in diameter which have the appearance of aggregates of small nodules. These clusters of small nodules, so-called “super-nodules”, change their size and shape upon annealing. Large nodules are also reported by Kaempf [64] for drawn PET and Großknuth for poly(methyl methacrylate) [65]. Nodular structures in glassy polymers, prepared in a different way, will also be reported in chapter 7. For completeness two other models based on the idea of local ordering should be mentioned, first Pechhold’s meander model [66] and secondly the model of Privalko and Lipatov [67]. For an elaborated overview, the reader is referred to Sperling [68].

Especially wide angle x-ray diffraction and neutron scattering methods have been used to elucidate the existence of regions of local ordering. The results do not always clearly proof the existence of ordering. A number of recent publications on polycarbonates suggest that non-linear (banana-like) axially aligned chain segments build these regions of local ordering [69-72]. Molecular dynamics simulations on polycarbonate indicate that there exists some weak intermolecular preference for

distances of about 5 to 6 Å [73]. This may be an indication of the areas of enhanced order as found in the references cited above. Earlier X-ray diffraction experiments on poly(ethylene terephthalate) do not show any evidence of ordering beyond a distance of 4Å [74]. In chapter 6, however, molecular dynamics simulation results will be presented which compare well with the X-ray diffraction experiments but also show intermolecular order at a distance of around 9 Å.

### List of Symbols

$a_i$	activity of the component i [-]
$A$	empirical plasticization constant [K]
$A^*$	empirical diffusional constant [ $\text{cm}^2/\text{s}$ ]
$b$	Langmuir affinity factor [1/bar]
$B$	empirical constant [ $\text{cm}^3/\text{s}$ ]
$B_i$	non-ideality factor [-]
$c$	concentration [ $\text{cm}^3(\text{STP})/\text{cm}^3\text{polym.}$ ]
$c_{\text{sat}}$	saturation concentration [ $\text{cm}^3(\text{STP})/\text{cm}^3\text{polym.}$ ]
$c_H$	concentration of penetrant molecules sorbed in the Langmuir mode [ $\text{cm}^3(\text{STP})/\text{cm}^3\text{polym.}$ ]
$c_H'$	Langmuir capacity factor [ $\text{cm}^3(\text{STP})/\text{cm}^3\text{polym.}$ ]
(C.E.D.)	volumetric cohesive energy density [ $\text{J}/(\text{m}^3 \text{K})$ ] in equation (6): molar (C.E.D.) [ $\text{cal}/(\text{mol K})$ ]
$c_L$	elastic strain factor [ $\text{cm}^3/\text{mol}$ ]
$d$	distance between reflection planes [m]
$D$	diffusivity [ $\text{cm}^2/\text{s}$ ]
$D_0$	diffusion coefficient at infinite temperature [ $\text{cm}^2/\text{s}$ ]
$D_D$	diffusion coefficient in the Henry mode [ $\text{cm}^2/\text{s}$ ]
$D_H$	diffusion coefficient in the Langmuir mode [ $\text{cm}^2/\text{s}$ ]
$E_D$	activation energy of diffusion [ $\text{J}/\text{mol}$ ]
$f_i$	fugacity of the component i [bar]
$f(s)$	chain flexibility factor [-]
$H_1^\infty$	Henry's constant at infinite small fugacity [ $\text{cm}^3(\text{STP})/(\text{cm}^3\text{polym. bar})$ ]
$k_D$	Henry's law constant [ $\text{cm}^3(\text{STP})/(\text{cm}^3\text{polym. bar})$ ]
$M_p$	molecular weight of the polymer repeating unit [g/mol]
$M_1$	molecular weight of the penetrant molecule [g/mol]
$n$	order of reflection
$N_A$	Avogadro's constant [1/mol]
$p$	pressure [bar]
$p^0$	saturation pressure [bar]



---

P	permeability [ $\text{cm}^3(\text{STP}) \text{ cm} / (\text{cm}^2 \text{ s cmHg})$ ]
R	universal gas constant [ $\text{J}/(\text{mol K})$ ]
S	solubility [ $\text{cm}^3(\text{STP})/(\text{cm}^3 \text{ polym. cmHg})$ ]
$T_g$	glass transition temperature [K]
$T_{g0}$	glass transition temperature of the penetrant free polymer [K]
$T_{gm}$	glass transition temperature of the penetrant/polymer system [K]
$v$	specific volume of the polymer [ $\text{g}/\text{cm}^3$ ]
$v$	molar volume of a segment site [ $\text{cm}^3/\text{mol}$ ]
$v_0$	specific occupied volume of the polymer chains constants [ $\text{g}/\text{cm}^3$ ]
$V_{av}$	average partial molar volume averaged over all components $i$ [ $\text{cm}^3/\text{mol}$ ]
$V_{FH2}$	average hole free-volume [ $\text{cm}^3/\text{g}$ ]
$V_h$	molar volume of holes [ $\text{cm}^3/\text{mol}$ ]
$V_i$	partial molar volume of the component $i$ [ $\text{cm}^3/\text{mol}$ ]
$V_0$	molar hard core volume of polymer segment [ $\text{cm}^3/\text{mol}$ ]
$V_2^*$	specific critical hole free-volume for a jump [ $\text{cm}^3/\text{g}$ ]
$z$	coordination number
$Z_{av}$	average coordination number of the swollen polymer phase [-]
$Z_i$	lattice coordination number for the component $i$ [-]
$\alpha$	plasticization parameter [ $\text{cm}^3 \text{ polym.}/\text{cm}^3(\text{STP})$ ]
$\Delta c_p$	molar heat capacity jump at the glass transition temperature [ $\text{cal}/(\text{molK})$ ]
$\Delta H_i^{\text{mix}}$	partial molar enthalpy of mixing [ $\text{J}/\text{mol}$ ]
$\delta_{ip}$	binary mixture solubility parameter [ $(\text{J}/\text{mol})^{1/2}$ ]
$\epsilon_h$	hole formation energy [ $\text{J}/\text{mol}$ ]
$\phi_a$	volume fraction amorphous polymer phase [-]
$\phi_i$	volume fraction of the component $i$ sorbed in the polymer [-]
$\phi_1$	volume fraction penetrant [-]
$\phi_s$	sum of all volume fraction $\phi_i$ [-]
$\phi_p$	volume fraction polymer [-]
$\gamma$	overlap factor
$\lambda$	diffusional jump length [m]
$\lambda_{\text{aff}}$	Langmuir affinity factor [1/bar]
$\lambda^*$	wavelength of the X-rays [m]
$\rho(\lambda_{\text{aff}})$	distribution function for the Langmuir affinity function
$\chi$	Flory-Huggins interaction parameter [-]
$\xi$	ratio of the critical molar volume of a solvent jumping unit over the critical molar volume of the polymer jumping unit [-]
$\sigma^2$	penetrant cross section [ $\text{m}^2$ ]

---

$\sigma_0$	solubility coefficient [ $\text{cm}^3(\text{STP})/(\text{cm}^3\text{polym. bar})$ ]
$\theta$	scattering angle [-]
$\omega_1$	weight fraction of the penetrant [-]

## References

- (1) W.J. Koros, M.W. Hellums, Transport Properties, in: Encyclopedia of Polymer Science and Engineering, Supplement, J.Wiley & Sons, 1989
- (2) H.L. Frisch, S.A. Stern, Diffusion of Small Molecules in Polymers, CRC Critical Reviews in Solid State and Materials Science, 11(2) (1983) 123
- (3) E. Smit, Modelling of the diffusion of gases through membranes of novel polyimides, Ph.D. Thesis, 1991, Enschede/The Netherlands
- (4) E. Hensema, Polyoxadiazoles and polytriazoles gas separation membranes, Ph.D. Thesis 1991, Enschede/The Netherlands
- (5) P. Meares, The diffusion of gases through polyvinyl acetate, J.Am.Chem.Soc. 76 (1954) 3415
- (6) W.W. Brandt, Model calculation of the temperature dependence of small molecule diffusion in high polymers, J.Phys.Chem., 63 (1959) 1080
- (7) A.T. DiBenedetto, Molecular properties of amorphous high polymers, 1. A cell theory for amorphous high polymers, J.Polym.Sci. A, 1 (1963) 3459
- (8) R.J. Pace, A. Dadyner, Statistical mechanical model for diffusion of simple penetrants in polymers, J.Polym.Sci., Polym.Phys., 17 (1979) 437,453,465
- (9) M.H. Cohen, D. Turnbull, Free-volume model of the amorphous glass transition, J.Chem.Phys., 31 (1959) 1164
- (10) H. Fujita, Organic vapors above the glass transition temperature, in: Diffusion in Polymers, J. Crank and G.S. Park, Acad. Press, NY, 1968
- (11) W.M. Lee, Selection of barrier materials from molecular structure, Polym.Eng.Sci., 20 (1980) 65
- (12) J.S. Vrentas, J.L. Duda, Diffusion in polymer-solvent systems, 1. Reexamination of the free-volume theory, J.Polym.Sci. Polym.Phys., 15 (1977) 403
- (13) I. Blume, E. Smit, M.Wessling, C.A. Smolders, Diffusion in glassy and rubbery polymers, Makromol. Chem., Macromol. Symp., 45 (1991) 237-257
- (14) F.R. Sheu, R.T. Chern, Effects of packing density on the gas transport properties of poly(phenolphthalein phthalate), J.Polym.Sci. Polym. Phys., 27 (1989) 1121
- (15) G.F. Sykes, A.K. St.Clair, The effect of molecular structure on the gas transmission rates of aromatic polyimides, J.Appl.Polym.Sci., 32 (1986) 3725

- 
- (16) K.I. Okamoto, K. Tanaka, H. Kita, M. Ishida, M. Kakimoto, Y. Imai, Gas permeability and permselectivity of polyimides prepared from 4,4'-diaminotriphenylamine, *Polymer J.*, 24 (1992) 451
- (17) C.J. Lee, Correlation of elastic modulus, cohesive energy density and heat capacity jump of glassy polymers, *Polym.Eng.Sci.*, 27(13) (1987) 1015
- (18) E.R. Hensema, M.H.V. Mulder, C.A. Smolders, On the mechanism of gas transport in rigid polymer membranes, submitted to *J.Appl.Polym.Sci.*
- (19) B. Wunderlich, Study of the change in specific heat of monomeric and polymeric glasses during the glass transition, *J.Phys.Chem.*, 64 (1960) 1052
- (20) N. Hirai, H.Eyring, Bulk viscosity of polymeric systems, *J.Polym.Sci.*, 37 (1959) 51
- (21) W. Wrasidlo, Thermal analysis of polymers, *Adv.Polym.Sci.*, 13 (1974) 3
- (22) W.F. van Gunsteren, H.J.C. Berendsen, Groningen Molecular Simulation Library, 1987
- (23) E. Smit, M.H.V. Mulder, C.A. Smolders, H. Karrenbeld, J. van Eerden, D. Feil, Modelling of the diffusion of carbon dioxide in polyimide matrices by computer simulation, *J.Membrane Sci.*, 73 (1992) 247
- (24) W.R. Vieth, H.H. Alcalay, A.J. Frabetti, Solution of gases in oriented poly(ethylene terephthalate), *J.Appl.Polym.Sci.*, 8 (1964) 2125
- (25) G.R. Mauze, S.A. Stern, The dual mode solution of vinyl chloride monomer in poly(vinyl chloride), *J.Membrane Sci.*, 18 (1984) 99
- (26) Y. Kamiya, D. Bourbon, K. Mizoguchi, Y. Naito, Sorption, dilation and isothermal glass transition of poly(ethyl methacrylate)-organic gas systems, *Polymer J.*, 24 (1992) 443
- (27) A.R. Berens, G.S. Huvar, Interaction of polymers with near-critical carbon dioxide, ACS Symp. Ser. 406, *Supercritical Fluid Science and Technology* (Ed. K.P. Johnston, J.M.L. Penninger)
- (28) A.J. Kovacs, La contraction isotherme du volume des polymeres amorphes, *J.Polym.Sci.*, 30 (1958) 131
- (29) W.J. Koros, D.R. Paul, A. Rocha., Carbon dioxide sorption and transport in polycarbonate, *J.Polym.Sci., Polym.Phys.*, 14 (1976) 687
- (30) J.H. Petropoulos, Quantitative analysis of gaseous diffusion in glassy polymers, *J.Polym.Sci., Polym.Phys.*, 8 (1970) 1797
- (31) W.J. Koros, D.R. Paul, Effect of partially immobilizing sorption on permeability and the diffusion time lag, *J.Polym.Sci., Polym.Phys.*, 14 (1976) 675-685
- (32) M.W. Hellums, W.J. Koros, G.R. Husk, D.R. Paul, Fluorinated polycarbonates for gas separation applications, *J. Membrane Sci.*, 46 (1989) 93
- (33) J.R. Fritzpatrick, B. Ellis, X-Ray diffraction studies of the structure of amorphous polymers, in: R.N. Haward, *The physics of glassy polymers*, Applied Science Publ., London, 1973
-

- (34) W.J. Koros, D.R. Paul, CO<sub>2</sub> sorption in poly(ethylene terephthalate) above and below the glass transition temperature, *J.Polym.Sci., Polym.Phys.*, 16 (1978) 1947-1963
- (35) W.J. Koros, D.R. Paul, Observations concerning the temperature dependence of the Langmuir sorption capacity of glassy polymers, *J.Polym.Sci., Polym.Phys.*, 19 (1981) 1655
- (36) G.K. Fleming, W.J. Koros, Dilation of polymers by sorption of carbon dioxide at elevated pressures, 1. silicone rubber and unconditioned polycarbonate, *Macromolecules* 19 (1986) 2285
- (37) G.K. Fleming, W.J. Koros, Dilation of substituted polycarbonates caused by high pressure carbon dioxide sorption, *J.Polym.Sci., Polym. Phys.*, 28 (1990) 1137-1152
- (38) Y. Kamiya, T. Hirose, K. Mizoguchi, K. Terada, Sorptive dilation of poly (vinyl benzoate) and poly(vinyl butyral) by carbon dioxide, *J.Polym. Sci. Polym. Phys.*, 26 (1988) 1409 - 1424
- (39) H. Funke, Sorption von Reingasen in Polymeren und an Zeolithen bei Drücken bis 70 bar, Ph.D. Thesis, 1991, University of Heidelberg, Germany
- (40) D. Bourbon, Y. Kamiya, K. Mizoguchi, Sorption and dilation properties of poly(p-phenylene sulfide) under high pressure carbon dioxide, *J.Polym. Sci., Polym.Phys.*, 28 (1990) 2057-2069
- (41) G.H. Weiss, J.T. Bender, M.F. Shlesinger, Continuous-site model for Langmuir gas sorption in glassy polymers, *Macromolecules* 25 (1992) 990
- (42) J.S. Vrentas, C.M. Vrentas, Sorption in glassy polymers , *Macromolecules* 24 (1991) 2404
- (43) J.S. Vrentas, C.M. Vrentas, Isotherm Shape for penetrant sorption in glassy polymers, *J.Appl.Polym.Sci.*, 45 (1992) 1497
- (44) H. Hachisuka, T. Sato, T. Imai , J. Tsujita, A. Takizawa, T. Kinoshita, Glass transition temperature of glassy polymers plasticized by CO<sub>2</sub> gas, *Polymer J.*, 22 (1990) 77
- (45) T.S. Chow, Molecular interpretation of the glass transition temperature of polymer-diluent systems, *Macromolecules* 13 (1980) 362
- (46) J.G.A. Bitter, Effect of crystallinity and swelling on the permeability and selectivity of polymer membranes, *Desalination* 51 (1984) 19
- (47) J.G.A. Bitter, Transport mechanisms in membrane separation processes, Plenum Press, New York 1991
- (48) G.G. Lipsomb, Unified thermodynamic analysis of sorption in rubbery and glassy materials, *AIChE Journal*, 36 (1990) 1505
- (49) D. Raucher, M. Sefcik, Sorption and transport in glassy polymers (gas-polymer-matrix model), in: *Industrial Gas Separation, ACS Symp. Ser. 223* (1983) 111
- (50) T.A. Barbari, W.J. Koros, D.R. Paul, Gas sorption in polymers based on Bisphenol-A, *J.Polym. Sci. Polym. Phys.*, 26 (1988) 729

- 
- (51) E.A. DiMarzio, J.H. Gibbs, Chain stiffness and the lattice theory of polymer phases, *J.Chem.Phys.*, 28 (1958) 807
  - (52) E. Guth, H. Mark, Viscosity of solutions, *Monatsh. Chem.* 65 (1934) 93
  - (53) P.J. Flory, *Principles of Polymer Chemistry*, Cornell University Press, Ithaca, NY, 1953
  - (54) J.S. Higgins, R.S. Stein, Recent developments in polymer applications of small-angle neutron, X-ray and light scattering, *J.Appl. Cryst.* 11 (1978) 346
  - (55) I. Voigt-Martin, J. Wendorff, Amorphous polymers, in: *Encyclopedia of Polymer Science and Engineering*, Vol 1., J. Wiley & Sons, 1985
  - (56) G.S.Y. Yeh, A structural model for the amorphous state of polymers: folded- chain fringed-micellar grain model, *J.Macromol. Sci.-Phys.*, B6 (1972) 451
  - (57) G.S.Y. Yeh, Morphology of amorphous polymers, *Crit.Rev.Macromol.Sci.* 1 (1972) 173
  - (58) P.H. Geil, Morphology of amorphous polymers, *Ind.Eng.Chem., Prod.Res.Dev.*, 14 (1975) 59
  - (59) G.S.Y. Yeh, Crystallization of PET from the glassy amorphous state, *J.Macromol. Sci.-Phys.*, B1(2) (1967) 235
  - (60) K. Neki, P.H. Geil, Morphology-property studies of amorphous Polycarbonate, *J. Macromol. Sci.-Phys.*, B(8) 1-2 (1973) 295
  - (61) G.S.Y. Yeh, Order in amorphous polystyrenes as revealed by electron diffraction and diffraction microscopy, *J.Macromol.Sci.-Phys*, B(6) 3 (1972) 451
  - (62) Symposium on "Physical structure of the amorphous state", *J.Macromol. Sci.,-Phys.*, B(12) (1976)
  - (63) "Organisation of macromolecules in the condensed phase", *Faraday Discuss. Chem.Soc.*, 68 (1979) 26
  - (64) G. Kaempf, H. Orth, Regularly arranged superstructures in stretched high polymers, *J. Macromol. Sci.-Phys.*, B11(2) (1975) 151
  - (65) K.P. Großkurth, Netzwerkstrukturen in Polymethylmethacrylat, *Prog. Coll.& Polym. Sci.*, 66 (1979) 281
  - (66) W. Pechhold, M.E.T. Hauber, E. Liska, The meander model of condensed polymers, *Kolloid Z.Z. Polym.*, 251 (1973) 818
  - (67) V.P. Privalko, Y.S. Lipatov, Entanglement concept and chain conformations in bulk amorphous polymers, *Makromol. Chem.*, 175 (1972) 641
  - (68) L.H. Sperling, *Physical Polymer Science*, J. Wiley & Sons 1992
  - (69) G.R. Mitchell, A.H. Windle, The effect of annealing on the local structure of glassy polycarbonate, *Coll.&Polym.Sci.*, 263 (1985) 263
  - (70) H.R. Schubach, B. Heise, Structure and anisotropy in polycarbonate. I. Short range order of amorphous polycarbonate revealed by WAXS, *Coll.&Polym.Sci.*, 264 (1986) 335
-

- (71) M. Pietralla, H.R. Schubach, M. Dettenmeier, B. Heise, Structure and anisotropy in PC, II. WAXS, anisotropic heat conduction and birefringence in oriented samples, *Prog. Coll. & Polym. Sci.*, 71 (1985) 125
- (72) L. Cervinka, E.W. Fischer, K. Hahn, B.-Z. Jiang, G.P. Helman, K.-J. Kuhn, On the intermolecular order in amorphous polycarbonate. Neutron scattering results and model calculations, *Polymer* 28 (1987) 1287
- (73) M. Hutnik, F.T. Gentile, P.J. Ludovice, U.W. Suter, A.S. Argon, An atomistic model of amorphous glassy polycarbonate of 4,4'-Isopropylidenediphenol, *Macromolecules* 24 (1991) 5962
- (74) G.W. Longman, R.P. Sheldon, G.D. Wignall, Investigation of short range ordering in polymers by means of radial distribution functions derived from X-ray diffraction, *J. Mat. Sci.*, 11 (1976) 1339

## Chapter 3

### Experimental Methods Permeation, Sorption and Dilution

#### 3.1. Introduction

Understanding the mass transport behaviour of polymeric membranes requires an experimental investigation of the transport characteristics, *i.e.*, permeability, diffusivity and solubility. These characteristics are related to each other obeying equation (1).

$$P = D * S \quad (1)$$

Often, two of these parameters are determined experimentally and the third one is calculated from equation (1). The permeability, diffusivity and solubility are in the most ideal case of a polymer/penetrant system, *i.e.*, an inert gas in a rubbery polymer, independent of the amount of the penetrant present in the matrix and furthermore constant in time. However, in most other cases, concentration and time dependence cannot be neglected.

In this chapter, experimental methods to determine these concentration and time dependences will be described. First, the polymers used for these experiments, their chemical synthesis and physical properties will be described. The following parts will concentrate on the experimental methods which determine the polymer properties permeability, diffusivity and solubility. In a last part a new technique investigating the volume increase of the polymer due to mass uptake will be discussed extensively. The description of these experimental techniques is rather detailed because the number of publications in this field is tremendously high and a precise description of similarities and differences in experimental procedures seems necessary to be able to compare results presented in this thesis with already published ones.

### 3.2. Polymer Synthesis and Characterization

For the investigation of the influence of the chemical structure of the polymer on its mass transport properties, especially on sorption and dilation, a number of polyimides based on the dianhydride 6FDA [4,4'-(2,2,2-trifluoro methyl)ethylidene]-bis[1,3-isobenzofuran-dione]) were prepared by reacting the dianhydride with a diamine. Detailed information about reaction conditions and yields can be found in [1,2]. For clarity, the reaction shown in figure 1 is an example for the synthesis route of 6FDA with the para isomer of phenylenediamine 4PDA. In the first step of a two step reaction a poly(amic acid) is formed by a polycondensation reaction.

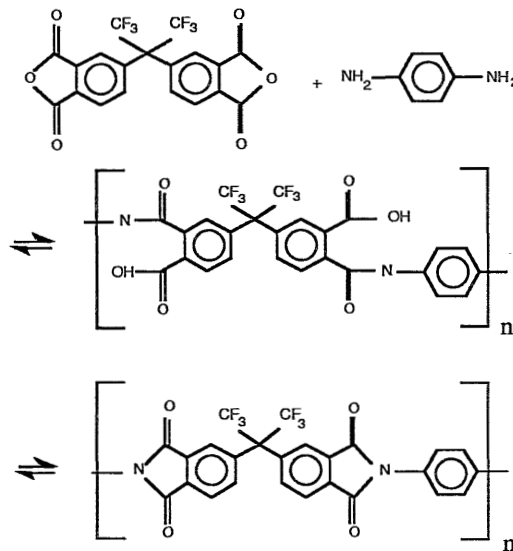


Figure 1. Reaction scheme for the synthesis of 6FDA-4PDA polyimide

In a second step, the imidization reaction, a chemical ring closure reaction is performed by using a mixture of acetic anhydride and a tertiary amine-base like pyridine. The polymers synthesized are listed in figure 2. The calorimetric data like glass transition temperature  $T_g$  and the jump in heat capacity  $\Delta c_p$  at  $T_g$  were obtained by DSC measurements performed on a Perkin Elmer DSC-4 calorimeter at heating rates of 20°C/minute. Densities of the polymers were measured with a set-up which is described by Park [3]. Here, basically, the weight of a polymer sample is measured in air and in a liquid (water or iso-octane) and the difference of the two weights is an accurate measure for the density of the polymer. The data for the glass transition temperature and densities listed in figure 2 agree well with the data reported in [2,4]. Differences for  $\Delta c_p$  are certainly caused by different film histories.



Polymer Structure	Name	$T_g$ [°C]	$\Delta c_p E2$ [cal/(gK)]	density [g/ml]	free volume $v_f$ [cm <sup>3</sup> /g]
	6FDA-4PDA	364	5.76	1.481	0.099
	6FDA-3PDA	313	3.10	1.467	0.105
	6FDA-3/4PDA(1:1)	324	4.04	1.477	0.101
	6FDA-NDA	417	5.54	1.379	0.139
	6FDA-DAF	401	3.55	1.492	0.09
	6FDA-MDA	330	6.99	1.382	0.114
	6FDA-44ODA	289	3.86	1.424	0.106
	6FDA-34ODA	267	3.37	1.413	0.111
	6FDA-SDA	302	3.84	1.422	0.109

Figure 2. Structures and physical properties of polyimides synthesized

Polymer films were prepared by casting a 10-15 wt% solution of the polyimide in DMAc on a glass plate which was dried for two days under a stream of nitrogen. The films were released from the glass plate by immersion in a water bath. Samples were then dried for at least 2 weeks in a vacuum oven at 150°C to remove the residual solvent. No residual solvent could be found in the IR-spectra. Often a heating step above the glass transition temperature is considered as a means to remove those solvent molecules which cannot be detected by infrared spectroscopy. However, this procedure was not applied to the samples because this heat treatment often transforms samples with smooth surfaces and geometry into “wavy” samples. Dilation experiments with such a distorted sample would be difficult. Therefore, in order to maintain a drying procedure which is the same for the sorption samples as for the dilation samples, all samples were prepared as described above.

### 3.3. Permeation

The experimental method determining the permeability of a polymer is based on the principle that molecules permeating through a polymer film from the high pressure, upstream side of a membrane into an evacuated constant volume on the low pressure, downstream side will lead to an increase of pressure in this constant volume. The experimental principle (a) together with a schematic illustration of experimental signals from the pressure transducers (b) are shown in figure 3.

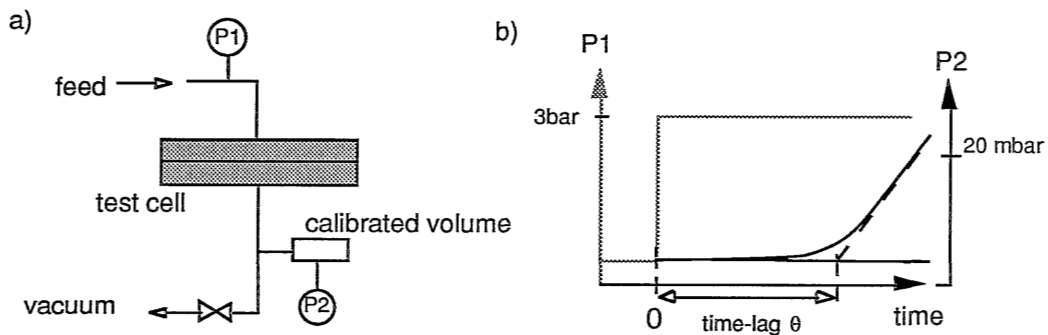


Figure 3. Permeability and time-lag measurement apparatus (a); typical signals obtained from the pressure transducers during an experiment (b)

For times smaller than  $t=\theta$ , the whole system is evacuated so that no penetrant molecules remain in the membrane. Starting at  $t=0$  with an upstream pressure  $p_1$ , i.e.,  $p_1 = 3$  bar in figure 3, and vacuum on the downstream side, the total amount permeated through the membrane into the calibrated volume changes in time from

a non-linear increase in the transient state into a linear increase in the steady state when an equilibrium concentration profile in the membrane is reached. From the slope of this steady state pressure increase  $\Delta p_2/\Delta t$ , one can calculate the permeability of a penetrant through a polymeric membrane according to equation (2)

$$P = \frac{\Delta p_2}{\Delta t (p_1 - p_2)} \frac{V_c L}{R T A} * 22400 \quad (2)$$

where  $V_c$  is the calibrated volume,  $R$  the universal gas constant,  $T$  the experimental temperature,  $L$  the membrane thickness,  $A$  the membrane surface area and  $(p_1 - p_2)$  the pressure difference over the membrane. Since  $p_2$  does hardly change with respect to  $p_1$ , the driving force  $(p_1 - p_2)$  can be assumed to be equal to  $p_1$ . The permeability of a polymer is given in the unit Barrer throughout this thesis.

$$1 \text{ Barrer} = 10^{-10} \frac{\text{cm}^3 (\text{STP}) \text{ cm}}{\text{cm}^2 \text{ s cmHg}} \quad (3)$$

The intersection of the extrapolation of the steady-state flux with the x-axis is the so-called time-lag  $\theta$ . In order to obtain reliable data for the time-lag, the evacuation time for the whole membrane must be sufficiently long so that all penetrant molecules have been removed and no concentration profile remains in the membrane. The time-lag is correlated with the diffusion coefficient for ideal Fickian, hence concentration independent, diffusion by equation (4) [5].

$$D = \frac{L^2}{6 \theta} \quad (4)$$

However, in the case of significant polymer swelling induced by the penetrant molecules, diffusion coefficients become concentration dependent and the mathematical relation between diffusion coefficient and driving force appears to be more complex. But still, because of its simplicity, equation (4) is often used in order to *estimate* diffusion coefficients [2,6].

$$\theta(c) = \frac{L^2 \int_0^c w D(w) \left[ \int_w^c D(u) du \right] dw}{\left[ \int_0^c D(u) du \right]^3} \quad (5)$$

A more complex relation (equation (5)) for the concentration dependent time-lag has

been developed by Frisch [7]. To solve this integral, a relation for the concentration dependent diffusion coefficient must be assumed. Often, empirical relations used are linear in  $c$  according to equation (6)

$$D = D_0(1 + \beta c) \quad (6)$$

or exponential in  $c$  according to equation (7).

$$D = D_0 \exp\{\beta c\} \quad (7)$$

Here  $D_0$  is the diffusion coefficient at zero concentration and  $\beta$  is a factor called the plasticization factor. Integration of equation (5) with equation (6) results in

$$\theta(c) = \frac{L^2 \left[ \frac{1}{15} \beta^2 c^2 + \frac{5}{24} \beta c + \frac{1}{6} \right]}{D_0 \left[ \frac{1}{8} \beta^3 c^3 + \frac{3}{4} \beta^2 c^2 + \frac{3}{2} \beta c + 1 \right]} \quad (8)$$

This equation will be used later in paragraph 3.5. to evaluate time-lag experiments carried out at different upstream pressures, hence different concentrations.

### *High pressure permeation*

Permeation and time-lag experiments described until now have been determined at low upstream pressures. For highly sorbing gas at high pressures ( $p > 15$  bar) the time-lag is a meaningless parameter. At high penetrant concentrations the permeability of glassy polymers becomes time-dependent while the sorption remains constant. Slow relaxation processes in the polymer matrix cause slow changes in the transport behaviour of the membrane. A special set-up, shown in figure 4, was designed to investigate this time dependent permeation behaviour.

The set-up consists of two permeation cells and the experimental technique used is based on the same principle as shown in figure 3. The measurement volume  $V_m$  was calibrated using a standard polymer film obtained from the National Bureau of Standards/CO, U.S.A.. In the case of gas mixtures as a feed, the composition of the feed and permeate can be analysed using gas chromatography. Figure 5 shows a hypothetical time-dependent increase of the permeability over a certain time period. The permeability at time  $t$  is determined by measuring the permeability for a time period ( $< 5$  minutes) which is negligibly small with respect to the total experimentation time. Since experiments may last longer than a whole day, the experimental set-up was automated by a Programming Logic Control Unit (PLC).

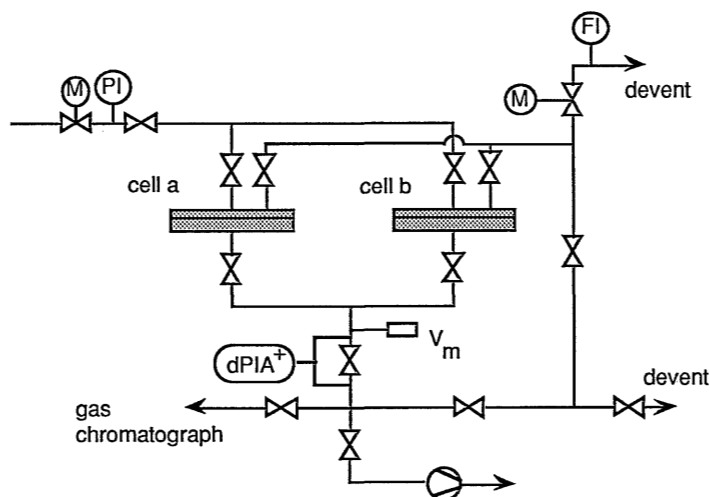


Figure 4. Automated permeation set-up for high pressure permeation

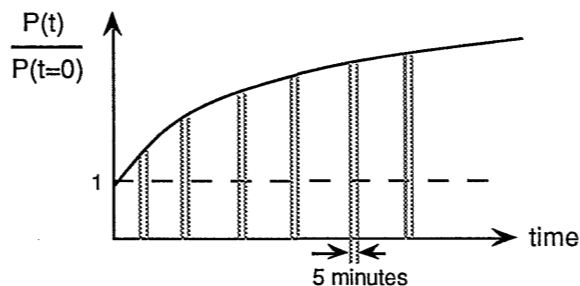


Figure 5. Hypothetical time dependent permeation behaviour of a glassy polymer at elevated pressures

### 3.4. Sorption

In the introduction to this chapter the permeability has been introduced as the product of diffusivity and solubility. The solubility of a penetrant in a polymer is characterized by its sorption isotherm, which relates the equilibrium concentration in the polymeric matrix to the applied activity or pressure. Measurements of the gas solubility can be performed by gravimetric methods using a microbalance [8,9], a quartz spring [10] or by pressure decay methods. Since the gravimetric methods have uncertainties due to buoyancy problems and thermally induced convective

flows, a pressure decay method was chosen. Here, single volume and dual-volume types can be distinguished [11] as shown in figure 6. In a closed, constant volume containing a polymer sample and a gas, the pressure decreases in time due to the sorption of the gas into the polymer. The equilibrium concentration at a certain pressure starting with a polymer with no sorbed penetrant can be simply calculated using the ideal gas law according to equation (9).

$$c = \frac{\Delta p (V_c - V_p)}{RT V_p} \quad (9)$$

$V_c$  is the cell volume,  $V_p$  is the polymer volume and  $\Delta p$  the final pressure decay. The single volume set-up has the disadvantage that the mass uptake occurring during the inlet of the gas must be extrapolated from the measured signal after closing the inlet valve. This disadvantage is overcome by the dual-volume set-up. Here, the total amount of gas in the closed dual-volume system is exactly known on forehand because the system itself is completely closed. This set-up accurately measures the *equilibrium* sorption value. However, for both set-ups the pressure decay is of considerable value and the calculation of diffusion coefficients of the pressure decay signal in time is not straightforward because a decreasing pressure represents a time-dependent boundary condition in the mathematical description of the mass transport [12].

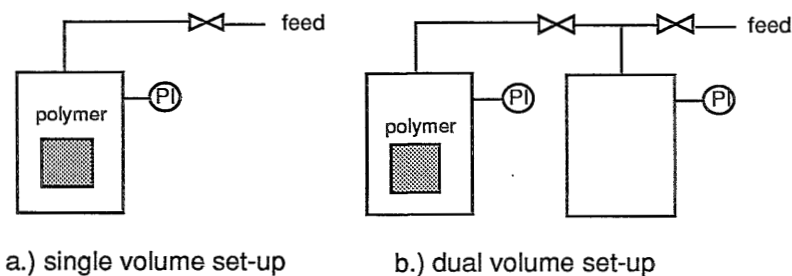


Figure 6. Pressure decay sorption set-ups; (a) single volume and (b) dual volume set-up

In this work a set-up was assembled that actually is an intermediate between a single and a dual volume pressure decay method. A schematic picture is shown in figure 7. The set-up consists of two cells of which one contains the polymer sample and the second one is an empty reference cell. Both cells are placed in a thermostated liquid bath. Additionally, the whole set-up is placed in a thermostated air bath having the same temperature as the liquid bath. The pressure decay is measured as a

minute pressure *difference* decay between the cells. The final pressure decay in a sorption experiment is small compared to the total pressure in the system so that the problem of time dependent boundary conditions can be assumed to be negligible.

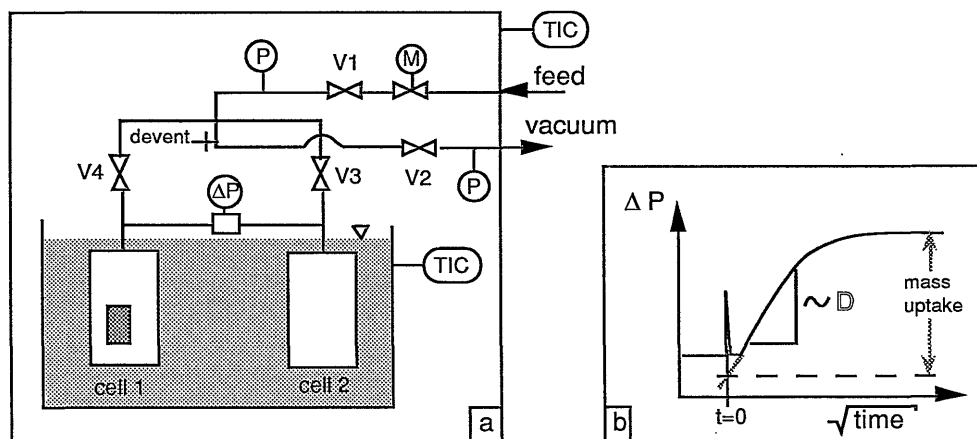


Figure 7. Pressure difference decay sorption set-up (a) and a schematic picture showing a typical signal from the pressure difference transducer (b)

Sorption isotherms were obtained by the following experimental procedure: the cells were evacuated for at least 10 hours and then suddenly pressurized to the pressure  $p$  by opening valves 3 and 4 together (pressure difference peak in figure 7b). After a very short time (around 5 s) valves 3 and 4 were closed again and the pressure decrease in the sample cell compared to the reference cell could be observed due to the sorption of penetrant molecules into the polymer film until equilibrium was reached. Additional pressurization was used to obtain higher sorption values. During the time when valves 3 and 4 were open sorption has already occurred as described for the single volume pressure decay method. This missing initial sorption was later calculated by extrapolating the recorder plot to the time  $t=0$ . Extrapolation was carried out by fitting the data from the recorder plot, after transforming the time axis into a square-root-of-time axis, to a straight line. The reason for this type of extrapolation is related to the mass transport itself which is mathematically characterized by equation (10).

From the pressure change in time an effective diffusion coefficient can be calculated from the slope of the relative mass uptake versus the square root of time [5]

$$\frac{M_t}{M_\infty} = \frac{4}{\sqrt{\pi}} \sqrt{\frac{Dt}{L^2}} \quad (10)$$

where  $M_t$  is the mass uptake at time  $t$ ,  $M_\infty$  the mass uptake at infinite time,  $D$  the diffusion coefficient and  $L$  the membrane thickness. The diffusion coefficient obtained is an effective diffusion coefficient within the concentration range corresponding to the pressure range of the previous sorption run and the actual one. Figure 9 shows the sorption kinetics and figure 10 the calculated concentration dependent diffusion coefficients for the system  $\text{CO}_2/\text{PIXU 218}$  at room temperature. It can be seen clearly that the diffusion coefficient of  $\text{CO}_2$  is strongly dependent on its concentration in the matrix. The resulting sorption isotherm which actually shows the well known concave shape [13] for glassy polymers is shown in figure 11.

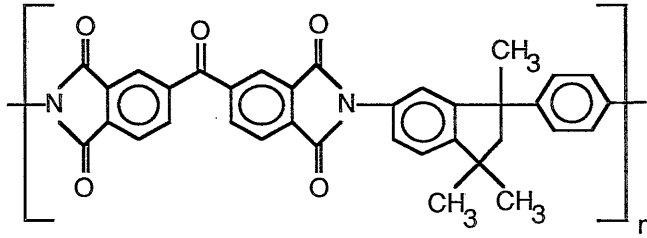


Figure 8. Chemical structure of the polyimide PIXU 218 from Ciba Geigy

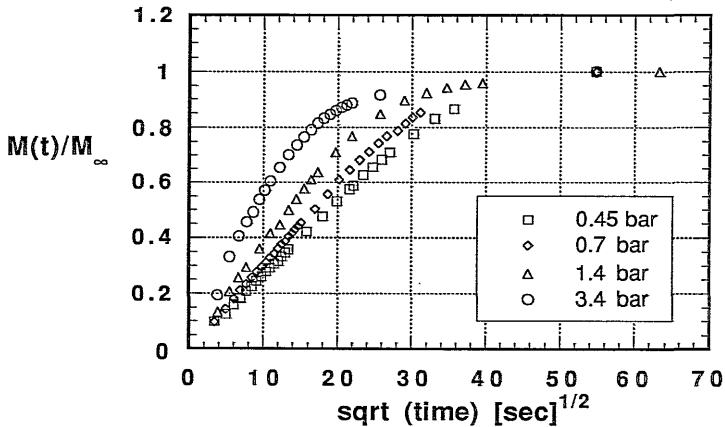


Figure 9. Sorption kinetics for the sorption of  $\text{CO}_2$  in PIXU 218 at  $T=25^\circ\text{C}$ ; sorption kinetics is measured starting from the equilibrium value, for instance  $p=0.7$  bar, to the next higher pressure ( $p=1.4$  bar)



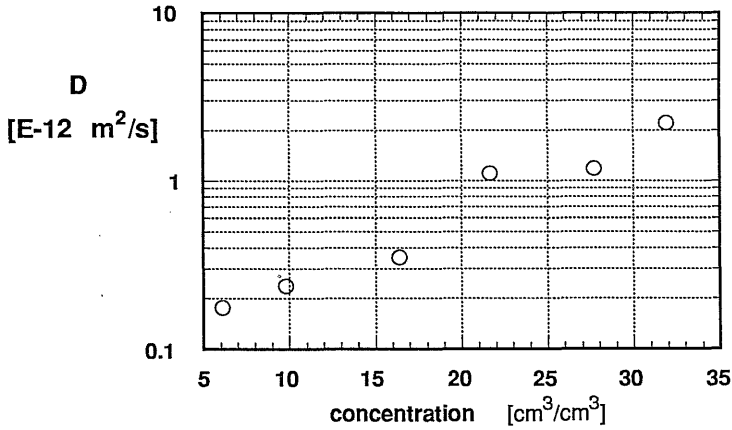


Figure 10. Diffusion coefficients of  $\text{CO}_2$  in PIXU 218 at  $T=25^\circ\text{C}$  calculated with sorption data from figure 9 using equation (10)

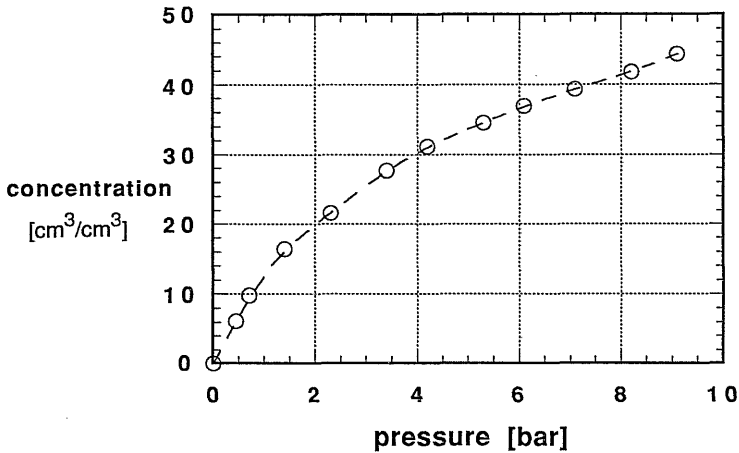


Figure 11. Sorption isotherm for the sorption of  $\text{CO}_2$  into PIXU 218 at  $T=25^\circ\text{C}$

Because the sorption set-up used throughout the experimental part of this thesis was somewhat different to those normally reported in literature, the sorption isotherm for an extensively investigated polymer/penetrant systems was measured again in order to test the validity of the present sorption results. Sorption isotherms were measured for polycarbonate and compared with data reported in literature [14]. The results are shown in figure 12. Good agreement of our data with literature data can be concluded on the basis of these results.

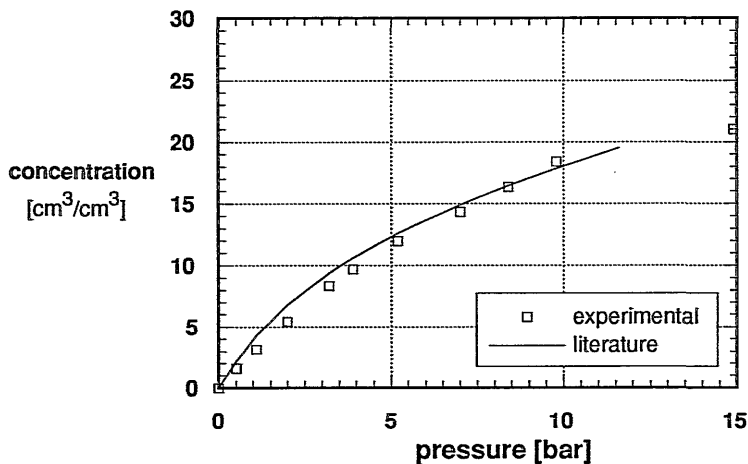


Figure 12. Comparison of the sorption of  $\text{CO}_2$  in polycarbonate at  $T=35^\circ\text{C}$  with data published in [14]

### 3.5. Comparison of Diffusion Coefficients obtained from Different Experimental Methods

In paragraph 3.3. and 3.4. different methods have been described to determine concentration dependent diffusion coefficients. Of course, it is of interest how the results obtained compare with each other. For this purpose, the time-lag analysis for the diffusion of  $\text{CO}_2$  in 6FDA-3PDA carried out according to equation (4) for the concentration independent diffusion as well as equation (5) for the concentration dependent diffusion can be compared with diffusion coefficients obtained from sorption experiments.

The choice of the empirical relation describing the concentration dependent diffusion coefficient (equation (6) or (7)) is arbitrary. No systematic investigation concerning the physical meaning of the plasticization factor  $\beta$  has ever been carried out. Since the equation seems to be of empirical nature, a prediction whether the concentration dependence will be linear or exponential can not be made beforehand. In the case of  $\text{CO}_2$  diffusion in 6FDA-3PDA the linear function for the concentration dependent diffusion coefficient was chosen. For the determination of  $D_0$  and  $\beta$ , the time-lag at different upstream pressures must be measured. Knowing the sorption equilibrium  $c=f(p)$  one can create a plot of the time-lag  $\theta$  versus the upstream concentration and finally fit equation (8) to these data as shown in figure 13. The non-linear least square fitting of the data resulted, for the permeation of  $\text{CO}_2$

through 6FDA-3PDA at 25 °C, in:

$$D_0 = 0.32 \cdot 10^{-12} \frac{\text{m}^2}{\text{s}}$$

$$\beta = 0.162 \frac{\text{cm}^3 \text{ polym.}}{\text{cm}^3 \text{ (STP)}}$$

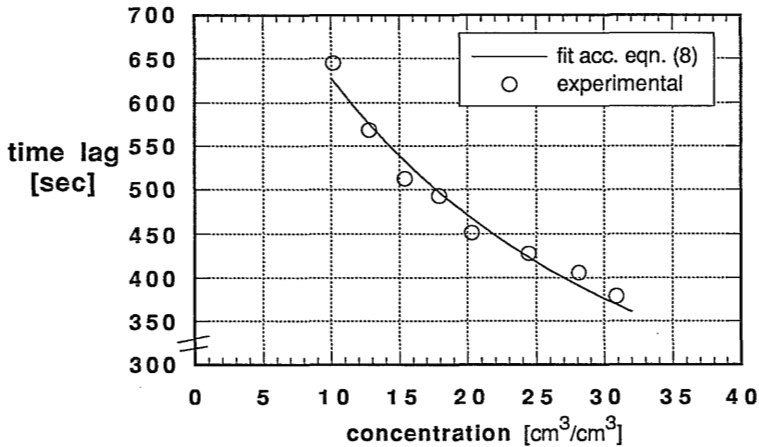
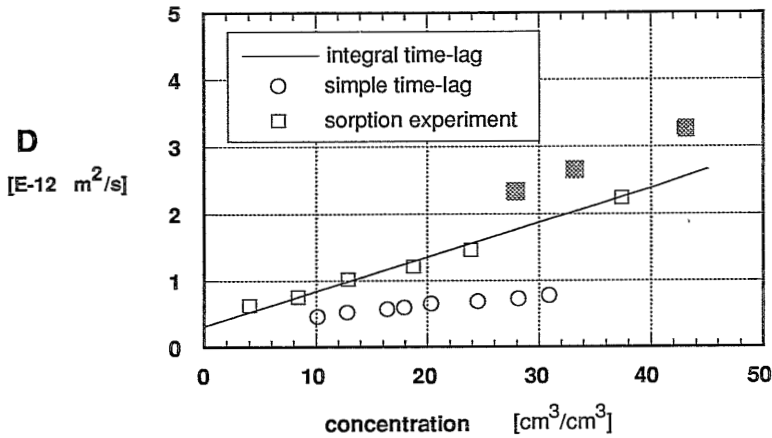


Figure 13. Time lags for the permeation of CO<sub>2</sub> through 6FDA-3PDA depending on the upstream pressure at T=25°C; solid line represents the data fit according to equation (8)

In figure 14, the concentration dependent diffusion coefficients are compared with each other. The solid line represents the diffusion coefficients obtained by the fitting procedure as described above. A considerable deviation exists between the *estimated* diffusion coefficients using equation (4) and those obtained by the “integral time-lag” equation (equation (8)). The excellent agreement between integral time-lag data and diffusion coefficients obtained experimentally from sorption kinetics points out the necessity to use equation (5) if a *realistic* value of D is required. However, if the diffusion coefficients of one specific penetrant in a certain narrow class of polymers must be determined, equation (4) is sufficient to determine trends within this set of polymers. Finally, from the comparison of the three methods it can be concluded that the diffusion coefficients obtained with the three methods agree well for the limit of zero concentration as pointed out in table 1.



**Figure 14.** Comparison of different methods for the determination of the concentration dependent diffusion coefficients for the system 6FDA-3PDA/CO<sub>2</sub> at T=35°C

**Table 1.** Comparison of diffusion coefficients in the limit of zero concentration for different experimental techniques for the system 6FDA-3PDA/CO<sub>2</sub>

technique	D <sub>0</sub> [E-12 m <sup>2</sup> /s]
integral time-lag	0.32
simple time-lag	0.33
sorption experiments	0.34* (0.18)

\* without shaded rectangles in figure 14

Similar experiments have been carried out for other polyimides and the same trends have been observed in those cases.

### 3.6. Dilation

For the determination of the swelling of a polymer induced by the sorbed gas, a new, automatized experimental technique has been developed. A pressure cell with two glass windows was constructed containing a hanging polymer strip as shown in

figure 15. The polymer strip is fixed at the top of the cell and placed on a porous clamping fixture of 9 cm length. This construction guaranteed a stable position of the polymer sample and, furthermore, contact of the total sample surface with the gas phase. The sample was usually around 10 cm long. Upon gas uptake the polymer swells isotropically as it has been demonstrated in literature [15]. The movement of the end of the strip towards the bottom of the cell, which is visible through the windows, is a measure for the penetrant induced dilation. The pressure and the temperature in the cell are computer controlled. Normally, in literature, the displacement of the end of the strip was observed with a cathetometer [16]. This technique, however, does not allow the measurement of the kinetics of volume increase [17]. In contrast to the common experimental approach, the observation of the displacement of the end of the film strip was automatized by using a line scan camera. This newly developed technique made the measurement of *dilation kinetics* possible.

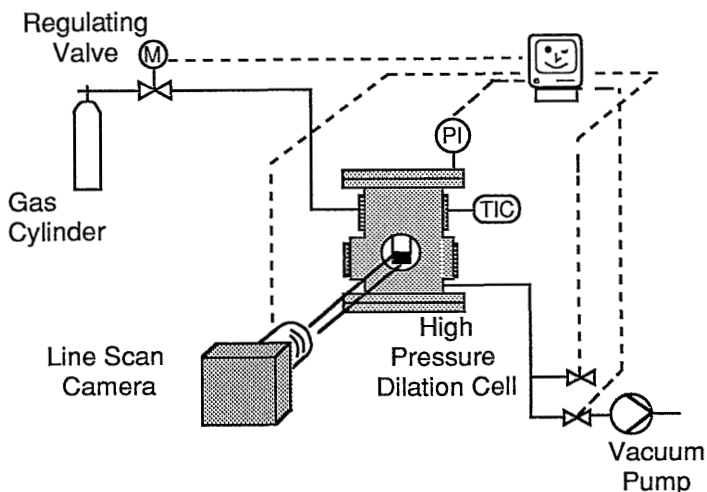


Figure 15. Automatized high pressure dilation set-up

A light source outside the cell illuminated the cell so that a little non-transparent mark at the end of the polymer strip was well visible. This mark is the optical indication of the end of the strip. For the accuracy of the experiments, it did not matter whether this mark actually was a gold strip sputtered on the polymer strip surface, a little tape strip or a small metal strip. The line scan camera consisting of a line of 2064 light sensitive diodes measured the light intensity depending on the local position. The resolution of such a line scan camera is equal to the distance of the diodes. This distance was determined by calibration experiments, and

corresponded to a value of  $5.2\ \mu\text{m}$  which actually meets the specifications of the producer. A "photo" or line scan of the end of a strip hanging in the cell is shown in figure 16. At the place of the non-transparent mark, the intensity drops to zero. A sudden change in light intensity cannot be observed because of light bending effects at the edge of the mark. However, the width of the transition region from the high light intensity to the low intensity did not change if the pressure or temperature was changed. Various numerical techniques transforming this *transition region* into a single value, the *transition point*, have been investigated. The most accurate and reliable way is the definition that the end of the strip is represented by that diode which shows the first time an intensity of zero coming from diodes with a low counter. This transition point can then be followed in time depending on the pressure and temperature. The automatization of the experimental procedure enables the determination of the transition point every 9 seconds.

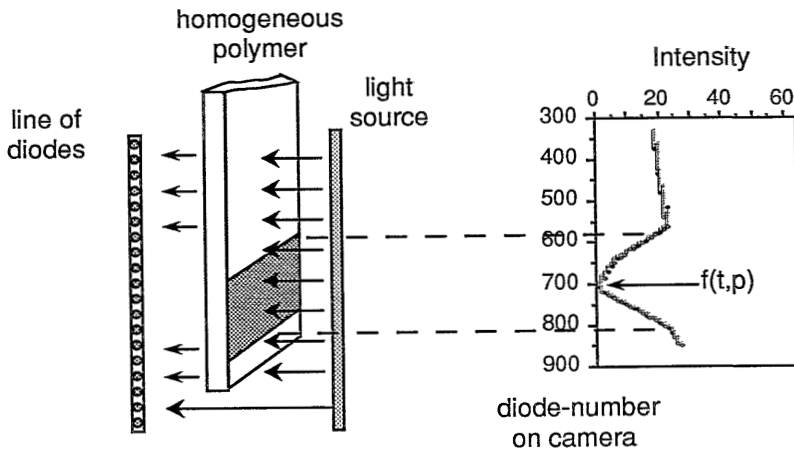


Figure 16. Measurement principle of the line scan camera used in the high pressure dilation set-up

Dilation experiments were normally carried out stepwise in pressure steps of three bars ranging from 0 to 30 bars. At each pressure step, the dilation kinetics was measured for a fixed experimentation time. From the equilibrium values of each pressure step, which are normally reached within the experimentation time, the dilation isotherm can be determined as shown in figure 17 for a polyimide (PIXU 218/Ciba Geigy) with  $\text{CO}_2$  at  $T=25^\circ\text{C}$ . The dilation isotherm shows the same shape as the sorption isotherm which is in contradiction with earlier published sorption and dilation data (see chapter 2) [18]. This, however, will be worked out in more detail in chapter 4.

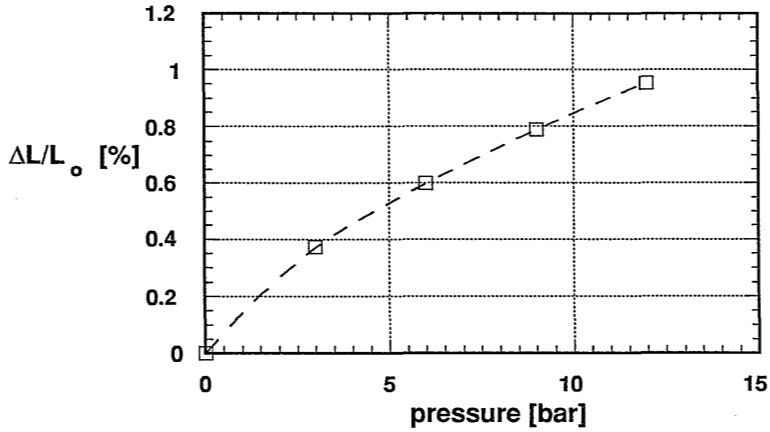


Figure 17. Dilation isotherm of CO<sub>2</sub> in PIXU 218 at T=25°C

Together with the sorption isotherm (figure 11) and the assumption of isotropic swelling [15], the volume increase depending on the amount of penetrant sorbed in the polymer matrix can be determined, as shown in figure 18. The derivative of this experimentally obtained relation represents the partial molar volume  $V_{\text{CO}_2}$  of CO<sub>2</sub> in this polymer.

$$V_{\text{CO}_2} = 22400 \frac{\partial \frac{\Delta V}{V_0}}{\partial c} \quad (11)$$

This partial molar volume depends on the polymer structure (see chapter 4) and actually gives the value for the volume increase of the penetrant/polymer system if one mole of penetrant is sorbed in the matrix. In the case of the system PIXU 218/CO<sub>2</sub> the partial molar volume is slightly concentration dependent; in most other cases reported in chapter 4.4.  $V_{\text{CO}_2}$  is concentration independent. This leads to the conclusion that every molecule sorbed in the matrix dilates the matrix to the same (average) extent which is not in agreement with Dual Mode Sorption theory.

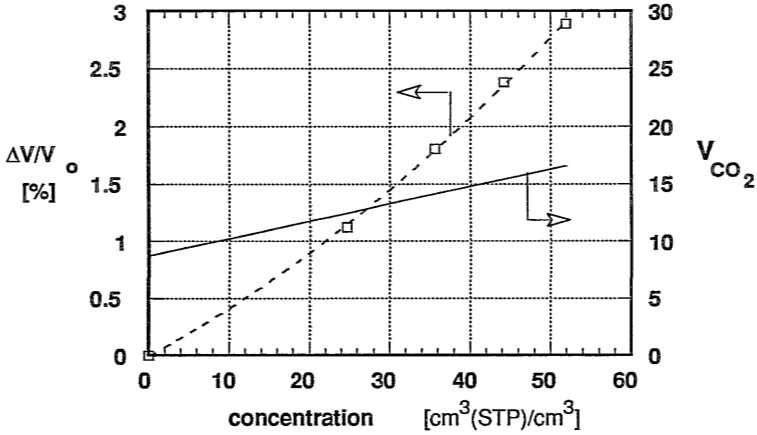


Figure 18. Relative volume increase and partial molar volume of PIXU 218 at  $T=25^{\circ}\text{C}$  depending on the concentration  $\text{CO}_2$

A peculiar phenomenon can be observed comparing the dilation and sorption kinetics of  $\text{CO}_2$  in the polyimide PIXU 218 for a pressure step from 0 to 3 bar as shown in figure 19. In this figure the time axis is transformed into the square-root-of-time axis as usually done for mass transport kinetics.

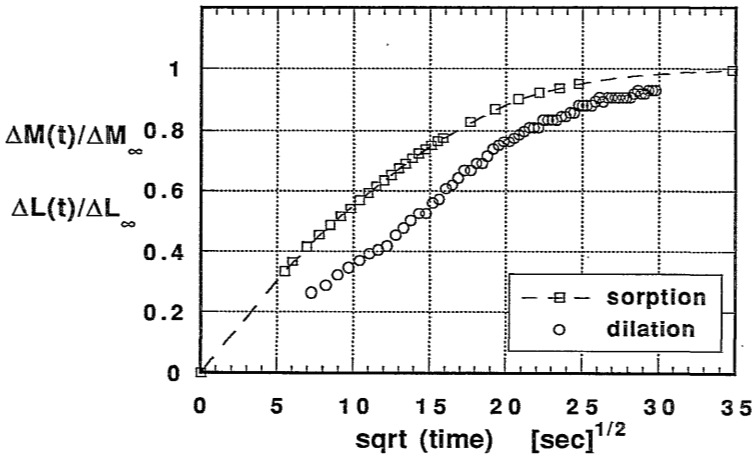


Figure 19. Comparison of the sorption and dilation kinetics for  $\text{CO}_2$  sorption in PIXU 218 at  $T=25^{\circ}\text{C}$



It can be seen clearly that there exists a considerable delay time between the mass uptake and the length increase. Two causes seem to exist for the shift of the dilation kinetics towards larger times. First, the speed of pressure increase in the dilation cell is finite whereas the pressure increase in the sorption set-up is a step function as shown in figure 20. The pressure in the dilation cell first increases with a pressure step from 0 to 0.8 bar and then increases continuously to the pressure level required. The regulation of the pressure in the dilation cell was chosen in this manner because a sudden pressurization from vacuum towards  $p=3$  bar would have risked the chance that the sample would change its position upon pressurization. However, from figure 20 it also can be concluded that mass transport into the film occurs already at the very beginning of the experiments because of the initial pressure step from 0 to 0.8 bar. The continuous increase in pressure from 0.8 to 3 bars, however, represents certainly a time-dependent boundary condition in the mathematical description of the mass transport kinetics.

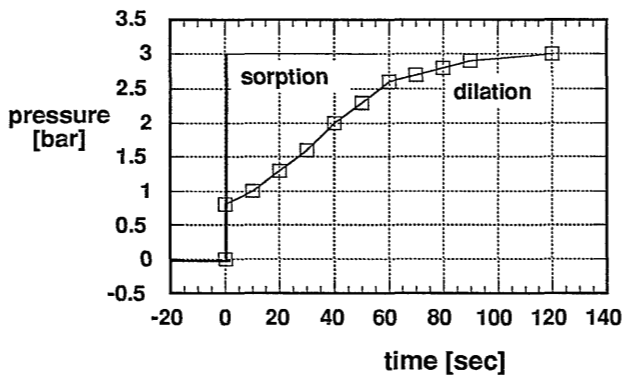


Figure 20. Comparison of the pressurization step for the sorption and dilation set-up

Secondly, the observed delay time in dilation has to be considered as a mass transfer problem and might be closely related to the film thickness of the polymer sample. Figure 21 represents schematically the problem of comparing sorption and dilation kinetics. Penetrant molecules diffuse into the *depth* of the polymer film until the concentration is equal over the whole film thickness. The dilation kinetics, however, is a time-dependent phenomenon in the *length* direction of the film. It is not clear a priori whether dilation can already be observed at  $t=0$  when the first molecules are sorbed in the surface layer of the film or whether dilation starts at the time when the first molecules have reached the middle of the strip as it is suggested by the delay between sorption and dilation kinetics and as it is also found in literature for some special cases of liquid sorption into glassy polymers [19].

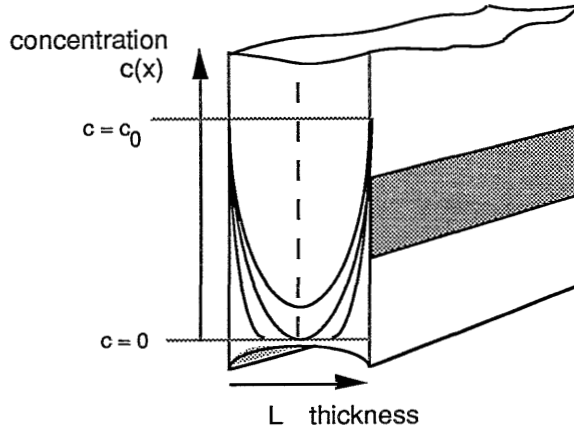


Figure 21. Schematic representation of concentration profiles in the dilation sample when time proceeds

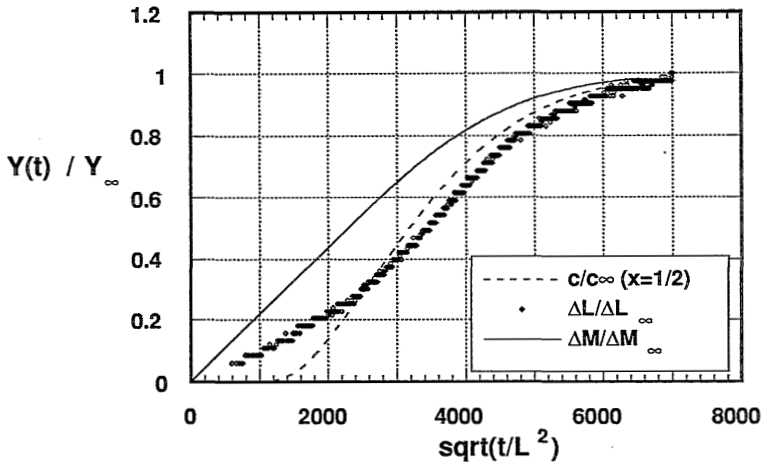


Figure 22. Comparison of the calculated total mass uptake and the concentration in the middle of the polymer film with experimentally determined dilation kinetics for the system 6FDA-DAF at  $T=25^{\circ}\text{C}$  and a film thickness of  $122\ \mu\text{m}$

The kinetic data for the sorption of  $\text{CO}_2$  in a polyimide 6FDA-DAF can be analyzed as usually done by plotting the relative mass uptake versus the square root of time normalized for the membrane thickness. Experimental mass uptake data agree very well with the calculated values (equation (12)) which are shown in figure 22. The dilation kinetics of a  $122\ \mu\text{m}$  thick sample is plotted in the same way. Both the mass

uptake and the dilation kinetics are compared with the calculated relative concentration increase in the middle ( $x=L/2$ ) of the polymer strip. This concentration increase depending on the time is given by equation (13) [5].

$$\frac{M(t)}{M_{\infty}} = 1 - \frac{8}{\pi^2} \sum_{m=0}^{\infty} \frac{1}{(2m+1)^2} \exp \left\{ -\frac{D(2m+1)^2 \pi^2 t}{L^2} \right\} \quad (12)$$

$$\frac{c(t)}{c_{\infty}} \left( x = \frac{L}{2} \right) = 1 - \frac{4}{\pi} \sum_{m=0}^{\infty} \frac{(-1)^m}{(2m+1)} \exp \left\{ \frac{D(2m+1)^2 \pi^2 t}{L^2} \right\} \quad (13)$$

From a certain bending point on, for  $\Delta L(t)/\Delta L_{\infty} > 0.35$ , the length of the polymer strip changes simultaneously with the concentration in the middle of the film but not with the total mass uptake. This supports therefore clearly the second argumentation given above for the delay in dilation. The delay between these two curves, *i.e.*, for the concentration in the middle of the film and for dilation, however, might also be caused by limitations in the pressure regulations as explained above. A significant deviation of the delayed dilation curve from the concentration curve can be observed in figure 22 below  $\Delta L(t)/\Delta L_{\infty} < 0.35$ . Here the dilation increases in a less pronounced way than the total mass uptake but more quickly than the concentration in the middle of the film. This phenomenon can only be observed if samples are sufficiently thick. If samples are very thin (solid line in figure 23) it only *seems* that there is no dilation as long as the concentration in the middle of the film is equal to zero. The camera cannot take any picture at shorter times because the pressure has not been fully adjusted; however, if this would be faster, a dilation curve such as the one shown in figure 22 would probably be obtained, too.

In fact, the critical parameter in this consideration on the bending point is the ratio of the diffusion coefficient and the squared film thickness (see equation (12) and (13)). The statement that the deviation between the concentration in the middle of the film and the dilation kinetics becomes less pronounced and may even disappear if the film thickness becomes smaller than a critical value can be checked by increasing the experimental temperature. Increasing the temperature increases the diffusion coefficient which actually has nearly the same effect as decreasing the film thickness. Temperature dependent experiments have been carried out with the 122 $\mu\text{m}$ -sample also used in figure 22.

Results are shown in figure 23. With increasing temperature the dilation curves of this thick sample shift towards the dilation kinetics curve of the thin sample. Furthermore, the bending points (circles in figure 23) shift to smaller times and

smaller  $\gamma$ -values which indicates that from a critical value for the ratio of diffusion coefficient and squared film thickness this bending point cannot be observed with this experimental set-up.

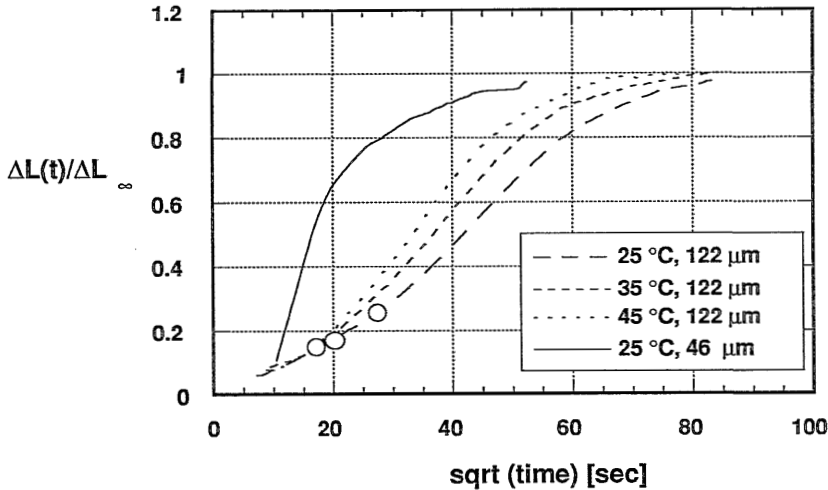


**Figure 23.** Dilation kinetics for the system 6FDA-DAF/CO<sub>2</sub> at different temperatures and different sample thicknesses; circles show bending points in the curve

It is reasonable to conclude that the observed dilation signal in this region is caused by a hindered swelling visualized in figure 21 as bent edges at the end of the film strip. From a certain time on, which depends on the ratio of diffusion coefficients and squared film thickness, dilation progresses simultaneously with the concentration in the middle of the film. Finally from this elaborated explanation of the phenomena occurring during sorption and dilation *kinetics*, it must be concluded, as it was also done for the equilibrium sorption and dilation experiments, that every sorbed penetrant molecule dilates the polymer instantaneously and to the same average extent.

## References

- (1) G.R. Husk, C.E. Cassidy, K.L. Gebert, Synthesis and characterization of a series of polyimides, *Macromolecules* 21 (1988) 1234

- 
- (2) E. Smit, Modelling the diffusion of gases through membranes of novel polyimides, Ph.D. Thesis, University of Twente, The Netherlands, 1991
  - (3) H.C. Park, Separation of alcohols from organic mixtures by pervaporation, Ph.D. Thesis, University of Twente, The Netherlands, 1993
  - (4) K. Tanaka, M. Okano, H. Toshino, H. Kita, K. Okamoto, Effect of methyl substitutions on permeability and permselectivity of gases in polyimides prepared from methyl-substituted phenylenediamines, *J.Polym.Sci., Polym.Phys.*, 30 (1992) 907
  - (5) J. Crank, *The Mathematics of Diffusion*, 2nd Edition, Clarendon Press, Oxford (1975)
  - (6) J.S. McHattie, W.J. Koros, D.R. Paul, Gas transport properties of polysulphones: 1. Role of symmetry of methyl group placement on bisphenol rings, *Polymer*, 32 (1991) 840
  - (7) H. Frisch, The time-lag in diffusion, *J.Phys.Chem.*, 62 (1957) 93
  - (8) Y. Kamiya, K. Mizoguchi, Y. Naito, T. Hirose, Gas sorption in poly(vinyl benzoate), *J.Polym.Sci., Polym.Phys.*, 24 (1986) 535
  - (9) H. Funke, Sorption von Reingasen in Polymeren und an Zeolithen bei Drücken bis zu 70 bar, Dissertation 1991, Universität Heidelberg, Germany
  - (10) R.G. Wissinger, M.E. Paulaitis, Swelling and sorption in polymer-carbondioxide mixtures at elevated pressures, *J.Polymer Sci., Polym. Phys.* 25 (1987) 2497
  - (11) W.J. Koros, D.R. Paul, Design considerations for measurement of gas sorption in polymers by pressure decay, *J.Polym.Sci., Polym. Phys.*, 14 (1976) 1903
  - (12) J.S. Chiou, D.R. Paul, Sorption and transport of CO<sub>2</sub> in PVF<sub>2</sub>/PMMA blends, *J.Polym.Sci., Polym.Phys.*, 32 (1986) 2897
  - (13) W.R. Vieth, K.J. Sladek, A model for diffusion in a glassy polymer, *J. Colloid Sci.*, 20 (1965) 1014
  - (14) W.J. Koros, A.H. Chan, D.R. Paul, Sorption and transport of various gases in polycarbonate, *J.Membrane Sci.* 2 (1977) 165
  - (15) D.S. Pope, W.J. Koros, G.K. Fleming, Measurement of thickness dilation in polymer films, *J.Polym.Sci., Polym.Phys.*, 27 (1989), 1173
  - (16) T. Hirose, K. Mizoguchi, Y. Kamiya, Dilation of polyethylene by sorption of carbon dioxide, *J.Polym.Sci., Polym.Phys.*, 24 (1986) 2107
  - (17) Y. Kamiya, T. Hirose, Y. Naito, Sorptive dilation of polysulfone and poly(ethylene terephthalate) films by high pressure carbon dioxide, *J.Polym.Sci., Polym.Phys.*, 26 (1988) 159
  - (18) G.K. Fleming, W.J. Koros, Dilation of substituted polycarbonates caused by high pressure carbon dioxide sorption, *J.Polym.Sci., Polym.Phys.*, 28 (1990) 1137
  - (19) N.L. Thomas, A.H. Windle, Diffusion mechanics of the system PMMA-methanol, *Polymer*, 22 (1981) 627
-



# Chapter 4

## Sorption and Dilation of Polymer-Carbon Dioxide Systems

### 4.1. Introduction

The ultimate characteristics of a polymer which make it valuable as a membrane material are its permeability and selectivity. A membrane material with a high permeability together with a high selectivity is generally required for the fabrication of a perfect membrane. In the past 20 years, a huge amount of effort has been invested into the development of highly selective polymeric materials. In the theoretical field, parallel with the achievements made in the improvement of permeability and selectivity, various theoretical models have been developed to describe and understand the permeation behaviour of penetrant molecules through polymer membranes. An elaborate overview is given in chapter 2. It can be seen from this overview that neither the kinetic part of the permeability, the diffusion, nor the thermodynamic part, the sorption, is completely understood.

In this chapter, experimental results of the sorption of CO<sub>2</sub> in polymers and the induced volume increase, called dilation, will be presented and interpreted within the theoretical framework given in chapter 2. The goal of this chapter is to develop a meaningful molecular picture on sorption and dilation processes in order to build up a basis on which, later on, relaxation phenomena occurring in solution-diffusion membranes can be discussed. Most experiments have been carried out with glassy 6FDA-based polyimides. Carbon dioxide was chosen as a model gas because of the reported plasticization effects of CO<sub>2</sub> on glassy polymers which we finally want to understand. Similar results may be expected from highly swelling gases like ethane, propane, ethylene etc. [1].

Three models describing the sorption behaviour of glassy polymers have been introduced:

- the Dual Mode Sorption model [2]
- the Flory-Huggins model of Vrentas and Vrentas [3] based on the glass transition temperature depression
- the elastic strain corrected Flory-Huggins model of Bitter [4].

In the first part of this chapter various experimental results will be interpreted using the above mentioned models. Basic equations will partly be repeated in order to facilitate reading. A list of symbols can be found attached to chapter 2. A final choice from these three models will be made on the basis of this analysis and a detailed interpretation of new experiments and literature data will be presented.

#### 4.2. The T<sub>g</sub>-Depression based Model of Vrentas and Vrentas

Vrentas and Vrentas developed a model [3] in which they consider the glass transition depression of the polymer by sorbed penetrant molecules as a key point in characterizing the effect of the penetrant on the polymer structure and therefore on the sorption behaviour. Equation (1) shows their final equation relating the applied pressure  $p$  to the volume fraction of penetrant  $\phi_1$  in the polymer matrix.

$$\frac{p}{p^0} = \phi_1 \exp \left\{ (1 - \phi_1) + \chi (1 - \phi_1)^2 \right\} \exp(F) \quad (1)$$

with

$$F = \frac{M_1 \omega_2^2 \Delta c_p \frac{dT_{gm}}{d\omega_1}}{R T} \left( 1 - \frac{T}{T_{gm}} \right) \quad (2)$$

$p^0$  is the vapour pressure of the pure liquid penetrant,  $M_1$  the molecular weight of the penetrant,  $T$  the experimental temperature,  $\chi$  the Flory-Huggins interaction parameter,  $\omega_1$  the mass fraction of the penetrant,  $\Delta c_p$  the jump in the heat capacity at  $T_g$ ,  $T_{gm}$  the glass transition temperature of the polymer-penetrant system and  $dT_{gm}/d\omega$  the derivative of the function describing the composition dependence of the glass transition temperature.

Figure 1 shows schematically two possible curves describing the glass transition temperature of a polymer penetrant system depending on the mass fraction of penetrant sorbed in the polymer. A linear relation has been found for sorption of CO<sub>2</sub> in glassy polymers [5]. On the other hand, a logarithmic type of relation has been used to describe vapor sorption in polystyrene [6]. However, it is not known beforehand which relation has to be used for a system investigated. For low mass fractions the two relations describing the concentration dependence of the  $T_g$  do not differ very much. But at higher mass fractions differences are significant and depending on the relation chosen, model predictions differ also considerably.



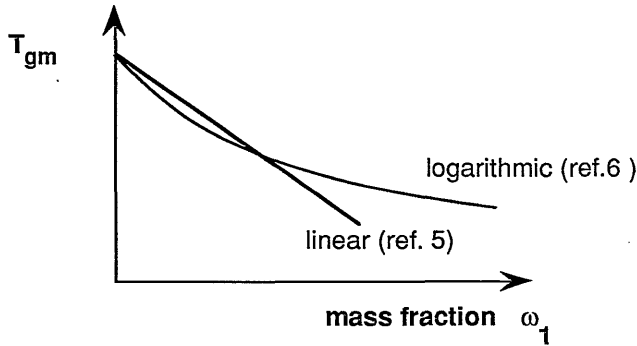


Figure 1. Linear and logarithmic relation describing the composition dependence of the glass transition temperature of two different polymer-penetrant systems

New sorption experiments for the sorption of CO<sub>2</sub> in meta and para isomer polyimides 6FDA-PDA were analyzed according to the model of Vrentas *et al.* The only difference between the polymers is the meta or para bond of a phenylene ring in the polymer backbone. Physical characteristics which are required as inputs for the model are listed in table 1 of chapter 3. The problem of choosing one of the two relations describing the glass transition temperature depression on forehand was avoided by introducing a second order polynomial with adjustable coefficients as shown in equation (3).

$$T_g = T_{g0} - (A \omega_1^2 + B \omega_1) \quad (3)$$

If A equals zero equation (3) changes into the linear relation. If, on the other hand, A is larger than zero the logarithmic relation is numerically represented by equation (3). Hence the isotherms (equation (1)) were fitted with an adjustable  $\chi$ -parameter and two adjustable polynomial coefficients. As shown in figure 2, a good fit of the sorption data could be obtained, certainly caused by the two fitting parameters in the second order polynomial. No reasonable fit could be obtained when the linear or logarithmic relation for the T<sub>g</sub>-depression was chosen beforehand. Fixing the Flory-Huggins parameter and fitting the sorption isotherms with the parameters A and B did not result in a satisfactory fit, either.

The whole sorption isotherms of 6FDA-4PDA and 6FDA-3/4PDA(1:1) are well represented by the model calculation. Only for the sorption isotherm of 6FDA-3PDA the experimental data deviate from the model. Over a large part of the pressure range experimental values are higher than the calculated ones.

Apparently, the model has difficulties in describing strongly concave shaped sorption isotherms.

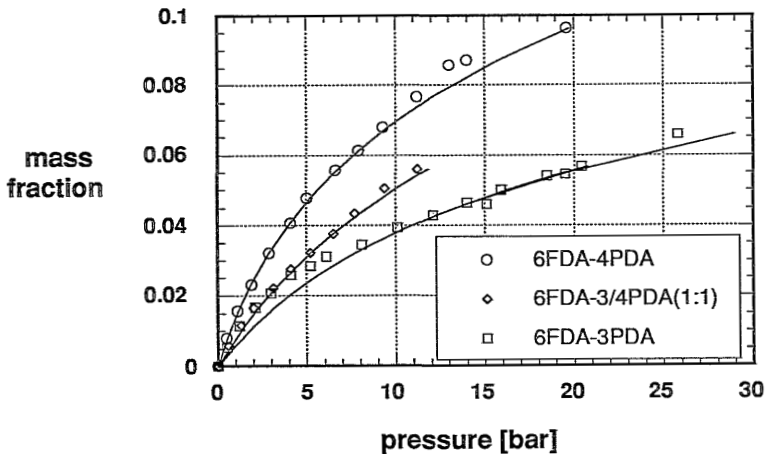


**Figure 2.** Sorption isotherms for the sorption of  $\text{CO}_2$  in isomeric 6FDA-PDAs at  $T = 35^\circ\text{C}$ ; solid lines represent the best fit obtained with the model of Vrentas and Vrentas [2]

Table 1 shows that considerable differences exist for the magnitude of the glass transition temperature depression depending on the polymer investigated. This deviation is expressed by the differences in the two polynomial constants A and B. However, the most significant output of the analysis is the fact that the Flory-Huggins  $\chi$ -parameters differ significantly although the chemical structure of the polymer is the same. This is in contradiction to the general understanding that the physico-chemical interaction between polymer and penetrant should not or only slightly depend on the meta or para substitution of the phenylene ring in the polymer backbone.

**Table 1.** Fitted model parameters for meta/para isomer polyimides according to the model of Vrentas and Vrentas [2]; 6FDA-3/4PDA (1:1) is a random copolymer consisting of 50% of the meta and 50% of the para isomer

polymer	A	B	$\chi$
6FDA-4PDA	0.048	1807.8	2.40
6FDA-3/4PDA(1:1)	0.140	1939.5	1.92
6FDA-3PDA	0.008	2588.4	2.19

The order of magnitude for the  $\chi$ -parameters is quite reasonable; for polycarbonate/ $\text{CO}_2$  Vrentas *et al.* found  $\chi=1.75$  [3]. However, the fact that the  $\chi$ -parameters differ considerably for polymers which are chemically identical has been the reason why the data presented later on in this chapter are not analyzed in this context.

#### 4.3. The Dual Mode Sorption Model and the Partial Molar Volume of Gases in Polymeric Glasses

A strong argument which is believed to support the Dual Mode Sorption model is the fact that the volumetric behaviour of a glassy polymer can actually be predicted from the sorption experiment [7]. The volume of the glassy polymer should increase *linearly* with the applied pressure because only the molecules sorbed in the Henry mode swell the polymer matrix whereas the Langmuir population is trapped in pre-existing microcavities without disturbing the polymer matrix. The volume of the polymer-penetrant system can then be predicted by using equation (4):

$$V(c) = V_p + k_D p \frac{V_{\text{CO}_2}}{22400} \quad (4)$$

Here  $V(c)$  is the volume of the polymer-penetrant system,  $V_p$  is the volume of the pure polymer,  $k_D$  the Henry constant obtained from the sorption experiment and  $V_{\text{CO}_2}$  the partial molar volume. The partial molar volume actually gives the volume increase of the polymer if one mole of the penetrant is sorbed in the polymer matrix. In the dual mode sorption model the partial molar volume is assumed to be independent of the polymer structure and can be taken from tabulated experimental liquid parameters.

Our own sorption and dilation experiments carried out with  $\text{CO}_2$  and the polyimides listed in table 1 of chapter 3 are in contradiction to these findings and so are experiments carried out by Kamiya *et al.* [8] and Funke [9]. As an illustration, the experimental data for the sorption of  $\text{CO}_2$  in the polyimide 6FDA-3PDA and the dilation of the polymer will be worked out in detail.

Figure 3 shows the sorption isotherms together with the dilation isotherms of two different samples for the polymer-penetrant system at  $T = 35^\circ\text{C}$ . The dilation as well as the sorption isotherms are well reproducible. Furthermore, comparing the dilation and the sorption isotherms in figure 3 shows that the two curves have almost the same shape. In fact, the shape of the dilation isotherm is in contradiction

with the prediction according to the Dual Mode Sorption (DMS) model which shows a linear volume increase with increasing pressure.

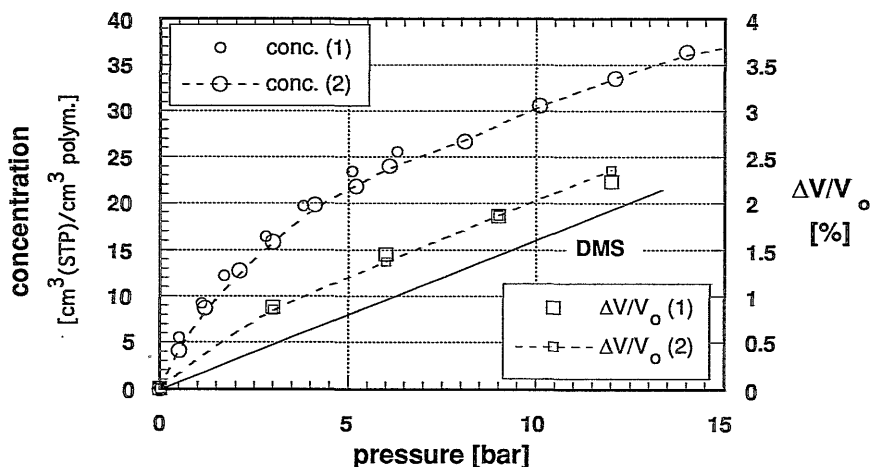
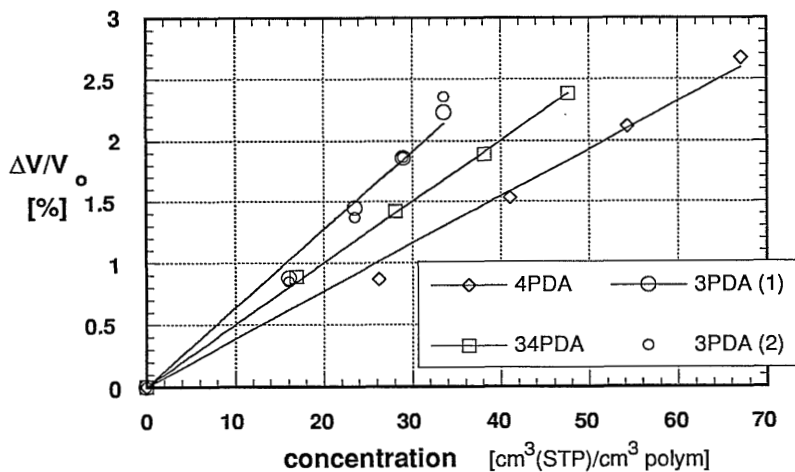


Figure 3. Sorption and dilation isotherms for the polyimide 6FDA-3PDA (two samples) at  $T=35^{\circ}\text{C}$ ; the actual volumetric behaviour is compared with the prediction of the Dual Mode Sorption model (DMS)

The fact that both curves have the same shape suggests that *every* gas molecule (not only the Henry population) dilate the polymer. If every gas molecule sorbed into the matrix will dilate the polymer to the same extent, a cross-plot of the sorption and dilation isotherms will result in a straight line. Figure 4 shows such cross-plots for 6FDA-PDA polyimides which differ only in the meta or para position of the phenylene ring (for sorption isotherms see figure 2). A perfect linear relation can be observed for the polyimides 6FDA-4PDA and 6FDA-3/4PDA(1:1). The curve for 6FDA-3PDA seems to have a slightly convex shape. We do not consider this latter fact as an evidence for Dual Mode Sorption behaviour; we just assume a linear relationship as it is found for the other two polymers. In the following paragraph, however, a suggestion will be given for the slight deviation from the linear relation in the case of 6FDA-3PDA.

Sticking to the argument in terms of the Dual Mode Sorption model would lead to the conclusion that *both* populations, Henry and Langmuir, swell the matrix. The extent to which the Langmuir species swells the polymer is not known on forehand but is a polymer-specific property. As a consequence the volumetric behaviour of the polymer-penetrant system is not predictable anymore. Indeed, it raises the question whether the discrimination between two penetrant populations with two different

swelling abilities, *i.e.*, two partial molar volumes, is physically real. Or in other words whether the picture of one average, polymer specific penetrant partial molar volume would reflect reality better.



**Figure 4.** Cross-plots of the equilibrium dilation obtained from dilation experiments versus the equilibrium concentration obtained from sorption experiments for isomeric polyimides 6FDA-PDA at  $T=35^{\circ}\text{C}$

Since these experimental observations are in contradiction to experiments carried out by Koros *et al.* [7,10] on the system polycarbonate (PC) and  $\text{CO}_2$  and therefore also in contradiction to the Dual Mode Sorption theory, additional experiments were carried out with this system in order to check again the reliability of the experiments in our laboratory and the validity of the findings on the dilation of polycarbonate by  $\text{CO}_2$ .

Experiments were carried out with samples from extruded polycarbonate films supplied by DSM/Netherlands. Whether the dilation samples were cut perpendicular to or in the direction of extrusion did not influence the dilation behaviour. Experiments carried out with a sample heated above its glass transition temperature and then slowly cooled down also did not vary from those obtained with "as-received" films. In figure 5 the experimental results are compared with those published in reference 10. The concentration axis was changed into a mass fraction axis because this kind of axis is used in reference 10. The curve for polycarbonate is convex in this kind of cross-plot because the volume increases proportionally with the pressure (see also figure 3) in the case of PC and the sorption

isotherm is concave.

Our experimental values are generally higher than the published data. However, if one keeps in mind that PC is a glassy polymer and that the mass transport behaviour of a glassy polymer is sensitive to the history of the sample, than a maximum deviation of less than 10% between experimental and published data is not unreasonable.

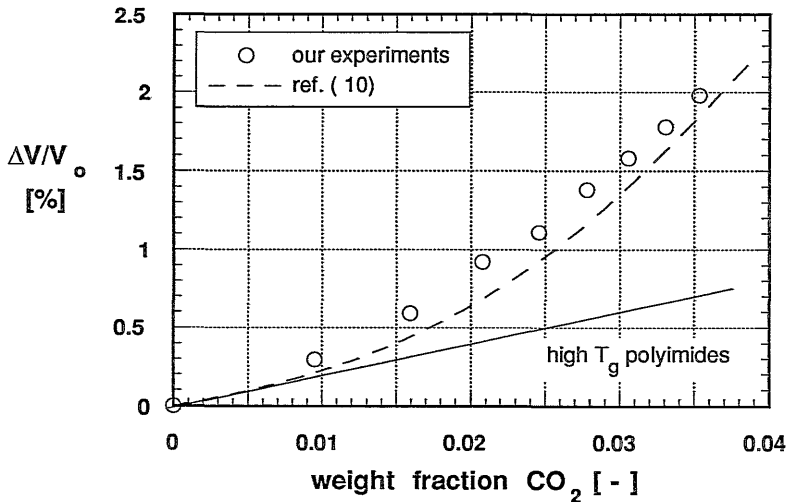


**Figure 5.** *Relative volume increase depending on the mass fraction sorbed for polycarbonate/CO<sub>2</sub>; solid line visualizes schematically the linear volume increase of polyimides with increasing penetrant concentration*

Besides that, the dashed line stems from an interpolation carried out with only two data points available for the concentration range observed in [10]. In fact, the curve based on literature data follows very well the trend of the new experimental data demonstrating the validity of the experimental findings for the system polycarbonate/CO<sub>2</sub>. The solid line in figure 5 schematically visualizes the fact that a linear relation between the mass fraction sorbed and the dilation is found for the polyimides investigated in this chapter. It also emphasizes again (see chapter 3) the contradiction between our experimental evidence and the interpretation in terms of the Dual Mode Sorption model.

A comment must be made about the number of data points taken at low pressures. In the low pressure range, dilation experiments were carried out by increasing the pressure in small pressure steps because, here, the most important informations about the fictitious, so-called Langmuir-sites may be obtained. At high pressures the

Langmuir sites are assumed to be saturated and do not influence sorption and dilation behaviour. At low pressures, however, they should be the most "active". No dilation data have been reported in literature which concentrate on this small pressure range from 0 to 15 bars. Most publications show dilation isotherms where the dilation is measured in five bar pressure steps up to 60 bars. The first data point is obtained at  $p = 5$  bar. Valuable information is lost because the size of the pressure steps taken is actually too large. For the dilation isotherms of polyimides the pressure range was scanned using 3 bar pressure steps. By this means, at least a few more data points could be obtained in the interesting pressure range from 0 to 15 bars.

It has been shown in this paragraph that dilation and sorption experiments carried out with polyimides and  $\text{CO}_2$  do not support the Dual Mode Sorption model with the same strong evidence as experiments of PC and  $\text{CO}_2$ . Because of the criticisms described in chapter 2 and the contradictions in the volumetric behaviour of penetrant-polymer systems, experimental results will not be interpreted further in terms of the Dual Mode sorption model.

#### **4.4. The Partial Molar Volume of Carbon Dioxide in Rubbery and Glassy Polymers**

Dilation and sorption experiments have been carried out for a number of other polyimides. Three dimensional structures of the repeat units for the polymer 6FDA-MDA, 6FDA-DAF and 6FDA-NDA, which are very similar in chemical structure, are shown in figure 6. The only difference between the polymers is the flexibility of the diamine units. This difference in chain flexibility can be clearly correlated to the glass transition temperatures of the polymers. An increasing glass transition temperature indicates a decreased chain flexibility [11,12].

The relative change in volume of the three polymers as a function of the concentration of sorbed  $\text{CO}_2$  is plotted for all three polymers in figure 7. As shown before in figure 4, the volumetric behaviour depends strongly on the polymer type. The data in figures 4 and 7 suggest that the partial molar volume which is proportional to the slope of the curves in these figures increases as the glass transition temperature of the polymer decreases.

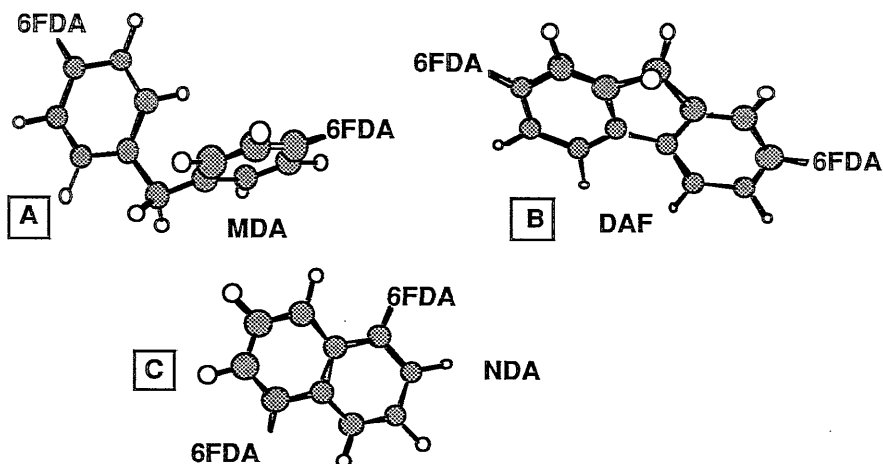


Figure 6. Three-dimensional structures of 6FDA-MDA(4,4'-methylene-bis[benzeneamine]) (A), 6FDA-DAF(2,7-diaminofluorene) (B) and 6FDA-NDA(1,5-diaminonaphthalene) (C)

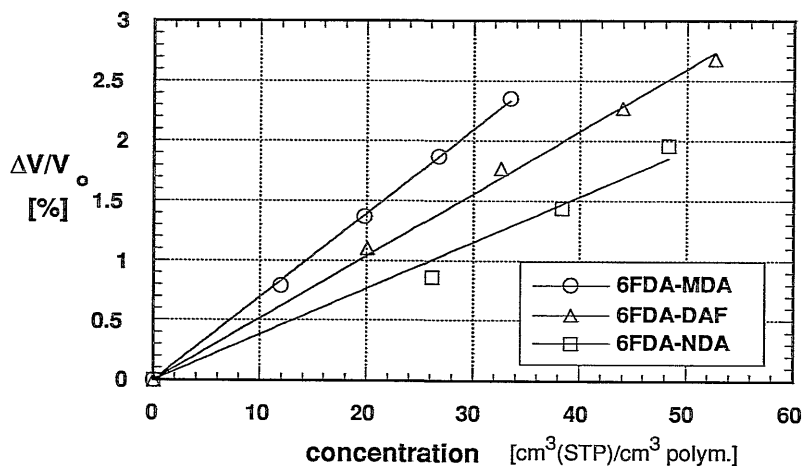


Figure 7. Crossplots of equilibrium dilation obtained from dilation experiments versus the equilibrium concentration obtained from sorption experiments for the sorption of CO<sub>2</sub> in 6FDA-DAF, 6FDA-MDA and 6FDA-NDA at T=35°C

In table 2 the partial molar volumes of the polymers studied are listed together with their glass transition temperatures. The trend of a decreasing partial molar volume with an increasing glass transition temperature can be observed clearly for both series of polyimides.



**Table 2.** Glass transition temperatures and partial molar volumes of CO<sub>2</sub> at T=35°C for polyimides which differ in terms of chain flexibility

polymer	T <sub>g</sub> [°C]	partial molar volume V <sub>CO<sub>2</sub></sub> [cm <sup>3</sup> /mol]
6FDA-MDA	330	15.7
6FDA-DAF	401	11.1
6DFA-NDA	417	8.5
6FDA-3PDA	313	14.3
6FDA-3/4PDA(1:1)	329	11.2
6FDA-4PDA	364	8.7

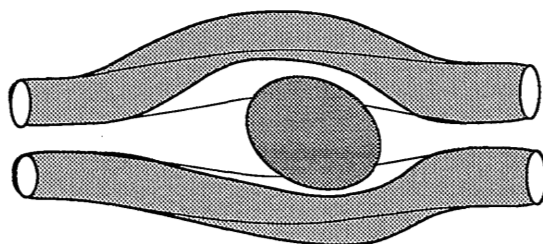


**Figure 8.** Schematic representation of the microscopic swelling process; thin lines represent the original position of the polymer chains in the unswollen state

A penetrant molecule placed between polymer chains disrupts partly the original structure if the sorption takes place in locations where the available volume between the chains is smaller than the actual volume of the penetrant molecule. This disruption as visualized in figure 8 requires energy to overcome attractive forces between the chains which may be described in the form of Lennard-Jones potentials and coulombic electrostatic potentials. Furthermore, the energy which is required to change the conformation of the polymer chains: rotational alterations of sp<sup>3</sup>-bonds and out-of-plane bending of sp<sup>2</sup>-bonds may be responsible for the change of the chain conformation. The ease of accommodating such alterations in a certain polymer segment may be defined as the chain flexibility.

The glass transition temperature of a polymer as a bulk material property is

assumed to be strongly influenced by both intermolecular forces and the chain flexibility. However, it is difficult to distinguish between the two effects. In an analysis on the influence of the intermolecular forces represented by the cohesive energy density (C.E.D.) no relation at all could be found for a number of different polymers [13] between the  $T_g$  and (C.E.D.). Theoretically, Gibbs and DiMarzio have shown that the glass transition temperature is strongly dependent on the chain flexibility expressed by a flexibility energy term. In contrast, variations in intermolecular interactions hardly influenced the glass transition temperature in their model. Privalko and Lipatov [14] present experimental evidence supporting the Gibbs-DiMarzio theory for polymers with only carbon-carbon and oxygen-carbon single bonds in the polymer backbone. Polymers with bulky aromatic groups in the main chain have not been considered. Based on these considerations it is reasonable to assume for further argumentations that the glass transition temperature is an adequate measure for chain flexibility. The data presented in table 2 led to the following conclusion: an increasing partial molar volume with decreasing glass transition temperature represents the fact that a more flexible polymer matrix can dilate more easily and to a larger extent than a stiff matrix for the same molar mass uptake.

A few other polymers like polydimethylsiloxane (PDMS), ethylenpropylene rubber (EPDM), polysulfone (PSF), polycarbonate (PC), poly(styrene maleicacid) block-copolymer (SMA, from DSM/NL) were also investigated with respect to their sorption and dilation behaviour. For a number of other polymers, sorption and dilation results can be found in literature. From the argumentation carried out above it would be interesting to see whether the flexibility argument holds also for very different polymers over a wider range of glass transition temperatures. Hence, all available literature data together with our own experimental data of partial molar volumes have been plotted versus the glass transition temperature of the polymers in figure 9. Reference data plotted in this figure together with the references are listed in appendix A following this chapter.

Apparently, the relation between the flexibility of a polymer chain and the partial molar volume of  $\text{CO}_2$  in the polymeric matrix holds for very different polymer types over a glass transition temperature range from around  $-120^\circ\text{C}$  up to  $+400^\circ\text{C}$ . In a semi-logarithmic plot the data points do not fall perfectly on one straight line but scatter in a broad zone of increasing partial molar volume with decreasing  $T_g$ . The scatter is certainly caused by the fact that not only alteration of the chain conformation by chain bending and bond rotation but also the overcoming of attractive intermolecular forces between polymer chains plays a certain role in the swelling of the polymer matrix. The effect of chain flexibility is clearly present.

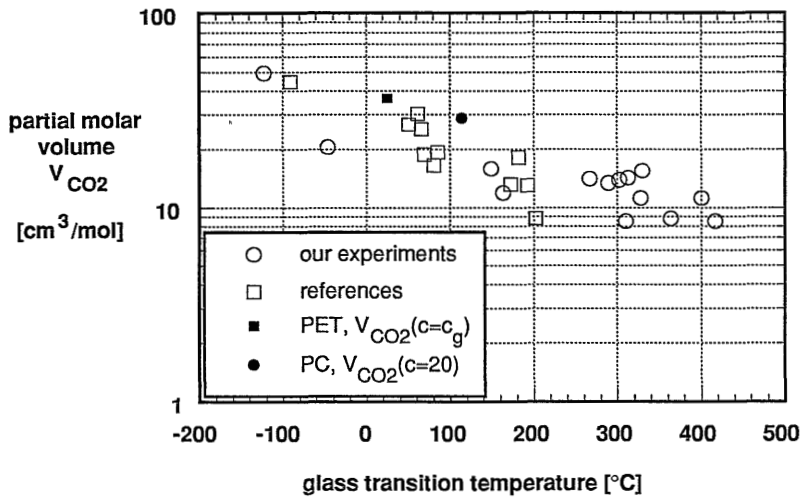


Figure 9. Partial molar volume of  $\text{CO}_2$  in glassy and rubbery polymers at  $T=35^\circ\text{C}$  depending on the glass transition temperature of the polymer; full dots are explained in the text below

The fact that some of the cross-plots of volume increase and concentration show a slightly convex shape may be related to the fact that the sorption of  $\text{CO}_2$  depresses the glass transition temperature. The  $T_g$ -depression would result in an increasing chain flexibility and hence in a stronger increase in volume of the polymer/penetrant system. This hypothesis is supported by experiments carried out by Kamiya [15] with PET and  $\text{CO}_2$ . PET changes from a glassy into a rubbery polymer as the penetrant concentration increases due to the glass transition temperature depression effect of the sorbed carbon dioxide (see fig. 2.7.). The partial molar volume changes from 18.9 for the glassy to 36.7  $\text{cm}^3/\text{mole}$  for the rubbery polymer. The  $T_g$  at this concentration is equal to the experimentation temperature  $T=25^\circ\text{C}$ . This data point is plotted in figure 9 as a full rectangle. Considering the  $T_g$ -depression induced by the sorbed  $\text{CO}_2$  (see chapter 7), a glass transition temperature at  $c=20 \text{ cm}^3(\text{STP})/\text{cm}^3\text{polym.}$  for PC can be calculated and the related partial molar volume can be taken from figure 5. This data point is plotted as full circle in figure 9.

#### 4.5. The Elastic Strain Corrected Flory-Huggins Model of Bitter [4]

Bitter's assumption of local ordering as a cause of topological constraints in the polymer matrix and the introduction of strained polymer chains due to the presence of penetrant molecules in the derivation of the free energy of a polymer-penetrant

system led to a final equation describing the sorption equilibrium as given in chapter 2. The basis of the model is schematically depicted in figure 10. Polymer chains are fixed in a three-dimensional space by so-called "local orderings" and run from one of these constraints to another one. In between these local orderings the polymer matrix is amorphous. A crucial factor in Bitter's model is the chain flexibility described by the factor  $f(s)$ .

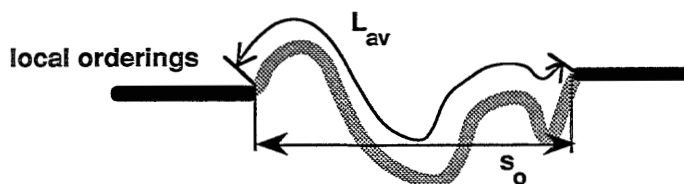


Figure 10. Schematic representation of the polymer parameters affecting the flexibility term  $f(s)$  in the Elastic Strain Corrected Flory-Huggins model (ESCFH) of Bitter

$$f(s) = \frac{L_{av} - s_0}{s_0} \frac{y}{y-1} \quad (5)$$

$L_{av}$  is the average chain length between two local constraints,  $s_0$  is the shortest distance between these constraints and  $y$  is the chain flexibility in the unswollen polymer. Basically,  $y$  is the chance of a new segment to be placed on an adjacent lattice position and is therefore always larger or equal to one. If  $y$  equals 1, the new segment can only be placed in one new position and the polymer chain is infinitely stiff. The factor  $y/(y-1)$  describes the polymer conformation. In contrast,  $(L_{av}/s_0)-1$  has a morphological character, although it is also a measure for the chain flexibility. The more  $L_{av}$  approaches  $s_0$  the stiffer is the polymer chain. However, if  $L_{av}$  and  $s_0$  are sufficiently different, the stiffness of the polymer chain is determined predominantly by  $y$ . Assuming that variations in  $L_{av}$  and  $s_0$  between polymers are negligible, an increasing value of  $f(s)$  represents a decreasing chain flexibility. Clearly,  $f(s)$  is a property of the pure polymer. Unfortunately, Bitter does not give any suggestion for a polymer characteristic that is correlated to  $f(s)$  which might be determined experimentally.

Because the physical picture of an elastically strained network developed by Bitter is in agreement with the experimental results on the dilation of polymers presented in 4.3., an attempt will be made in this paragraph to get more information on the model parameters. Sorption isotherms for the sorption of  $\text{CO}_2$  in different polyimides have been measured and will be analyzed using Bitter's equation (6).

$$c_i = \frac{H_i^\infty f_i}{1 - \phi_s} \exp\{B_i \phi_i\} \quad (6)$$

$H_i^\infty$  is the Henry's law coefficient at infinitely low fugacity  $f_i$ ;  $\phi_s$  is the sum of all volume fractions  $\phi_i$  of penetrants  $i$  and  $B_i$  is a constant expressing the non-ideality of the polymer-penetrant system. In the case of the sorption of a single component equation (6) changes into (7)

$$c_i = \frac{H_i^\infty f_i}{1 - \phi_i} \exp\{B_i \phi_i\} \quad (7)$$

with

$$\phi_i = \frac{\frac{c_i V_i}{\phi_a}}{\frac{c_i V_i}{\phi_a} + 22400} \quad (8)$$

$c_i$  is the volumetric concentration of the penetrant per unit volume of polymer in [ $\text{cm}^3$  (STP)/ $\text{cm}^3$  polymer] as determined in a sorption experiment,  $V_i$  the partial molar volume of the penetrant in the polymer and  $\phi_a$  the amorphous polymer volume fraction in which sorption takes place. Because the polyimides investigated do not show any crystallinity and, in a numerical sense, the extent of local ordering is negligibly small compared to the amorphous polymer fraction,  $\phi_a$  is assumed to be equal to one for further calculations.

If the sorption isotherm  $c_i=f(p)$  or  $c_i=f(f)$  is determined experimentally, the model parameters must be determined by fitting equation (9) instead of equation (7) since the latter is an implicit function in concentration.

$$f_i = p_i = \frac{1 - \phi_i}{H_i^\infty} c_i \exp\{-B_i \phi_i\} \quad (9)$$

$\phi_s$ ,  $\phi_i$  and  $B_i$  contain as an unknown parameter the partial molar volume of the penetrant. However for the polyimides under investigation, the partial molar volume has already been determined experimentally. As it was done regarding the volumetric behaviour, 6FDA-MDA, 6FDA-DAF, 6FDA-NDA on one hand and isomeric 6FDA-PDAs on the other hand were analyzed using equation (9). Although fitted with equation (9), the results are shown in figure 11 and 12 (by switching axes) in the usual form of a sorption isotherm showing the penetrant concentration as a

function of the applied pressure.

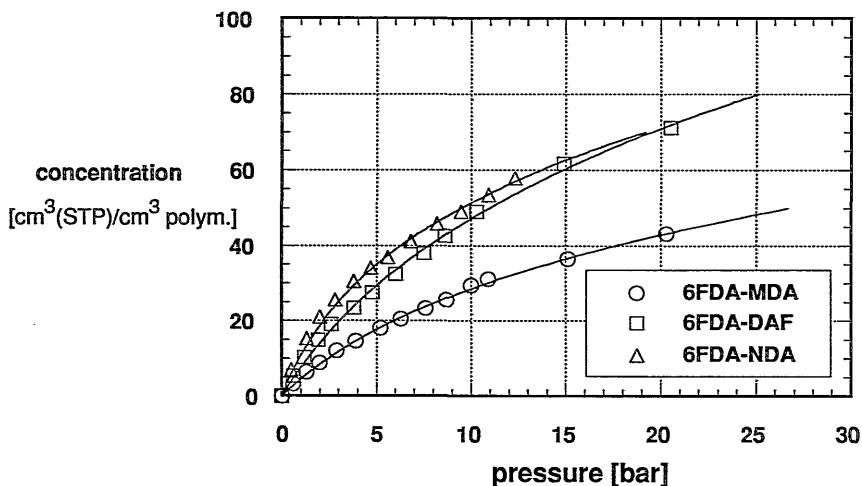


Figure 11. Experimental sorption isotherms for the sorption of CO<sub>2</sub> in 6FDA-MDA, 6FDA-DAF and 6FDA-NDA at T=35°C in comparison with ESCFH-model fit (solid lines)

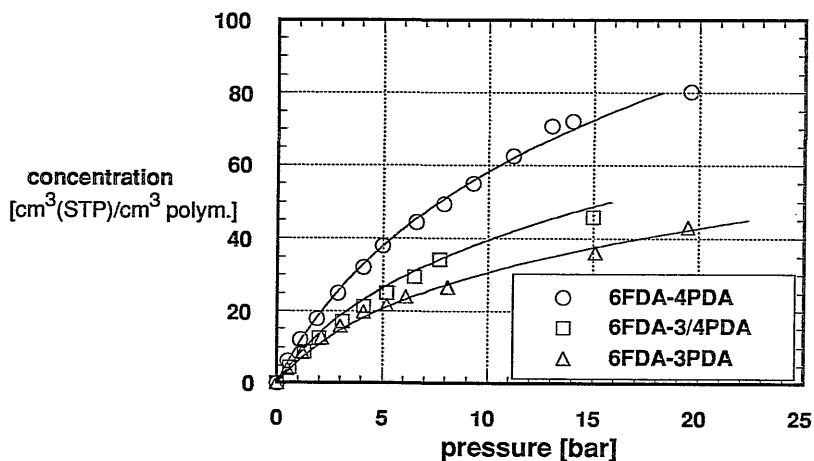


Figure 12. Experimental sorption isotherms for the sorption of CO<sub>2</sub> in isomeric 6FDA-PDAs at T=35°C in comparison with ESCFH-model fit (solid lines)

The solid lines show the fit according to equation (9). In all cases the model fits the data very well. For the isomeric 6FDA-PDAs, a comparison of fitted model parameters of the Dual Mode Sorption model and the elastic strain corrected Flory-

Huggins Model of Bitter are shown in table 3a and 3b. Both models represent the sorption isotherms over the whole concentration range very well.

**Table 3a.** Dual Mode Sorption model parameters describing the solubility of CO<sub>2</sub> in isomeric 6FDA-PDAs;  $\chi^2$  is a statistical parameter indicating the quality of the fit

polymer	$k_D$	$c'_H$	b	$\chi^2$
6FDA-3PDA	1.07	24.7	0.36	2.2
6FDA-3/4PDA(1:1)	0.98	45.4	0.15	5.2
6FDA-4PDA	1.64	89.7	0.14	3.81

units:  $k_D$  in [ $\text{cm}^3$  (STP)/( $\text{cm}^3$  bar)];  $c'_H$  in [ $\text{cm}^3$ (STP)/ $\text{cm}^3$ ]; b in [1/bar]

**Table 3b.** Model parameters for the model of Bitter describing the solubility of CO<sub>2</sub> in isomeric 6FDA-PDAs;  $\chi^2$  is a statistical parameter indicating the quality of the fit

polymer	$H_i^\infty$	$B_i$	$\chi^2$
6FDA-3PDA	7.83	-49.6	4.3
6FDA-3/4PDA(1:1)	9.1	-46.6	9.5
6FDA-4PDA	12.71	-36.1	3.1

units:  $H_i^\infty$  in [ $\text{cm}^3$  (STP)/( $\text{cm}^3$  bar)];  $B_i$  in [-]

The quality of the fit is represented by the statistical parameter  $\chi^2$  which is a measure for the deviation between the actual data points and the fitted model. A low value of  $\chi^2$  represents a good fit. The statistical parameter  $\chi^2$  is found on the average to be lower for the Dual Mode Sorption model. However, this is due to the fact that this model contains one more fitting parameter.

The strength of a model does not only depend on the ability to fit sorption isotherms for a single polymer. The physical significance of the fitted model parameters in comparison with parameters obtained for other polymers must be evaluated in order to be able to make a statement concerning the strength of a model. The model of Bitter contains the two fitting parameters  $B_i$  and  $H_i^\infty$ , given in equation (10) and (11) respectively, which are functions of topological and thermodynamic parameters. Detailed explanations about the symbols can be found in chapter 2.

$$B_i = \left\{ \frac{V_i}{9 v} \frac{2 f(s) - 1}{f(s)^2} + 2 \frac{V_i}{R T} \delta_{ip}^2 + \frac{V_i}{V_{av}} \frac{Z_i}{Z_{av}} \right\} \quad (10)$$

and

$$H_i^\infty = \frac{K_H}{f_{sat,i}} \exp\left\{-\frac{V_i}{R T} \delta_{ip}^2\right\} \quad (11)$$

with

$$K_H = \frac{Z_a \phi_a}{Z_i V_i} 22400 \exp\left\{-\left(1 + \frac{V_i}{3 v f(s)}\right)\right\} \quad (12)$$

In both cases, the fitting parameter depends on the flexibility term  $f(s)$ . Substituting equation (12) in (11) and combining a few constant terms, one obtains

$$H_i^\infty = A \frac{1}{f_{sat,i}} \exp\left\{-\left(1 + \frac{V_i}{3 v f(s)}\right)\right\} \quad (13)$$

with

$$A = \frac{Z_a \phi_a}{Z_i V_i} 22400 \exp\left\{-\frac{V_i}{R T} \delta_{ip}^2\right\} \quad (14)$$

Taking the logarithm of equation (13) one obtains equation (15). Simplification leads to equation (16) which predicts a linear relation between the logarithm of the Henry coefficient and the inverse of the flexibility parameter  $f(s)$ . In order to verify this prediction, the solubility of one gas in polymers with different chain flexibility should be investigated.

$$\ln(H_i^\infty) = \ln\left(\frac{A}{f_{sat,i}}\right) - 1 - \frac{V_i}{3 v f(s)} \quad (15)$$

$$\ln(H_i^\infty) = C_1 - \frac{C_2}{f(s)} \quad (16)$$

with

$$C_1 = \ln\left(\frac{A}{p_{sat,i}}\right) - 1 \quad (17)$$

and



$$C_2 = \frac{V_i}{3 v} \quad (18)$$

For this purpose, a number of sorption isotherms for the sorption of CO<sub>2</sub> in glassy as well as rubbery polymers published in the past will be analyzed. No attempt has ever been made to compare all these published data. Because all published sorption isotherms are fitted by the Dual Mode Sorption model and the model parameters are listed in the papers, sorption isotherms are well documented. The sorption isotherms of CO<sub>2</sub> for around 50 different polymers have been calculated using the Dual Mode Sorption parameters and these data were *refitted* using the model of Bitter in order to calculate the parameters H<sub>1</sub><sup>∞</sup> and B<sub>1</sub>. For all polymers taken from references, where no degree of crystallinity was published, it was assumed that the polymer matrix is amorphous and φ<sub>a</sub>=1. Because the partial molar volume of CO<sub>2</sub> in these polymers is not known on forehand, estimates obtained from figure 9 were used. The partial molar volume of CO<sub>2</sub> in different polymers follows an empirical relation:

$$V_{CO_2} = 26.07 \exp \{ -0.0027 T_g [^{\circ}C] \} \quad (19)$$

However, the data points do not always fall on this line. This might raise doubts about the procedure following further on. To check the sensitivity of the model parameters B<sub>1</sub> and H<sub>1</sub><sup>∞</sup> on the value of the partial molar volume, the solubility of CO<sub>2</sub> in the polyimide 6FDA-SDA was fitted with the real value of V<sub>i</sub> and then compared with V<sub>i</sub>-values 25% smaller and larger than the actual value. Results of the calculations are listed in table 4.

**Table 4.** *Effect of variations of the partial molar volume V<sub>CO<sub>2</sub></sub> on the fit parameters in the elastic strain corrected model of Bitter for the solubility of CO<sub>2</sub> in the polyimide 6FDA-SDA at T=35°C*

V <sub>CO<sub>2</sub></sub>	ΔV [%]	H <sub>1</sub> <sup>∞</sup>	B <sub>1</sub>	B <sub>1</sub> <sup>*</sup>
13.9	0	8.43	-43.8	-43.8
10.4	-25	8.39	-57.5	-54.7
17.4	+25	8.47	-35.5	-33.0

\*linearly predicted

A 25% change in the partial molar volume results in a 0.5% change in the Henry coefficient. Since B<sub>1</sub> is linearly related to the partial molar volume V<sub>CO<sub>2</sub></sub>, it can be

expected that a certain percentage change of  $V_i$  should result in the same percentage change of  $B_i$ . The prediction of  $B_i$  according to this linear recalculation is listed in column 5 of table 4. Differences between the fitted  $B_i$  and the linearly predicted one are between 5 and 7%. Both changes demonstrate that the model of Bitter is not very sensitive to the value of the partial molar volume. An estimation of  $V_i$  for other polymers using equation (19) seems therefore reasonable. In cases where the partial molar volumes have been determined experimentally, these values were used in the fit procedure. The results of the determination of the model parameter for 52 different polymers published in literature and 14 polymers characterized by our sorption experiments together with glass transition temperatures are listed in table B1 and B2 in appendix B. For the polymers taken from literature the references are also listed in the appendix. All sorption isotherms are fitted very well by the model.

Since the relationship of the flexibility parameter  $f(s)$  and the glass transition temperature  $T_g$  with the actual chain flexibility are equal (a high value of  $f(s)$  or  $T_g$  respectively, represents a stiff polymer) the Henry coefficients obtained from the fitting calculations are plotted versus the inverse glass transition temperature of each polymer as it is suggested by equation (16) in figure 13. The glass transition temperatures actually range from  $-120^\circ\text{C}$  up to  $420^\circ\text{C}$ , representing PDMS as the rubbery polymer with the lowest  $T_g$  and 6FDA-NDA as the glassy polymer with the highest  $T_g$ .

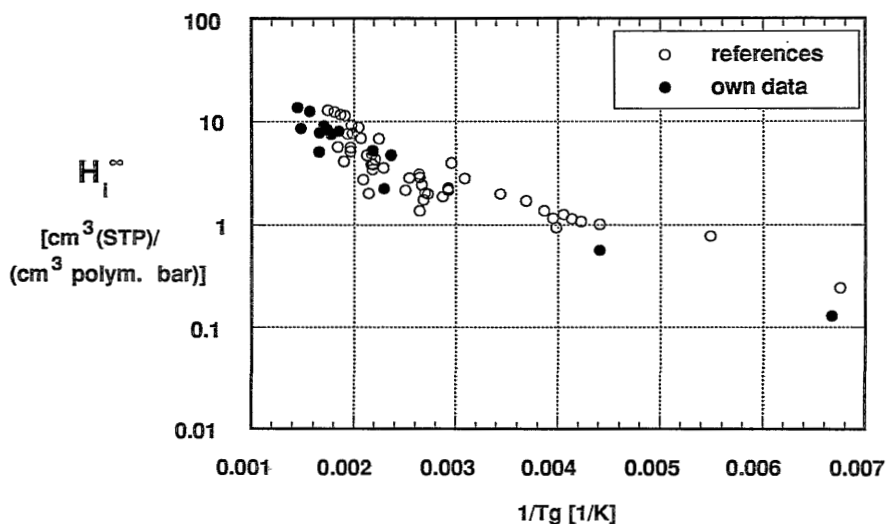


Figure 13. Henry coefficients for the solubility of  $\text{CO}_2$  in glassy and rubbery polymers at  $T=35^\circ\text{C}$  versus the inverse glass transition temperature of each polymer

Figure 13 shows clearly that there exists a unique linear relationship between the logarithm of the Henry coefficient and the inverse glass transition temperature. This figure together with equation (16) suggests furthermore that the glass transition temperature as a physical characteristics of the polymer is related to the flexibility term  $f(s)$  in the model of Bitter. Again, as for the partial molar volume, a certain scattering can be observed. Especially at high  $T_g$ s, the Henry coefficients can vary by a factor of 4 between different polymers with the same  $T_g$ . This actually should be expected because the fact that the solubility would be only dependent on the polymer chain conformation but not on thermodynamic interaction would be unreasonable. No intensive evaluation of physico-chemical interaction between polymer and penetrant was possible due to lack of time. But theoretically, this effect is already considered in the model in terms of the solubility parameters. For the non-ideality factor  $B_i$  no clear relation can be deduced from the fitted data in appendix B. Up to now  $B_i$  remains therefore a fitting parameter which, from a theoretical point of view, should have physical significance but which is hard to correlate to any bulk physical property of the polymer.

Another point which remains open in the analysis of this model is the capability of the model to describe the sorption isotherm of a polymer penetrant system that changes from a glassy system into a rubbery system as the penetrant concentration increases with increasing pressure. A sorption isotherm representing such a polymer penetrant system is shown in chapter 2, figure 7. The model of Bitter can only describe these systems if the non-ideality factor varies with concentration. A negative  $B_i$  stands for a glassy polymer whereas a positive value can be found for rubbery polymers. Bitter suggests that the difference between these two classes of polymers can be found in the morphological factor  $L_{av}/s_0$ . A change in the sign of  $B_i$  can only be obtained if the term

$$\frac{V_i}{9v} \frac{2f(s) - 1}{f(s)^2} \quad (20)$$

in equation (10) becomes smaller with increasing concentration compared to the two terms

$$2 \frac{V_i}{RT} \delta_{ip}^2 + \frac{V_i}{V_{av}} \frac{Z_i}{Z_{av}} \quad (21)$$

This actually means for a system undergoing glass transition that drastic morphological changes must occur in terms of alterations of the local orderings present in the polymer matrix.

#### 4.6. Conclusions

Three models describing the thermodynamic equilibrium between a gaseous phase of CO<sub>2</sub> and the sorbed CO<sub>2</sub> in a polymer have been compared with each other. Based on the rigorous analysis of experimental data, the elastic strain corrected Flory-Huggins model has been chosen as the model that describes polymer-penetrant systems most adequate. The molecular picture behind the model agrees well with the experimental results of an increasing partial molar volume with decreasing glass transition temperature. Furthermore, the model predicts a decreasing Henry coefficient with increasing chain flexibility. This prediction is confirmed by the analysis of around 70 different polymers. A unique linear relationship is found plotting the logarithm of the Henry coefficient versus the inverse glass transition temperature.

#### References

- (1) Y. Kamiya, D. Bourbon, K. Mizoguchi, Y. Naito, Sorption, dilation and isothermal glass transition of poly(ethyl methacrylate)-organic gas systems, *Polymer J.*, 24 (1992) 443
- (2) W.R. Vieth, H.H. Alcalay, A.J. Frabetti, Solution of gases in oriented poly(ethylene terephthalate), *J.Appl.Polym.Sci*, 8 (1964) 2125
- (3) J.S. Vrentas, C.M. Vrentas, Sorption in glassy polymers, *Macromolecules* 24 (1991) 2404
- (4) J.G.A. Bitter, Transport mechanisms in membrane separation processes, Plenum Press, New York 1991
- (5) H. Hachisuka, T. Sato, T. Imai, J. Tsujita, A. Takizawa, T. Kinoshita, Glass transition temperature of glassy polymers plasticized by CO<sub>2</sub> gas, *Polymer J.*, 22 (1990) 77
- (6) T.S. Chow, Molecular interpretation of the glass transition temperature of polymer-diluent systems, *Macromolecules* 13 (1980) 362
- (7) G.K. Fleming, W.J. Koros, Dilation of polymers by sorption of carbon dioxide at elevated pressures, 1. Silicone Rubber and unconditioned polycarbonate, *Macromolecules* 19 (1986) 2285
- (8) D. Bourbon, Y. Kamiya, K. Mizoguchi, Sorption and dilation properties of poly(p-phenylene sulfide) under high pressure carbondioxide, *J.Polym. Sci., Polym.Phys.*, 28 (1990) 2057-2069
- (9) H. Funke, Sorption von Reingasen in Polymeren und an Zeolithen bei Drücken bis 70 bar, Ph.D. Thesis, 1991, University of Heidelberg, Germany
- (10) G.K. Fleming, W.J. Koros, Dilation of substituted polycarbonates caused by high pressure carbon dioxide sorption, *J.Polym.Sci., Polym. Phys.*, 28 (1990) 1137-1152
- (11) E.A. DiMarzio, J.H. Gibbs, Chain stiffness and the lattice theory of polymer phases, *J.Chem.Phys.*, 28 (1958) 807
- (12) E.A.DiMarzio, J.H. Gibbs, Nature of the glass transition and the glassy state, *J.Chem.Phys.*, 28 (1958) 373

- (13) W.A. Lee, J.H. Sewell, Influence of cohesive forces on the glass transition temperatures of polymers, *J.Appl.Polym.Sci.*, 12 (1968) 1397
- (14) V.P. Privalko, Y.S. Lipatov, Glass transition and chain flexibility of linear polymers, *J.Macromol.Sci.-Phys.*, B9(3) (1974) 551
- (15) Y. Kamiya, T. Hirose, Y. Naito, K. Mizoguchi, Sorptive dilation of polysulfone and poly(ethylene terephthalate) films by high-pressure carbon dioxide, *J.Polym.Sci., Polym.Phys.*, 26 (1988) 159-177

## Appendix A

## Partial Molar Volumes of CO<sub>2</sub>-Polymer Systems

The polymer properties listed in appendix A and B have the following units:

$V_{CO_2}$	[cm <sup>3</sup> /mol]
$T_g$	[°C]
Henry Coeff.	[cm <sup>3</sup> (STP)/(cm <sup>3</sup> polym. bar)]
$B_i$	[-]

polymer	T <sub>g</sub>	V(CO <sub>2</sub> )	remark-#	reference
PET	69	18.9	1	1
PVB	65.5	25.3		2
PVBu	51	26.8		2
PEMA	61	30.5		3
PPS	85.5	19.3		4
TMPC	202	8.8		5
HFPC	172	13.2		5
PBU	-91	44.4		6
PVA	80	16.6	2	7
CTA	182	18.1		7

*Table A1. Reference data for the partial molar volume of carbon dioxide in different polymers*

- (#1) The partial molar volume of CO<sub>2</sub> plasticized PET at T=35°C and p=32bar is equal to  $V_{CO_2}=36.7$  cc/mole.
- (#2) measured at T=51°C; however, Kamiya shows that the partial molar volume of CO<sub>2</sub> is insensitive for temperature variations [1]. Therefore, it is appropriate to enclose PVA in this list and in figure 9.

### References

- (1) Y. Kamiya, T. Hirose, Y. Naito, K. Mizoguchi, Sorptive dilation of polysulfone and poly(ethylene terephthalate) films by high-pressure carbon dioxide, J.Polymer Sci.

- Polym. Phys., 26 (1988) 159
- (2) Y. Kamiya, T. Hirose, K. Mizoguchi, K. Terada, Sorptive dilation of poly(vinyl benzoate) and poly(vinyl butyral) by carbon dioxide, J.Polymer Sci. Polym., Phys., 26 (1988) 1409
  - (3) Y. Kamiya, D. Bourbon, K. Mizoguchi, Y. Naito, Sorption, dilation and isothermal glass transition of poly(ethyl methacrylate)-organic gas systems, Polymer J., 24 (1992) 443
  - (4) D. Bourbon, Y. Kamiya, K. Mizoguchi, Sorption and dilation properties of poly(p-phenylene sulfide) under high pressure carbondioxide, J.Polym. Sci., Polym.Phys., 28 (1990) 2057
  - (5) G.K. Fleming, W.J. Koros, Dilution of substituted polycarbonates caused by high pressure carbon dioxide sorption, J.Polym.Sci., Polym. Phys., 28 (1990) 1137
  - (6) Y. Kamiya, Y. Naito, K. Mizoguchi, Sorption and partial molar volume of gases in polybutadiene, J.Polym. Sci., Polym. Phys., 27 (1989) 2243-2250
  - (7) H. Funke, Sorption von Reingasen in Polymeren und an Zeolithen bei Drücken bis 70 bar, Ph.D. Thesis, 1991, University of Heidelberg, Germany

## Appendix B

### Fitted Parameters for the ESCFH-Model of Bitter

polymer	Tg	V(CO <sub>2</sub> )	Henry Coeff.	error Hi	Bi	error Bi	reference
6FDA-SDA	302	13.9	8.43	0.6	-43.8	2.8	*
6FDA-MDA	330	15.5	5.12	0.2	-30.7	1.3	*
6FDA-44ODA	289	13.4	7.53	0.6	-52.9	1.5	*
6FDA-34ODA	267	14.1	8.15	0.8	-43.3	3.8	*
6FDA-DAF	401	11.2	8.59	0.4	-26.8	1.5	*
6FDA-4PDA	364	8.7	12.71	1.3	-36.1	3.7	*
6FDA-34PDA	313	11.2	9.6	1.3	-46.6	7.3	*
6FDA-3PDA	328	14.3	7.83	0.8	-49.6	4.2	*
6FDA-NDA	416	8.5	13.76	0.78	-52.4	3.1	*
PDMS	-123	49.4	0.128				*
EPDM	-46	20.6	0.56				*
SMA	163	11.9	2.26		-95.3		*

(\*) our experiments

**Table B1.** Model parameters for the ESCFH-model of Bitter determined from our sorption experiments

polymer	Tg	V(CO <sub>2</sub> )	Henry Coeff.	error Hi	Bi	error Bi	reference
PSF	186	13	5.25	0.27	-80.93	3.5	1
PH	94	20.2	1.98	0.05	-90.5	2.3	1
PEI	215	14.6	8.85	0.5	-81.9	3.1	1
PC	150	15.9	4.73	0.2	-58.7	2.23	1
PA	184	15.8	5.21	0.14	-65.3	1.6	1
PSF	186	13	4.87	0.2	-66.7	2.6	2
TMPSF	242	11	7.65	0.22	-94.4	2	2
DMPSF	180	13	4.37	0.13	-90.98	2.5	2
DMPSF-Z	197	12	4.77	0.17	-92.22	2.8	2
PET	69	18.9	2.28				3
PPO	210	14.8	6.9	0.17	-40.6	1.2	4
PPO(BR)(36)	233	13.9	9.3	0.3	-47.4	1.5	4
PPO(BR)(91)	262	12.9	11.8	0.4	-54.1	1.85	4
6FDA-CDA	235	13.8	5.62	0.4	-49.1	4.51	5
6FDA-pAPPS	269	12.6	5.68	0.4	-45.4	4.6	5
6FDA-mAPPS	184	15.9	3.89	0.3	-65.9	6.1	5
6FDA-pAPPP	253	13.2	4.18	0.25	-50.1	4.8	5
PMDA-mAPPS	193	15.5	2.01	0.1	-31.5	4.3	5
CA(1.75)	205	15.0	2.75	0.15	-31.8	4.1	6
CA(2.45)	187	15.7	3.92	0.16	-20.7	1.9	6
CA(2.84)	185	15.8	3.46	0.15	-11	1.8	6
PVC	75	21.3	1.88		-40.6		7
NBPC	235	13.8	5.16	0.26	-48.6	3.22	8
PBZ	185	15.8	3.46	0.08	-58.9	1.76	8
BPBZ	164	16.7	3.62	0.16	-51.7	3.3	8
PEMA	69	21.6	2.18	0.01	-6.3	0.26	9
PMMA	120	18.9	2.85	0.11	-30.7	1.9	9
PS acetoxoy	126	18.6	2.16	0.08	-16.8	1.8	10
PS methoxy	105	19.6	1.37	0.05	-19.2	2.3	10
HFPC	172	16.4	6.86	0.3	-36.1	1.4	11
PVB	66	21.8	4.04	0.11	-20.3	0.8	12
PVBu	51	22.7	2.83	0.04	-14.1	0.4	12
PPha-tere	299	11.6	12.9	0.82	-51.5	3.1	13
PPha-1/1	279	12.3	12.45	0.8	-52	2.9	13
PPha-iso	249	13.3	11.5	0.8	-49.5	3.2	13
PS	100	19.9	1.74	0.05	-46.3	2.5	14
SMMA80	98	20.0	2.04	0.06	-46.6	2.13	14
SMMA40	102	19.8	2.45	0.1	-33	2.2	14
SMMA10	105	19.6	2.89	0.09	-22.6	1.3	14
PMMA	106	19.6	3.11	0.08	-19.2	1.04	14
PTMSP	230	14.0	7.71	0.4	-7.3	0.35	15
PMA	18	24.8	1.98				16
PMA 25/75	-2	26.2	1.71				16
PMA 50/50	-15	27.1	1.37				16
PMA 75/25	-20	27.5	1.15				16
PECH	-22	27.7	0.95				16
LDPE	-125	45.0	0.24				17
Perbunan 18	-46	29.5	1.01				18 (*)
Perbunan(Ger)	-36	28.7	1.08				18 (*)
Hycar 25	-31	28.3	1.14				18 (*)
Hycar 15	-26	28.0	1.26				18 (*)

(\*) Tg interpolated from ref. (19); solubility interpolated at T=35°C from temperature dependent solubilities

Table B2. Model parameters for the ESCFH-model determined from reference sorption data



- (1) T.A. Barbari, W.J. Koros, D.R. Paul, Gas sorption in polymers based on bisphenol-A, *J. Polym. Sci., Polym. Phys.*, 26 (1988) 729
- (2) J.S. McHattie, W.J. Koros, D.R. Paul, Gas transport properties of polysulphones: 1. Role of symmetry of methylgroup placement on bisphenol rings, *Polymer* 5 (1992) 840
- (3) Y. Kamiya, Y. Naito, K. Mizoguchi, Sorptive dilation of polysulfone and poly(ethylene terephthalate) films by high pressure carbon dioxide, *J. Polym. Sci., Polym. Phys.*, 26 (1988) 159
- (4) R.T. Chern, F.R. Sheu, L. Jia, V.T. Stannett, H.B. Hopfenberg, Transport of gases in unmodified and arylbrominated 2,6-dimethyl-1,4-poly(phenylene oxide), *J. Membrane Sci.*, 35 (1987) 103
- (5) T. Hirose, Y. Mi, S.A. Stern, A.K. St. Clair, The solubility of carbon dioxide and methane in polyimides at elevated pressures, *J. Polym. Sci., Polym. Phys.*, 29 (1991) 341
- (6) A.C. Puleo, D.R. Paul, The effect of degree of acetylation on gas sorption and transport behaviour in cellulose acetate, *J. Membrane Sci.*, 47 (1989) 301
- (7) M.J. El-Hibri, D.R. Paul, Effects of uniaxial drawing and heat treatment on gas sorption and transport in PVC, *J. Appl. Polym. Sci.*, 30 (1985) 3649-3678
- (8) J.S. McHattie, W.J. Koros, D.R. Paul, Effect of isopropylidene replacement on gas transport properties of polycarbonates, *J. Polym. Sci., Polym. Phys.*, 29 (1991) 731-746
- (9) J.S. Chiou, D.R. Paul, Gas sorption and permeation in poly(ethyl methacrylate), *J. Membrane Sci.*, 45 (1989) 167-189
- (10) A.C. Puleo, N. Muruganadam, D.R. Paul, Gas sorption and transport in substituted polystyrenes, *J. Polym. Sci., Polym. Phys.*, 27 (1989) 2385
- (11) G.K. Fleming, W.J. Koros, Dilatation of substituted polycarbonates caused by high pressure carbon dioxide sorption, *J. Polym. Sci., Polym. Phys.*, 28 (1990) 1137
- (12) Y. Kamiya, T. Hirose, K. Mizoguchi, K. Terada, Sorptive dilation of poly(vinyl benzoate) and poly(vinyl butyral) by carbon dioxide, *J. Polymer Sci., Polym. Phys.*, 26 (1988) 1409
- (13) F.R. Sheu, R.T. Chern, Effects of packing density on the gas transport properties of poly(phenolphthalein phthalate)s, *J. Polym. Sci., Polym. Phys.*, 27 (1989) 1121-1133
- (14) P.C. Raymond, D.R. Paul, Sorption and transport of pure gases in random styrene/methyl methacrylate copolymers, *J. Polym. Sci., Polym. Phys.*, 28 (1990) 2079
- (15) N.A. Plate, A.K. Bokarev, N.E. Kaliuzhnyi, E.G. Litvinova, V.S. Khotimskii, V.V. Volkov, Y.P. Yampolskii, Gas and vapor permeation and sorption in PTMSP, *J. Membrane Sci.*, 60 (1991) 13-24
- (16) J.S. Chiou, W.J. Barlow, D.R. Paul, Sorption and transport of gases in miscible poly(methyl acrylate)/poly(epichlorhydrin) blends, *J. Appl. Polym. Sci.*, 30 (1985) 1173-1186

- (17) Y. Kamiya, T. Hirose, K. Mizoguchi, Dilation of polyethylene by sorption of carbon dioxide, *J. Polym. Sci., Polym. Phys.*, 24 (1986) 2107
- (18) G.J. von Amerongen, Influence of structure of elastomers on their permeability to gases, *J. Polym. Sci.*, 5(3) 1950 307-332
- (19) H. Nijhuis, Removal of trace organics from water by pervaporation, Ph.D. Thesis, 1990, University of Twente

## Chapter 5

# Relaxation Phenomena in Dense Gas Separation Membranes

### 5.1. Introduction

In chapter 4 it has been demonstrated that dilation of a polymer matrix can be related to the polymer chain flexibility. Furthermore, using Bitter's elastic strain corrected Flory-Huggins model [1] a relation could be presented that shows a decreasing Henry coefficient with increasing chain flexibility. This elastic strain corrected Flory-Huggins model assumes areas of local order as mutual, physical crosslinks. However, the polymer chains are not chemically crosslinked in these areas and therefore may be subject of alteration in the case of large swelling stresses. In this chapter, experiments will be presented which were mostly carried out at high penetrant concentrations in order to develop a better understanding on swelling induced morphology alterations. These alterations can be observed as time-dependent polymer characteristics and can be generally covered by the technical term "relaxation phenomena". Relaxation is used in the sense of Van Krevelen [2] meaning that "relaxation is the time-dependent return to an equilibrium (or to a new equilibrium) after a disturbance".

### 5.2. Relaxational Permeation

Characterization of the transport properties of tailor-made polymers by means of permeation experiments is mostly carried out at very mild conditions, *i.e.*, at very low concentrations or pressures ( $p < 10$  bar). At these low concentrations, the presence of the penetrant molecules in the polymer does not affect the polymer morphology. The permeability of an inert gas through a rubbery polymer is normally independent of the penetrant concentration or pressure, respectively. At relatively moderate pressures the permeability for a penetrant through a glassy polymer decreases with increasing upstream pressure, hence with increasing concentration. This behaviour is well-known for glassy polymers because the solubility decreases more strongly with increasing pressure than the diffusivity increases. In the following, only glassy polymers will be considered. Permeation

experiments carried out for the permeation of  $\text{CO}_2$  through the polyimide 6FDA-MDA shows this typical behaviour; a decrease in the permeability from around 26 Barrer at 3 bar to 23.2 Barrer at 10 bar upstream pressure can be observed.

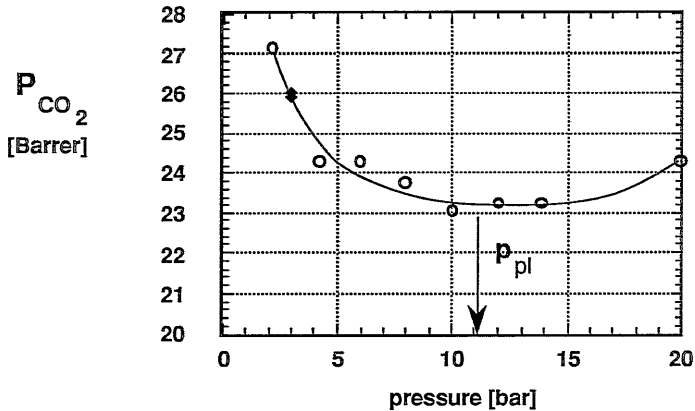


Figure 1. Permeation of  $\text{CO}_2$  through 6FDA-MDA at  $T=32^\circ\text{C}$  depending on the upstream pressure; the full dot represents a film from another synthesis batch (value taken from [3])

However, increasing the upstream pressure further reveals a peculiar phenomenon that also has previously been observed for other polymers [4,5]. The permeability increases again with increasing upstream pressure. The minimum pressure above which the permeability increases is called the plasticization pressure  $p_{pi}$ . In literature, plasticization in the context of mass transport through polymers is often used as a term that basically covers all unexpected transport phenomena which are difficult to interpret. It is furthermore reported that the permeability above the plasticization pressure is time-dependent as shown in figure 2.

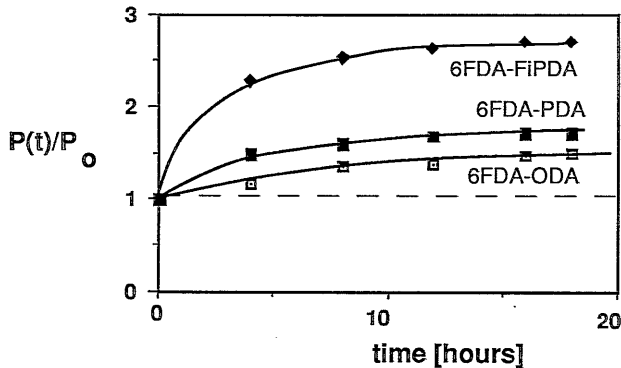


Figure 2. Relative time-dependent permeation of  $\text{CO}_2$  for different polyimides at  $T=25^\circ\text{C}$  and  $p=30$  bar [6]

Similar results were obtained by Puleo *et al.* [4,5] for the permeation of CO<sub>2</sub> through cellulose acetate and modified polystyrene films. However, no detailed analysis of the time-dependent permeation has been carried out until now.

For this purpose, a series of different experiments were carried out with the polyimide 6FDA-MDA. First, the permeabilities shown in figure 1 were measured as a function of time. The experimentation time was generally 24 hours. Indeed, it could be observed that the permeability becomes a function of time above the plasticization pressure. A typical experimental result is shown in figure 3 for a pressure step from 17 to 20 bar. In order to normalize the extent of permeability increase, the actual permeability  $P(t)$  is divided by  $P_0$  which is the permeability when the constant concentration profile is reached after an initial instationary period (time-lag). To eliminate any thickness dependence in the mass transport analysis, the experimental time was divided by the squared membrane thickness. A logarithmic time axis was chosen to emphasize the small changes in permeability at long experimentation times.

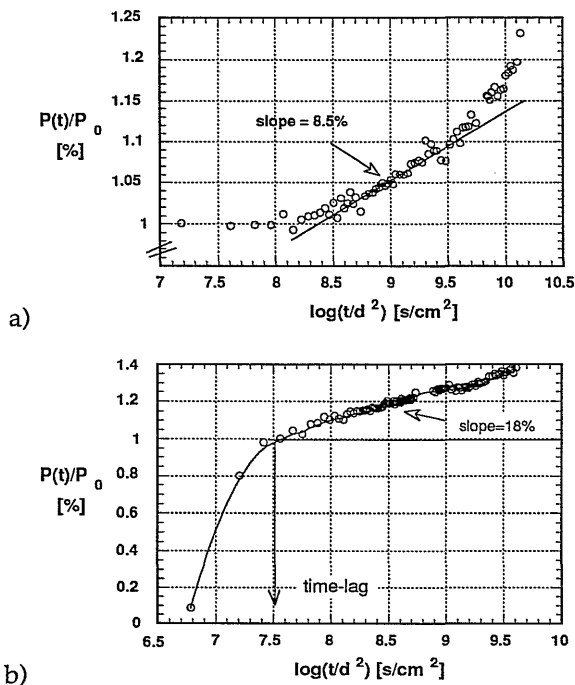


Figure 3. Relative permeation of CO<sub>2</sub> through 6FDA-MDA depending on the time (a) for a pressure step from 17 to 20 bars (b) for a pressure step from 0 to 20 bars at  $T=32^\circ\text{C}$

For an upstream pressure step from 17 to 20 bar, shown in figure 3a, the permeability is almost constant for  $\log(t/d^2)$ -values of 7 to 8. For longer times the permeability increases resulting in a relative permeability increase of around 8.5% per decade. Such time dependent changes of any polymer property will be described in the following as a relaxational phenomenon which result from the penetrant induced dilational stresses exerted on the polymer matrix. Regarding the results in figure 3a one has to keep in mind that this film was used already at lower pressures and cannot be considered as virgin. In order to evaluate this effect of film history, a virgin film was also used for a pressure step from 0 to 20 bars. The result is shown in figure 3b.

Figures 3a and b show clearly that the results for experiments carried out at the same upstream pressure, may differ considerably. For the virgin film a drastic increase in the relative permeability can be observed ranging from 0.1 to 1. This increase can be related to the phenomenon of time-lag due to the build-up of the concentration profile in the membrane. In the case of a polymer which is not "plasticized", no relaxational response of the permeability can be measured after the time-lag and the permeability then stays constant. (This was experimentally verified for pressures lower than 11 bar.) However, for a pressure step from 0 to 20 bars the permeability increases linearly on a logarithmic time scale after passing the time-lag. This *linear* increase cannot be found in the experiment for a pressure step from 17 to 20 bar shown in figure 3a. In this case, the permeability stays constant in the early stages and then increases steadily.

Comparing the slope of the permeability as a function of time, one also can observe significant differences: 8.5% (decade 8.5 to 9.5) for the pressure step from 17 to 20 bar and 18 % (decade 7.5 to 9.5) for the pressure step from 0 to 20 bar. In order to get more insight in these discrepancies, new experiments were carried out with virgin films at different upstream pressures. The main characteristic, namely the slope of the relaxational permeability curve, is listed together with the upstream pressure in table 1. The curves obtained show in general the same characteristic shape as shown in figure 3b.

*Table 1. Slope of the time-dependent relative permeability of CO<sub>2</sub> in 6FDA-MDA for pressure steps from zero to different upstream pressures*

p [bar]	slope[%]
14	5.3
20	18
26	27

From these experiments it can be concluded that the relaxation processes occurring in the polymer matrix become faster as the upstream pressure, and hence the penetrant concentration, is increased. Since no equilibrium value is reached within the experimentation time, no conclusion can be drawn about the absolute value of the permeability increase due to relaxations. The fact that relaxation processes become more pronounced at higher pressures fits with the molecular picture developed in chapter 4. The swelling stresses in the polymeric matrix induced by the sorbed penetrant molecules become obviously larger as the penetrant concentration increases leading to more pronounced relaxation processes. At this point, however, it is not possible to define the exact nature of these relaxation processes. Some slow long-chain motions in the amorphous part are possible as well as alterations of the local orderings. Even slow long-chain motions in the amorphous part of the polymer matrix *induced* by alterations of local orderings are possible. To obtain more information about this question, spectroscopic experiments like IR-, Raman- and NMR-spectroscopy should be very valuable.

The question remains why the shape of the curve for a pressure step from 17 to 20 bar deviates from the one for a pressure step from 0 to 20 bar and why the slope of the relaxational permeability is considerably smaller for the former. The answer can be found in the experimental protocol. The membrane which has been investigated for the small pressure step (17 to 20 bar) has already had a certain relaxation history at pressure steps which ended at 14 and at 17 bar. However, this additional time is not considered when resetting the time to zero for each new experiment at a higher pressure. This problem will be worked out in more detail below.

Any property  $y$  which is a function of time obeying equation 1

$$y(t) = a t + b \quad (1)$$

can be shifted along the time axis into a new time frame  $t' = t - t_0$  obeying equation 2

$$y(t' + t_0) = a (t' + t_0) + b = a t' + b' \quad (2)$$

without changing its slope  $a$ . Only the intersection with the  $y$ -axis varies upon shifting. This is not valid for a property that changes linearly with the *logarithm* of time.

For an untreated or unused polymer film, the time  $t=0$  is in fact the beginning of the experiment. For films which have been characterized by consecutive additional pressure steps above the plasticization pressure, the time  $t=0$  is not known at all. One may think that the time at which the membrane was characterized at lower

pressures must be added to the experimentation time. However, this neglects the fact that the penetrant induced stresses are smaller at smaller pressures compared to the actual experimental situation.

Assuming the general validity of a linear relationship between the permeability and the logarithmic time, only a certain percentage of the experimentation times at lower pressures was added to the actual experimental time until a linear relation was obtained. The results of this shifting procedure are shown in figure 4 a and b. The first time dependent permeation experiment for a virgin membrane was carried out at 14 bar upstream pressure. Consecutive runs were carried out at 17 and 20 bar. The data for the permeabilities at 17 bar upstream pressure in figure 4a take 30% of the experimentation time at 14 bar into account. The obtained slope in figure 5a for the relaxational permeability is 9.5 % per decade.

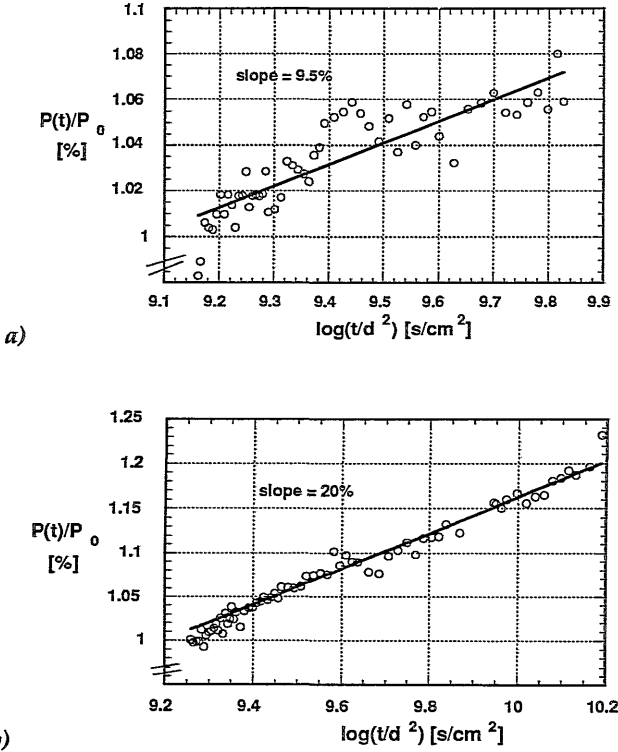


**Figure 4.** History corrected time-dependent permeation of CO<sub>2</sub> through a 6FDA-MDA membrane which had already a permeation history at 14 bar upstream pressure; a.) additional pressure step from 14 to 17 bar; b.) consecutive pressure step from 17 to 20 bar



For the experiment at 20 bar upstream pressure, the experimental time for the 14 bar experiment was taken into account for 10% and the 17 bar experiment for 25%. The obtained slope in figure 4b for the relaxational permeability is 20%. (The uncorrected curve is shown in figure 3). At this point the choice of the absolute value of shifting the starting point appears rather arbitrary; however the extent of shifting has to fulfil a few general conditions as shown later in this chapter.

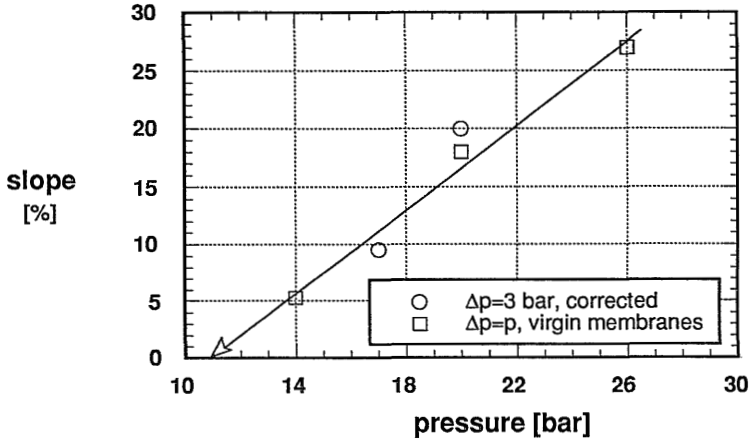


Figure 5. Slope of the time-dependent permeability of  $\text{CO}_2$  through 6FDA-MDA at different upstream pressures for virgin membranes and membranes with considered history

The absolute values of the percentage of experimentation times considered in the film history is chosen in such a way that the slope of the corrected permeability approaches the slope of the time-dependent permeability of a virgin membrane. The results of this data treatment are shown in figure 5. One can conclude from this figure that there will be no time-dependent permeation for pressures below around 11 bar upstream pressure since at  $p=11$  bar the extrapolated slope will be equal to zero. This indeed agrees well with the experiments shown in figure 1. As long as in this figure the permeability decreases with increasing pressure no time-dependence can be observed. As soon as the permeability increases with increasing upstream pressure, mass transport across the membrane is time-dependent.

The data treatment given above can be defined mathematically: the time-dependent permeability of a virgin film at a certain pressure  $p$  can be expressed for times larger than the time-lag (see figure 3b) as

$$\frac{P(p,t)}{P_0(p)} = 1 + a \log\left(\frac{t}{d^2}\right) \quad (3)$$

Considering  $m$  previous permeation experiments at lower pressures  $p_m$  the

experimentation time  $t$  for the permeation experiment at  $p > p_m$  can be corrected in such a way that

$$\frac{P^*(p, t^*)}{P_0^*(p)} = 1 + a \log \left( \frac{t + \sum_{n=1}^m x_n t_n}{d^2} \right) \quad (4)$$

and the slopes  $a$  of both figures are equal.  $x_n$  is the percentage of the experimentation time  $t_n$  used for the experiment at the pressure  $p_n$ . No definite statement can be made at this moment regarding the absolute values of the permeabilities  $P_0(p)$  and  $P_0^*(p)$  which are not influenced by relaxation phenomena. However, since the permeability alterations seem to stem from irreversible or very slowly reversible morphology alterations, different experimental procedures in the sequence of pressure and vacuum application on the upstream side of the membrane may cause variations in the initial values of  $P_0$ .

The sum of the effective experimentation times  $x_n \cdot t_n$  of low pressure experiments will be called "aging time". This aging time has no relation with the "physical aging time" introduced by Struik [7]. Struik defines physical aging as a gradual continuation of the glass formation in the vicinity below the glass transition temperature stemming from the non-equilibrium of the supercooled glass. The aging phenomena considered here are clearly of a different nature: sorbed penetrant molecules dilate the polymer matrix and the stresses exerted by the penetrant molecules can be so large that any instantaneous, elastic dilation response upon sorption may change into a relaxational dilation response which goes along with a relaxational permeability. This hypothesis will be discussed in detail in the second part of this chapter.

Before doing so, the physical significance of the aging time and a number of conditions linked to the aging time must be discussed:

- the aging times must be chosen such that the slopes of the time-dependent permeability on a logarithmic time-scale are equal for the virgin and the aged membrane
- for a film history of only one experimental run at an upstream pressure lower than the actual experimental upstream pressure, the aging time  $x_1 \cdot t_1$  cannot be equal to or larger than the actual experimentation time  $t_2$ 

$$x_1 \cdot t_1 < t_2$$
- for a film history with various consecutive pressure steps and equal experimentation times per step, the aging time at a low pressure must be smaller than the aging time at any higher pressure. This is due to the fact that swelling stresses are smaller at lower pressures than at higher pressures

$$x_n * t_n < x_{n+m} * t_{n+m} \text{ if } t_n = t_{n+m}$$

Additionally, one may say that under the conditions of pressure steps causing *linearly* related swelling stress steps in the polymer matrix and equal experimentation times  $t$ , the aging time can be calculated from

$$\sum_{n=1}^m x^n t .$$

The physical significance of the aging time for permeation was tested by the following experiment: the membrane which was used for permeation experiments at 14, 17 and 20 bar upstream pressure was left for four weeks at ambient atmosphere. This membrane showed after the permeation test at 20 bar a total aging time of 32 hours. This aging time is the sum of 10% of the experimentation time at 14 bar, plus 25% of the experimentation time at 17 bar upstream pressure plus the full experimentation time at 20 bar. A new permeation experiment was carried out for a pressure step from zero up to 20 bar after being four weeks at ambient atmosphere. One would expect that the aging time which actually is a measure for the extent of penetrant induced swelling stresses, would decrease because the internal stresses vanish as the CO<sub>2</sub> is desorbed at ambient atmosphere. The polymer matrix can consolidate back into the direction of a morphology similar to the virgin membrane. This is indeed the case: additionally to the experimentation time for the new experiment an aging time of 11 hours must be added (obtained from the above described correction procedure). This is considerably lower than the aging time of 32 hours. The concept of the aging time does have significance. However, the aging time is not predictable beforehand, but has to fulfil a number of conditions. The decrease in aging time may be correlated to the aging time as Struik understands it. This type of aging is experimentally accessible by permeation experiments with a highly permeable, inert gas like helium. The aging behaviour of unswollen membranes has already been pointed out by Pinnau [8].

### 5.3. Relaxational Dilation

In this paragraph time-dependent dilation experiments will be presented. First, a number of peculiar experimental details will be shown which will then be interpreted on the basis of a new qualitative model. In chapter 4 dilation experiments were described which have been carried out taking pressure steps of 3 bar mostly. Within an experimentation time of, for instance, 5000 seconds dilation equilibrium was reached for pressures smaller than 15 bar and a polymer film thickness of around 75  $\mu\text{m}$ . Because this time period had to be specified in the software for each pressure step, all experiments did last this specific time but dilation equilibrium had already been reached earlier. At higher pressures however,

equilibrium could not be reached within the 5000 seconds. In order to demonstrate this non-equilibrium, the relative dilation as a function of time at different pressures is shown in figure 6.

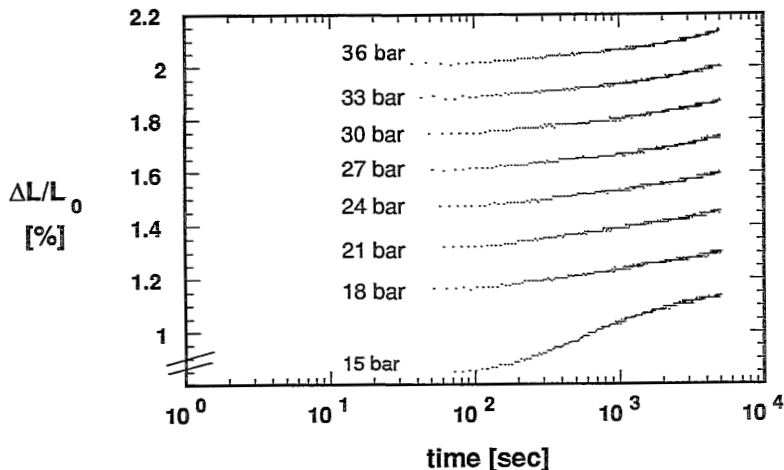


Figure 6. Consecutive dilation experiments at pressures  $p \geq 15$  bar for the system  $\text{CO}_2$ -6FDA-DAF at  $T=25^\circ\text{C}$

The dilation experiment at  $p=15$  bar is the last example of the stepwise increased pressure range where an equilibrium is reached within the experimentation time. The dilation kinetics at higher pressures is totally different in shape compared to the kinetics at 15 bar or 3 bar (see figure 22 in chapter 3). The fact that equilibrium at high pressures is not reached is somewhat unexpected. One would expect that the equilibrium is reached more quickly at high pressures, since the diffusion coefficient is highly concentration dependent. An interpretation of these non-equilibria will be given later in this chapter. Before that, a number of other experimental observations will be described.

For the experiments at pressures larger than 15 bar the last data point at  $t = 5000\text{s}$  is assumed as a pseudo-equilibrium. Using these pseudo-equilibrium data, the dilation isotherm for the sorption of  $\text{CO}_2$  in 6FDA-DAF can be plotted. Besides the dilation experiments in pressure steps of 3 bar, consolidation experiments with decreasing pressure steps of 10 bar were also carried out. The "equilibrium" values of all these experiments are plotted in figure 7.

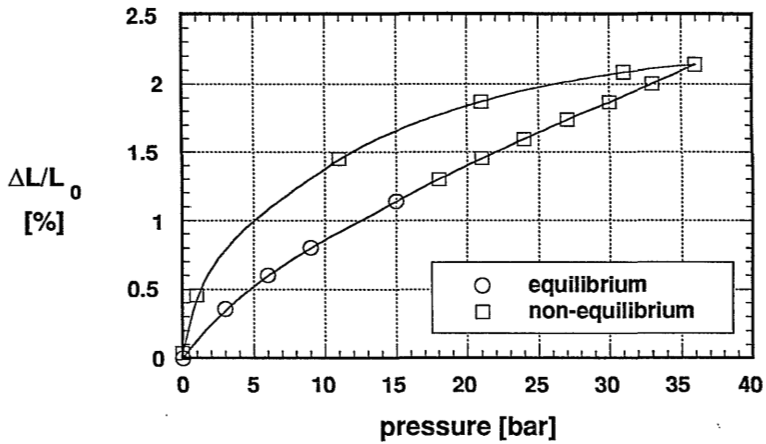


Figure 7. Dilation and consolidation isotherms for the system of  $\text{CO}_2/6\text{FDA-DAF}$  at  $T=25^\circ\text{C}$ ; equilibration times are 5000s for dilation and 8000s for consolidation

In figure 7 the consolidation process upon desorption does not follow the dilation isotherm but shows a hysteresis where data points for consolidation fall clearly above the dilation isotherm. This phenomenon has also been measured for the polyimide PIXU 218 but data are not shown here (for the chemical structure see figure 3.8). Several authors mentioned already this dilation hysteresis [9,10] and it can be considered as a general behaviour of glassy polymers. More information can be obtained from the consolidation kinetics shown in figure 8.

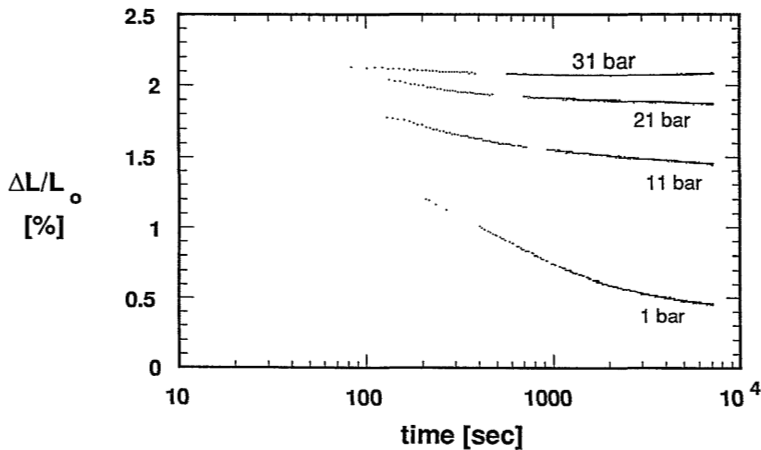


Figure 8. Consolidation kinetics for the desorption of  $\text{CO}_2$  from 6FDA-DAF at  $T=25^\circ\text{C}$  in pressure steps of 10 bar

A pressure decrease from 36 to 31 bar practically does not show any consolidation. A pressure decrease from 31 to 21 bar shows significantly less consolidation than the pressure decrease from 11 to 1 bar. Evacuation at  $p=0$  bar for 7000 seconds results in a residual dilation value of 0.19% (not shown) as a pseudo-equilibrium; further evacuation for 72 hours decreases this residual dilation down to 0.05%.

In figure 8 it seems that the consolidation kinetics at lower pressures are faster than at higher pressures. However, this conclusion must not be drawn because only the relative consolidation  $\varepsilon_{rel}^-(t, p_1)$  defined as

$$\varepsilon_{rel}^-(t, p_1) = \frac{\Delta L(t, p_1) - \Delta L_{cd}(p_1)}{\Delta L_{cd}(p_2) - \Delta L_{cd}(p_1)} \quad (5)$$

with

$$p_2 > p_1$$

can give valuable information about the *kinetics* of the consolidation process. For this purpose the relative consolidation  $\varepsilon_{rel}^-(t, p_1)$  as defined in equation 5 is plotted versus the time in figure 9. Only small times are shown to point out differences between the consolidation kinetics. From the three different pressure steps shown in figure 9, one can conclude clearly that the consolidation kinetics is faster at higher pressures or concentration, respectively.

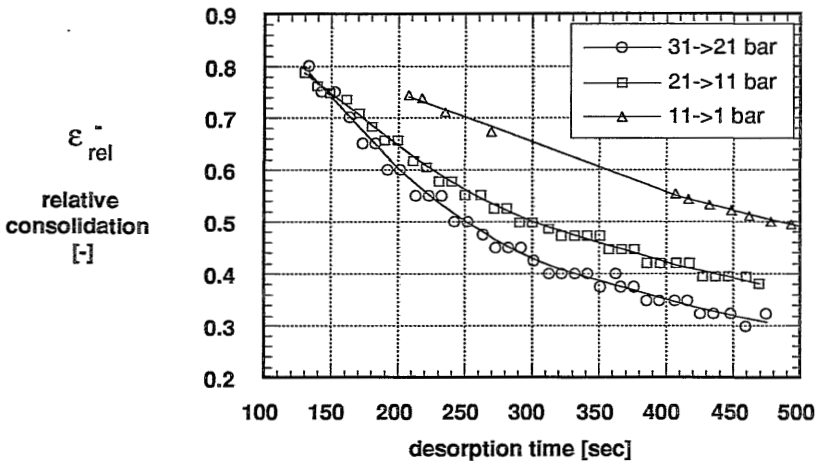


Figure 9. Relative consolidation kinetics at different pressure levels for the desorption of  $CO_2$  at  $T=25^\circ C$

The experiments presented on 6FDA-DAF/ $\text{CO}_2$  at  $T=25^\circ\text{C}$  lead to the following conclusions:

- 1) A considerable hysteresis behaviour can be observed between dilation and consolidation isotherms. Consolidation isotherms lie always above dilation isotherms.
- 2) No distinct time-dependent regions can be observed in the consolidation kinetics; instead, the curves are rather smooth.
- 3) The consolidation kinetics at higher penetrant concentration is faster compared to that at low penetrant concentrations.
- 4) The amount of residual dilation after dilation experiments at high concentrations depends strongly on the time of evacuation after the experiment. The time-scale for these relaxational consolidation processes at "zero" penetrant concentration is much larger than the time-scale for the consolidation due to desorption of the penetrant molecules at higher pressures.

Similar dilation experiments with  $\text{CO}_2$  as a sorbing gas have been carried out with the polyimide 6FDA-MDA at  $T=35^\circ\text{C}$ . However, no desorption experiments were carried out. Instead, the dilation kinetics resulting from *incrementally* increasing pressure steps of 3 bar were compared with *integral* pressure steps from, for example, 0 to 20 bar. A result generally obtained for such an integral pressure step is shown in figure 10.

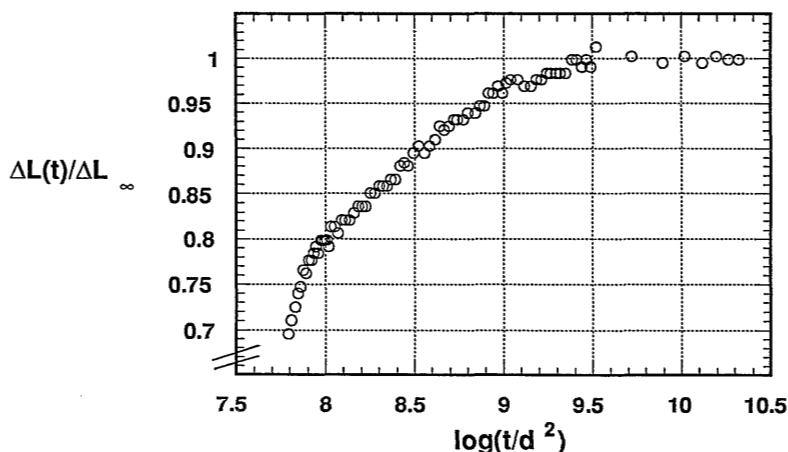


Figure 10. Dilation kinetics for the sorption of  $\text{CO}_2$  in 6FDA-MDA at  $T=35^\circ\text{C}$  for an integral pressure step from  $p=0$  bar to  $p=20$  bar

Different distinct regimes can be distinguished when plotting the relative length dilation versus a logarithmic time-axis. The time has been divided by the squared

membrane thickness in order to eliminate thickness effects for different polymer films. The first regime ( $\Delta L(t)/\Delta L_\infty < 0.78$ ) stands for the actual sorption process where the length increase of the sample follows the concentration in the middle of the film in time (see also figure 3.21 and 3.22). We will refer to this behaviour as Fickian and the relative amount of Fickian dilation will be called  $\phi_F$ . The Fickian dilation is followed by apparently two regimes which are considerably slower. The regimes will be called relaxational dilation regimes. The relative extent of these relaxation dilations will be called  $\phi_R$ . The last regime is actually the dilation equilibrium.

Similar dynamic responses have been observed by Berens *et al.* [11] for the weight gain in a sorption experiment of poly(vinylchloride) with different organic vapours like ethanol, acetone and vinylchloride. Berens *et al.* modelled their system phenomenologically by assuming that the total mass uptake consists of ordinary Fickian mass uptake and secondly of mass uptake due to relaxation.

$$M(t) = M(t)_F + M(t)_R \quad (6)$$

This approach can be transformed easily to dilation experiments:

$$V(t) = V(t)_F + V(t)_R \quad (7)$$

Assuming isotropic swelling with  $\varepsilon = \Delta L/L_0$

$$V = V_0 (1 + \varepsilon)^3 \quad (8)$$

and neglecting second order and third order terms at low relative dilation equation (7) can be transformed into

$$V = V_0 (1 + 3\varepsilon) \quad (9)$$

This proportionality means that instead of investigating the volume increase it is also valid to investigate the length increase without losing any significant information. This will be done in the following: normalizing the absolute length increase at a time  $t$  by the equilibrium length increase, equation 7 can be rewritten as

$$\frac{\Delta L(t)}{\Delta L_\infty} = \frac{\Delta L(t)_F}{\Delta L_\infty} + \frac{\Delta L(t)_R}{\Delta L_\infty} = \phi_F + \phi_R \quad (10)$$

Adapting the mathematical treatment of viscoelastic properties of polymers, the relative relaxational length increase can be written as a sum of phenomenological functions representing a distribution of first order processes with rate constants  $k_j = 1/\tau_j$  where  $\tau_j$  is the relaxation time.



$$\phi_R = \sum_{n=1}^{\infty} \phi_{R,n} \left( 1 - \exp\left(-\frac{t}{\tau_{Rn}}\right) \right) \quad (11)$$

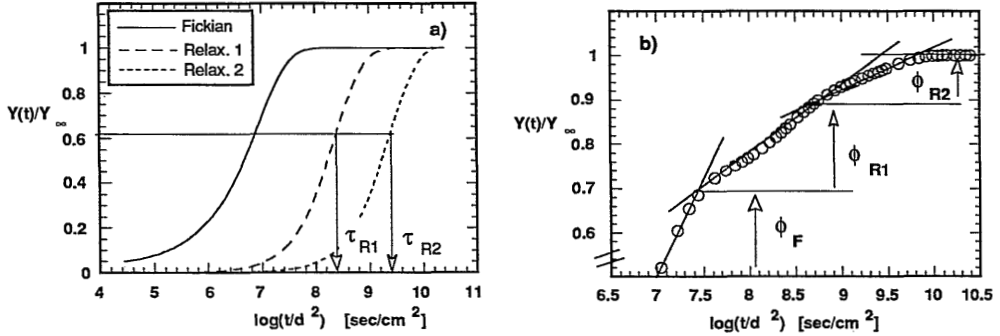


**Figure 11.** (a) Fickian length increase and two relaxational functions  $y(t)/y_{\infty}=1-\exp[-t/\tau]$  plotted versus the logarithmic, membrane thickness normalized time for different (membrane thickness normalized) relaxation times  $\tau_{R1}=2.5E8$  and  $\tau_{R2}=2.5E9$  s/cm<sup>2</sup> ( $d=60\mu\text{m}$ ); (b) Summation of percentages of the three functions according to the above described procedure ( $\phi_F=0.7$ ,  $\phi_{R1}=0.2$ ,  $\phi_{R2}=0.1$ ); data points are calculated, solid lines have no mathematical meaning but solely point out the three regimes

The mathematical treatment described above is shown in figure 11. The total relative dilation is equal to the sum of the Fickian and relaxational dilation regimes. In figure 11a, the relative Fickian dilation and two relaxational dilation kinetics are shown separately. The relaxation times for the latter two can be determined assuming that  $t=\tau_{Ri}$ ; the corresponding  $y$ -value equals  $Y(t)/Y_{\infty}=1-\exp\{-1\}=0.632$ . Therefore, the relaxation times can easily be determined by reading from the plot the corresponding time for  $Y(t)/Y_{\infty}=0.632$ . Figure 11b shows the fictitious case that the total length dilation consists of 70% Fickian, 20% of the first relaxational and 10% of the second relaxational dilation. The data points are calculated values. The solid lines point out the fact that the three regimes can be easily distinguished if a logarithmic instead of linear time-scale is chosen. Therefore, the only reason for the logarithmic time-scale is to *visualize and identify* the different regimes and to *simplify* the determination of the membrane thickness normalized relaxation times. In figure 12 the graphical procedure described above is applied to the data plotted in figure 10.

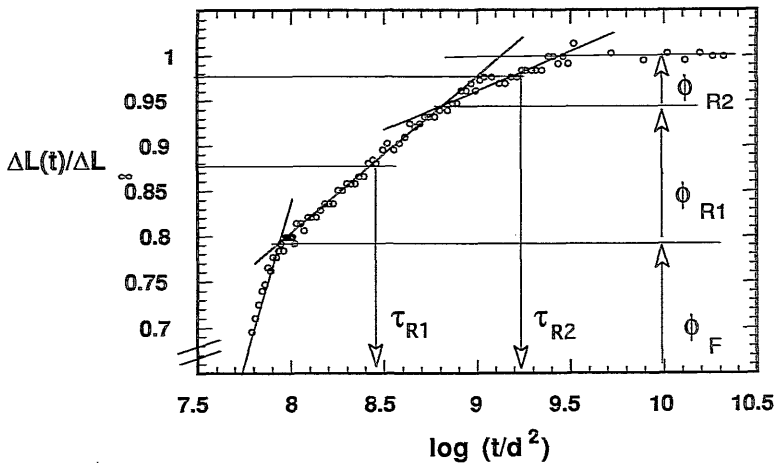


Figure 12. Graphical identification and quantification of different regimes in the experimental dilation kinetics for the sorption of  $\text{CO}_2$  in 6FDA-MDA at  $T=35^\circ\text{C}$  for an integral pressure step from  $p=0$  bar to  $p=20$  bar; relaxation times can be determined according to the procedure described in the text

The representation of the data by two relaxational functions are definitely sufficient and accurate. This has been verified by fitting experimental data for a number of different experiments numerically. Differences between fitted and graphically obtained relaxation times are smaller than 10%. Differences for the dilation fractions are smaller than 5%. Therefore, a tedious fit procedure for all experiments is not necessary because the determination of the model parameters from the figures is as accurate as the fitting procedure, but quicker.

An important question must be answered, before interpreting the experimental results presented until now and in the following paragraphs: the question arises whether the dilation at high pressure is or is not an *instantaneous* response following the sorption or, in other words, whether the dilation results directly represent sorption phenomena. In chapter 3 it has been shown for kinetic dilation experiments at low pressures that every sorbed molecule dilates the polymer instantaneously and to the same extent. This was additionally confirmed by cross-plotting sorption and dilation isotherms in chapter 4. At high pressures and especially for large integral pressure steps the sorption set-up used is not adequate to determine accurate sorption kinetics in the later stages of the sorption processes. At high pressures the two cells are going to act like a thermometer: any small temperature fluctuation between the two cells at high pressures will cause a pressure difference fluctuation. These fluctuations hardly effect the determination of the equilibrium concentration, but it makes the analysis of the sorption kinetics in the later stages difficult.

Unfortunately, no hard experimental evidence can be presented which supports or contradicts the hypothesis of instantaneous dilation upon mass uptake at high pressures. In earlier work [12] we had observed a still increasing volume of the polymer/penetrant system although mass uptake appeared to have reached equilibrium. On the other hand, similar sorption kinetics as the dilation kinetics presented here were also observed by Sanders [13] for the sorption of carbon dioxide in poly(ether sulfone).

In the following discussion it will be kept in mind that ideal Fickian sorption results in instantaneous dilation. Furthermore it will be assumed *that a time-dependent volume increase, hence volumetric relaxation processes, represent mass uptake due to relaxational processes occurring in the polymer matrix*. However, the time-dependence of the relaxational dilation and mass uptake processes do not have to be necessarily equal.

In the figures 13a and b, 14 and 15 results of kinetic dilation experiments are shown. The first column in figure 13 and 14 contains an identification code; the second column represents the conditions at which the experiments were carried out. Here, the time-axis runs vertically while the horizontal axis stands for the applied pressure. This second column represents therefore exactly the history of the polymer sample. The third column contains the actual experimental results in the same form as represented in detail in figure 15. Taking a resolution of two diodes for the line scan camera as the worst case, the accuracy for the relative length increase  $\Delta L(t)/\Delta L_\infty$  is  $1.2 \cdot 10^{-4}$ . The fourth column contains the fitting parameters. The relaxation times  $\tau_{Rn}$  were left out because no systematic trend between relaxation time and experimental conditions could be found. Instead, the first relaxation time  $\tau_{R1}$  scatters around  $2.5 \cdot 10^8$  s/cm<sup>2</sup> and the second one  $\tau_{R2}$  around  $2.5 \cdot 10^9$  s/cm<sup>2</sup>.

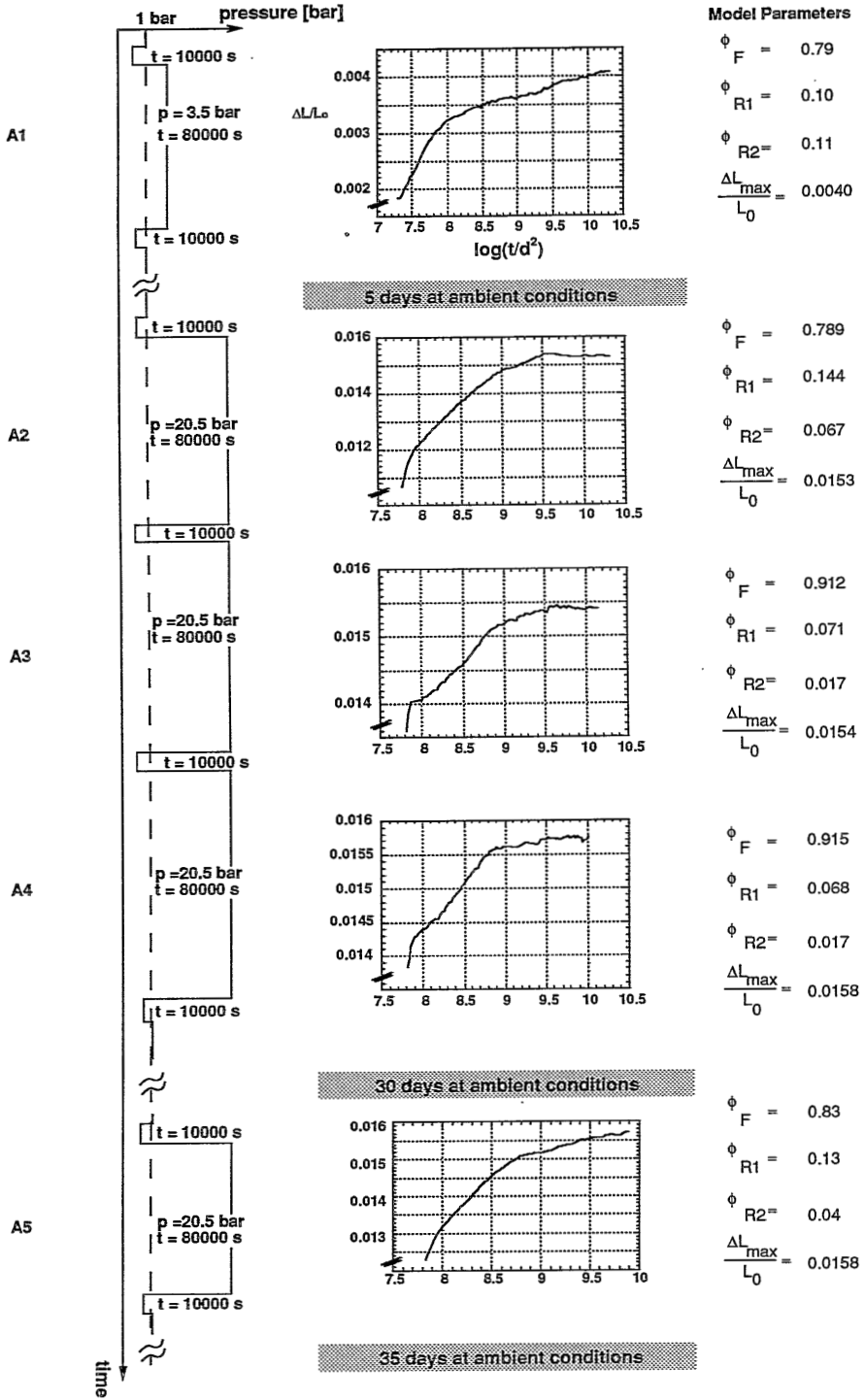


Figure 13a. Relaxational dilation experiments for the sorption of CO<sub>2</sub> in 6FDA-MDA at 35°C

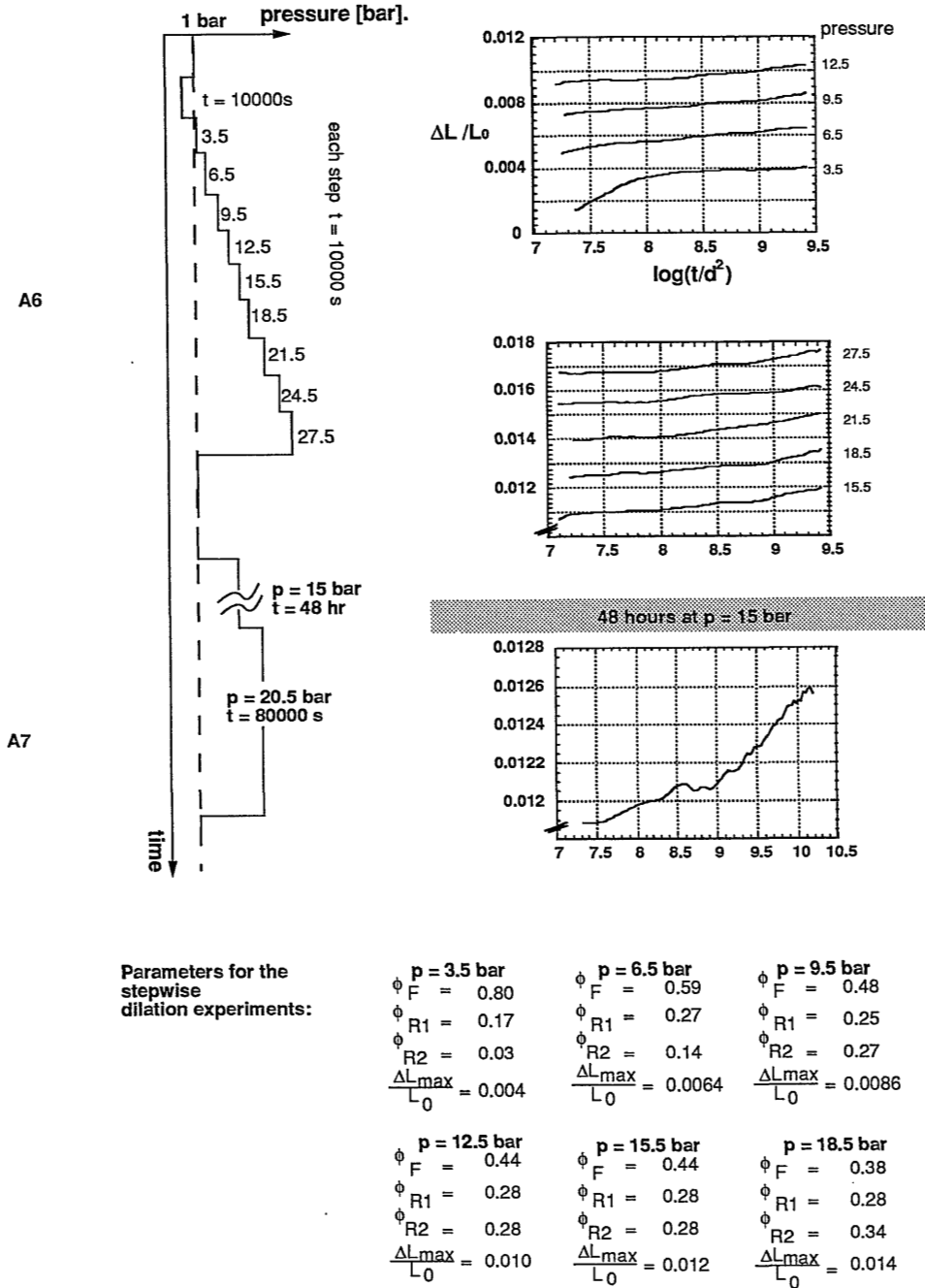


Figure 13b. Relaxational dilation of 6FDA-MDA by sorption of  $CO_2$  at  $35^\circ C$  (continuation of figure 13a)

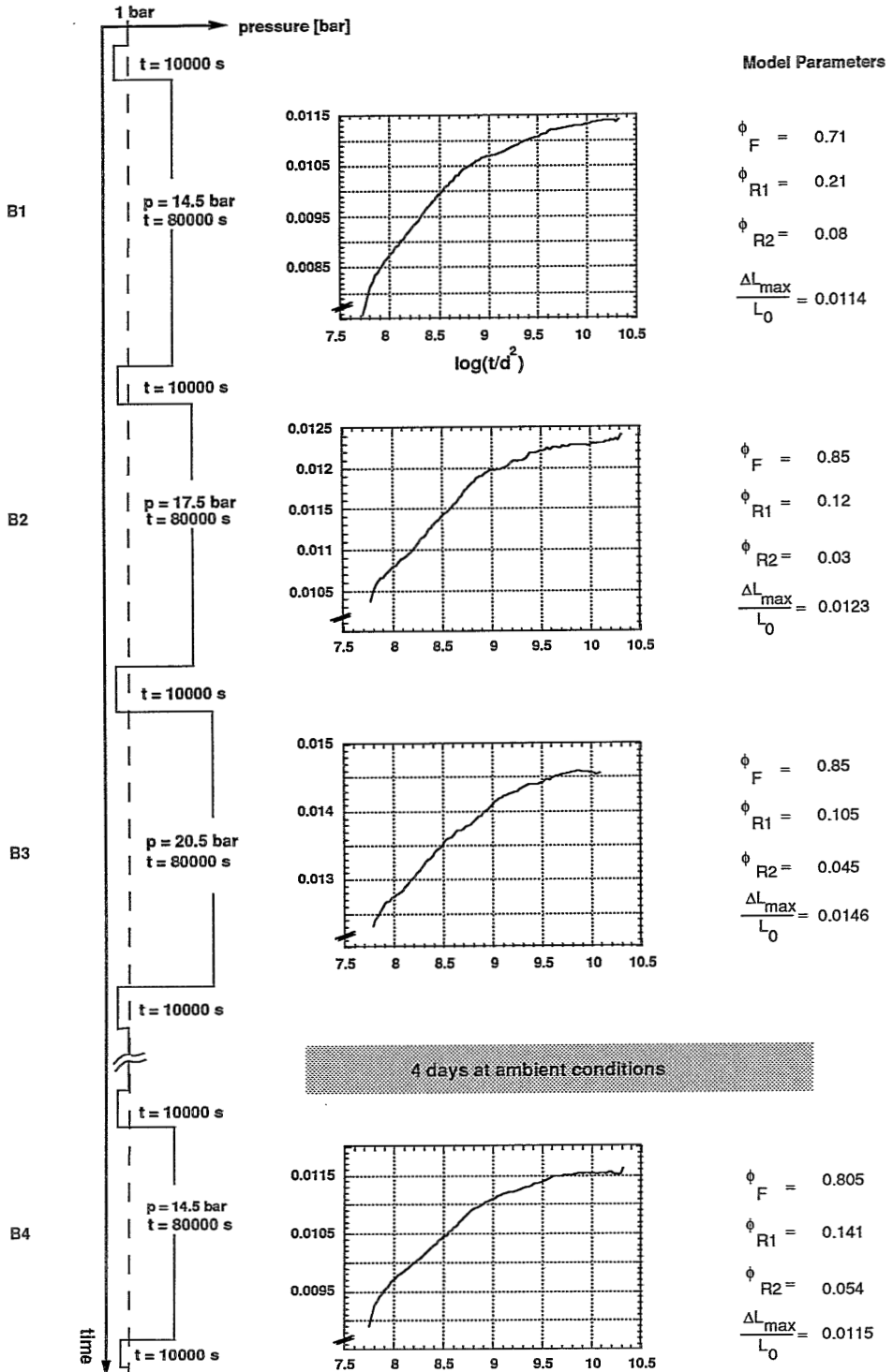


Figure 14. Relaxational dilation of a second sample of 6FDA-MDA by sorption of CO<sub>2</sub> at 35°C

The following trends can be found in the experiments presented for 6FDA-MDA/CO<sub>2</sub> at T=35°C:

- 1) The Fickian dilation fraction  $\phi_F$  of the experiments A2 to A5 shows a very pronounced influence of the swelling history. The results are summarized in table 2 and partly visualized in figure 15. The Fickian volume dilation fraction in a second experiment (A3) which follows briefly after the first one (A2) at the same pressure is considerably larger than the  $\phi_F$  in the first experiment. A third experiment does not show any further increase in  $\phi_F$  (A4). Leaving the sample for 30 days at ambient conditions results in a considerable decrease of  $\phi_F$  (A5) but with a value still larger than the initial one (A2).

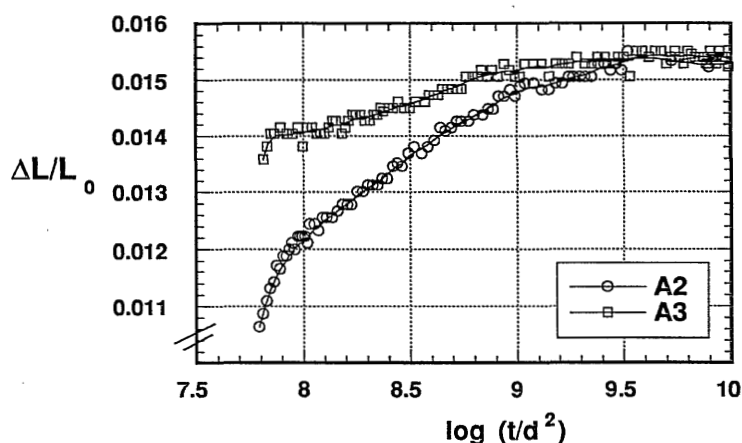


Figure 15. Direct comparison of the dilation kinetics for two consecutive runs (A2 and A3) for 6FDA-MDA at  $p=20$  bar and  $T=35^\circ\text{C}$ ; see figure 13a for further experimental details

Table 2. Fitting parameters and relative dilation for the system 6FDA-MDA for consecutive experiments at  $p=20$  bar and  $T=35^\circ\text{C}$

	A2	A3	A4	A5
$\phi_F$	0.79	0.91	0.92	0.83
$\Delta L_{\max}/L_0$	0.0153	0.0154	0.0158	0.0158

N.B.: Between A4 and A5 a different treatment was given (see text)

- 2) In table 2 the values for the relative length dilation at a constant pressure are also listed. It might seem that the relative length dilation increases slightly with the number of runs. But looking at the experiments B1 and B4 in figure 14 which are both carried out at  $p=14.5$  bar but which are different in their history shows no significant increase or conditioning effect.
- 3) A general trend can be observed in the shape of the curves for the dilation kinetics. If a dilation experiment is carried out quickly after the former one (A3 after A2; B2 after B1) a small horizontal part in the dilation kinetics curve can be observed right after the Fickian dilation part of the curve. This horizontal part lies exactly at that position of the time-scale where one would expect the equilibrium state for purely Fickian dilation.
- 4) For integral pressure steps the relaxation times  $\tau_{R1}$  and  $\tau_{R2}$  do not depend on the pressure and therefore not on the penetrant induced stress on the polymer matrix.
- 5) Above 18 bar no dilation equilibrium can be reached within experimentation time for a stepwise pressure increase as done in A6. This observation is in agreement with similar experiments carried out with 6FDA-DAF and  $\text{CO}_2$  at  $T=25^\circ\text{C}$  as shown in figure 7. A dilation experiment for a pressure step from 15 to 20 bar (A7) confirms this observation clearly.
- 6) Dilation experiments with a stepwise pressure increase (A6) show an increasing relaxational dilation fraction with increasing pressure. Therefore, the extent of relaxation seems to increase with increasing pressure in stepwise experiments. However, the extent in the first relaxation regime  $\phi_{R1}$  stays almost constant but the amount in the second regime  $\phi_{R2}$  increases. The relaxation times  $\tau_{R2}$  for experiments above 15 bar become even larger than the total experimentation time. This expresses actually the fact that no equilibrium is reached within the experimentation time.
- 7) Comparison of the experiments A7 and A2 points out clearly that the shape of the dilation kinetics curve depends strongly on the equilibrated starting pressure but not on the final pressure. Equilibrium is indeed reached coming from vacuum whereas no equilibrium is established in the same experimentation time in A7 coming from 15 bar.



#### 5.4 Qualitative model for the description of relaxational dilation phenomena

In the foregoing paragraph a number of experimental trends have been found which seem somewhat difficult to interpret. The model suggested in the following paragraphs will try to cover these phenomena in a qualitative way. The model assumes that penetrant molecules need a certain energy  $E_i$  to nest in certain sites in the polymer matrix. At low gas or vapour activity only those places can be involved where a low energy is sufficient for the penetrant molecules to occupy them. These loci are easy to dilate or they are even preexisting in the glassy matrix. The larger the dilation will become, due to high sorption values, the more energy it will require to occupy a new position in the matrix. This picture can be supported by sorption experiments at different temperatures. Huvard *et al.* [14] measured the sorption isotherms of CO<sub>2</sub> in poly(ethylene terephthalate) over a wide range of temperatures. For different temperatures they determined at a certain concentration the related pressure. The slope of a plot showing the logarithm of the pressure versus the inverse temperature (Van't Hoff plot) at a certain penetrant concentration is directly related to the isosteric heat of sorption. Different Van 't Hoff plots at different concentration gives the concentration dependence of the heat of sorption. The fact that the isosteric heat of sorption increases or becomes less negative, respectively, with increasing penetrant concentration gives direct support for the picture developed above.

In the following, sorption phenomena will be considered to directly represent dilation phenomena as it has been discussed in the foregoing paragraph. In a sorption experiment at a pressure  $p_1$ , clearly below the plasticization level, all loci  $n_i$  which require an energy  $E_i \leq E(p_1)$  can be occupied by penetrant molecules. Upon desorption the number of the loci  $n_i$  and the energy level to occupy them does not change for a second sorption cycle. If the pressure is increased from  $p_1$  to  $p_2$ , all loci  $n_j$  can be occupied by molecules which require energies  $E_j < E(p_2)$ . This process may also be reversible if no *morphological* alterations in the polymer matrix occur. This was experimentally verified by consecutive dilation experiments at a constant pressure of 3 bar. Such experiments are very reproducible. However, there will be a situation in which the penetrant induced stresses on the polymer matrix are of such a magnitude that the morphology will not remain unaffected. In the light of Bitter's modified Flory-Huggins model these alterations may occur in the local orderings. A change in the morphology of local ordering has then a direct impact on the amorphous part of the polymer matrix.

The next assumption in this model is that these morphological alterations find their expression in a decrease of the energy levels for the penetrant molecules to occupy certain positions. Or in other words, if  $n(E_j)$  is the number of molecules directly sorbed at the energy level  $E(p_2)$  in the virgin polymer, then the morphology

alterations result in an increase of available loci  $n_{\text{total}}$  for this energy level. The amount  $n_F$  of loci available in the virgin polymer will be called "Fickian" whereas the newly created number will be called "relaxational"  $n_R$ .

$$n_{\text{total}} = n_F + n_R \quad (11)$$

Since the morphological alterations and therefore the creation of new sites  $n_R$  are slow in nature, the ordinary Fickian sorption and the relaxational sorption are easy to distinguish.

If now all penetrant molecules are desorbed by applying a vacuum, the polymer remains with more Fickian sorption sites belonging to the pressure level  $p_2$  than the virgin one. Depending on the time between the first sorption experiment and a second one at the same applied pressure, the sorption and hence the dilation kinetics may be very different. In an experiment (A3) briefly after the first sorption experiment (A2) (with only a three hour vacuum period in between, see paragraph 5.3.), the new "Fickian" sorption sites (the former relaxational sites) will be the sum of the old Fickian sorption sites  $\phi_F(A2)$  plus the relaxational sites  $\phi_{R1}(A2)$  of the first experiment. This actually corresponds to the observation 1 in the foregoing paragraph. If the second experiment were carried out at a considerably later time, for instance one month later, the former relaxational sites (new Fickian sites) relax back into a situation similar to their virgin situation. The number of Fickian sites observed in that last experiment, i.e.,  $\phi_F(A5)$ , will be close to the number of Fickian sorption sites in the first experiment  $\phi_F(A2)$ . This corresponds also to the observation 1 in the foregoing paragraph.

In order to be able to observe these phenomena, one condition must be fulfilled: the relaxation process for the creation of new Fickian sites must be considerably faster than the back-relaxation into the original situation. Actually, this hypothesis is easy to accept if one accepts the fact that the molecular motion of polymer chains are faster in the presence of solvent or plasticizer molecules. This "lubrication" effect [15] of  $\text{CO}_2$  molecules on polymer chains is nicely demonstrated by the following experiment: a polymer strip of uncrosslinked Nitrilbutylrubber (NBR) (10cm \*1cm \*0.1cm) was placed in the dilation set-up at  $p=10$  bar  $\text{CO}_2$ . After three days the strip was roughly twice as long due to the creep induced by the weight of the polymer sample itself. Another polymer strip of the same polymer hanging in ambient atmosphere did not extend more than 10% in length within 2 months. With this in mind it can be understood that the relaxation process in the presence of  $\text{CO}_2$  for the sorption experiment is faster than the back-relaxation in the polymer which contains no penetrant molecules.

Considering the situation where briefly after the first experiment (A2) a second one

---

(A3) is performed, the question arises whether in the second experiment additionally to the increased Fickian sorption the same extra amount of relaxational sorption will occur so that the polymer would dilate more than in the first experiment. This must be denied since an infinite number of successive experiments would disintegrate the material. In the experiments presented here, no significant increase in dilation can be observed in subsequent experiments at the same pressure. However, in even more strongly swelling penetrants like organic vapours these progressive effects are possible as will be reported later. But generally, an equilibrium dilational value is reached for a certain maximum sorption belonging to the same pressure level ( $p_2$ ). The fact that still to some extent of the relaxational modes  $\phi_{R1}$  and  $\phi_{R2}$  are observable in the experiment A3 may be explained by the fact that during the evacuation for 10000 seconds some back relaxation will have occurred. This effect stays the same for successive identical pressure steps with the same pretreatment (A4).

Until now only experiments with integral pressure steps have been considered where the penetrant concentration in the polymer film changes from concentration  $c=0$  at  $t=0$  to an equilibrium concentration  $c=c_{\text{equil}}$  at  $t=\infty$ . Now we consider the situation where an equilibrium concentration  $c_{1,\text{equil}}$  is already present in the polymer when the next pressure step ( $p_1$  to  $p_2$ ) is applied. Following the argumentation in the first part of this paragraph, a part of the sites for the pressure step from  $p_1$  to  $p_2$  has been occupied in the pressure step from 0 to  $p_1$  by relaxation phenomena. This part would have been "Fickian" sorption sites for the pressure step from  $p_1$  to  $p_2$ . But since they are already occupied, these sites will not contribute to the Fickian fraction in the increase in  $\Delta L/L_0$  for this step. As a consequence the ratio of relaxational sites to "Fickian" sites increases. Carrying out successive pressure steps should result in a decreasing "Fickian" sorption site fraction with increasing pressure. One may even find the experimental situation that no "Fickian" behaviour will be found anymore. This argumentation is in agreement with the experiments A6, A7 and with observation 5 following figure 15.

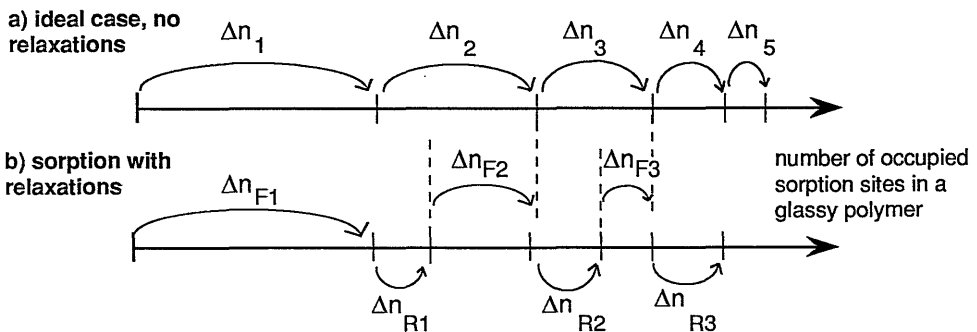


**Figure 16.** Visualization of the phenomenon of disappearance of the Fickian dilation part in dilation kinetics for incrementally increasing pressure steps

The arrow diagrams in figure 16 a and b compare the situation (a) without any relaxational sorption with (b) the situation of relaxational sorption. From this figure one can clearly see that the Fickian part of the dilation kinetics decreases with incrementally increasing pressure steps as it was described above.

Until now only dilation phenomena, for incrementally increasing pressure and concentration steps, have been considered in this discussion. However, the proposed model can also account for the consolidation process and here especially for the hysteresis behaviour shown in figure 8. It has been shown that relaxational sites can act as Fickian sites in a second run briefly after the first one. This actually means that there exists no energetical difference between these two sites for gas molecule penetrating into the matrix. This is of course also true for the molecules leaving the polymer in a desorption step between the two successive sorption runs. The question, which *molecules* will leave the polymer first, the Fickian or relaxational ones, is therefore inadequate. The *polymer* will consolidate with those sites which have been formed quickly and without large "effort", hence the Fickian ones, as visualized in figure 17.

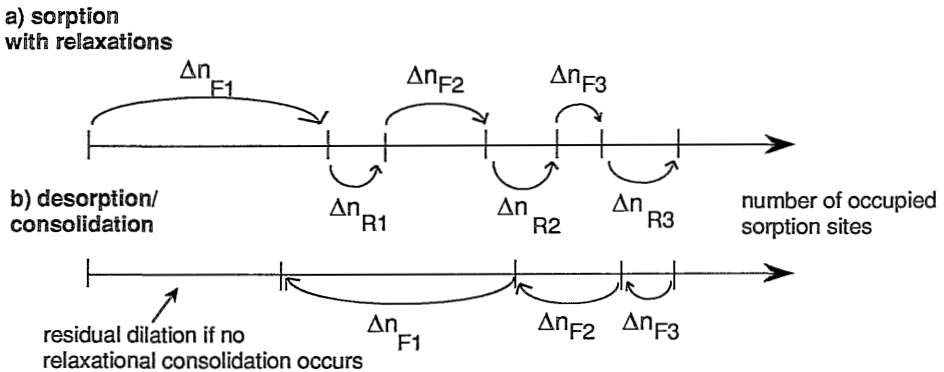


Figure 17. Visualization of the phenomenon of hysteresis between (a) the dilation and (b) the consolidation isotherm

The penetrant molecules, however, even may interchange between former Fickian and relaxational sites because these are energetically equally easy to occupy. At low pressures coming from elevated pressures, these quick consolidation processes coincide with slow relaxational processes stemming from a pressure decrease step at a higher pressure level. The rate constants for these relaxation processes can not be distinguished from quick processes and the consolidation kinetics shows no distinct regions as the dilation kinetics does. Instead, the consolidation kinetics has a rather smooth shape as it was shown in figure 8.

Due to the smaller lubrication effect for a negative pressure step compared to the positive pressure step in dilation, the consolidation relaxations will be even slower than the dilation relaxations (see conclusion 1 following figure 9). One may even assume that the consolidation relaxations cannot be observed on the experimental time scale and therefore a residual dilation will be found.

All these interpretations are based on the assumption that any observed dilational phenomenon results from mass uptake (although the two processes dilation and sorption do not have to be equally fast). Therefore, one should be able to observe the hysteresis behaviour also for the sorption and desorption isotherms. Koros *et al.* [9] carried out sorption/desorption and dilation/consolidation experiments for CO<sub>2</sub> in polycarbonate. As can be seen in figure 18, the sorption and desorption experiments show indeed the same hysteresis behaviour supporting the argumentation given above.

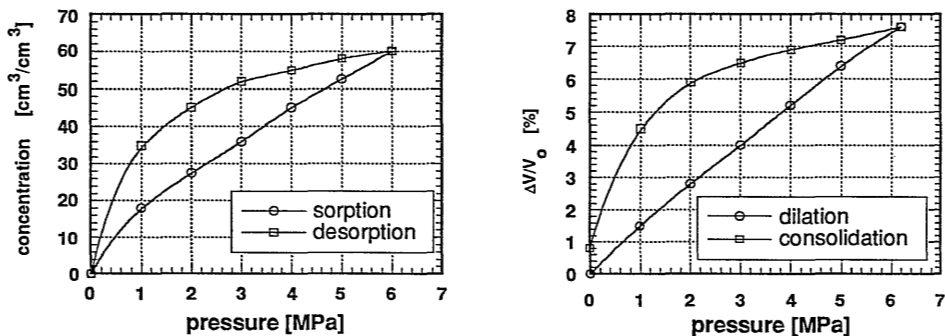


Figure 18. Sorption/desorption and dilation/consolidation experiments for the system polycarbonate/CO<sub>2</sub> at T=35°C (replotted from [9])

Finally the question may arise whether the film history of the virgin film, *e.g.*, annealing, has an influence on the sorption/dilation kinetics. From the viewpoint of the model it must be argued that a densification of the polymer matrix by annealing should result in a decrease of the number of Fickian sites and an increase of relaxational sites. In fact, it should result in an opposite effect compared to a preswelling treatment (see figure 15). No experiments of our own can be presented here due to lack of time. But sorption experiments published by Hopfenberg [16] on the system hexane/polystyrene clearly support this argumentation. Figure 19 shows that preswelling of polystyrene microbeads results in a very quick sorption equilibrium whereas annealing of the beads results in a considerable amount of relaxational sorption. Besides the effects in the kinetics it also can be seen that the total amount sorbed depends on the history. However, in a number of subsequent sorption cycles an "equilibrium" was reached.

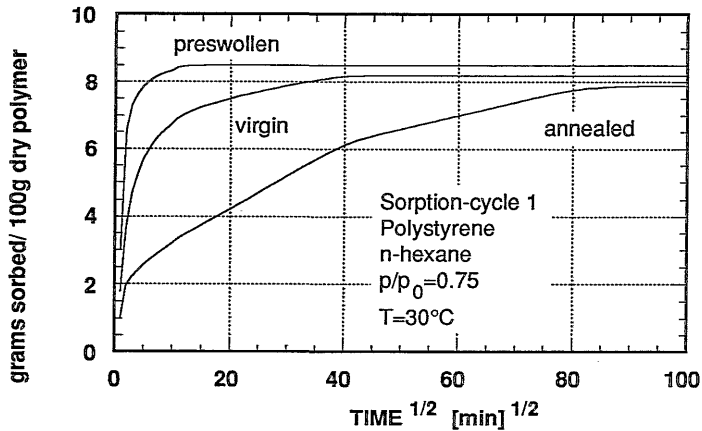


Figure 19. Sorption kinetics of *n*-hexane in polystyrene micro-beads having different histories (replotted from [16])

### 5.5. Swelling Related Phenomena occurring in Separation Processes making use of Solution-Diffusion Membranes

The morphological changes in the polymer matrix introduced by the swelling stresses of absorbed  $\text{CO}_2$  molecules led to an increase in the permeability of gaseous  $\text{CO}_2$  through a glassy polyimide membrane, as described in 5.2. In the following paragraph a number of different examples will be presented on peculiar mass transport phenomena occurring in solution-diffusion membranes made from glassy polymers. All the phenomena are caused (in the opinion of the author) by penetrant induced stresses on the polymer matrix. Generally, rubbery polymers react purely elastically in volume dilation upon mass uptake. However, for glassy polymers the restricted polymer chain flexibility at experimental temperatures below the glass transition temperature often results in a relaxational mass transport behaviour.

In pervaporation, where the feed is a liquid mixture, similar phenomena as those described in 5.2. can be observed. Park [17] has investigated the effect of the degree of preswelling on the pervaporation flux through a glassy polymer membrane made from a homogeneous blend of poly(vinyl alcohol) and poly(acrylic acid). The liquid feed consisted of 10 wt% methanol (MeOH) and 90 wt% methyl-tertiarybutylether (MTBE). In general, the polymer membranes sorb more MeOH than MTBE and differences in fluxes of the pure components are clearly related to differences in solubility. If the pervaporation experiment is carried out with a dry, unswollen membrane, the total flux for a membrane of 20  $\mu\text{m}$  thickness is around 50  $\text{g}/(\text{m}^2\text{h})$

for the above mentioned feed mixture. This does not change if the total membrane is immersed and preswollen in the same liquid mixture of MeOH/MTBE as the feed mixture used for the pervaporation experiment. However, preswelling in mixtures which contain more methanol than the feed mixture has a drastic impact on the flux and the selectivity of the membrane. The higher the methanol content in the preswelling mixture, and therefore the higher the preswelling, the higher will be the total flux. The selectivity of the membrane will then be diminished.

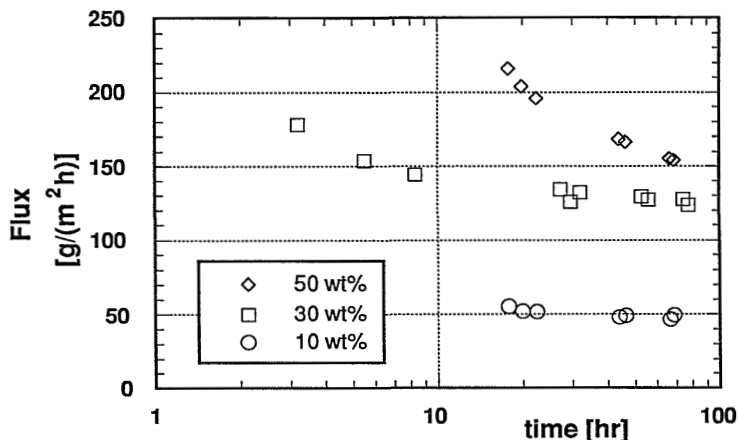


**Figure 20.** Time-dependent pervaporation flux of a 10/90 wt% MeOH/MTBE mixture through a 30/70wt% PVA/PAA polymer blend membrane having different degrees of preswelling; legend gives the weight percent of MeOH in the swelling mixture of MeOH/MtBE (taken from [17])

This phenomenon is in accordance with the physical picture developed in the foregoing paragraphs. The highly swelling component methanol introduces morphological alterations in the amorphous polymer matrix which result in higher fluxes. The enhanced fluxes, however, will decrease slowly in time as shown in figure 20. This decrease in time seems in contrast with the increasing permeability for the permeation experiments reported in 5.2. The reason is however simple: the preswollen membrane placed in the pervaporation cell contains in the very beginning a constant concentration profile over the whole membrane thickness belonging to a higher level of methanol sorption than in the actual situation during pervaporation. The application of a vacuum at the downstream side of the membrane and a lower alcohol content at the feed side than during swelling result in a consolidation process which is quick for the desorption of "Fickian" sites but slow for the relaxational ones. The slow consolidation process results in a slow flux decline and a slow selectivity increase (not shown). Membranes preswollen in 30/70 and 50/50 wt% feed mixtures change in time for more than 80 hours but do not

reach during that period the actual flux of the dry membrane or the membrane preswollen in the feed mixture. Similar relaxation phenomena have been observed by Radovanovic [18] for pervaporation experiments with cellulose-triacetate membranes and ethanol/water feed mixtures. Upon a pulse change in feed composition, fluxes change slowly but did not reach equilibrium within an experimentation time of 3 days.

At this point a few words on the permselectivity of polymeric matrices under different swelling conditions seem adequate. Koros [19] states as an empirical rule: "Structural modifications that simultaneously inhibit chain packing and the torsional mobility around flexible linkages in the polymer backbone tend to cause either simultaneous increases in both permeability and permselectivity or a significant increase in permeability with negligible loss in permselectivity". Actually, 'structural' means in this citation chemical modification. Concerning the permselectivity, this empirical rule can be reversed regarding the point of chain flexibility. The enhancement of torsional mobility (by preswelling) around less flexible linkages in the polymer backbone decreases the selectivity while enhancing the flux. This is in fact what can be observed in a swollen membrane; in gas separation the selectivity decreases drastically as the feed pressure is increased for a gas mixture containing highly swelling carbon dioxide (see chapter 1 figure 6); a similar conclusion is valid in the pervaporation experiments of Park. The swelling of the polymer matrix increases the flexibility of the polymer backbone as it is also suggested by  $^2\text{H}$ -NMR studies [20]. This increased backbone mobility is apparently responsible for the loss in selectivity.

Another severe problem regarding the properties of solution-diffusion membranes seems to be related to the swelling of the polymer matrix by penetrant molecules: namely, a decreasing selectivity with decreasing membrane thickness. This phenomenon has been mentioned first by Spitzen et. al. [21] for pervaporation experiments with ethanol/water mixtures using homogeneous membranes made from poly(acrylonitrile) (PAN). In pervaporation experiments for mixtures of acetic acid/water with three different polymers PAN, PVC and PSF, Koops observed the same thickness behaviour of the selectivity [22]. In figure 21, taken from Koops' work, the permeate composition is shown as a function of the membrane thickness. Below a certain critical membrane thickness (around 10  $\mu\text{m}$ ), the water content in the permeate decreases drastically resulting in a decreased selectivity. Koops interprets this phenomenon by means of solvent induced crazing. Craze initiation in this context is defined as a "localized collective dilational reorganization of stiff chain segments accompanied by matrix break-up" [23]. Thin membranes may not have an unswollen layer on the downstream side of sufficient thickness to prevent craze growing. Here, in fact, the induced swelling stresses cause an *irreversible*, disastrous failure of the polymer matrix.



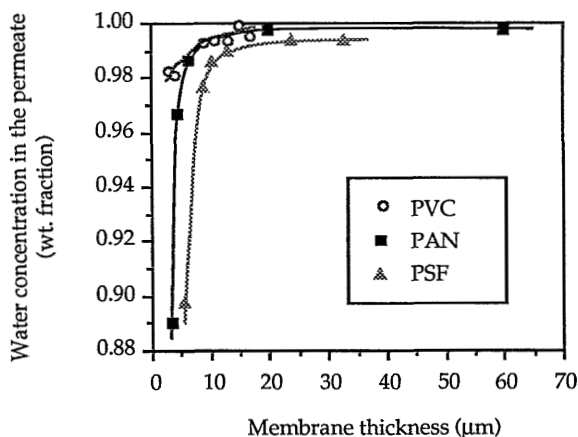


Figure 21. Water content in the permeate as a function of membrane thickness for the dehydration of 80/20 wt% acetic acid/water at  $T=80^{\circ}\text{C}$  by pervaporation [22]

For gas separation membranes, Toy *et al.* [24] have also observed a decreasing selectivity with decreasing membrane thickness. The membrane used for the separation of propane/methane and butane/methane mixtures was a homogeneous poly(trimethyl silylpropene) PTMSP film. The higher swelling component butane showed a more dramatic decrease in selectivity in its mixture with methane than propane. For both separations the selectivity also decreased with increasing feed pressure, hence increasing penetrant concentration.

Junginger [25] has carried out experiments which support the global picture developed. Homogeneous membranes made out of PAN with a thickness of around  $15\ \mu\text{m}$  were used for pervaporation experiments with feed mixtures of MTBE and MeOH. Starting from pure MTBE, feed compositions were increased up to pure MeOH using the same membrane for every experiment. A pseudo-equilibrium was reached after the pulse change in the feed composition after around 24 hours. This was far too long for ideal Fickian diffusion behaviour and the effects can be explained in the way time-dependent permeabilities in paragraph 5.2 were explained. The total flux increased with increasing MeOH content. Decreasing the methanol content stepwise again towards pure MTBE resulted in a hysteresis effect where the fluxes for the decreasing MeOH concentration were above the fluxes for the increasing methanol concentration in the feed. This observation is thus in accordance with conditioning effects observed by Park and described in paragraph 5.3. The membranes deteriorate, however, after a certain time of usage at different feed mixtures. The flux increases dramatically, simultaneously with a disastrous decrease in selectivity. This failure of the membrane can only be explained in

accordance with the interpretation of Koops who states that the gradient in penetrant induced swelling stresses in a thin film which then introduces non-selective, highly permeable matrix break-ups (crazes).

Coming back to thin film problems, deviations between thick films ( $d > 20 \mu\text{m}$ ) and thin films can also be observed in gas separation with highly swelling gases like  $\text{CO}_2$ . This phenomena will be described and discussed in the last part of this chapter. Bi-layer membranes have been prepared using the polyimide 6FDA-4PDA as a highly selective top layer and the highly permeable poly(trimethyl silylpropene) PTMSP or poly(dimethylsiloxane) PDMS as a supporting layer. First a layer of 6FDA-4PDA dissolved in DMAc was cast on a glass plate. The solvent was evaporated in a nitrogen glove box for 24 hours. After this drying step, a 2 wt% polymer solution of PTMSP (supplied by Prof. Nakagawa/Japan) in toluene was cast upon the polyimide film. A second drying step in the glove box was applied. The resulting membrane consists of layers of around  $3 \mu\text{m}$  polyimide and  $14 \mu\text{m}$  PTMSP. The exact thickness of layers could not be determined because no distinct transition between the layers could be observed under the electronmicroscope. In the case of PDMS as support, a  $75 \mu\text{m}$  film of PDMS was cast on the polyimide film. After casting this PDMS-layer was thermally crosslinked in an oven at  $T=80^\circ\text{C}$  for 2 hours. After removal from the glass plates the bi-layer membranes were dried in a vacuum oven at  $T=70^\circ\text{C}$  for two days. The selective properties were tested as described in chapter 2.2. Pressure-normalized fluxes ( $P/l$ ) and selectivity values  $\alpha$  for permeation experiments using gas mixtures of 25 vol%  $\text{CO}_2$  and 75 vol%  $\text{CH}_4$  at 4 bar upstream pressure are listed in table 3.

*Table 3. Pressure-normalized  $\text{CO}_2$  fluxes ( $P/l$ ) and selectivities  $\alpha$  for bi-layer membranes determined for 25/75 vol%  $\text{CO}_2/\text{CH}_4$  gas mixtures at  $T=30^\circ\text{C}$  and 4 bar upstream pressure*

membrane	$d_{\text{total}}$	$P/l_{\text{CO}_2}$	$\alpha_{\text{CO}_2/\text{CH}_4}$
PI/PTMSP	17	21.5	37
PI/PDMS	78	17.0	41

units:  $d$  [ $\mu\text{m}$ ];  $P/l$  [ $10^{-6}\text{cm}^3(\text{STP})/(\text{cm}^2\text{s cmHg})$ ];  $\alpha$  [-]

The selectivities for both membranes are almost equal to the intrinsic, ideal selectivity  $\alpha_{\text{ideal}}=40$  of 6FDA-4PDA membranes obtained from pure gas experiments. Thus, the thin layer of 6FDA-4PDA on the "support" layers can be considered as homogeneous and pinhole free. With these membranes permeation

experiments using pure CO<sub>2</sub> as the permeating gas were carried out at different upstream pressures. Five permeation experiments were carried out at each upstream pressure and the average value was taken as the actual permeability. No time-dependent experiments were carried out. The results of these experiments are shown in figure 22.

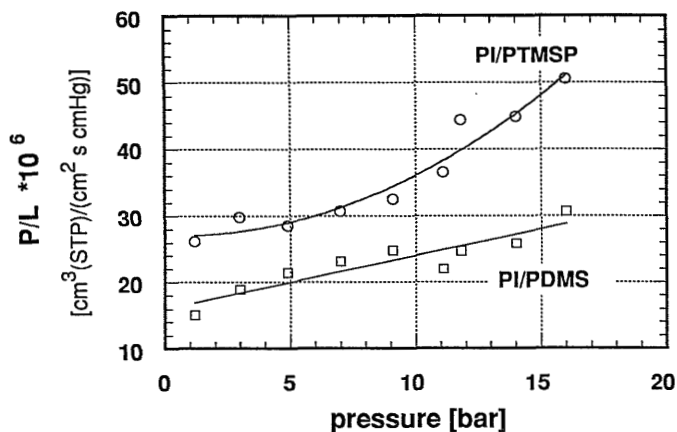


Figure 22. Pressure-normalized CO<sub>2</sub> flux through two bi-layer membranes with the polyimide (PI) 6FDA-4PDA and the support materials PTMSP or PDMS, respectively, at different upstream pressures and T=30°C

With increasing upstream pressure the permeability of CO<sub>2</sub> increases significantly. From experiments with thick single layer membranes one would expect a decreasing P/l-value with increasing upstream pressure for the glassy polymers 6FDA-4PDA and PTMSP while the permeability of PDMS should be independent of the upstream pressure at the pressure range investigated.

Pinnau [8] has obtained comparable results for permeation experiments with CO<sub>2</sub> through an asymmetric membrane made from PSF. After a small drop in the permeability with increasing pressure, the permeability increases as shown in figure 23 which is, again, in contradiction to the behaviour of thick films. These differences apparently result from the ability of thick films to *maintain* transport characteristics under swelling stresses, whereas thin films alter in morphology. These morphological alterations finally result in higher values for the pressure-normalized fluxes.

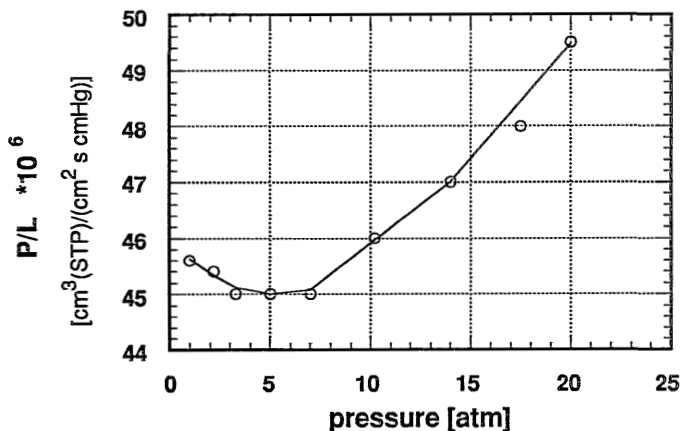


Figure 23. Pressure-normalized CO<sub>2</sub> flux through an integrally-skinned asymmetric poly(sulfone) membrane at T=35°C, replotted from [8]

## 5.6. Conclusions

Penetrant induced swelling stresses cause morphological alterations of the polymeric matrix which can be measured by permeation and dilation experiments. Depending on the level of swelling stresses and the time of exposure, time-dependent permeation of glassy polymers can be very complex. In order to account for the effect of these stresses, a new characteristic for the history of the membrane has been introduced: the aging time. Conditions which have to be fulfilled by the aging time are presented.

The morphological alterations can also be followed as a relaxational volume increase following the ordinary, 'instantaneous' Fickian volume increase as a much slower process. The distinction between Fickian and relaxational sorption sites is used to interpret different sorption kinetics for virgin, preswollen and annealed polymer samples. Furthermore, the model explains the hysteresis behaviour for sorption/desorption or dilation/consolidation processes, respectively. Based on this picture, a variety of "peculiar" phenomena observed in separation processes making use of solution-diffusion membranes are explained. Selectivities depending on the membrane thickness, decreasing selectivities with increasing feed activity and conditioning effects are undoubtedly linked to morphological alterations induced by the penetrant molecules themselves.

---

**References**

- (1) J.G.A. Bitter, Transport mechanisms in membrane separation processes, Plenum Press, 1991
- (2) D.W. van Krevelen, Properties of polymers, 3rd edition, Elsevier, 1990
- (3) E. Smit, Modelling of the diffusion of carbon dioxide in polyimide matrices by computer simulation, *J.Membrane Sci.*, 73 (1992) 247
- (4) A.C. Puleo, D.R. Paul, The effect of degree of acetylation on gas sorption and transport behaviour in cellulose acetate, *J.Membrane Sci.*, 47 (1989) 301
- (5) A.C. Puleo, N. Muruganadam, D.R. Paul, Gas sorption and transport in substituted polystyrenes, *J.Polym. Sci. Polym. Phys.*, 27 (1989) 2385
- (6) BRITE Project RI/B-0098/NL, Membrane separation of CO<sub>2</sub> and H<sub>2</sub>S from mixtures with gaseous hydrocarbons
- (7) L.C.E. Struik, Physical aging in amorphous polymers and other materials, Elsevier, 1978
- (8) I. Pinnau, Skin-formation of integral-asymmetric gas separation membranes made by dry/wet phase inversion, Ph.D. Thesis, University of Texas at Austin, 1991
- (9) D.S. Pope, G.K. Fleming, W.J. Koros, Effect of various exposure histories on sorption and dilation in a family of polycarbonates, *Macromolecules* 23 (1990) 2988
- (10) Y. Kamiya, D. Bourbon, K. Mizoguchi, Y. Naito, Sorption, dilation and isothermal glass transition of Poly(ethyl methacrylate)-organic gas systems, *Polymer J.*, 24 (1992) 443
- (11) A.R. Berens, H.B. Hopfenberg, Diffusion and relaxation in glassy polymer powders: 2. separation of diffusion and relaxation parameters, *Polymer*, 19 (1978) 489
- (12) M. Wessling, S. Schoeman, Th. v.d.Boomgaard, C.A. Smolders, Plasticization of gas separation membranes, *Gas Sep.&Purif.*, 5 (1991) 222
- (13) E.S. Sanders, Penetrant-induced plasticization and gas permeation in glassy polymers, *J.Membrane Sci.*, 37 (1988) 63
- (14) W.J. Koros, D.R. Paul, G.S. Huvard, Energetics of gas sorption in glassy polymers, *Polymer*, 20 (1979) 956
- (15) Plasticizers, J.K. Sears, N.W. Touchettes, in: *Encyclopedia of Polymer Science and Engineering*, Supplement, J.Wiley & Sons, 1989
- (16) H.B. Hopfenberg, The effect of film thickness and sample history on the parameters describing transport in glassy polymers, *J.Membrane Sci.*, 3 (1978) 215
- (17) H.C. Park, Separation of alcohols from organic liquid mixtures by pervaporation, Ph.D. Thesis, University of Twente, 1993
- (18) P. Radovanovic, Influence of mixing of the feed on pervaporation flux and selectivity and time-dependence of flux and selectivity in pervaporation of ethanol-water mixtures through CTA membranes, Internal report University of Twente, 1985
- (19) W.J. Koros and M.W. Hellums, Gas separation membrane material selection criteria: differences for weakly and strongly interacting feed compositions, *Fluid*

- Phas.Equil. 53 (1989) 339
- (20) P.B. Smith, D.J. Moll,  $^2\text{H}$  NMR investigation of the plasticization effects induced by high-pressure carbon dioxide gas on the molecular dynamics of polymers, *Macromolecules*, 23 (1990) 3250
  - (21) J.W.F. Spitzen, G.H. Koops, M.H.V. Mulder, C.A. Smolders, *Proc.3rd.Int.Conf.Pervap. Proc.Chem.Ind.*, Bakish [ed.], Nancy, France, 252 (1988)
  - (22) G.H. Koops, Dehydration of acetic acid by pervaporation; material science aspects, Ph.D. Thesis, University of Twente, 1992
  - (23) H.H. Kausch, *Polymer fracture; polymers/properties and applications 2.Vol*, Springer Verlag, 1987
  - (24) L. Toy, I. Pinnau, J.G. Wijmans, Composite membranes for the recovery of higher hydrocarbons from natural gas, presented at the AICHE-Meeting, Miami/FL, Nov. 1992
  - (25) S. Junginger, Pervaporation of organic mixtures using polyacrylonitrile membranes, M.Sc. Thesis University of Dortmund/University of Cincinnati 1992

## Chapter 6

# A Molecular Dynamics Study on the Amorphous State of Poly(ethylene terephthalate) and Poly(ethylene isophthalate)

### 6.1. Introduction

The molecular structure and the morphology of glassy amorphous polymers has been subject of numerous research efforts in the past. Motivation for this research is the need of a relation between the structure on a molecular level and bulk material properties. Especially, mechanical and mass transport properties of glassy as well as rubbery polymers have been investigated theoretically by Molecular Dynamics (MD) simulations. In MD simulations, the atomic structure of a polymer is mimicked in three-dimensional boxes with a box length of 20-30 Å containing around 2000 atoms. The atoms may be present in the box as a large number of low molecular weight molecules in the case of the simulation of normal liquids or as a small number of high molecular weight molecules in the case of polymers.

Mathematical incorporation of all bonded and non-bonded interactions between these molecules allows the study of the trajectory of any single atom in this system. For example, placing a single low molecular weight molecule in a polymeric host matrix and following the path of this molecule in time confirmed the hopping mechanism of diffusion in the polymer [1] as it was postulated some 40 years ago by Meares [2]. Advanced simulation techniques allow already the prediction of macroscopic diffusion coefficients for different polymers with an accuracy of one order of magnitude [3].

For all these simulations it is *assumed* that the simulated three-dimensional structure represents the structure of the bulk material. Instead of spotting at the motion of one particular atom, MD simulations will be used in this chapter to investigate the local structure in this simulated box. Up to now no attempt has been made to compare the polymer structure simulated by MD with experimental evidence.

Experimentally, the local structure of amorphous glassy polymers has been investigated by scattering techniques like neutron and X-ray scattering. The question behind these experimental investigations, whether the polymer chain can be regarded as a random coil [4] or whether the amorphous matrix contains some degree of local ordering [5], is intensively discussed and still not solved. It is of considerable importance for the sorption model for polymers developed by Bitter [6]. A more detailed description of these local ordering phenomena is given in chapter 2.4. For polycarbonate a number of experimental studies indicate that there exists some level of enhanced local ordering although the polymer appears to have no measurable degree of crystallinity. Preliminary MD simulations support these results [7]. In this chapter we will concentrate on the question whether the structure simulated with MD can be, in general, compared with experimental results. Furthermore, the question whether X-ray scattering experiments can be used for the determination of local ordering will be elucidated.

## 6.2. Details of the Molecular Dynamics Simulation

Molecular Dynamics programs have been developed, successfully applied and even commercialized (ProSimulate, Discover, InsightII) for the simulation of dynamic behaviour of systems containing large numbers of atoms. For the purpose of simulating low molecular weight systems like liquids and for simulating proteins, a widely used program package is GROMOS [8]. It has been applied with some modifications for the simulation of a penetrant molecule,  $\text{CO}_2$ , in a polymeric host matrix [1].

The principle of the MD simulation will be explained briefly: the total energy of the simulated system is the sum over all bonded and non-bonded interactions between all atoms.

$$E_{\text{tot}} = E_{\text{bonded}} + E_{\text{non-bonded}} \quad (1)$$

The bonded energy can be subdivided in stretching, bending and torsional energies:

$$E_{\text{bonded}} = E_{\text{bond}} + E_{\text{angle}} + E_{\text{dihedral}} + E_{\text{improper}} \quad (2)$$

with

$$E_{\text{bond}} = \sum \frac{1}{2} K_{\text{bond}} (r - r_0)^2 \quad (3)$$

$$E_{\text{angle}} = \sum \frac{1}{2} K_{\text{angle}} (\theta - \theta_0)^2 \quad (4)$$

$$E_{\text{dihedral}} = \sum K_{\text{dihedral}} (1 + \cos(n\Phi - \delta)) \quad (5)$$



$$E_{\text{improper}} = \sum \frac{1}{2} K_{\text{improper}} (\psi - \psi_0)^2 \quad (6)$$

The non-bonded energies arise from van der Waals and electrostatic interaction:

$$E_{\text{non-bonded}} = E_{\text{vdW}} + E_{\text{electrostatic}} \quad (7)$$

with

$$E_{\text{vdW}} = \sum C_{12} \frac{1}{r_{ij}^{12}} - \sum C_6 \frac{1}{r_{ij}^6} \quad (8)$$

$$E_{\text{electrostatic}} = \sum \frac{q_1 q_2}{4\pi \epsilon_0 r_{ij}} \quad (9)$$

Here, the 1,2- and 1,3-van der Waals interactions stemming from next and next-next neighbour bonds are excluded and special parameters are used for the 1,4-van der Waals interactions. Force constants  $K$ , equilibrium values for the interatomic distances and angles, static electric charges and van-der-Waals constants were taken from Charmm after conversion to the GROMOS force field. The summation in equation (3) to (6) and (8) and (9) runs over all atoms pairs. The total energy is a function of all atomic positions at a certain time  $t$ . Any force acting on the atoms in the system can be obtained from the gradient of the potential energy.

$$\vec{F}_i(t) = -\vec{\nabla}_i E(\dots, \vec{x}_i(t), \dots) \quad (10)$$

Dividing the force by the mass of the atom gives the acceleration. Numerical integration gives the new velocity  $\vec{v}$  and position  $\vec{x}$  at the new time  $t+\Delta t$ :

$$\vec{v}_i\left(t+\frac{\Delta t}{2}\right) = \vec{v}_i\left(t-\frac{\Delta t}{2}\right) + \vec{F}_i(t) \frac{\Delta t}{m} \quad (11)$$

$$\vec{x}_i(t+\Delta t) = \vec{x}_i(t) + \vec{v}_i\left(t+\frac{\Delta t}{2}\right) \Delta t \quad (12)$$

In this numerical procedure, the velocities  $\vec{v}$  are calculated at half integral times whereas positions  $\vec{x}$  and forces  $\vec{F}$  are calculated at integral times.

At the beginning, at  $t=t_0$ , all positions of the atoms are assigned and the topologies of the molecules are specified. Each atom gets a random velocity so that

$$n k T\left(t+\frac{\Delta t}{2}\right) = \sum m \vec{v}\left(t+\frac{\Delta t}{2}\right)^2 \quad (13)$$

is obeyed and the temperature  $T$  is equal to the required experimental temperature ( $n$  is number of degrees of freedom). Simulations in this chapter are carried out in the  $N,p,T$  ensemble meaning that the number  $N$  of atoms, the pressure  $p$  of the

system and temperature  $T$  are kept constant. Therefore, the volume of the simulated system which is actually placed in a cubic box remains variable. Surface effects at box surfaces can be avoided by introducing periodic boundary conditions. This actually means that copies of the actual box are placed around the box under investigation. The procedure to prepare such a box with a reasonable total energy and volume is tedious and will be described briefly:

1. Random placement of 5 energy minimized polymer chains of the type  $C_6H_5-(COO-C_2H_4-OOC-C_6H_4)_{11}-COO-C_2H_4-OOC-C_6H_5$  in a box with box length of 120-150Å.
2. Shrinking of the box at a very high pressure ( $10^5$  bar) down to a volume smaller than the experimental specific volume of the polymer by using a softcore potential instead of the normal van-der-Waals potential. This softcore potential neglects repulsive forces and allows close contacts of atoms. Charges on atoms are artificially set to zero. For a detailed description of this shrinking procedure the reader is referred to [9].
3. Energy minimization of the box with hardcore (vdW) potentials and charges, at  $p=1$ bar.
4. Equilibration run at a constant pressure  $p=1$  bar and  $T=298$  K for 20 ps.
5. Production run over 10 ps. During this run quantities like energies, velocities and coordinates are stored every 0.01ps. The data stored can be used later for further computations.

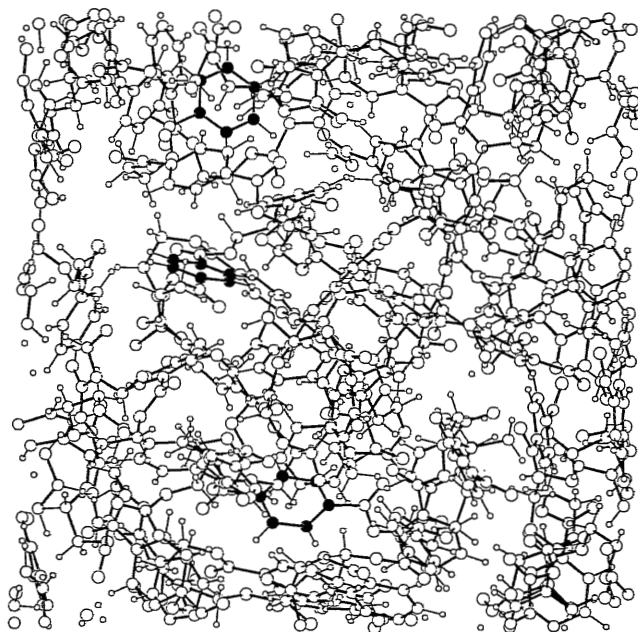


*Figure 1. Representative box of poly(ethylene terephthalate) used for MD simulations*

An important element of the molecular dynamics simulation is the proper treatment of long-range non-bonded interactions. For the purpose of smaller computation times, the long-range non-bonded interactions were truncated after 8.5 Å which is a reasonable cut-off for non-ionic systems. Figure 1 shows the box after the equilibration run. The box length after shrinking, energy minimization and equilibration is 24.8Å. The volume fluctuates during the equilibration and production run. Deviations from the average box size length are 0.1Å. Because the simulation is carried out in  $(N,p,T)$  ensemble the volume of the box is actually a simulated characteristic and can therefore be compared with experimental values.

### 6.3. Methods to Analyse the Amorphous State of Glassy Polymers

The structure of an amorphous polymer can be investigated by means of X-ray scattering experiments. Because X-ray scattering as a characterization tool for polymers used as membrane materials is rather undeveloped, a description of this technique will be given.

Experimentally, first the scattering intensity as a function of the scattering angle is measured. A typical scan for an amorphous glassy polymer is given in figure 2. This intensity curve shows four diffuse maxima. It has been mentioned earlier in chapter 2 that the angle, at which the first maximum occurs, is sometimes used to calculate an average d-spacing according to the Bragg relation [10,11]. This value for the d-spacing is then associated to an average distance between chains. The proper treatment of an intensity-scattering angle pattern is rather extensive and will be briefly outlined here. A detailed description is given in [12].

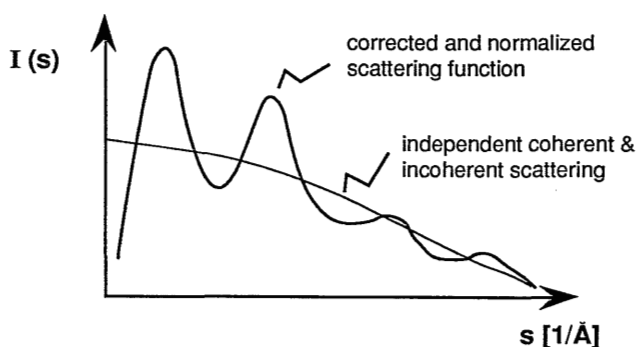


**Figure 2.** X-ray scattering pattern from an amorphous polymer; the scattering intensity is plotted versus  $s=4\pi/\lambda\sin\theta$  where  $\theta$  is the angle of the incident beam and  $\lambda$  the wave length of the X-ray

The experimentally obtained intensity curve must be smoothed by interpolation using cubic splines. Corrections for polarization and absorption must be applied. Now, the obtained intensity curve is the sum of an independent scattering component which would be observed if no structure would be present and a scattering component which arises from the scattering of structural effects as visualized in figure 2.

A reduced intensity function  $i(s)$  can be obtained by calculating

$$i(s) = I(s) - \sum_i^n f_i^2(s) - I_{\text{comp}}(s) \quad (14)$$

where the last two terms can be calculated from tabulated values [13]. In order to weigh the obtained intensity function  $i(s)$  evenly the weighted reduced intensity function  $s \cdot i(s)$  is introduced. A schematic picture of such a function obtained from the scattering experiment in figure 2 is shown in figure 3. Only at this point of the data treatment *reasonable* information can be extracted from the amorphous scattering pattern. Therefore, the d-spacing value obtained from the untreated scattering experiment as described in chapter 2.3 is a rather dubious parameter.

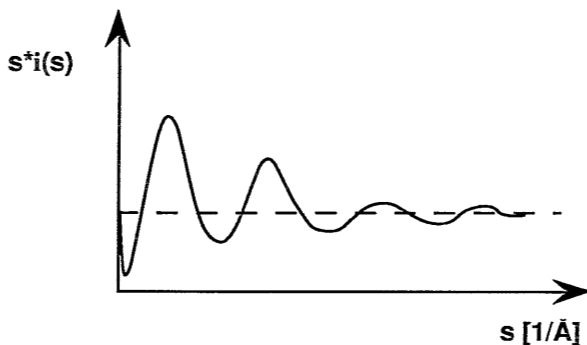


Figure 3. Reduced intensity function  $s \cdot i(s)$  obtained from corrected X-ray scattering pattern

A Fourier transformation of  $s \cdot i(s)$  according to equation (15)

$$H(r) = \frac{1}{2 \pi^2 r \rho} \int_0^{\infty} s i(s) \sin(s r) ds \quad (15)$$

results in a so-called experimental, total radial distribution function (RDF)  $H(r)$ .

In order to explain the meaning of a radial distribution function, let us consider a mono-atomic system with a certain distribution of atoms over space. The atomic density  $\rho(r)$  in a spherical shell of thickness  $dr$  and radius  $r$  (we put the center of the spherical shell at one of the atoms) is given by

$$\rho(r) = \frac{n(r)}{4\pi r^2 dr} \quad (16)$$

where  $n(r)$  is the number of atoms in the shell with the volume  $4\pi r^2 dr$ . The ratio of the atomic density depending on the radius and the average density gives the radial distribution function  $g(r)$ .

$$g(r) = \frac{\rho(r)}{\bar{\rho}} \quad (17)$$

In a perfect gas  $\rho(r)$  would be equal to  $\bar{\rho}$  resulting in  $g(r)=1$  because all atoms would be randomly distributed. In contrast, a perfect static crystal where atoms return periodically would result in a RDF which looks like a series of delta functions with infinite values at distances equal to the atomic distances and zero in-between. In amorphous systems like liquids, glasses and some polymers no neighbouring atoms can be observed below a distance of  $1\text{\AA}$  due to repulsive forces; hence, for  $r < 1\text{\AA}$ ,  $g(r)$  is equal to zero. At long distances  $g(r)$  will be equal to one because by definition amorphous systems have no long range order. Peaks in  $g(r)$  will represent a systematic distance correlation. In many applications in which the radial distribution function is integrated over total space it is convenient to define the total RDF  $h(r)$  by

$$h(r) = g(r) - 1 \quad (18)$$

The extension to multi-component systems is straightforward; considering the atom type  $i$  in the center of the spherical shell with the radius  $r$  and counting the number of atoms type  $j$  results in

$$\rho_{ij}(r) = \frac{n_{ij}(r)}{4\pi r^2 dr} \quad (19)$$

and equation (17) becomes

$$g_{ij}(r) = \frac{\rho_{ij}(r)}{\bar{\rho}_j} \quad (20)$$

The total pair RDF becomes for this specific pair

$$h_{ij}(r) = g_{ij}(r) - 1 \quad (21)$$

By this means a number of total *pair correlation functions* for different atom pairs can be defined. All these pair correlation functions are finally hidden in the total RDF  $H(r)$  which can be obtained from the experimental scattering curve.

Such pair radial distribution functions for certain atom pairs can be easily obtained from MD simulations. As a matter of fact it simply means counting the number of the species  $j$  at a certain distance  $r$  from the atom  $i$  and averaging over all  $i$ . Once all of the pair RDFs have been determined, two possibilities exist to calculate the total RDF according to Pings and Waser [14]. The first one (method 1) assumes angle independent scattering factors for scattering atoms  $i$ . Then the total RDF  $H(r)$  for multi-atomic systems is given by

$$H(r) = \sum_{i=1}^n \sum_{j=1}^n x_i x_j \frac{K_i K_j}{\left[ \sum K_i x_i \right]^2} h_{ij}(r). \quad (22)$$

$x_i$  and  $x_j$  are the mole fractions of the atom types  $i$  and  $j$  present in the total system and  $K_i$  and  $K_j$  are scattering constants equal to the number of electrons in the atoms  $i$  and  $j$ .

The second alternative (method 2) is somewhat more difficult because scattering of X-rays on a certain atom type is actually angle dependent. Two Fourier transforms must be carried out to obtain finally the total RDF  $H(r)$ . First, a certain intensity function  $i_{ij}(s)$  must be calculated for each pair  $ij$  according to:

$$i_{ij}(s) = \frac{4\pi\rho}{s} \int_0^{\infty} r_{ij} h_{ij}(r_{ij}) \sin(s r_{ij}) dr_{ij} \quad (23)$$

Experimentally the integration in equation (15) is normally carried out up to a finite value  $s_{\max}$  around  $16\text{\AA}^{-1}$ . Therefore, equation (23) needs to be calculated only for values of  $s$  smaller than  $s_{\max}$ . The scattering function  $i(s)$  can be calculated according to equation

$$i(s) = \sum_{i=1}^n \sum_{j=1}^n x_i x_j F_{ij}(s) i_{ij}(s) \quad (24)$$

with

$$F_{ij}(s) = \frac{f_i(s) f_j(s)}{\left[ \sum x_i f_i(s) \right]^2} \quad (25)$$

$f_i(s)$  and  $f_j(s)$  are the angle dependent scattering functions tabulated in [13]. In a last

Fourier transformation the total net RDF can be calculated using equation (15). These two numerical methods have never been applied to the investigation of the polymeric structure by means of a molecular dynamics study. In the following two paragraphs, results obtained using these two methods with MD simulated structures will be compared with experimentally obtained radial distribution functions published in literature.

#### 6.4. Choice of the Polymeric System

Within this thesis, most of the experimental work on the characterization of mass transport was carried out with polyimides. However, no X-ray diffraction experiments with polyimides have been published and a simulation of the RDFs of a polyimide could therefore not be compared with experimental evidence. On the other hand, poly(ethylene terephthalate) (PET) as a thermoplastic engineering plastic has been subject of intensive experimental investigations. The formation of nodular structures in homogeneous films led to the development of the folded-chain fringed-micellar grain model of Yeh [15] which is discussed in detail in chapter 2. Wignall *et al.* carried out X-ray diffraction experiments [16] in order to get more information about local ordering in PET. From the experiments it was not possible to obtain any conclusive evidence of local ordering in amorphous PET because the authors could assign almost all observed peaks to intramolecular distances. However, as shown in the paragraphs above, the total RDF of a polymer is actually a superposition of a number of different pair RDFs and is therefore still difficult to interpret. Experimentally obtained total radial distribution functions of three samples with different thermal histories replotted from [16] are shown in figure 4a, b and c. Albeit very different in shape, no interpretations regarding these differences were offered by the authors. Since these experimental RDFs will be compared later with results obtained from MD simulations, they will be discussed here in some more detail. Differences will be pointed out by *comparing* the RDFs; physical *interpretations*, however, are hardly possible at this point of the discussion but will be carried out in a following paragraph when spotting on pair radial distribution functions.

Sample A was quenched from the melt to room temperature. This sample was then annealed at  $T=65^{\circ}\text{C}$  just below the glass transition temperature for 100 hours. A third sample was prepared by heating sample A just above  $T_g$  at  $T=90^{\circ}\text{C}$  for 100 hours and finally quickly cooled to room temperature. The authors did not point out that during this heat treatment the polymer is actually in its rubbery state so that the heat treatment must be regarded as a quenching step from the rubbery state rather than an annealing treatment. The experimental RDFs for the two samples with different quench conditions (sample A and C) are shown in figure 4a. For the sample quenched from the melt distinct maxima and minima can be observed over the

range from 0.05 up to 0.5 nm. For the sample C, quenched from the rubbery state, distinct maxima and minima can only be observed up to distances of 0.3 nm. From  $r=0.3$  nm on, the RDF is almost flat. Comparing the RDF of the annealed sample (B) with the sample A in figure 4b, one can clearly see that the peaks in the distance range from 0.3 to 0.5 nm become smaller and broader whereas the first two peaks become larger and narrower after annealing. Furthermore, the second peak shifts towards smaller  $r$ -values.

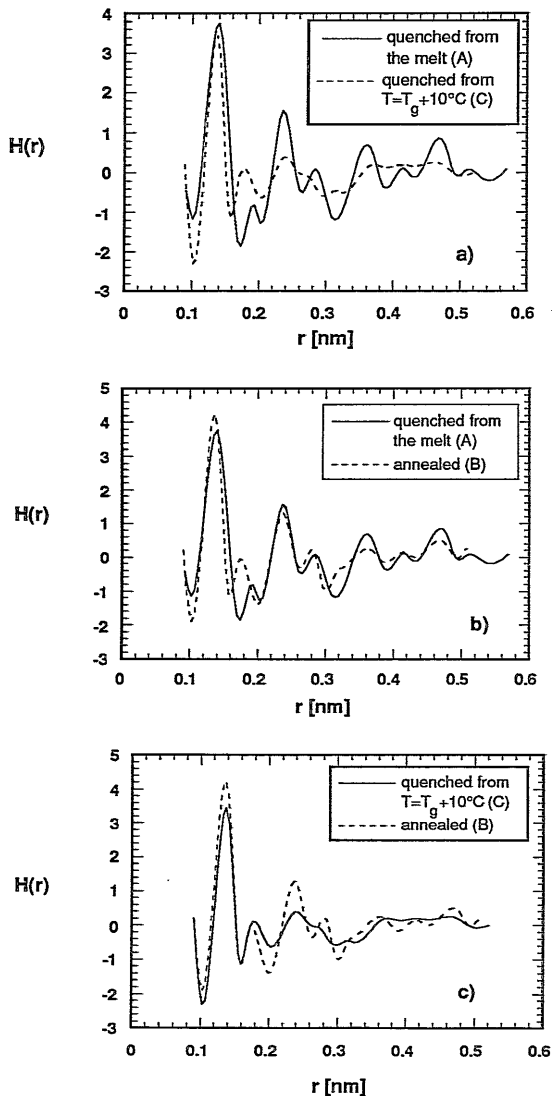


**Figure 4.** Experimental radial distribution functions obtained from PET ( $T_g=78^\circ\text{C}$ ) samples having different thermal histories: a) quenched from the melt, b) annealed for 100h at  $T=65^\circ\text{C}$  and c) quenched from  $T=T_g+10^\circ\text{C}$ , replotted from [14]



One may also compare the annealed sample (B) with the sample quenched from the rubbery phase (C) as done in figure 4c. Since sample B was not annealed after a quenching step as sample C had experienced, physical interpretation of the differences between the two RDFs is not valid. The comparison is, however, illustrative and makes the statement acceptable that there definitely exist significant differences between RDFs obtained from polymer samples having different thermal histories.

Wignall *et al.* could assign most of the peaks to intramolecular distances (in one chain) and concluded therefore that no intermolecular ordering (between different chains) exists. However, the difficulty to interpret these experimentally obtained RDFs is demonstrated by the fact that the authors could not find any intramolecular distance for the second peak at around  $r=0.19$  nm. Furthermore, no explanation was given for the considerable differences in the radial distribution functions of the three different samples as pointed out above.

Because of the availability of these data, PET was chosen as a model system for the molecular dynamics simulations. The advantage of MD simulations is the fact that besides the total RDF also the pair RDFs are known. Some more general information can be obtained to which extent intermolecular distance correlations are hidden in the total RDF. These intermolecular correlations may be overshadowed by intramolecular correlations and therefore hardly detectable. These (up to now hypothetical) local orderings may give considerable support to the model of Bitter who assumes local ordering as topological constraints in his elastic strain corrected Flory-Huggins model used for interpreting sorption isotherms.

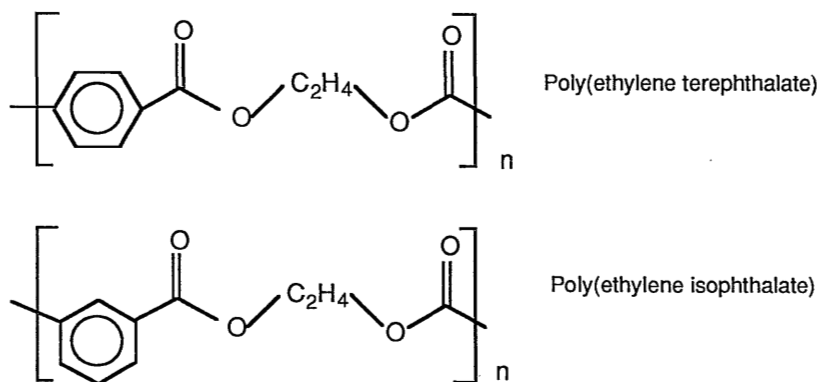


Figure 5. Chemical structures of poly(ethylene terephthalate) (PET or pPET) and poly(ethylene isophthalate) (mPET)

The second reason why PET is an interesting polymer to analyse is the fact that the

meta isomer poly(ethylene isophthalate) (mPET) has a totally different mass transport behaviour. As it is found for polytriazoles and polyimides too, the meta substitution of the phenylene group in poly(ethylene isophthalate) results in a lower diffusivity of dissolved molecules compared to the para isomer. For these two isomers the lower diffusivity can at least be correlated to a lower value for the total free-volume of meta substituted mPET. For certain polyimides and polytriazoles [17] as shown in chapter 2, free-volume and diffusivity are not at all correlated to each other. Therefore it has been speculated that not the *total amount* of the free-volume but also its *distribution* must be of considerable importance. Therefore an analysis of the free-volume distribution of PET and mPET may give some more evidence to these speculations.

## 6.5. Results and Discussion

### 6.5.1. General Considerations

Before presenting and discussing the results of the simulations, a nomenclature regarding the different atom types in poly(ethylene terephthalate) must be introduced. The chemical structure of PET with the identification codes are shown in figure 6. The nomenclature was adapted from the simulation package Charmm/Polygen. In these packages the atoms are classified according to their chemical nature and environment. Atomic names only serve to determine the interatomic interaction. In the sequel they will also be used to identify pair correlation functions. Since the aliphatic hydrogens are not equivalent to the aromatic hydrogens as far as their correlation to other atoms is concerned, pair correlation function invoking hydrogen atoms are actually sums of several distinguishable more fundamental correlation functions.

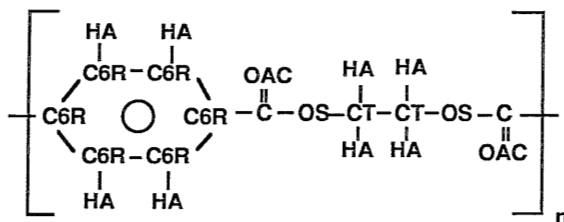


Figure 6. Nomenclature for different atom types in pPET and mPET

From the equilibrated structure as it is shown in figure 1, pair distribution functions were determined by averaging 500 structures from the production run. This was sufficient in order to obtain statistically reliable results. Because PET contains 6 different atom types, 21 different pair radial distribution functions must be

calculated for the calculation of the total radial distribution function. The principle for the determination of the pair RDF for the benzene ring carbon C6R and the hydrogen atoms HA is visualized in figure 6.

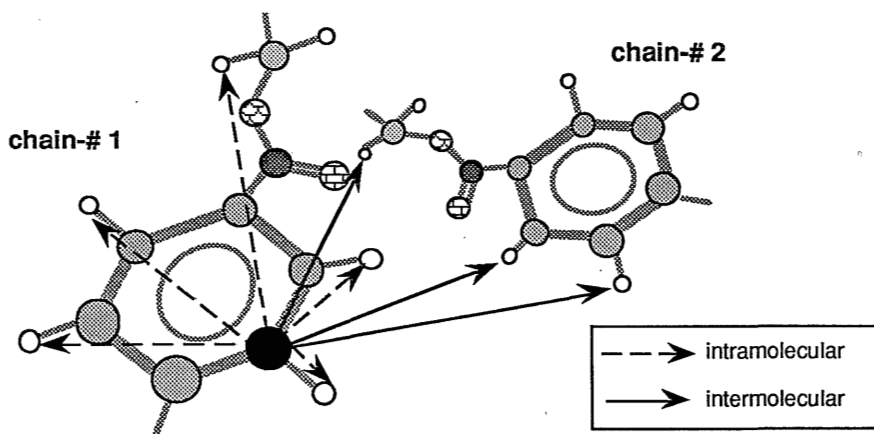


Figure 7. Schematic representation of the procedure for the determination of inter- and intramolecular pair distribution functions for the benzene ring carbon-hydrogen correlation

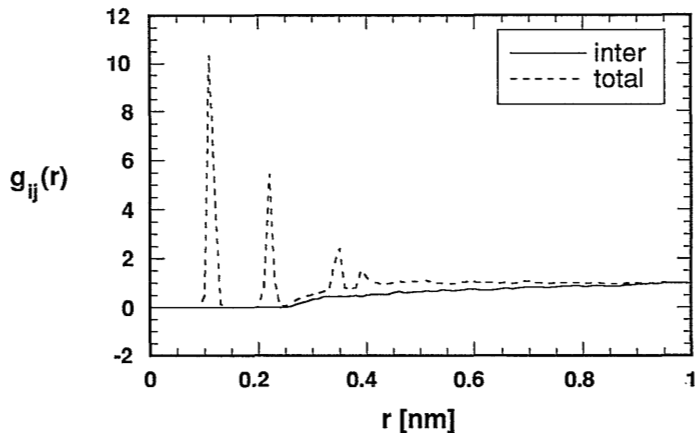


Figure 8. Inter- and total(inter+intra) pair distribution function  $g_{ij}(r)$  for the benzene ring carbon-hydrogen correlation

The distances between a certain benzene ring carbon and all hydrogen atoms in the same chain and in all other chains are calculated. If the distance falls in a certain interval  $r+dr$  the counter for this distance is increased by one. This procedure is repeated for all C6R-atoms in the box. The result will be a "total" pair radial distribution function for the atom pair C6R-HA containing inter- and intramolecular

correlations. An “inter” pair RDF is obtained if distances between C6R atoms in one chain and hydrogen atoms HA in the remaining four chains are considered. Figure 8 shows the result of such a calculation. Four distinct peaks in the “total” pair RDF  $g_{ij}(r)$  can be observed. Because no peaks can be observed in the “inter” pair RDF  $g_{ij}(r)$ , one can conclude that the peaks purely result from intramolecular distance correlations. In fact, these four peaks represent the four distances between the phenylring carbons and the phenylring hydrogen atoms. The hydrogen atoms bound in the aliphatic part of the chain can not be identified as peaks because this part of the chain is highly flexible compared to the benzene ring.

The total radial distribution function  $H(r)$  which can be compared with the experimentally obtained one must be calculated out of the 21 partial RDFs  $g_{ij}(r)$  according to the two procedures described in paragraph 6.3. Both alternatives have been used in order to determine any artificial difference arising from the different mathematical treatments. These eventual mathematically induced deviations may appear as undesired differences between experimental and simulated data. Results of the calculations are shown in figure 9.

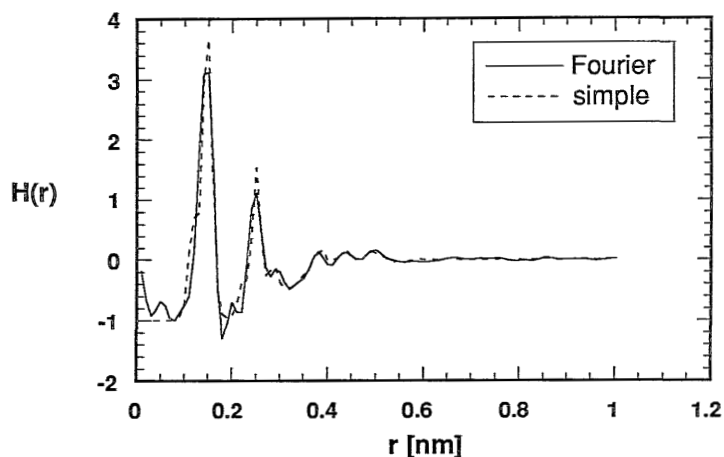


Figure 9. Comparison of radial distribution functions obtained with scattering angle independent electron scattering factors (simple, method 1) with scattering angle dependent factors (Fourier, method 2)

The results are very similar. However, in the  $H(r)$ -curve obtained with the angle dependent scattering factors, two more peaks appear compared with the  $H(r)$  obtained with the simple method. The first appears at a distance below  $1\text{\AA}$  and is therefore unrealistic. The second one appears at around  $2\text{\AA}$ . This is actually the same peak as the one Wignall *et al.* could not identify in their experimentally obtained X-ray patterns. The reason for the appearance can be found in the mathematical

treatment of the data because the simple method does not show any peak at that position. Fourier transformations which are not integrated properly to infinity, but which have a cut-off at a certain maximum  $s_{\max}$ , tend to have small peaks (truncation ripples) on the flanks of a large peak. Since the most realistic comparison between experimental and calculated results was desirable, the calculations were integrated to the same value  $s_{\max}=16\text{\AA}^{-1}$  as has been done for the experiments, and, therefore, it must be concluded that this peak comes from the cut-off in the integration step and has no physical significance. Similar effects have been observed by Boek [18] for the simulation of neutron scattering on ureum-water mixtures. For further considerations only RDFs  $H(r)$  obtained by the Fourier transformation route will be used.

### 6.5.2. The Total Radial Distribution Function of PET

The main aim of this study was the elucidation of the question whether a computer simulated structure actually represents the bulk material as it is used in experiments. For this purpose, the simulated radial distribution function  $H(r)$  must be compared with the experimental ones determined by Wignall *et al.* Each of the three experimentally determined  $H(r)$ s, which were earlier shown in figure 4, is compared now with the simulated total RDF in figure 10 a-c.

In figures 10a and b one can observe that the number of the maxima and minima are correctly reproduced by the simulated structure. However, the positions of the simulated peaks are always shifted towards larger distances. For the first two large peaks this is certainly caused by the numerical accuracy used during the determination of the radial distribution functions. Small variations of the equilibrium bond distances in the used force field can be the reason for shifts in the positions of the maxima to larger distances.

Comparing only the first four peaks of the simulations with the RDF of the sample quenched from the melt, a good agreement of the magnitude and shape of the peaks can be seen. In figure 10a the peaks in the simulated RDF at 0.38 nm, 0.41 nm and 0.5 nm are, however, considerably smaller than the experimentally observed peaks for the sample quenched from the melt. The annealed sample in contrast, agrees rather well regarding the peak height also at larger distances as shown in figure 10b. However, in both figures 10 a and b the minimum for the experimental RDFs at 0.31 nm is not at all resembled by the simulated RDF. Instead, the sample quenched from the rubbery state has almost the same  $H(r)$ -value at this minimum as shown in figure 10c. In this latter experimental RDF, on the other hand, no distinct minima and maxima can be observed for larger distances. It appears that single parts of the three experimental radial distribution functions can indeed be identified in the simulated RDF.

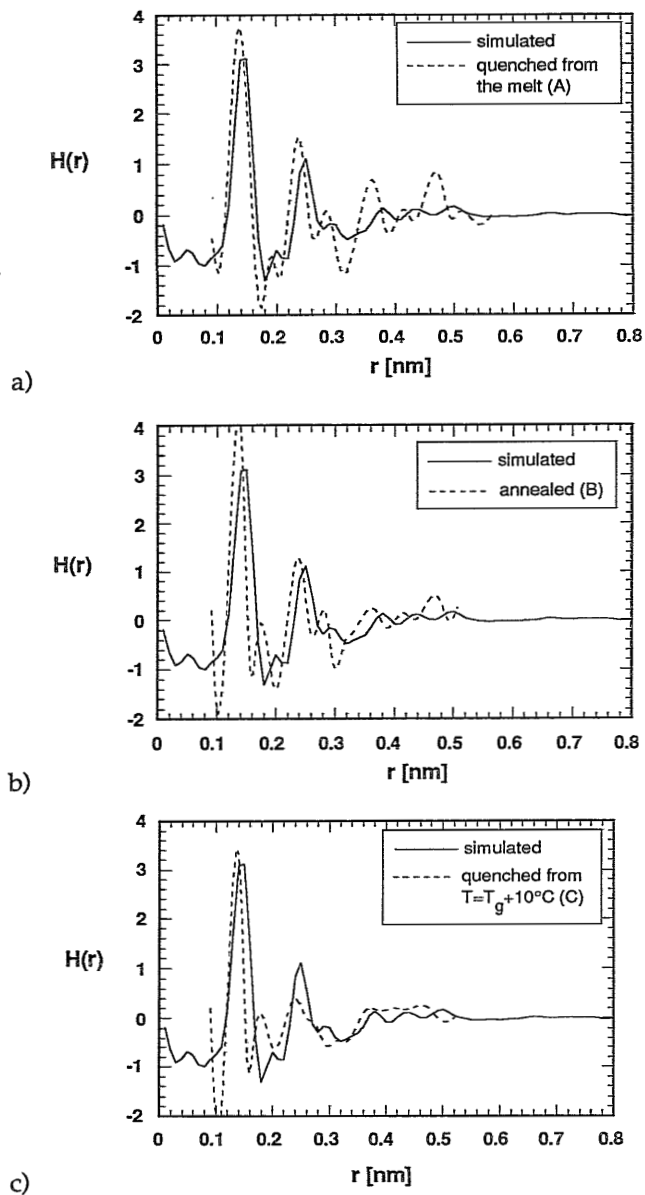


**Figure 10.** Comparison of the simulated radial distribution function with the one obtained experimentally from PET samples having different thermal histories as described in the legend and in paragraph 6.4

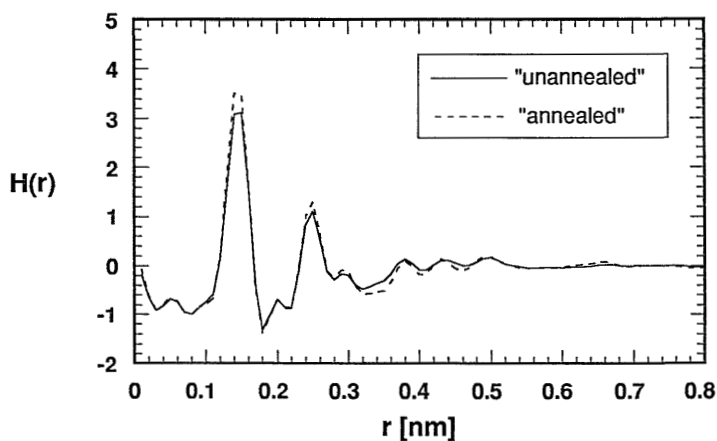
Unfortunately, the procedure by which the simulated box has been prepared cannot be compared to any thermal treatment as carried out experimentally. Nevertheless,

since the shape of the simulated RDF is in general agreement with the experimentally determined one, the statement that the simulated box represents the structure of the bulk polymer seems reasonable. One may ask how sensitive the simulated RDF actually is for changes in the chemical structure of the polymer or whether it is possible to obtain the same RDF with a different structure. In paragraph 6.5.4 we will show that minor changes in the chemical structure can cause significant differences in the total RDF.

The question remains whether the differences in the experimentally determined RDFs are related to any morphological effect induced by a thermal treatment and whether they can be simulated with MD. The following steps were carried out during MD runs in order to simulate annealing experiments:

1. 20 ps equilibration run at an elevated temperature of  $T=355$  K with a softcore potential and without electric charges
2. Energy minimization at  $T=355$  K with a hardcore potential and electric charges
3. Shrinking of the box with a softcore potential and without electric charges at  $T=298$  K
4. Energy minimization of the shrunk structure
5. Equilibration and production run as described earlier

The RDFs were determined from the production run and compared with the RDF of the "unannealed" box. Any change in the RDF may stem from intra- and intermolecular alterations. Changes in angles in a chain segment are responsible for intramolecular alterations. Intermolecular alterations represent morphological changes.



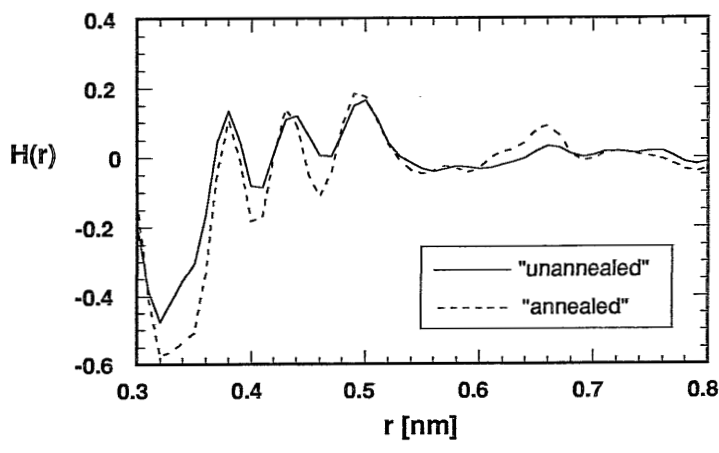


Figure 11. Effect of "annealing" on the simulated radial distribution function of pPET; figure 11b represents a particular part of figure 11a

In figure 11 the RDF of the original box is compared with the one obtained from the "annealed" box. A considerable difference for the total RDFs between the original box and the "annealed" one can be observed. Differences between maxima and minima become more distinct in the region of 0.3 up to 0.5 nm as shown in 11b. The minimum at  $r=0.31$  nm becomes considerably deeper and broader. These results are in contradiction with the findings of Wignall *et al.* shown in figures 10a and b. There, the differences between the maxima and minima become smaller upon annealing coming from the quenched, virgin film. Furthermore, the simulation of the annealing process also shows an increase of the first two large peaks at 0.15 and 0.25 nm. A third, interesting fact which can be observed in figure 11 must be pointed out. A small broad peak at 0.68 nm present in the original box becomes more distinct after annealing. Summarizing these observations one can say that the simulated annealing procedure results generally in a RDF containing more distinct extrema.

Recalling figure 10c, it may promote the speculation whether an annealing treatment of sample C (after quenching) would have resulted in similar effects as observed in the simulation. Since these data are not available, a definite conclusion can not be drawn. But it certainly can be concluded that those maxima and minima in the experimental RDFs which show changes upon a heat treatment, do also show changes in the simulated RDF. At a purely experimental stage, no further interpretations can be made on the nature of the changes in the RDF upon a heat treatment. For the molecular dynamics simulation, further detailed work can be carried out by analyzing *pair* radial distribution functions.



### 6.5.3. Pair Radial Distribution Functions

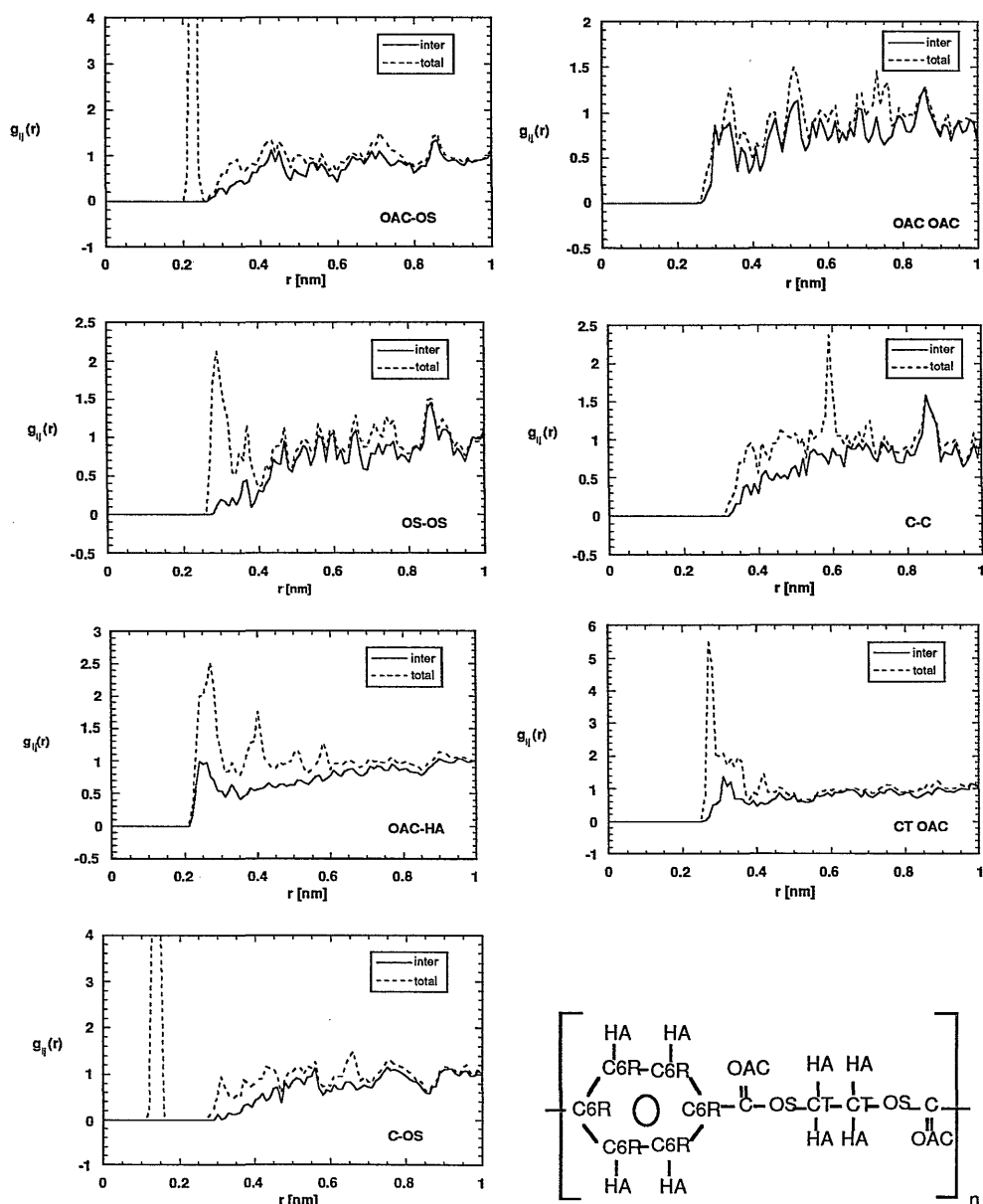


Figure 12. Pair radial distribution functions for atoms bond in the aliphatic part of the polymer chain

Since we have presented strong evidence that the simulated polymer box has the same structure as the bulk polymer, a closer look at pair radial distribution functions which build up the total RDF  $H(r)$  is allowed. Many of the 21 pair RDFs show only peaks resulting from chemical bonds and do not show any intermolecular correlations. These will not be presented here. In order to prohibit confusion, it must be mentioned that the word "total" in the legends of the plots shown in figure 12 stands for pair RDFs that cover all atoms. It is therefore the sum of inter- and intramolecular distance correlations.

All the pair radial distribution functions  $g_{ij}(r)$  shown in figure 12 contain distinct peaks in the intermolecular correlation function. Only pairs of atoms placed in the aliphatic parts of the polymer chain show any distance correlations. All intermolecular RDFs for the benzene ring carbons do not show any significant intermolecular correlation. Therefore, any type of parallel or offset alignment of the benzene rings cannot be found. Unfortunately, the local ordering found for the flexible part of the polymer repeat unit between two phenyl rings is hardly transferable into any three-dimensional picture of orientations until now.

One way of analyzing any parallel alignment of chain segments mathematically is by specifying vectors on the chain (for example from OS to OS atoms) and comparing their three-dimensional orientation to each other. Different types of vectors (OS-OS, C-C, C6R-C6R) were used but no indication of alignment was found. From all the intermolecular RDFs only one allows direct physical interpretation: the first peak in the intermolecular RDF of OAC-HA represents the phenomenon of some kind of hydrogen bonding. This distinct peak at 0.28 nm becomes more pronounced as the box undergoes an "annealing" treatment as shown in the appendix A to this chapter.

From all the pair RDFs it can be seen that the peaks resulting from intramolecular distances are much larger than those stemming from intermolecular ordering. The intramolecular peaks therefore have the largest input on the form of the total RDF  $H(r)$  as it is shown in the previous paragraph. Although local orderings can be found in the pair RDFs (which are not accessible experimentally), these do not have a considerable influence on the total RDF  $H(r)$ . Therefore, one must be careful in extracting information about the presence or absence of local ordering from the experimentally obtained total RDF  $H(r)$ . The conclusion of Wignall *et al.* that the investigated PET-samples do not show any local ordering is not so obvious in the light of the detailed simulations presented above.

Annealing of the box led to separation of peaks in the distance range of 0.3-0.5 nm and to a new distinct peak at 0.68 nm (see figure 11b). From the total radial distribution function it was not possible to decide whether these alterations stem from inter- or intramolecular changes. In order to get more insight in this problem,

the intermolecular pair radial distribution functions for the annealed and unannealed box were compared. One example is given in figure 13 for the carbonyl oxygen-carbonyl oxygen pair RDF. A drastic enhancement of local order due to the heat treatment can be concluded from this figure. Other pair RDFs showing similar phenomena are shown in the appendix A. These figures represent strong evidence that the changes in the experimentally obtained RDF  $H(r)$  caused by a heat treatment can also be linked to alterations in the intermolecular structure of the polymer matrix.

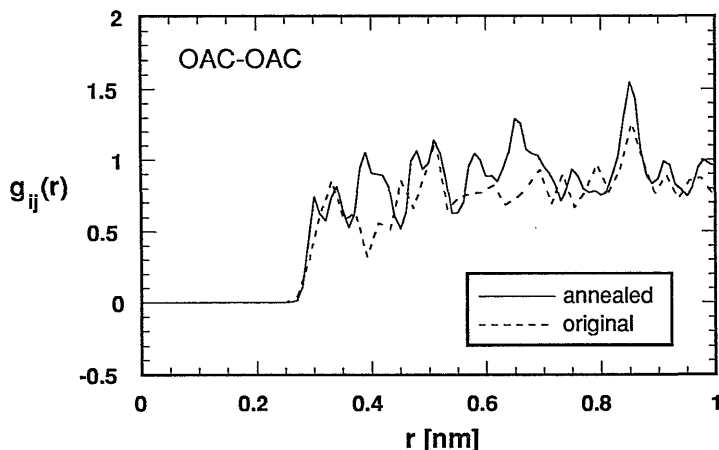


Figure 13. Pair radial distribution function for the carbonyl oxygen-carbonyl oxygen pair obtained from the annealed and unannealed box

#### 6.5.4. On the Morphology of Poly(ethylene terephthalate) and Poly(ethylene isophthalate)

Mass transport behaviour of aromatic polymers depends strongly on the position at which benzene rings are bonded in the polymer backbone. A para substitution generally results in a higher diffusivity compared to the meta substitution. In some cases, as with poly(ethylene terephthalate) and poly(ethylene isophthalate), the larger diffusivity can be explained by a larger amount of free-volume. However, in other cases such as polytriazoles and polyimides, the diffusivity may be larger for the polymer which has the lower absolute amount of free-volume. It has been speculated that not only the absolute value of the free-volume but also its distribution must be of considerable importance. The free-volume distribution is hardly measurable experimentally. A detailed comparison of structures built up by

meta- or para substituted polymers by means of MD simulations may give more insight into the problem.

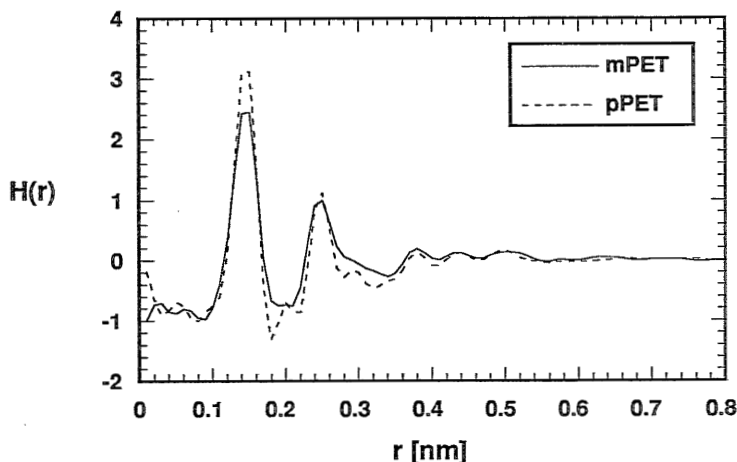


Figure 14. Radial distribution functions simulated for pPET and mPET

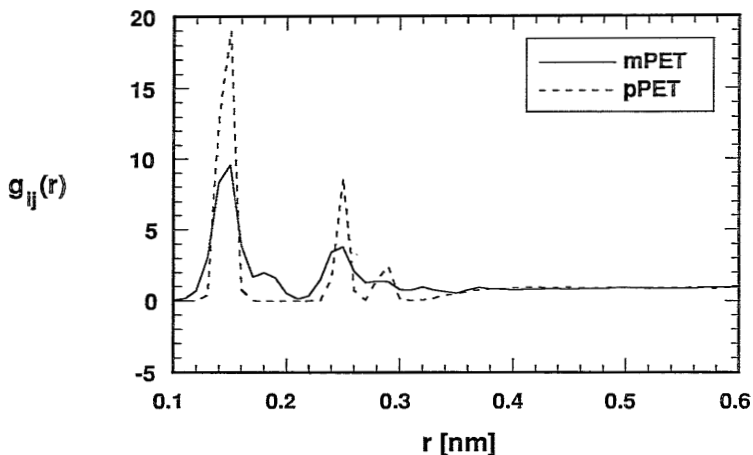


Figure 15. Total pair radial distribution function for the benzene ring carbon atoms for pPET and mPET

For this purpose 5 chains of poly(ethylene isophthalate) have been placed in a box according to the method described above. The final density during the production runs is the same as the one of PET. Therefore, the two boxes are a perfect tool to study the influence of the meta or para substitution on the free-volume distribution.

But before doing that, the structure of the simulated poly(ethylene isophthalate) (mPET) will be analyzed by means of radial distribution functions. The total radial distribution function  $H(r)$  for both pPET and mPET are shown in figure 14. Generally spoken, one can state that the first major peaks at  $r=0.15$  nm and  $r=0.25$  nm are smeared out while the following peaks at the range from 0.35 to 0.55 nm remain the same.

The reason for the smearing out of the first peaks can be found in the chemical structure of the polymer. Because the only difference between the two polymers is the position of the phenylring carbons connecting the polymer backbone, a pair radial distribution function for the pair C6R-C6R may give some more detailed information. This is shown in figure 15. Considerable differences can be observed between the meta and the para substituted polymer.

For pPET three sharp peaks can be seen representing the three carbon-carbon distances in the symmetric benzene ring. However, in the meta substituted benzene ring the positions of the carbons are at the same position but less strictly fixed resulting in a smaller peak height and a broader distribution. This, of course, has a direct impact on the total polymer. The intramolecular maxima for the atoms in the aliphatic part of the chain also become more diffuse (see Appendix B to this chapter) indicating a larger flexibility of the polymer chain segment. In fact, this observation is a direct support for the understanding that the lower glass transition temperature of mPET ( $T_g=68^\circ\text{C}$ ) stands for an enhanced chain flexibility compared with the higher  $T_g$  of pPET ( $T_g=78^\circ\text{C}$ ).

Smit [9] postulated that this increased chain flexibility leads to a better packing of the polymer chains. *Better* is meant in the sense of *more homogeneous* packing so that there exists a large amount of small free-volume pockets and a relatively small amount of large free-volume pockets. In contrast, a less flexible polymer would have the opposite structure: more inhomogeneous with large "holes" inside. This distribution of free-volume is experimentally hardly accessible. In a simulated box, however, this can be done easily.

Free volume distributions for both polymers were determined following the procedure of Ludovice [19]. Each atom in the box is considered as a sphere with its respective van der Waals radius. Randomly, a point within the periodic box was chosen. Because the coordinates of all atoms and their van der Waals radius are known, it could be checked whether the random point was placed in unoccupied volume. If so, the spherical trace volume of this point was increased gradually in discrete size steps (each related to a counter) until the surface of the trace volume touched for the first time the surface of a polymer chain atom. At this point, counters for volumes smaller than the trace volume were increased by one. Doing this  $N=10^6$  times gives a good representation of the box. The counters for each volume

normalized for the total number of tests  $N$  equals the relative probability that a free-volume pocket of this size can be found in the polymer box. The area under the curve should be equal to one.

$$\sum_{m=1}^N \frac{n(d)}{N} = 1 \quad (26)$$

The free-volume distribution of the para substituted poly(ethylene terephthalate) and the meta substituted poly(ethylene isophthalate) are shown in figure 16.

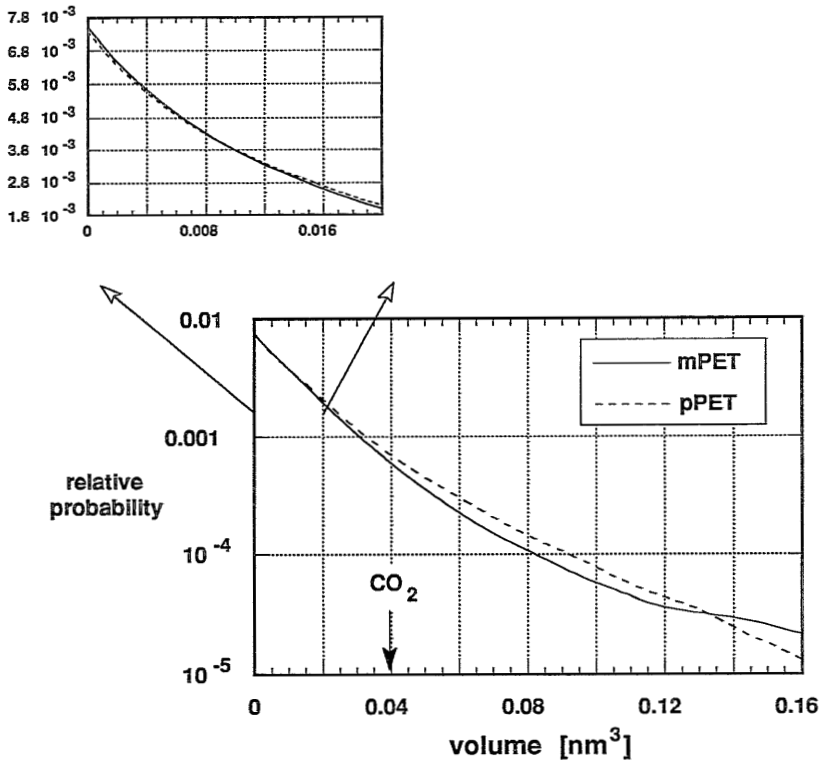


*Figure 16. Free-volume distributions obtained from boxes of pPET and mPET; the volume of a CO<sub>2</sub> molecule is indicated for comparison; upper graph is an enlargement of the cross-over of the curves at small free-volume pockets*

In the volume range from 0.01 nm<sup>3</sup> up to 0.13 nm<sup>3</sup> there are always more free-volume pockets present in pPET than in mPET. At very small volumes there exist slightly more pockets in the meta substituted polymer. The difference between the two graphs in the enlargement of figure 16 is statistically significant since it does not depend on the amount of traces carried out.

The results shown support the speculation about the packing tendency of flexible polymers as discussed above. At very large volumes, the probability for the existence of these volumes becomes larger for mPET. However, the probability is so small that it seems reasonable to say that these pockets do not have any significant influence on the mass transport behaviour of the simulated polymer. A more rigorous free-volume analysis using other methods may be even more valuable. Of importance in this context may be also the *connectivity* of the free-volume pockets.

## 6.6. Conclusions

In this chapter it has been shown that wide angle X-ray scattering experiments can be simulated by a Molecular Dynamics study. The simulations are in qualitative agreement with the experimental results. However, the radial distribution function is mainly determined by intramolecular distance correlations. Local ordering can better be observed in pair distribution functions but this has hardly any influence on the total simulated scattering pattern. Therefore, extracting information about intermolecular ordering from experimental scattering data must be carried out carefully. "Annealing" of the MD box showed an influence on the local ordering phenomena in the pair distribution function and thus on the total radial distribution function.

Meta- instead of para-substitution of a benzene ring in the polymer backbone causes a considerable alteration of the radial distribution function. Detailed analysis of the pair distribution function revealed that the chain flexibility is larger in the mPET compared to the pPET. A free-volume analysis of the mPET and pPET shows that over a wide volume range relevant for the transport of gaseous penetrants the probability to find a certain volume size is larger for pPET than for mPET. This can explain why two polymers with the same total amount of free-volume have very different diffusion coefficients.

## References

- (1) E. Smit E., M.H.V. Mulder, C.A. Smolders, H. Karrenbeld, J. van Eerden, D. Feil, Modelling of the diffusion of carbon dioxide in polyimide matrices by computer simulation, *J.Membrane Sci.*, 73 (1992) 247
- (2) P. Meares, The diffusion of gases through polyvinyl acetate, *J.Am.Chem.Soc.* 76 (1954) 3415
- (3) A.A. Gusev, U.W. Suter, Mobility of small molecules in dense polymers subject to thermal motions, submitted *J.Chem.Phys.*

- (4) P.J. Flory, Principles of Polymer Chemistry, Cornell University Press, Ithaca, NY, 1953
- (5) L.H. Sperling, Physical Polymer Science, 2nd edition, J. Wiley & Sons 1992
- (6) J.G.A. Bitter, Transport mechanisms in membrane separation processes, Plenum Press, New York, 1991
- (7) M. Hutník, F.T. Gentile, P.J. Ludovice, U.W. Suter, A.S. Argon, An atomistic model of amorphous glassy polycarbonate of 4,4'-Isopropylidenediphenol, *Macromolecules* 24 (1991) 5962
- (8) W.F. Van Gunsteren, H.J.C. Berendsen, Groningen Molecular Simulation Library, 1987
- (9) E.Smit, Modelling of the diffusion of gases through membranes of novel polyimides, Ph.D. Thesis, 1991, Enschede/The Netherlands
- (10) M.W. Hellums, W.J. Koros, G.R. Husk, D.R. Paul, Fluorinated Polycarbonates for gas separation applications, *J. Membrane Sci.*, 46 (1989) 93
- (11) S.G. Charati, A.Y. Houde, S.S. Kulkarni, M.G. Kulkarni, Transport of gases in aromatic polyesters: correlation with WAXD-studies, *J. Polym. Sci., Polym. Phys.*, 29 (1991) 921
- (12) G.R. Mitchell, in: Order in amorphous "state" of polymers, Ed.: S.E. Keinath, R.L. Miller, J.K. Rieke, Plenum Press, NY.
- (13) F. Hadju, G. Palinka, On the determination of the absolute intensity of X-rays scattered by a non-crystalline specimen, *J. Appl. Cryst.* 5 (1972) 395-401
- (14) C.J. Pings, J. Waser, Analysis of scattering data for mixtures of amorphous solids or liquids, *J. Chem. Phys.*, 48 (1968) 3016
- (15) G.S.Y. Yeh, A structural model for the amorphous state of polymers: folded-chain fringe-micellar grain model, *J. Macromol. Sci.-Phys.*, B6 (1972) 451
- (16) G.W. Longman, R.P. Sheldon, G.D. Wignall, Investigation of short range ordering in polymers by means of radial distribution functions derived from X-ray diffraction, *J. Material Sci.*, 11 (1976) 1339-1346
- (17) M. Wessling, Th. v.d.Boomgaard, M.H.V. Mulder, C.A. Smolders, Transport of gases through polymeric membranes, to be published *Makromol. Chem. Macromol. Symp.*
- (18) E.S. Boek, W.J. Briels, Molecular Dynamics simulation of aqueous urea solutions; to be published *J. Chem. Phys.*, Jan. (1993)
- (19) V.M. Shah, S.A. Stern, P.J. Ludovice, Estimation of the free-volume distribution in polymers by means of a Monte-Carlo Technique, *Macromolecules* 22 (1989) 4660-4662



## Appendix A

In this appendix partial radial distribution function obtained from the original box are compared with those obtained from the “annealed” box. Only *intermolecular* correlations are considered. And here, only those 5 of 21 are shown which have considerable local ordering in the original box. In general, one can conclude from these figures that the annealing procedure has an enhancing effect on those local orderings which preexist in the original box.

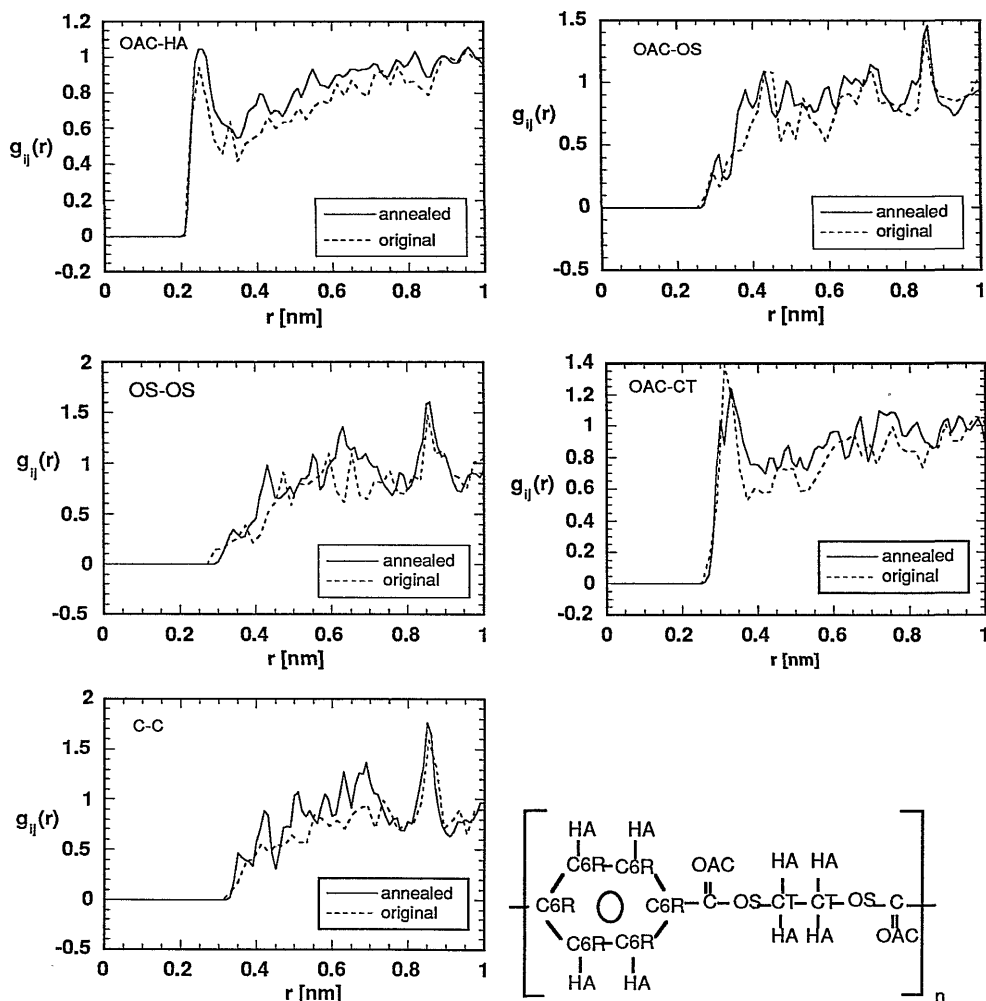


Figure 1. Comparison of pair radial distribution functions obtained from an unannealed (original) and an annealed polymeric box

## Appendix B

In this appendix pair radial distribution functions obtained from the meta and para isomeric polymers poly(ethylene isophthalate) and poly(ethylene terephthalate) are compared. Only the total RDFs (inter + intramolecular correlations) are shown.

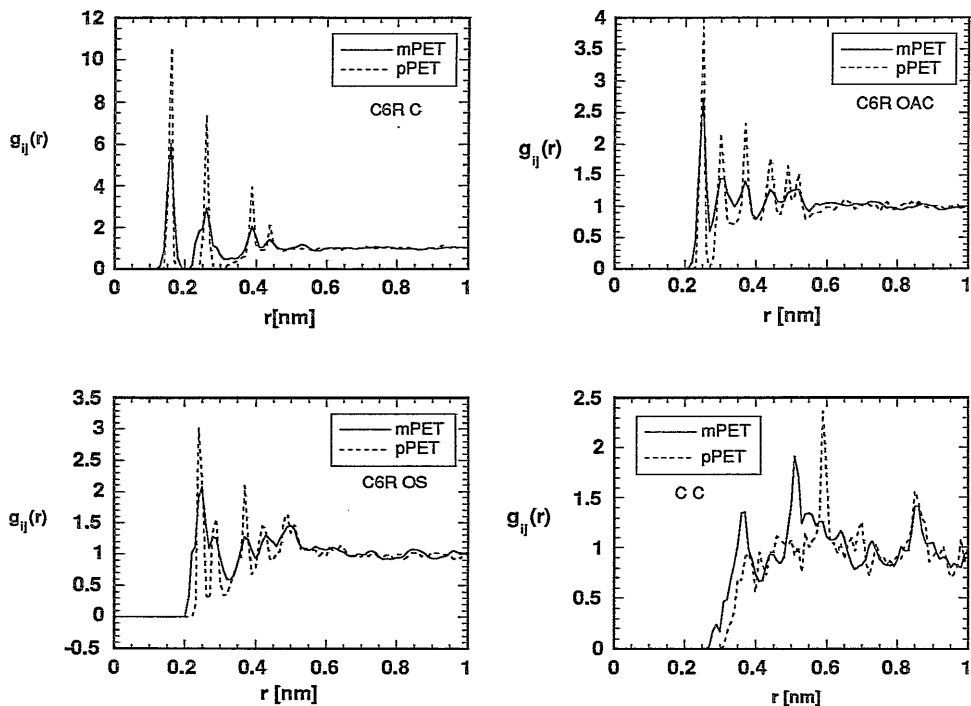


Figure 1. Comparison of some total pair radial distribution functions for mPET and pPET

# Chapter 7

## Carbon Dioxide Foaming of Glassy Polymers

### 7.1. Introduction

Microcellular foams prepared from thermoplastic materials have been developed in the past in order to reduce the amount of polymer used in mass produced items [1]. In this process, a glassy polymer is saturated with a non-reactive gas at high pressures and at room temperature. The pressure is released after gas uptake has reached equilibrium and the specimen remains supersaturated with gas since the release of absorbed gas in time is slow. If now the specimen is heated above its glass transition temperature, nucleation of a gas phase occurs and gas bubbles can grow in the matrix due to the drastically increased chain mobility in the rubbery state. An intensive, experimental study on nucleation and growth of gas bubbles was carried out by Kumar [2] for the system polycarbonate and CO<sub>2</sub>.

In this paper we will describe how this particular production process of porous glassy polymers can be used to investigate the influence of the absorbed non-reactive gas on the polymer matrix itself. First, we will present a detailed physical and mathematical description of mass and heat transport phenomena occurring during the preparation process. Experiments and calculations are carried out for the system polycarbonate/CO<sub>2</sub>. In a second part, we will illustrate that from this model an easy-to-use method can be developed which determines in a simple manner the glass transition temperature depression by absorbed gaseous penetrant molecules. Here, the experiments were carried out with the polyimide 6FDA-3PDA. (For the chemical structure, see fig 3.2).

The glass transition temperature depression is of special interest in the processing of thermoplastic materials into foams. During the extrusion process the dissolved CO<sub>2</sub> strongly influences the viscosity of the polymer melt. Often, the viscosity is empirically related to the difference between the processing temperature and the glass transition temperature, which is actually not known for the polymer/CO<sub>2</sub>

system because the  $T_g$ -depression is unknown. Furthermore, the  $T_g$ -depression is of special interest in membrane processes based on the solution-diffusion transport mechanism. In this case, the sorbed penetrant molecules alter the transport properties of the polymer in such a way that the polymer shows reduced selective properties [3].

In a third part, we will concentrate on the mechanism of the foam formation. From literature [2] it is clear that the nucleation mechanism of the bubbles is not completely understood. Therefore, a number of experiments on the nucleation mechanism of bubbles will be presented using polysulfone as a polymer.

Instead of using the same polymer for all experiments, different problems linked to the foaming process were tackled by experiments using different polymers. This had the advantage to demonstrate that the whole procedure of preparing microcellular foams can be applied to any kind of glassy polymer. Since the microcellular foams are only a small side project (however with a definite link to the main research topic of relaxation phenomena in dense gas separation membranes) not all the interesting problems could be worked out in detail. Some of the experiments touch only on a certain problem thereby initiating new questions.

## 7.2. Mass and Heat Transport Phenomena occurring during the Foaming Process of Polycarbonate

### *Experimental*

In recent publications on the production of microcellular glassy polymers, the analysis of the foamed samples concentrated on the number and size of bubbles depending on preparation parameters like pressure, temperature and foaming time. We have repeated the experiments on the system polycarbonate/ $\text{CO}_2$  with a different intention, as described in the introduction. The PC was kindly supplied as 100  $\mu\text{m}$  thick extruded sheets by DSM/The Netherlands. PC has a glass transition temperature of 150  $^\circ\text{C}$  and a density of 1.2  $\text{g}/\text{cm}^3$ .

First screening experiments were carried out as follows: the PC-sample was saturated at 40 bar  $\text{CO}_2$  for 24 hours at room temperature. Quickly after pressure release, the sample was dipped in a glycerol bath of 100 $^\circ\text{C}$  for 10 seconds. The sample turned from transparent into non-transparent (white) due to the nucleation of bubbles although the bath temperature was well below the glass transition temperature of the pure PC. The foamed samples were washed in a water/ethanol mixture for one hour and afterwards the samples were freeze-fractured in liquid nitrogen. A scanning electron micrograph of a typical structure is shown in figure 1.

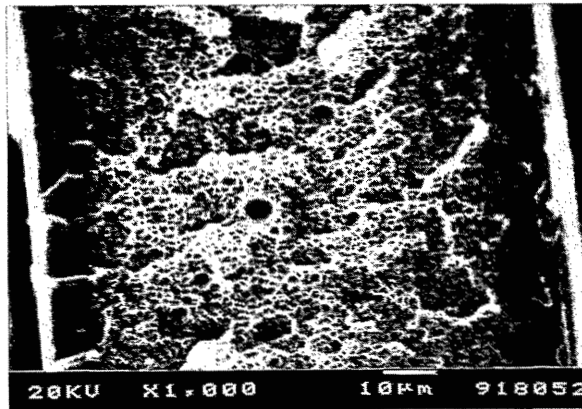


Figure 1. Microcellular polycarbonate foamed after supersaturation with carbon dioxide

Remarkably, the specimen shows, besides the bubbles observed earlier, a dense, non-porous layer at the outside of the film and an abrupt transition from the dense layer to the porous structure. This integral, unfoamed skin has been mentioned previously [4,5]; however, no *physical* explanation was formulated for the appearance of this skin. In the following part, a physical picture together with mass and heat transfer equations will explain the appearance and even predict the thickness of the dense layer.

### Discussion

As described above, the polymer specimen is saturated in a pressurization step (figure 2a) at a certain pressure for a fixed time at ambient temperature. During the pressure release step (2b), the polymer sample is exposed to an environment where the partial pressure of  $\text{CO}_2$  is nearly zero. Hence, the polymer is supersaturated and mass transport of  $\text{CO}_2$  out of the film takes place. A concentration profile of the penetrant in the film will be built up as shown in figure 2b. The shape of the concentration profile, which actually stands for the total penetrant concentration, depends on the time at which the sample is kept in this environment. Since any kind of sorbed penetrant lowers the glass transition temperature of a polymer to some extent, a concentration profile in a polymer sample is automatically accompanied by a glass transition temperature profile. Often, a simple relation (1) correlates the glass transition temperature of a polymer/penetrant system with the weight fraction of the penetrant [6].

$$T_g = T_{g0} - A c \quad (1)$$

$T_g$  is the actual glass transition temperature of the polymer/penetrant system,  $T_{g0}$  is the glass transition temperature of the polymer free of penetrant,  $c$  is the equilibrium concentration of penetrant in the polymer and  $A$  is an empirical plasticization parameter typical for this specific polymer/penetrant system.

A more complex function instead of equation (1) is also known [7]. However, equation (1) is adequate to account for the effect of sorbed penetrant molecules on the  $T_g$  of the polymer [8]. Kumar [2] observed that foaming is not possible for a polycarbonate sample containing 90 mg  $\text{CO}_2/\text{cm}^3$  polymer at temperatures below 60°C. Below this temperature no bubbles can be created since the polymer is then in its glassy state and the energy barrier for the activation of nucleation is too high. Kumar concluded that this confirms the occurrence of "a significant lowering of the glass transition temperature due to  $\text{CO}_2$  sorption". The value of the glass transition observed in this way correlates well with the value of  $T_g = 65^\circ\text{C}$  which can be calculated for the same system when applying equation (1) from Vrentas *et al.* [6].

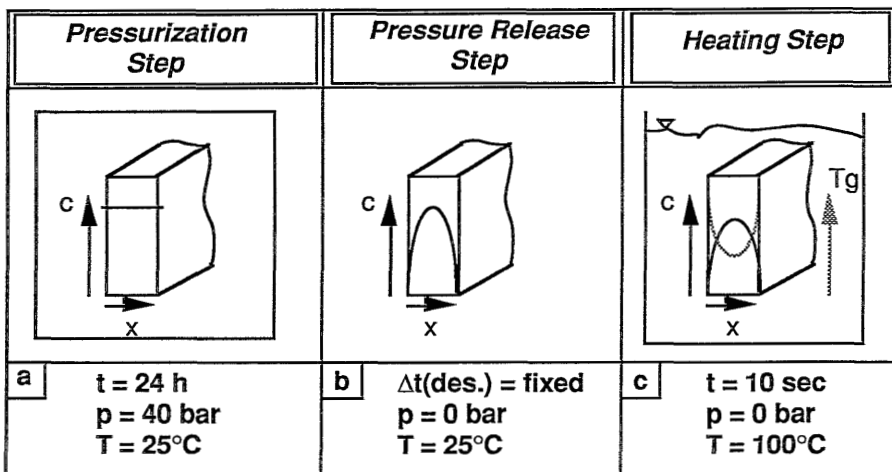


Figure 2. Basic foaming principle showing the individual preparation steps

The nucleation and growth of the bubbles in the inner part of the specimen is not completely, but rather well understood. The reasons for the existence of the outer skins, however, are not known at all yet. The following experiments in which the desorption time in the pressure release step is increased can elucidate the formation mechanism. An increased desorption time will result in a lower concentration profile and a related (increased) glass transition profile. If the sample with a certain concentration profile is dipped into the hot glycerol bath, desorption of  $\text{CO}_2$  will proceed but at the same time a temperature gradient is built up in the film. Now we formulate, on the basis of the above mentioned considerations, that exactly at that

position in the film where the sample temperature is equal to the glass transition temperature, the abrupt transition from a dense to a porous layer can be observed. Pores can only be formed in that part of the film where the  $T_g$  is lower than the local film temperature. For increasing desorption times in the pressure release step one actually expects, that the transition between the dense and porous layer will move towards the middle of the film. Figure 3 shows four polycarbonate samples foamed at the conditions mentioned above. The SEM-photos illustrate undoubtedly that the transition moves towards the middle of the film.

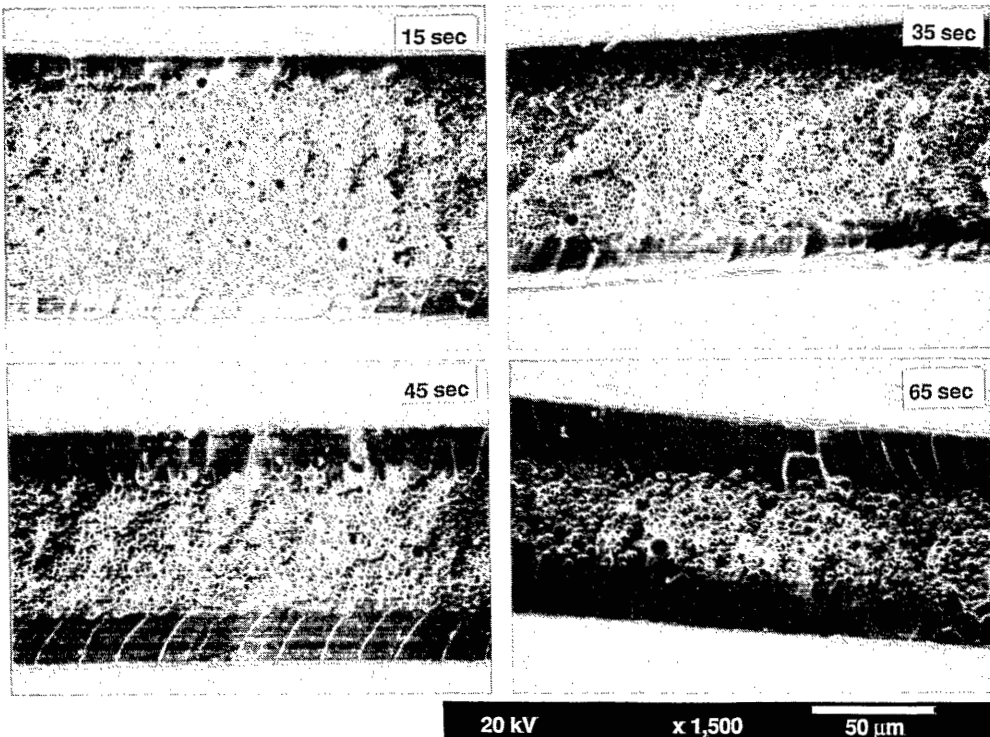


Figure 3. SEM-photos of microcellular PC films foamed at different desorption times during the pressure release step

### Mathematical Modelling

Mathematically, mass and heat transport phenomena occurring during the different preparation steps can be described by partial differential equations as schematically shown in figure 4. The first partial differential equation describes the diffusive transport of the penetrant out of the film during the pressure release step. Here, a constant diffusion coefficient is assumed and the concentration profiles at each time step during the calculations are computed numerically by using a FTCS-method [9]. The polymer film was subdivided into 500 slices. Further input data for the calculations are listed in table 1.

It is assumed for further calculations, that during the heating step in the liquid bath the concentration of  $\text{CO}_2$  in the outer layers remains zero and, hence, desorption proceeds. The sample with a concentration profile obtained for a specific desorption time in the pressure release step is now exposed to boundary conditions which characterize the heating step. In a first numerical procedure, the heat transport into the film at a fixed time step is calculated. In a second procedure, a diffusion coefficient is calculated depending on the temperature in each slice according to an Arrhenius relation.

$$D(T)=D_0 \exp\{-E_d/RT\}. \quad (2)$$

$D(T)$  is the diffusion coefficient at the local temperature  $T$ ,  $D_0$  is the diffusion coefficient at infinite temperature and  $E_D$  the activation energy of diffusion. A new concentration profile can be calculated with these local diffusion coefficients in a third procedure using the same numerical algorithm as for the pressure release step.

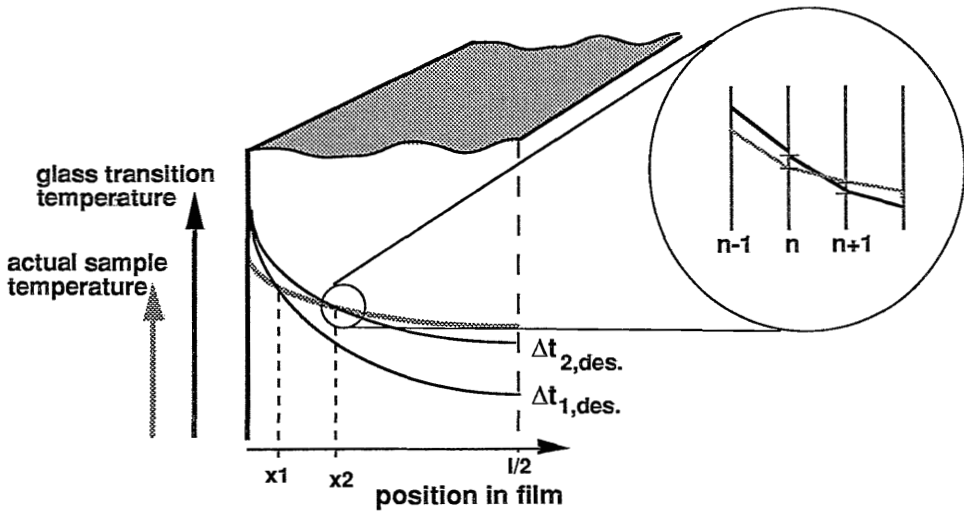


Figure 4. Temperature and glass transition temperature profiles as a function of the desorption time:  $\Delta t_1$  for desorption in the pressure release step is smaller than  $\Delta t_2$

Finally the glass transition profile at this fixed time step can be calculated from the newly calculated concentration profile by using equation (1). This  $T_g$ -profile can be compared with the actual temperature profile in the film. Since the mass transport is very slow compared to heat transport, the temperature profile (grey line in figure 4) will quickly move closer towards the glass transition temperature profile. The transition zone (which we want to determine) is defined as that slice in the polymer



film where the actual temperature is equal to the local glass transition temperature. This was evaluated numerically by controlling the sign of the temperature difference between the glass transition temperature and the actual temperature of the specimen at a specific slice. The position of the transition layer depends strongly on the desorption time in the pressure release step. Layer thicknesses are smaller for shorter desorption times  $\Delta t_{1,des}$ , shown as position  $x_1$  in figure 4. For a longer desorption time the transition moves into the film towards position  $x_2$ . In order to compare the experimental results with the mathematical description, average skin layer thicknesses at both sides of the PC-specimen were determined from SEM photos and plotted versus the square root of time [10] in figure 5.

*Table 1. Variables and parameters for the model calculations*

property	value	Ref.
$P_{CO_2}$	40 bar	
$c_{CO_2}(40bar)$	$44.5 \text{ cm}^3(\text{STP})/\text{cm}^3$	[11]
$c_{CO_2}(0bar)$	$0 \text{ cm}^3(\text{STP})/\text{cm}^3$	
$T_{go}$	$150^\circ\text{C}$	
$T_{bath}$	$100^\circ\text{C}$	
$D_O$	$0.018 \text{ cm}^2/\text{sec}$	[12]
$E_D/R$	$4.5 \cdot 10^3 \text{ K}$	[12]
$D$	$1.5 \cdot 10^{-8} \text{ cm}^2/\text{sec}$	*
$l$	$100 \mu\text{m}$	
$A$ (in equation (1))	1.785	[6]

\* our experiments;  $T=25^\circ\text{C}$

Since the shift of the transition layer into the film appears to be mass transport limited, a linear relation between the square root of desorption time and the layer thickness must be expected. Indeed, the linear relation can be observed as shown in figure 5. Even the mathematical model fits the experimental data quite well confirming the physical and mathematical picture developed in the foregoing paragraphs. For short desorption times the experimental data fit the model calculations very well. The calculations were stopped because of lack of computer time. At longer desorption times the layer thicknesses for both sides of the film diverge. This might be caused by different polymer chain packing densities in the film depending on the thermal history during the extrusion process.

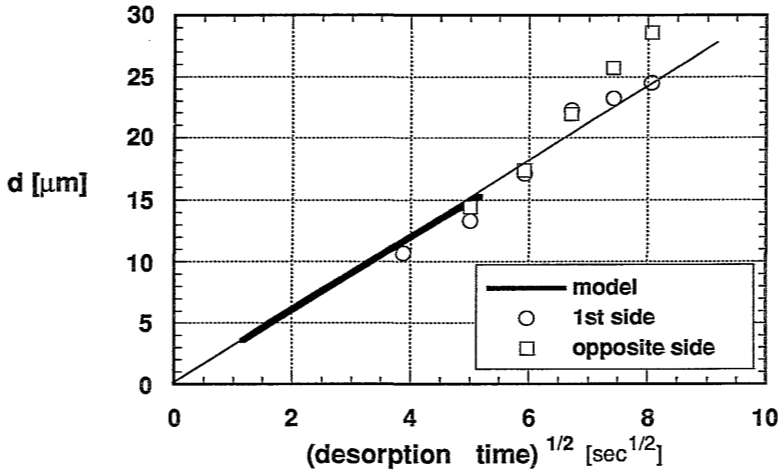


Figure 5. Comparison of model calculation with experimental skin layer thicknesses

### Nodular Structure

A closer look at cross-section of the homogeneous, dense outer layers of the foamed specimen reveals a peculiar structure. The layer is not really dense and homogeneous as it was before the foaming experiment but shows a nodular structure on the SEM photos as can be seen in figure 6.

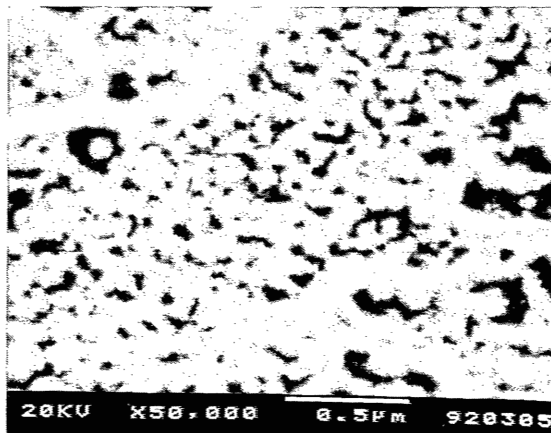


Figure 6. SEM-photo of the nodular structure found in the cross-section of the skin layer of a microcellular polycarbonate sample

The conditions at which the samples were prepared are the same as mentioned above. In order to investigate at which step in the process the nodular structure occurs, the preparation procedure was stopped at different stages and the sample was analyzed by SEM. No nodules at all can be observed before the saturated sample was exposed to the heating step in the hot glycerol bath. These experiments confirm that the observed nodules are not artefacts introduced by the preparation techniques for the electronmicroscope analysis. Nevertheless, the influence of sample preparation conditions for the SEM analysis was also investigated. The samples are normally sputtered with gold at an argon pressure of 0.1 torr for around 3 minutes at a current of 15 mA and the specimen 55 mm underneath the gold electrode. Sometimes, gold deposition on a smooth inorganic glass surface also results in a nodular structure, but the nodule size becomes then zero upon extrapolation to zero sputter time.

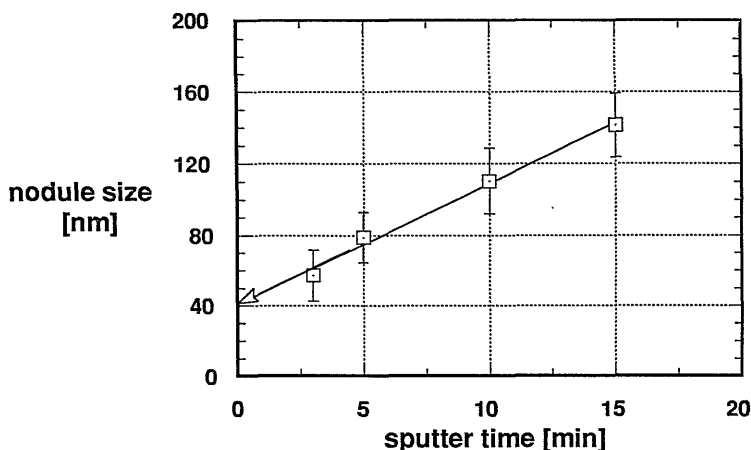


Figure 7. Nodule size depending on the sputter time

The same PC-sample was sputtered stepwise for different sputter times. In between two sputter steps the nodule size was measured on SEM photos at the same position of the fracture surface of the specimen. With increasing sputter time the size of the nodules in the cross-section of the non-porous outer layer of the PC-specimen increased as shown in figure 7. From the slope of the curve an average deposition rate can be calculated, which actually meets the specification of the apparatus well. Extrapolation to zero sputter time results in the actual nodule size of 40 nm.

Atomic force microscopy (AFM) was used to reconfirm and to illustrate in more detail this particular structure. No structure at all was found in untreated samples. After foaming, a grainy nodular structure was found in the cross-section of the dense outer layer as shown in figure 8. Here, the nodule size is in the range of 50 -

200 nm. The discrepancy between the AFM and the SEM photos might simply be caused by the fact that the AFM analyzed surfaces do not represent the small part of the layer observed in the SEM-photo. With the AFM used, it was hardly possible to spot on a specific surface area of the specimen.

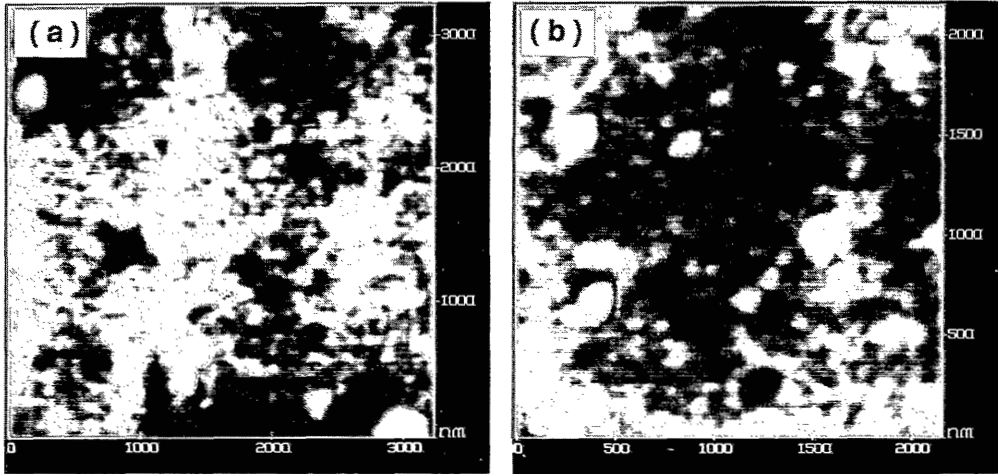


Figure 8. Atomic force microscopy photo of the nodular structure of the skin layer; picture size represents a surface of (a)  $3\mu\text{m} \times 3\mu\text{m}$  and (b)  $2\mu\text{m} \times 2\mu\text{m}$

The physical reasons for the creation of these nodules are not so obvious. From figure 6 it *seems* as if the nodular structure is built out of ball-like entities with voids in between. However, the creation of such spherical surfaces would be very energy intensive because of the disentanglement of the dense, glassy polymer matrix. Energy might be sufficiently supplied in the form of the high temperature of the heating step and the extraordinary high supersaturation. On the other hand nodules in amorphous dense polymer films have been reported by Yeh [13] and Geil [14]. The occurrence of these nodules in amorphous polymers and the tendency of amorphous polymers to crystallize upon heat treatment lead to the development of the model of Yeh [15]. This model describes local ordering by the folded-chain fringed micellar grain model which is actually a type of bundle model [16]. Bundle models generally assume small ordered regions showing strong, narrow distance correlations which are superposed by disordered regions showing very broad distance correlations as described in chapter 2.

The nodular structures reported by Geil are small in size and have generally a diameter of around  $30\text{\AA}$ . These nodules can aggregate into “super-nodules” depending on the thermal history of the sample because aggregation of nodules may minimize their intergrain surface energy. Since a heat treatment as well as  $\text{CO}_2$ -sorption both have the potential to enhance ordering phenomena, *e.g.*, crystallization in amorphous PET [17], it seems also reasonable that during the

preparation of the microcellular foams the polymer sample experiences such extreme conditions, *i.e.*, high penetrant concentration and high temperature, that the creation of such “super-nodules” out of areas of enhanced local ordering in the sense of bundle models may be favourable. At this point and time no definite decision on the validity of one or the other physical interpretation can be made. More experiments like permeation experiments which would give information on the density and eventually porosity of the toplayer are required to elucidate this problem.

### 7.3. Sorption induced Glass Transition Temperature Depression of the Polyimide 6FDA-3PDA

Polyimides are polymers with outstanding thermal, mechanical and chemical properties. A family of polyimides based on hexafluoro-dianhydride units has attracted considerable interest in the last five years in the field of membrane technology. These polymers show high permeabilities and high selectivities for gas mixtures. However, highly sorbing penetrants like CO<sub>2</sub> swell the polymer significantly and the selective properties are reduced significantly. Relaxation phenomena occur in the form of time dependent gas permeabilities and swelling volumes [3]. These phenomena are globally summarized in the term plasticization. Since plasticization can be related to a depression of the glass transition temperature, it is of general interest to what extent the  $T_g$  of a polyimide, which might be used as a membrane material, is depressed by the presence of sorbed CO<sub>2</sub>. Most of the methods described in literature, however, are not very suitable or even impracticable for polymers with glass transition temperatures higher than 200°C. The method described in the first part of this paper is very easy to use and might be suitable for this purpose.

The polyimide used is 6FDA-3PDA; chemical structure, physical characteristics, *i.e.*, density, molar mass and glass transition temperature are listed in chapter 3.2. Films of around 100 µm thickness were cast from a DMAc solution. The solvent was evaporated in a nitrogen flushed glove box. Afterwards the films were dried in a vacuum oven at 70°C for at least one month in order to guarantee the complete removal of residual solvent. The foaming experiments were carried out in the same way as those described above.

Not only the desorption time in the pressure release step was varied but also the bath temperature and the applied pressure. Depending on the difference between the bath temperature and the actual  $T_g(p)$ , different foam structures can be obtained (see figure 9). In general, the average cell diameter increases with increasing bath

temperature at a constant saturation pressure [2]. Figure 9a shows a foam structure where small cylindrical pores of 0.5  $\mu\text{m}$  diameter are embedded in a solid polymer matrix. In the sample shown in figure 9b, large honeycomb-like pores, 10  $\mu\text{m}$  in size, are separated by thin walls of polymer matrix.

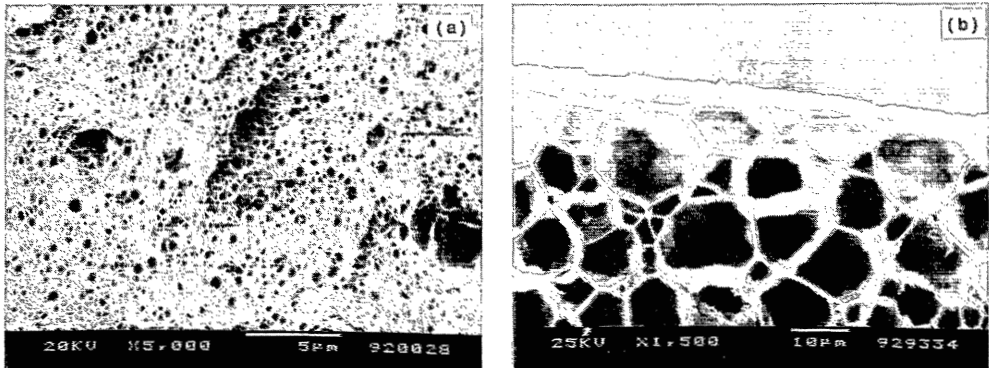


Figure 9. Microporous polyimide foamed by carbon dioxide at (a)  $p_{\text{CO}_2}=35$  bar and  $T=135^\circ\text{C}$  and (b)  $p_{\text{CO}_2}=20$  bar and  $T=220^\circ\text{C}$

In a new experimental series the desorption time was varied at each bath temperature. The thickness of the dense, outer layer was measured and was plotted in figure 10 normalized for the initial film thickness versus the square root of the desorption time. In this figure the normalization of the layer thickness was chosen since a maximum value of 0.5 for  $d/d_0$  means that no foaming occurs in the specimen.

For bath temperatures of 137, 157 and 237 $^\circ\text{C}$ , respectively, the samples always show a microcellular structure for the desorption times investigated. However, at 114 $^\circ\text{C}$  no foaming could be observed anymore after desorption times of around 15 seconds. Hence, the  $T_g$  drops from initially 312 $^\circ\text{C}$  to around 114 $^\circ\text{C}$  at a saturation pressure of 50 bars. During the experiments it was clearly seen that the samples which were foamed at 114 $^\circ\text{C}$  with a saturation pressure of 50 bars did not turn white for desorption times larger than 20 sec. For these desorption times the glass transition temperature of the sample was always larger than the bath temperature.

It is therefore possible to observe the glass transition temperature depression by decreasing systematically the bath temperature, even without using a scanning electron microscope. The temperature where no foaming occurs (the sample does not undergo a transparent/white transition) is then the actual glass transition

temperature.

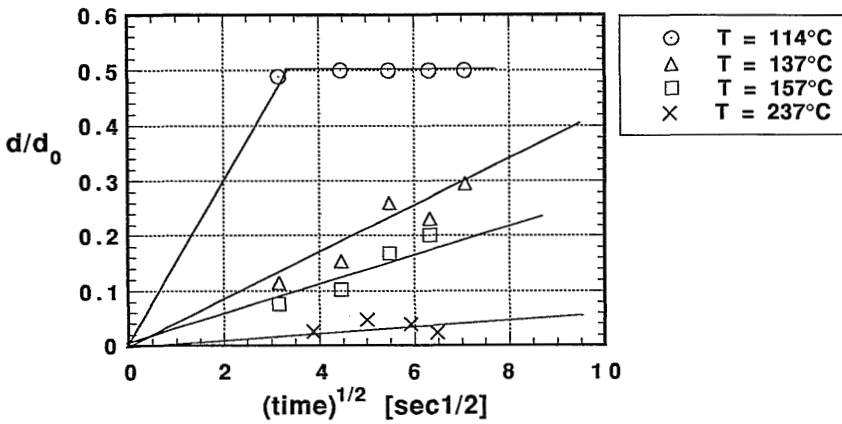


Figure 10. Thickness of the dense layer depending on the desorption times in the pressure release step at different foaming temperatures and a saturation pressure of  $p_{CO_2}=50\text{bar}$

The SEM analysis of the polyimide microcellular foams revealed another phenomenon that has not been mentioned before in literature. Under certain preparation conditions, the foam will show a bimodal bubble size distribution as shown for two different samples in figure 11.

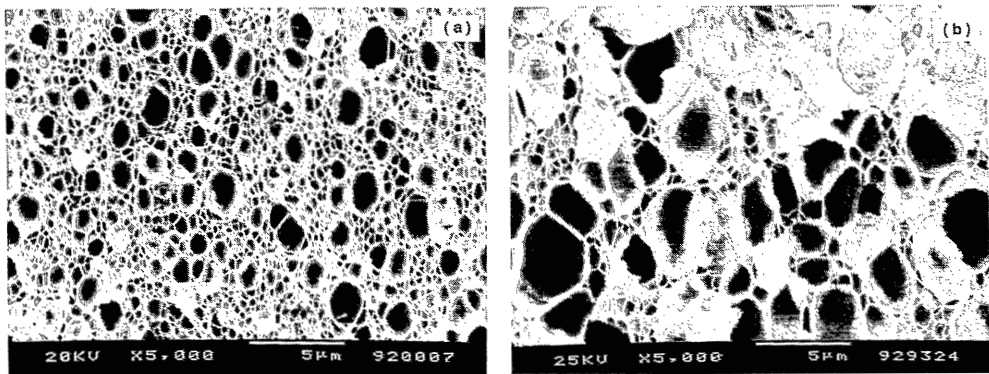
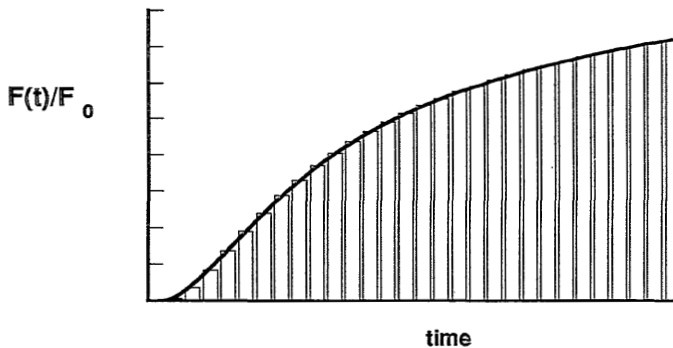


Figure 11. Polyimide microcellular foams showing bimodal bubble size distributions foamed at  $p=35\text{ bar}$  and different temperatures: (a)  $T=169^\circ\text{C}$  and (b)  $T=175^\circ\text{C}$

The striking characteristic is that the second series of smaller bubbles lies in between larger bubbles belonging to the first population. The explanation for this phenomenon can be found in the fact that the nucleation of bubbles starts at a time  $t=t_0$  while new nuclei are formed and grow out to bubbles as time proceeds. This can be described by equation (3) [18]:

$$F(t) = F_0 \exp \left\{ -\frac{\tau}{t} \right\} \quad (3)$$

in which  $\tau$  is a measure of the transient time necessary to reach the equilibrium nucleation frequency  $F_0$ , and  $F(t)$  is the time dependent nucleation frequency characterizing the number of nuclei formed per time and volume unit. Let us consider a polymer/penetrant phase that starts to form a number of nuclei continuously in time and let us furthermore assume that this continuous process can be idealized as a finite sum of discrete time steps at which new generations of nuclei will be formed. The continuous function for the ratio of  $F(t)/F_0$  can be approximated by discrete steps in the number of nuclei as shown in figure 12.



*Figure 12. Visualization of the discrete formation of generations of nuclei which can grow out to bubbles*

A first generation will grow in time as shown in figure 13a and subtract gas from its surrounding. Now, a "second generation" nuclei develops which also can grow. The second generation, however, cannot grow as much as the first generation because of the lower concentration of penetrant in the polymer matrix (figure 13b). This process of nucleation will continue, but as soon as the penetrant concentration has reached a critical concentration at which the corresponding glass transition temperature is equal to the sample temperature no further nucleation and growth can occur. (If this would not be the case, the described mechanism would result in a perfect selfsimilar, fractal foam morphology.)



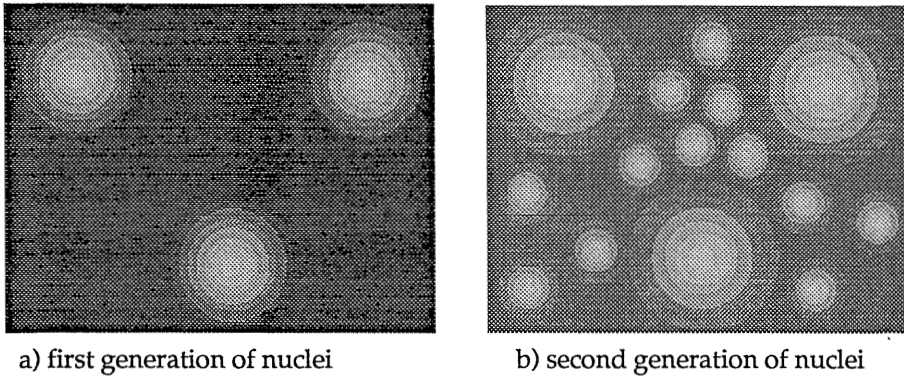


**Figure 13.** Schematic picture explaining the existence of a bimodal bubble size distribution; grey scale visualizes penetrant concentration in the polymer matrix (dark grey/high concentration and light grey/low concentration); a third generation of nuclei stays absent (see text)

From the SEM-photos in figure 11 it can also be seen that there exist more small pores than larger ones. This is in accordance with the prediction of equation (3) that, in the early stages of nucleation, the number of nuclei formed at later times must be larger than the amount of nuclei formed in the early times.

At this point it is, however, not known whether nucleation actually occurs homogeneously or heterogeneously. This will be worked out in more detail in the following paragraph.

#### 7.4. Tracing the Glassy State of Polysulfone by Nucleation of Gas Bubbles

Cell nucleation in the amorphous rubbery phase was assumed to be homogeneous in nature [2] following an Arrhenius type of relation for the nucleation rate  $n_{\text{hom}}$

$$n_{\text{hom}} = c_0 f_0 \exp\left\{\frac{-\Delta G}{k T}\right\} \quad (4)$$

where  $c_0$  is the concentration of the sorbed gas molecules in the polymer,  $f_0$  the frequency factor for gas molecules joining the nucleus,  $k$  Boltzman's constant,  $T$  the foaming temperature and  $\Delta G$  the activation energy for nucleation. The activation energy  $\Delta G$  is obeying equation (5) .

$$\Delta G = \frac{16 \pi \gamma^3}{3 (p_s - p_0)^2} \quad (5)$$

$\gamma$  is the surface energy between the polymer and the gas phase,  $p_s$  the saturation pressure during the pressurization step and  $p_0$  the environmental pressure at which the foaming will be carried out. Equation (4) predicts that a temperature increase should result in a drastic increase of the number of bubbles formed in the polymer. Experimentally, Kumar found contradictory results: the nucleation rate was independent of the foaming temperature leading to the conclusion that "traditional theories are clearly not applicable". However, it was not suggested that nucleation may also occur in a heterogeneous manner.

Considering the glassy polymer phase as having a free-volume distribution (see also chapter 6), heterogeneous nucleation is not unrealistic. Free-volume or density fluctuations are frozen in the polymer matrix during the glass formation. The larger free-volume pockets may already exist in the matrix in such an energetical situation that they only need a little bit of "internal" pressure so that they can grow out to bubbles.

One can support this idea of heterogeneous nucleation in loci of larger frozen-in density fluctuations experimentally by carrying out annealing experiments. On cooling, thermal density fluctuations of a rubbery polymer are frozen-in at the glass transition temperature. At much lower temperatures than  $T_g$  the polymer will densify very slowly. These relaxational densification processes can be enhanced if the polymeric glass undergoes a heat treatment at a temperature just below  $T_g$ . Such a heat treatment results in a much more homogeneous polymer matrix, therefore having less loci where heterogeneous nucleation can easily occur.

In order to test this *hypothesis* of heterogeneous nucleation at frozen-in density fluctuations, the following experiments were carried out: polysulfone samples (cast from a DMAc solution, 100  $\mu\text{m}$  thick,  $T_g=190^\circ\text{C}$ ) were heated above the glass transition temperature at  $T=204^\circ\text{C}$  for 20 hours and, afterwards, they were quenched in water at  $T=20^\circ\text{C}$ . Two samples were heated again at  $T=204^\circ\text{C}$ . One of the samples was directly quenched in liquid nitrogen whereas the other one remained in the oven. The oven was switched off and cooled down slowly to  $50^\circ\text{C}$  within 6 hours. The first sample (A) represents a sample which has basically frozen-in the density fluctuations of the rubbery state. The second sample (B) can be considered as an annealed sample because it undergoes a very slow glass formation process. From the above mentioned theoretical considerations, one should expect that sample A has a higher bubble density than sample B after foaming. Cross sections of the two samples foamed at  $T=140^\circ\text{C}$  and a saturation pressure of  $p=40$  bar  $\text{CO}_2$  are shown in figure 14 (other foaming parameters are the same as mentioned before).

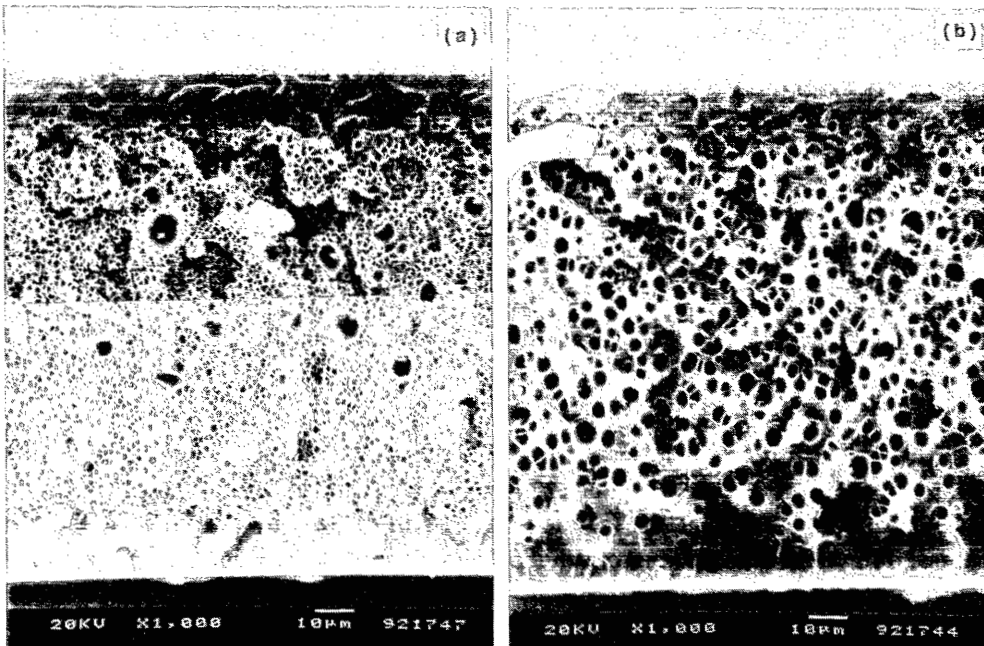


*Figure 14. Microcellular polysulfone foamed at the same preparation conditions; the samples have, however, different thermal histories: (a) quenched from the glassy state, (b) slowly cooled down through the glass transition region*

*Table 2. Influence of the thermal history of the polymer film on the bubble density of CO<sub>2</sub> foamed PSF at T=140°C and p<sub>CO<sub>2</sub></sub>=40 bar*

sample	number of bubbles [1/mm <sup>2</sup> ]
A	2.02 E+05
B	0.32 E+05
C	1.68 E+05

Clearly, the number of bubbles in sample A is significantly larger than in sample B supporting the idea of heterogeneous nucleation at frozen-in density fluctuations. Table 2 shows the results of the counting analysis of the pictures. Besides the two samples shown in figure 9, table 2 contains also the information on a sample (C) which did not undergo the second heat treatment at 204°C (so this was a water quenched sample after one heating step). In fact, due to the practically same quench conditions, the number of bubbles in sample A and C are almost equal.

## 7.5. Conclusions

The nucleation of gas bubbles in homogeneous polymer films supersaturated with CO<sub>2</sub> was used to develop a simple method for the investigation of the T<sub>g</sub>-depression due to the sorption of penetrant molecules. The physical picture proposed, together with the mathematical model, describes the observed macroscopical structure, consisting of a porous inner layer enclosed by interfacial dense layers, very well. The method was applied to investigate the T<sub>g</sub>-depression of a polyimide which was saturated with CO<sub>2</sub> at 50 bars. A considerable drop in the glass transition from T<sub>g0</sub>= 312°C to T<sub>g</sub>= 114°C was observed which clearly demonstrates the plasticizing effect of this penetrant.

A nodular structure in the outer, dense layers of the foamed sample was observed using SEM. This structure could be reconfirmed by atomic force microscopy. Two interpretations are suggested: (a) the nodules are formed by density segregation necessitating a disentanglement of the glassy polymer matrix, or (b) they grow out of regions of enhanced local ordering following the physical picture of bundle models. No definite decision for one or the other interpretation can be made.

Foaming experiments with polysulfone samples having different thermal histories suggest that the nucleation mechanism underlying the foaming process is heterogeneous in nature. Loci of nucleation are the larger free-volume pockets which are embedded in a more densified polymer matrix.

## References

- (1) J.E. Martini, N.P. Suh, Waldman F.A., US Patent No.4.473.665, 1984
- (2) V. Kumar, J.E. Weller, Microcellular polycarbonate -PartI: Experiments on bubble nucleation and growth, ANTEC (1991) 1401
- (3) M. Wessling, S. Schoeman, Th. v.d.Boomgaard, C.A. Smolders, Plasticization of gas separation membranes, *Gas Sep. & Purif.*, 5 (1991) 222
- (4) V. Kumar, Process-synthesis for manufacturing microcellular thermoplastic parts, Ph.D. Thesis, Massachusetts Institutue of Technology, U.S.A., 1988
- (5) S.B. Hadenbrook, L.P. Harasta, S.T. Falkenberry, R.D. Bomba, U.S. Patent 4.761.256, 1988
- (6) J.S. Vrentas, C.M. Vrentas, Sorption in glassy polymers, *Macromolecules*, 24 (1991) 2404
- (7) T.S. Chow, Molecular interpretation of the glass transition temperature of polymer-diluent systems, *Macromolecules*, 13 (1980) 362

- 
- (8) H. Hachisuka, T. Sato, T. Imai, J. Tsujita, A. Takizava, T. Kinoshita, Glas transition temperature of glassy polymers plasticized by CO<sub>2</sub> gas, *Polymer J.*, 22 (1990) 77
  - (9) W.H. Press, B.P. Flannery, S.A. Teukolsky, W.T. Vetterling, *Numerical Recipes*, Cambridge University Press, 1989
  - (10) J. Crank, *Mathematics of diffusion*, Oxford, Cleardon Press, 1975
  - (11) G.K. Fleming, W.J. Koros, Dilation of substituted polycarbonates caused by high pressure carbon dioxide sorption, *J.Polym.Sci., Polym. Phys.*, 28 (1990) 1137-1152
  - (12) D.W. van Krevelen, *Properties of polymers*, Elsevier, Amsterdam (1990)
  - (13) G.S.Y. Yeh, Order in amorphous polystyrenes as revealed by electron diffraction and diffraction microscopy, *J.Macromol. Sci.-Phys.*, B6(3), 451-464 (1972)
  - (14) K. Neki, P.H. Geil, Morphology-property studies of amorphous polycarbonate, *J.Macromol.Sci.-Phys*, B8(1-2) 295-341 (1973)
  - (15) G.S.Y. Yeh, A structural model for the amorphous state of polymers: folded-chain fringed micellar grain model, *J.Macromol.Sci.-Phys.*, B6(3), 465-478 (1972)
  - (16) I. Voigt-Martin, J. Wendorff, Amorphous polymers, in: *Encyclopedia of Polymer Science and Engineering*, Vol 1., J. Wiley & Sons, 1985
  - (17) K. Mizoguchi, T. Hirose, Y. Naito, Y. Kamiya, CO<sub>2</sub>-induced crystallization of poly(ethylene terephthalate), *Polymer* 28 (1987) 1298-1302
  - (18) A.G. Walton, Nucleation in liquids and solids, pg. 225, in: *Nucleation*, A.C. Zettlemayer A.C. (Ed.), Marcel Dekker, NY 1969



## Appendix I

# Modelling the Permeability of Polymers A Neural Network Approach

M. Wessling, A. Bos, M.v.d.Linden  
M.Bos, W.E.v.d.Linden, M.H.V. Mulder

### 1. Introduction

Mass transport properties of polymer films are of special interest in the food packaging industry and in membrane technology [1]. The most important property of a polymeric material for these applications is the permeability, *i.e.*, the pressure- and thickness-normalized flux through the polymer film. The permeability of a gas through a polymer film depends on the physical characteristics of the gas and the polymer. In this communication we will solely focus on the influence of polymer properties on the permeability of carbon dioxide as a gas.

A considerable amount of research effort is spent on the correlation of mass transport properties of polymers having different chemical structures. A widely used and accepted theory is the correlation between the permeability and the free volume of the polymer [2]. However, this correlation does not strictly hold for all polymers [3]. A second correlation method that must be mentioned in this brief overview is the Permachor method [4] which is a group contribution method. Here, a certain numerical value is coupled to a specific chemical group present in the polymer repeat unit. The sum of these values for the different groups present in the polymer is linearly related to the permeability of a gas.

In our approach, a comparable assumption is made, namely, that the chemical structure of the polymer is the most important factor influencing the permeability. No artificial subdivision into groups is introduced, instead, the infrared spectrum of the polymer is assumed to contain the necessary information. Furthermore, it is assumed that the hidden information in the IR-spectrum is somehow correlated to the permeability.

The attempt to correlate IR-spectra to the permeability is not really new. In a U.S. patent, Gold [5] correlates the permeability of gases through a mixture of two epoxy resins with their IR-spectra. However, the mathematical tool used (Partial Least Square Regression) is probably not skilful enough for *different* polymers which may vary considerably in chemical structure.

## 2. Neural Networks

In this study, a neural network has been chosen as a mathematical tool to correlate the IR-spectrum to the permeability of the polymer. In neural network science, one tries to mimic mathematically the processing of input signals to an output signal similar to signal processing in biological neural systems [6]. Because of the non-linearity of the neural networks, this approach is very powerful in correlating complex input signals to somehow correlated output signals. Here, the complex IR-spectrum is the input signal and the permeability the output signal. Before focusing on the way of carrying out the study, the principle of neural networks will be briefly explained.

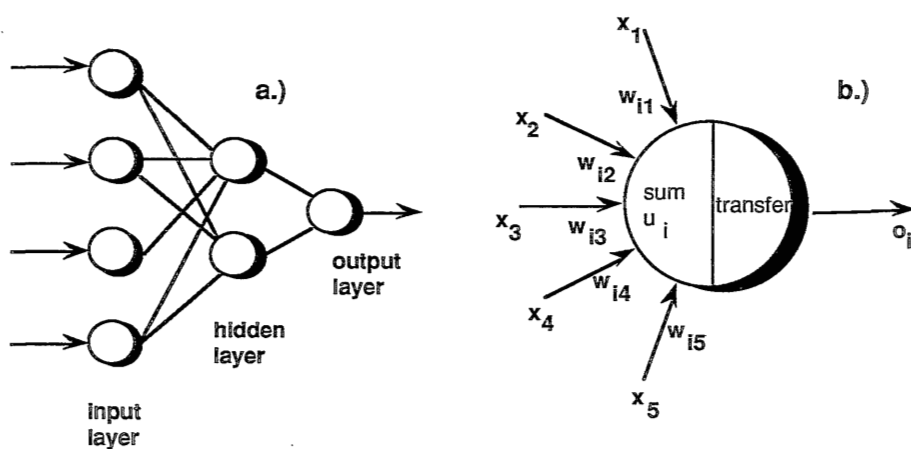


Figure 1. Schematic drawing of a neural network topology (a) and a processing element called neuron (b)

A neural network consists of a network of processing elements, so-called "neurons". These neurons are organized in layers in the network as shown in figure 1a. Every neuron calculates an output  $o_i$  out of all incoming inputs  $x_i$ . Generally, for a neuron  $i$ , all inputs  $x_j$  are weighted by a factor  $w_{ij}$  and then summed up to the final input  $u_i$ .

$$u_i = \sum_j w_{ij} x_j \quad (1)$$

This input can be transferred into the output  $o_i$  by a mathematical transfer or 'squashing' function. Different neurons can have different transfer functions: a sigmoid neuron transfers the input into the output according to equation 2 with  $\theta$  as a bias.



$$o_i = \frac{1}{1 + \exp\{-u_i + \theta\}} \quad (2)$$

On the other hand, a neuron having a radial base functions transfers directly all inputs  $x_j$  into an output according to equation (3).

$$o_i = \exp\left\{\frac{\sum_j (x_j - w_{ij})^2}{-2 \sigma_i^2}\right\} = \prod_j \exp\left\{\frac{(x_j - w_{ij})^2}{-2 \sigma_i^2}\right\} \quad (3)$$

The correct input-output relation of the network as a whole is "learned" from examples by adapting the weights iteratively. For the development of an optimal network which indeed correlates the permeability of a polymer to its IR-spectrum, a number of network parameters can be changed. Finally, a network with an optimal topology must be found concerning the kind of neuron used, the number of layers and the number of neurons per layer.

First an adequate number of neurons in the input layer is chosen. Secondly, a certain set of IR-spectra together with the permeabilities is presented to the network. (The way of presenting the IR-spectrum to the input layer will be explained later). In a third step, the network must be trained. This actually means, that the weights of neurons are changed in such a way that a minimum error is obtained between the predicted and experimental permeability. Training and testing was carried out in this study according to the *leave-one-out* method. One polymer is left out of the set of polymers and, after the network has been trained with the remaining polymers, the permeability of this polymer will be predicted on the basis of its IR-spectrum. The procedure will be repeated for all polymers in the training set.

In order to *measure* the predictive power of different network topologies a performance factor C has been defined (see equation 4). This performance factor C is equal to the ratio of the sum of all differences between the predicted output (output) and the experimental output (target output) and the sum of all differences between the average permeability  $P_{av}$  of all polymers and the experimental permeability.

$$C = \frac{\sum_n |\text{output} - \text{target output}|}{\sum_n |P_{av} - \text{target output}|} \quad (4)$$

The neural network does work predictively if C is smaller than 1. In the case of C=1 the prediction for an unknown polymer would be a permeability which is equal to the average permeability of all polymers in the set (which is, in fact, useless).

### 3. Infrared Spectroscopy

The question remains how an IR-spectrum, which is rather complex in nature, can be presented as a valuable, compact input to the neural network. We have chosen a curve fitting procedure using Legendre polynomials [7]. The IR-spectra were fitted in the range of  $400\text{-}2000\text{ cm}^{-1}$ . Depending on the number of polynomials used the quality of the representation of the IR-spectra can be influenced as shown in figure 2. A maximum set of 48 polynomials resulting in 48 input values for the network could be processed by the network. This, however, does not imply automatically an optimum input layer topology. Although 48 polynomials was not sufficient to fit every peak in the spectrum, the general form of the spectrum was well reproduced by this method.

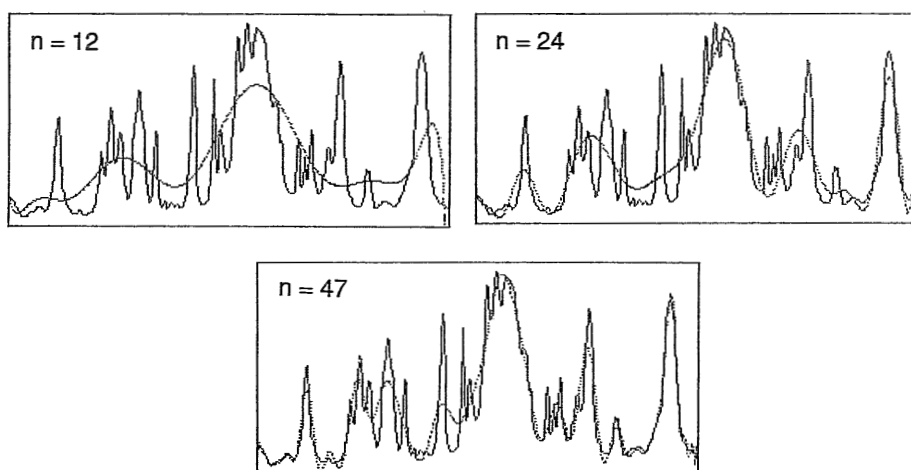


*Figure 2. Comparison of fitted and experimental IR-spectra for bisphenol-A polycarbonate at different numbers of Legendre polynomials*

### 4. Set of polymers

Not only the quality of inputs and the topology of networks but also the quality of the polymer set itself may strongly influence the success of neural network modelling. An optimum polymer set would consist of at least 50 different polymers (the more the better) with a very subtle change in polymer structure from one polymer family to another one. The polymers used in this study were all glassy polymers. Until now only 33 different polymers could be used for the modelling. The set of polymers consisted of tailor-made polyimides [8], polycarbonates [9], cellulosic polymers, polysulfones and aromatic polyesters. Polymers were dissolved in suitable solvents, cast on glass plates, dried in a nitrogen atmosphere for 24 hours

and finally dried for 2 weeks in a vacuum oven at 70°C. Permeabilities were measured at  $T=32^{\circ}\text{C}$  using a set-up described in [8].

## 5. Results and Discussion

A considerable amount of effort and computing time was invested in the optimization of the network topology; details of which are published in [10]. Besides the fitting of the Legendre polynomials other techniques were also used and compared with each other. Only the best results obtained until now are presented below. They were obtained with a neural network with 24 input neurons and 16 radial base function neurons in a single hidden layer. The IR-spectrum was fitted using 47 polynomials but only the first 24 were presented to the network. The network was trained in 3000 iterations for each polymer.

Figure 3 shows the predicted permeability for each polymer versus the experimental permeability. Both the y- and x-axis were chosen as a logarithmic axis because a linear axis would cluster most of the data points in the range of 1 to 20 Barrer (1 Barrer =  $10^{-10} \text{ cm}^3(\text{STP})\text{cm}/(\text{cm}^2 \text{ s cmHg})$ ). The solid line represents equal values for the predicted and experimental permeability.

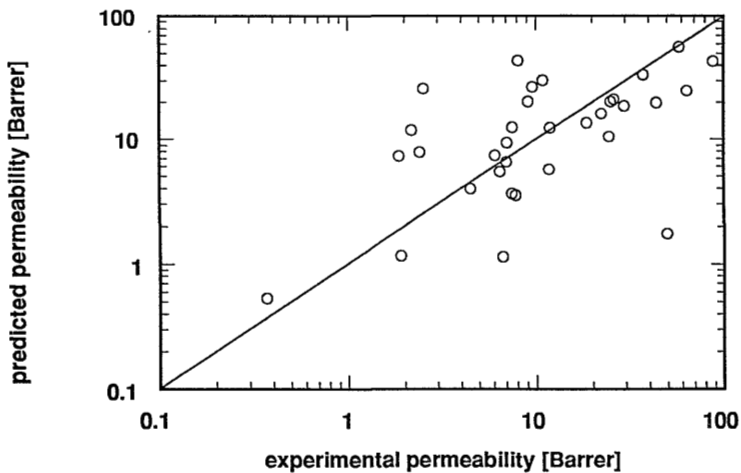


*Figure 3. Comparison of the permeabilities predicted by the neural network and the experimental permeability of carbon dioxide in different polymers*

A clear correlation between the predicted and the experimental permeability can be seen. This is also expressed in the performance factor of  $C=0.77$ . Furthermore, one has to keep in mind that extreme values for low as well as for high permeabilities

can only be obtained by *extrapolation* from the network trained by the leave-one-out method. This is actually done with a satisfying result for the two data points at 0.5 Barrer (phenoxy resin/Aldrich) and 100 Barrer (poly(2,6-diphenyl 1,4-phenylenoxide/Tenax GC, Enka), respectively.

On the other hand, some polymers do not fit well on the line. These are in general polymers having certain groups which occur only once in the whole set of polymers. Thus, if they are taken out during the leave-one-out training, the network is trained without this group. In the case of the polymer poly(vinyl butyrate)/Aldrich, the experimental permeability of 8.1 Barrer is significantly smaller than the predicted value of 43.8 Barrer. PIXU 218 from Ciba Geigy (see also chapter 3) shows a deviation into the other direction: the experimental permeability of 50 Barrer is totally underestimated by the prediction of 1.7 Barrer.

In summary, this short appendix shows that neural networks are able to relate the IR-spectrum of a polymer to its permeability for carbon dioxide. It can be expected that the enlargement of the polymer set would improve the quality of the prediction.

Concerning this correlation method one has to keep in mind that the weights of the final trained network do not have any physical significance. Only a systematic artificial manipulation of an input IR-spectrum, representing an alteration in the chemical structure of the polymer, together with the newly predicted permeability may give more insight in molecular aspects influencing the permeability and may finally save some time and effort in the tedious work of synthesizing new polymers for gas separation membranes. It is not clear yet whether history effects like annealing or residual solvent effects can be enclosed in the modelling. The authors are aware of the impact of such effects on the permeability. On the other hand, crystallization processes and roughly their extent as well as the residual solvent content are easy to determine using IR-spectroscopy. Certainly, this neural network method can also be applied to mechanical and thermal properties of polymers like the elastic modulus or the glass transition temperature, respectively.

## References

1. W.J. Koros, Barrier polymers and structures, ACS Symp.Ser. 423, 1989, pg 1.
2. W.M. Lee, Selection of barrier material from molecular structure, Polym.Eng.Sci., 20 (1980) 65
3. E. Hensema, M.H.V. Mulder, C.A. Smolders, On the mechanism of gas transport in rigid polymer membranes, submitted to J.Appl.Polym.Sci
4. D.W. van Krevelen, Properties of polymers, 3rd edition, Elsevier, 1990

5. H.S. Gold, U.S. patent 5.015.856, 1991
6. D.E. Rumelhardt, Parallel Distributed Processing, Vol. 1 and 2, MIT Press, 1986
7. W.H. Press, B.P. Flannery, S.A. Teukolsky, W.T. Vetterling, Numerical recipes, Cambridge University Press, 1989
8. I. Blume, E. Smit, M. Wessling, C.A. Smolders, Diffusion in glassy and rubbery polymers, Makromol. Chem., Macromol. Symp., 45 (1991) 237-257
9. K. Sommer, Correlation between primary chemical structure and property phenomena in polycondensates, Adv. Mat. 3,12, (1991) 590
10. A. Bos, M. Wessling, M. v.d.Linden, M.H.V. Mulder, M. Bos, W.E. v.d.Linden, Modelling the CO<sub>2</sub> permeability of polymer membranes with artificial neural networks, submitted to Anal. Chim. Acta



## Appendix II

**Phase Inversion Processes in Ternary Polymer Systems  
resulting in Fractal Patterns**

In this brief appendix, a technique for the preparation of fern-like, fractal patterns by phase inversion of a ternary polymer/solvent/nonsolvent will be described. The patterns shown on the cover page and in figure 1 have been prepared in the way described below.

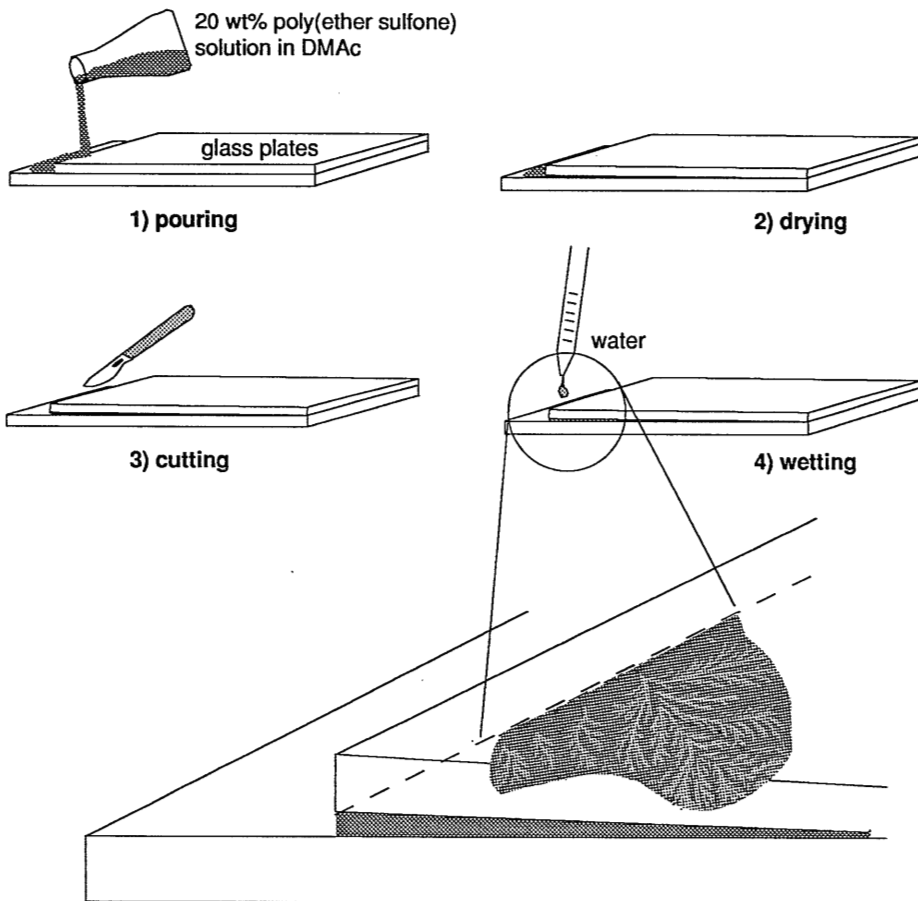


*Figure 1. Schematic drawing of the four steps for the preparation of fractal phase inversion patterns in a ternary polymer system*

First, a small glass plate is placed on a large one. A 20 wt% solution of poly(ether sulfone) PĒS in N,N-Dimethylacetamide DMAc is poured into the corner built by the sides of the small glass plate together with the surface of the large one. The glass plates are placed in a nitrogen flushed glove box to allow the polymer solution to dry for 24 hours. During this time, the polymer solution creeps between the glass plates and forms a very thin layer. After the drying procedure, the remaining polymer is removed from the corner of the glass plates by a scalpel. The final preparation step is wetting of the corner by a nonsolvent like water.

Exchange of solvent and nonsolvent in the thin layer between the glass plates takes place. As soon as the composition of the ternary mixture crosses the demixing gap, phase inversion takes places and the fractal patterns appear between the glass plates as shown in figure 1. Here, the dark parts of the fractal pattern are phase separated and appear opaque in the original.

For the correct preparation of these patterns, the thickness of the polymer layer between the glass plates is a crucial parameter. If *e.g.* a polymer film is simply cast on the larger glass plate and the second glass plate is placed afterwards on top of it, no fractal patterns but long, finger-like macrovoids will be the result of the experiment.



## SUMMARY

Solution-diffusion membranes are widely used for the separation of gaseous and liquid mixtures. The separation of air ( $O_2/N_2$ ), landfill gas ( $CH_4/CO_2$ ) and purge gas streams ( $NH_3/H_2$ ) in the ammonia synthesis are examples for state-of-the-art membrane gas separation processes. For the separation of liquid mixtures by means of a membrane process, i.e., pervaporation, the splitting of azeotropic mixtures of ethanol-water mixtures is a well established technique.

The separation is achieved by a homogeneous, very thin ( $<1\mu m$ ) polymer film. The polymer may be rubbery or glassy in nature. In cases where the polymer is rubbery, the amount of mass transported through the polymer matrix per time unit is time-independent. The penetrant molecules swell the polymer matrix to a certain extent and the swelling is *instantaneous* due to the high polymer flexibility in the rubbery state. Mass transport properties of glassy polymers are only constant in time if the amount of penetrant sorbed in the matrix is low as in the case of light and noble gases. This is not valid for highly sorbing gases like  $CO_2$  and  $SO_2$  and organic vapours. Often, selective properties can not be predicted from pure component experiments and the permeability becomes time-dependent. Furthermore, permselective properties of a glassy polymer membrane depend strongly on the thermal history of the membrane. In this thesis, a physical picture on molecular events underlying these relaxational alterations of mass transport properties in glassy polymer membranes will be developed.

Chapter 2 gives a broad overview on relevant theoretical and experimental literature information dealing with diffusion and sorption in polymer/penetrant systems. Since theoretical models describing the sorption behaviour of polymers are often related to the morphology of the polymer matrix, recent literature on this topic is reviewed, too.

Carbon dioxide has been chosen as a model penetrant. Experimental methods to determine the mass transport characteristics of  $CO_2$  in a polymer matrix are described in chapter 3. A newly developed technique determining the sorption induced swelling of a polymer-penetrant system is described in detail. This technique, based on an automated line scan camera, determines not only the *equilibrium* swelling but also the swelling *kinetics*. Since the rest of the thesis partly concentrates on the permeation, sorption and swelling behaviour of 6FDA-based polyimides, the synthesis and the physical properties of this polymer family is also described in chapter 3.

Experimental sorption and dilation results, i.e., swelling, for the 6FDA-based polyimides are presented in chapter 4. Analysing the data with the different

sorption models presented in chapter 2 reveals that a modified Flory-Huggins theory developed by Bitter describes the results most adequate. The theory is, furthermore, applied to sorption data for different glassy as well as rubbery polymers. A unique experimental relation between the logarithm of the Henry coefficient (obtained from the data analysis) and the inverse glass transition temperature is found. Assuming that the glass transition temperature is a measure for the polymer chain flexibility, this experimental relation is in agreement with the modified Flory-Huggins model. The model predicts a linear relation between the logarithmic Henry coefficient and an inverse chain flexibility parameter.

While chapter 4 focused on the *equilibrium* sorption, chapter 5 is focused on the *dynamics* by which sorption and, especially dilation equilibrium is reached. At elevated pressures, the dilation kinetics measured consists of three regimes: a so-called Fickian regime followed by two relaxational regimes. Using this discrimination of "relaxational" and "Fickian" sorption sites, differing results obtained by experiments at *same* experimental conditions and polymer samples having *different* histories can be explained. The relaxational regimes express slow morphology alterations in the polymer matrix due to swelling stresses exerted by sorbed penetrant molecules. In a glassy polyimide membrane, these alterations can also be observed as a slowly increasing CO<sub>2</sub> permeability. A number of unsolved phenomena occurring in solution-diffusion membranes are discussed with regard to the picture of a highly stressed polymer matrix.

The modified Flory-Huggins equation, which was used in chapter 4 for the interpretation of sorption data, is based on the assumption of areas of enhanced local ordering embedded in an amorphous matrix. Polymer chains are locally constrained in these regions. Such a degree of local ordering in polymers, which show no crystallinity in X-ray patterns, is hardly accessible experimentally. Results of Molecular Dynamics simulations on the amorphous state of poly(ethylene terephthalate) PET are described in chapter 6. PET was chosen as a model system because sufficient experimental X-ray results were available in literature which can be compared with X-ray simulations from the polymer box. Simulated and experimental X-ray patterns agree to such an extent that it is reasonable to say that the simulated polymer box represents the structure of the bulk polymer. Although amorphous, certain intermolecular distances between different polymer chains occur preferentially. At this moment, however, these preferential distances can not be translated into certain configurations of polymer chain segments.

Since mass transport properties of aromatic polymers depend strongly on the isomeric position of the benzene ring bound in the polymer chain backbone, a free-volume analysis of the simulated PET (para isomer) is carried out. The obtained free-volume *distribution* is compared with the one obtained from the simulated meta isomer poly(ethylene isophthalate). From this calculations it can be concluded

that the meta isomer has a lower content of larger volume elements compared to the para isomer. This result explains therefore the fact of a lower diffusion coefficient in meta isomers.

In chapter 6, carbon dioxide foamed glassy polymers are studied. A glassy polymer supersaturated with nitrogen forms a microcellular foam, if the polymer is quickly heated above its glass transition temperature. A glassy polymer supersaturated with CO<sub>2</sub> forms this foam-like structure at much lower temperatures which indicates the T<sub>g</sub>-depressing effect of CO<sub>2</sub>. Having this picture in mind, the overall sample morphology, i.e, a porous foam enclosed by dense outer skins, can be completely explained. The dense skins, however, are not homogeneous but show a nodular structure when analysed by SEM and AFM. Foaming experiments with samples having a different thermal history suggest that the nucleation mechanism underlying the foaming process is heterogeneous in nature.

The prediction of the permeability of CO<sub>2</sub> through different polymers using a neural network is studied in Appendix I. The neural network correlates the complex IR-spectrum of the polymer, which contains the necessary information on its chemical structure, to the permeability. The preliminary results presented are promising.



## SAMENVATTING

Synthetische kunststof membranen worden gebruikt voor het scheiden van gas- en vloeistofmengsels. Het scheiden van lucht in de componenten zuurstof en stikstof, biogas in methaan en kooldioxyde en het terugwinnen van waterstof uit ammoniak tijdens productie van laatstgenoemde stof zijn voorbeelden van hedendaagse gasscheidingsprocessen met membranen. Voor het scheiden van azeotrope vloeistofmengsels wordt vaak de membraantechniek pervaporatie gebruikt. Beide relatief nieuwe membraantechnieken (gasscheiding en pervaporatie) worden thans in de industrie toegepast.

Het scheiden wordt bereikt met behulp van een zeer dun, homogeen kunststof laagje met een dikte kleiner dan  $1\mu\text{m}$ , dat een grotere doorlaatbaarheid vertoont voor één van de componenten. Het materiaal (polymeer) kan een rubber zijn of glasachtige eigenschappen bezitten. Voor rubberachtige polymeren is de hoeveelheid massa, die op een bepaald tijdstip door het membraan wordt getransporteerd constant. De opgenomen vloeistof- of gasmoleculen doen het polymeer zwellen. Deze zwelling (dilatatie) treedt instantaan op omdat de grote polymeermoleculen in de rubberfase flexibel zijn en zich daarom goed kunnen aanpassen aan de nieuwe toestand. Transport van materie door glasachtige polymeren verandert niet in de tijd indien de hoeveelheid opgenomen materiaal in de polymere matrix klein is. De opname (sorptie) van edelgassen en lucht in kunststoffen is hiervan een voorbeeld. Andere gassen zoals kooldioxyde en zwaveldioxyde of organische dampen die in veel grotere mate worden opgenomen, vertonen dit gedrag daarentegen niet. Vaak kunnen de scheidende eigenschappen van het polymeer voor mengsels, waarbij één van de componenten in een grotere mate wordt opgenomen, dan ook niet meer worden voorspeld met het meten van de doorlaatbaarheid (permeabiliteit) van de zuivere componenten afzonderlijk. De permeabiliteit wordt dan tijds afhankelijk. Daarnaast hangen de scheidende eigenschappen van het polymeer sterk af van zijn voorbehandeling, zoals bijvoorbeeld al dan niet verhitting van het materiaal. In dit proefschrift wordt getracht de moleculaire processen, die tijdens de langzame veranderingen in de transporteigenschappen plaatsvinden, fysisch te beschrijven.

In hoofdstuk 2 wordt een overzicht gegeven van de literatuur met betrekking tot permeatie, diffusie en sorptie. Vaak wordt de morfologie van de polymeermatrix als uitgangspunt gekozen voor theoretische modellen die het zwelgedrag van polymeren beschrijven. Daarom wordt aan dit aspect aandacht geschonken.

Het gas kooldioxide ( $\text{CO}_2$ ) is als modelstof gekozen voor het laten zwellen van polymeren. Experimentele methoden die de transporteigenschappen van  $\text{CO}_2$  in een polymeer kunnen karakteriseren, worden in hoofdstuk 3 beschreven. Een nieuwe techniek die de zwelling van het polymeer door opname van gassen kan

kwantificeren, wordt uitgebreid beschreven. Een ééndimensionale videocamera gekoppeld aan een computer registreert nauwkeurig de uitzetting van een reepje polymeer in de tijd. Op deze wijze kan niet alleen de totale zwellingsgraad, maar ook de snelheid van zwellings- nauwkeurig worden bepaald. Omdat de meeste metingen aan verschillende polymeren van het type polyimide zijn uitgevoerd, wordt de synthese van deze polymeren en hun fysische eigenschappen kort beschreven.

Experimentele resultaten van de sorptie- en dilatatie- (zwellings-) metingen worden in hoofdstuk 4 gegeven. De Henrycoëfficiënt kan met de gevonden resultaten worden berekend. De analyse van de gegevens worden uitgevoerd met behulp van modellen die uitgebreid in hoofdstuk 2 zijn beschreven. Uit deze analyse volgt dat een aangepast Flory-Hugginsmodel het meest geschikte model is om zowel de zwellings- alsmede sorptie experimenten te beschrijven. Deze resultaten leveren samen met bevindingen over de opname van CO<sub>2</sub> door andere polymeren die in de literatuur zijn beschreven, een unieke relatie op: de logaritme van de Henry coëfficiënt is rechtevenredig met de reciproke van de glasovergangstemperatuur van het polymeer. Als men aanneemt dat de glasovergangstemperatuur een maat is voor de beweeglijkheid van de polymeerketen, dan is bovengenoemde experimentele relatie in overeenstemming met de voorspelling van het Flory-Huggings model.

In hoofdstuk 3 wordt de sorptie- en zwellingskinetiek bestudeerd. De resultaten van de zwellingskinetiek bij hoge drukken duiden op drie verschillende gebieden: één waar de diffusie volgens het model van Fick kan worden beschreven, gevolgd door twee gebieden waar relaxatieverschijnselen het belangrijkste zijn. Dit onderscheid biedt de mogelijkheid de opmerkelijke verschillen in de resultaten die gevonden zijn in monsters met een verschil in voorbehandeling te verklaren. Het polymeer ondergaat langzame morfologische veranderingen ten gevolge van de spanning in het materiaal dat wordt veroorzaakt door de opname van kleinere moleculen. Deze veranderingen kunnen aanleiding geven tot een ander relaxatiegedrag. Dergelijke veranderingen in het polymere materiaal komen ook tot uiting in een stijging in de permeabiliteit in de loop van een permeatie-experiment. Een aantal andere problemen die optreden in dergelijke membranen kan worden verklaard doordat het polymeermateriaal onder spanning staat.

De aangepaste Flory-Hugginsvergelijking, die in hoofdstuk 4 wordt gebruikt om de sorptie experimenten te verklaren, veronderstelt dat het polymeer uit een amorfe matrix bestaat, waarin kleine gebieden met hoge plaatselijke ordening aanwezig zijn. Polymeerketens kunnen in deze gebiedjes als het ware fysisch verknoopt worden beschouwd. Deze geordende structuren kunnen echter niet met röntgen-diffractie experimenteel als een kristallijne fase worden aangetoond. Daarom zijn om meer inzicht in de plaatselijke ordening te krijgen, theoretische berekeningen uitgevoerd aan amorf poly (ethyleen tereftalaat) (PET). Met behulp van moleculair dynamische

simulaties wordt het gedrag van dit polymeer in de loop van de tijd berekend. Aan de berekende structuur worden vervolgens theoretische röntgen diffractie experimenten gesimuleerd. Deze berekende resultaten zijn vergeleken met experimentele resultaten uit de literatuur. De gesimuleerde structuur komt redelijk overeen met de experimenteel gevonden structuur. Hoewel de gesimuleerde structuur amorf is, treden bepaalde intermoleculaire afstanden bijzonder vaak op, hetgeen een aanwijzing kan zijn voor plaatselijke ordening. Op dit moment kunnen echter de gevonden afstanden nog niet worden toegeschreven aan bepaalde verknoppingen in een geometrische structuur van de polymeerketens.

De eigenschappen voor stoftransport van aromatische polymeren hangen sterk af van de positie van de benzeenring in de hoofdketen. Een para gebonden benzeenring vertoont in alle gevallen een hogere diffusiecoëfficiënt in vergelijking met een meta gebonden benzeenring. Om dit verschijnsel beter te kunnen begrijpen is nagegaan hoeveel vrij volume aanwezig is in een polymeer box van het para isomeer van poly(ethyleen isofthalaat). De hiermee bepaalde vrij volume verdeling kan worden vergeleken met die van het meta isomeer. Uit deze berekeningen kan worden geconcludeerd dat het meta isomeer een kleiner gehalte aan grote vrije volume elementen heeft dan het para isomeer. Deze resultaten verklaren dus waarom twee polymeren met dezelfde hoeveelheid vrij volume toch grote verschillen in diffusiecoëfficiënten kunnen vertonen.

In hoofdstuk 6 worden polymeerschuim, gemaakt met CO<sub>2</sub> beschreven. Een glasachtig polymeer dat met stikstof oververzadigd is, vormt een microcellulaire schuim als het polymer snel boven zijn glasovergangstemperatuur wordt verwarmd. Eenzelfde glasachtig polymeer dat daarentegen met CO<sub>2</sub> is oververzadigd, vormt al een schuim bij een veel lagere temperatuur dan de oorspronkelijke glasovergangstemperatuur. Op deze manier kan de verlaging van de glasovergangstemperatuur ten gevolge van de aanwezigheid van CO<sub>2</sub> in het polymeer worden aangetoond. Met het optreden van de verlaging van de glasovergangstemperatuur kan dan ook de experimenteel gevonden totale structuur, een poreuze laag ingeklemd tussen twee dichte buitenlagen, volledig worden verklaard. Toch zijn de buitenste lagen niet geheel homogeen: als de buitenste laag met REM en AFM wordt geanalyseerd, worden nodulaire structuren gevonden. Schuimexperimenten met polymeer monsters die een verschillende voorbehandeling hebben ondergaan, tonen aan dat het nucleatie mechanisme voor het schuim een heterogeen proces is.

De voorspelling van de permeabiliteit van CO<sub>2</sub> door verschillende polymeren met behulp van een neurale netwerk wordt in Appendix I beschreven. Het neurale netwerk correleert het complexe IR-spectrum, dat alle noodzakelijke chemische informatie over de structuur van het polymeer bevat, aan de permeabiliteit door het polymeer. De voorlopige resultaten zijn veelbelovend.





## ZUSAMMENFASSUNG

Lösungs-Diffusions-Membranen werden heutzutage sowohl für die Trennung gasförmiger als auch flüssiger Gemische benutzt. Die Lufttrennung, die Trennung von CO<sub>2</sub> aus Biogas und die Trennung von Wasserstoff aus Ammoniaksynthesegas sind Beispiele für den Stand der Technik in der Membran-Gastrennung. Im Bereich der Flüssigkeitstrennung hat sich die Pervaporation bei der Trennung azeotroper Gemische, wie z.B. Ethanol/Wasser, industriell behaupten können.

Die Trennung dieser Gemische erfolgt mittels eines homogenen, sehr dünnen Polymerfilms. Das Polymer kann sowohl gummiartig als auch glasartig sein. Für den Fall eines gummiartigen Polymers, ist der Fluß durch die Membran zeitunabhängig. Die Polymermatrix quillt durch die Aufnahme der Penetrantmoleküle; jedoch tritt diese Quellung unmittelbar auf, da sich die Polymerketten im gummiartigen Zustand durch ihre hohe Beweglichkeit sehr schnell den sorptionsbedingten Veränderungen anpassen können. Stofftransport durch glassartige Polymere kann nur bei Penetrantmolekülen, die sich nur in kleinen Mengen im Polymer lösen, als konstant angenommen werden. Für gutlösliche Gase oder organische Dämpfe ist diese Annahme nicht mehr gültig. Die Permeabilität ist dann zeitabhängig und die selektiven Eigenschaften des Polymers können nicht mehr aus Reinkomponentenmessungen vorhergesagt werden. Außerdem hängen die Stofftransporteigenschaften eines glasartigen Polymers sehr stark von dessen Historie ab. Diese Dissertation versucht, ein physikalisches Bild zu entwickeln, das die molekularen Ereignisse, die diesen relaxationsartigen Veränderungen der Membran zu Grunde liegen, beschreibt.

Kapitel 2 gibt eine Übersicht über relevante theoretische und experimentelle Literaturstellen, die sich mit der Diffusion und Sorption in Polymeren beschäftigen. Viele der theoretischen Modelle, die das Sorptionsverhalten von Polymeren beschreiben, gehen von bestimmten Strukturvorstellungen über die Polymermatrix aus. Erläuterungen hierzu finden sich auch in vorliegendem Kapitel.

Kohlendioxid wurde für die Ausführung der Experimente als Modellpenetrant gewählt. Kapitel 3 beschreibt experimentelle Methoden zur detaillierten Charakterisierung des Stofftransportverhaltens von CO<sub>2</sub> in einer Polymermatrix. Eine neue Technik zur Bestimmung des sorptionsinduzierten Quellungsverhaltens von Polymer-Penetrant-Systemen wird dabei hervorgehoben. Mit Hilfe dieser Meßmethode, die auf dem Prinzip einer automatisierten einzeiligen Videokamera basiert, kann nicht nur das Quellungs*gleichgewicht*, sondern auch die Quellungs*kinetik* präzise gemessen werden. Experimente, die in dieser Dissertation beschrieben werden, sind hauptsächlich mit 6FDA-basierten Polyimiden ausgeführt worden; darum wird auch an dieser Stelle kurz auf deren Synthese und

physikalischen Eigenschaften eingegangen.

In Kapitel 4 werden die Resultate dieser Experimente erläutert. Die in Kapitel 2 erwähnten, verschiedenen Sorptionsmodelle werden anhand dieser Experimente überprüft. Dabei stellt sich heraus, daß ein modifiziertes Flory-Huggins-Modell die experimentellen Sorptions- und Quellungsexperimente am besten beschreibt. Dieses Modell wird danach zur weiteren Analyse von Sorptionsdaten gummi- als auch glassartiger Polymere, die in der Literatur publiziert sind, angewandt. Die daraus erhaltenen Henrykoeffizienten für die verschiedenen Polymere sind exponentiell mit der entsprechenden inversen Glasstemperatur korreliert. Nimmt man an, daß die Glasübergangstemperatur ein Maß für die Flexibilität von Polymerketten ist, so entspricht diese Relation der Vorhersage des modifizierten Flory-Huggins Modells.

Während Kapitel 4 die Gleichgewichtssorption und -quellung behandelt, wird in Kapitel 5 das Erreichen dieses Gleichgewichts, die Quellungskinetik, insbesondere bei hohen Drücken, analysiert. Die gemessene Quellungskinetik besteht im allgemeinen aus drei verschiedenen Teilbereichen: einem schnellen, sogenannten Fickschen Sorptionsbereich, dem im weiteren zwei langsame Relaxationssorptionsbereiche folgen. Anhand dieser Differenzierung von Fickschen und Relaxationssorptionsbereichen kann im folgenden dann auch das Phänomen erklärt werden, daß das kinetische Quellungsverhalten von Polymeren mit verschiedener Historie bei gleichen experimentellen Bedingungen sehr unterschiedlich ist. Die Relaxationssorptionsbereiche sind makroskopisch experimenteller Ausdruck langsamer Strukturveränderungen in der Polymermatrix, die in der durch sorbierte Penetrantmoleküle ausgeübten Spannung auf die Polymerketten ihren Ursprung finden. Diese langsamen Strukturveränderungen sind auch als eine in der Zeit langsam ansteigende Permeabilität beobachtbar. Verschiedene andere Probleme, die in Lösungs-Diffusions-Membranen beobachtet worden sind, werden im letzten Teil des Kapitels 5 mit Hilfe dieser Modellvorstellungen erklärt.

Das in Kapitel 4 zur Analyse der Sorptionsdaten herangezogene modifizierte Flory-Huggins-Modell basiert auf der Annahme, daß Polymere in aller Regel aus einer amorphen Matrix bestehen, worin sich kleine Inseln befinden, die sich durch eine erhöhte Nahordnung der Polymerkettensegmente auszeichnen. In diesen Inseln können die Polymerketten als physikalisch verknüpft betrachtet werden. Jedoch sind Nahordnungen experimentell bisher schwer erfaßbar. Ausführungen über molekular-dynamische Simulationen an Polyethylenterephthalate PET versuchen in Kapitel 6 den Begriff der Nahordnung in amorphen Polymersystem mit Leben zu füllen. PET wurde gewählt, da genügend experimentelle Ergebnisse zum Vergleich in der Literatur publiziert sind. An der simulierten Polymerstruktur wurden Röntgenbeugungs-experimente simuliert und mit publizierten experimentellen Ergebnissen verglichen. Aus dieser vergleichenden Studie wird geschlossen, daß die simulierte Polymerstruktur dem der eigentlichen Struktur sehr nahe kommt.

Obwohl die Struktur keine Anzeichen von Kristallinität besitzt, kann doch eine intermolekulare Nahordnung beobachtet werden. Jedoch ist es zu diesem Zeitpunkt nicht möglich, daraus auch eine geometrische Anordnung einzelner Polymerkettensegmente abzuleiten.

Stofftransporteigenschaften aromatischer Polymere hängen stark von der isomeren Position des Benzolrings in der Hauptkette ab. Paragebundene Benzolringe in der Hauptkette verursachen immer einen höheren Diffusionskoeffizienten im Vergleich zum meta-Isomer (bei gleichem oder sogar höherem totalen freien Volumen). Um diesen scheinbaren Widerspruch zu erklären, wurden an dem para-Isomer PET als auch an dem meta-Isomer Polyethylenisophthalate Berechnungen zur Bestimmung der Freien-Volumen-Verteilung ausgeführt. Dabei stellt sich heraus, daß das meta-Isomer einen geringeren Anteil größerer Freier-Volumen-Elemente besitzt als das para-Isomer. Das Resultat erklärt damit das Diffusionsverhalten von isomeren Polymeren.

In Kapitel 6, wird die Präparation von CO<sub>2</sub>-geschäumten, microzellularen Schäumen beschrieben. Ein glasartiges, mit Stickstoff übersättigtes Polymer formt eine schaumartige Struktur, sobald das Präparat eine Temperatur oberhalb der Glasübergangstemperatur erreicht. Wird anstelle von Stickstoff CO<sub>2</sub> benutzt, liegt diese Temperatur wesentlich niedriger als die eigentliche Glasübergangstemperatur. Ein solches Experiment deutet die glastemperaturniedrigende Wirkung von CO<sub>2</sub> an. Mit Hilfe dieser Interpretation kann dann auch die Struktur des Schaums, eine poröse Schaumstruktur eingebettet zwischen zwei äußeren dichten Schichten, erklärt werden. Durch Berechnungen instationärer Stoff- und Wärmetransportgleichungen kann dann auch die exakte Schichtdicke vorhergesagt werden. Die äußeren Schichten wirken wie homogene Polymerfilme, zeigen jedoch auf elektronenmikroskopischen und atomar-kraftfeldmikroskopischen Aufnahmen eine körnige, globularartige Struktur. Experimente mit unterschiedlich thermisch vorbehandelten Polymerpräparaten weisen darauf hin, daß die Schaumstrukturen durch einen heterogenen Nukleationsmechanismus entstehen.

Die Vorhersage der Permeabilität von CO<sub>2</sub> durch Polymermembranen mit Hilfe neuronaler Netzwerke wird in Appendix I dieser Dissertation untersucht. Das neuronale Netzwerk korreliert das komplexe IR-spektrum eines Polymers, das alle nötigen chemischen Informationen enthält, mit der Permeabilität. Die Ergebnisse dieser Experimente und Berechnungen sind vielversprechend und es empfiehlt sich eine Fortführung.

---

## LIST OF PUBLICATIONS

- M. Wessling, U. Werner, S.-T. Hwang, Separation of C<sub>8</sub>-isomers by means of pervaporation, Proc. 4th Int. Conf. Pervap. Proc. Chem. Ind., Bakish [Ed.], Ft. Lauderdale (1989)
- M. Wessling, U. Werner, S.-T. Hwang, Pervaporation of aromatic C<sub>8</sub>-isomers, J. Membrane Sci., 57 (1991) 257
- I. Blume, E. Smit, M. Wessling, C.A. Smolders, Diffusion through rubbery and glassy polymers, Makromol. Chem., Macromol. Symp., 45 (1991) 237
- M. Wessling, S. Schoeman, Th. v.d. Boomgaard, C.A. Smolders, Plasticization of gas separation membranes, Gas Sep. & Purif., 5 (1991) 222
- M. Wessling, Th. v.d. Boomgaard, C.A. Smolders, Molecular motions in glassy solution-diffusion membranes, Récents Progrès en Génie des Procédés, 6(21) (1992) 331
- M. Wessling, Th. v.d. Boomgaard, M.H.V. Mulder, C.A. Smolders, Transport of gases through polymeric membranes, accepted for publication in Makromol. Chem., Macromol. Symp.,
- K.M.P. Kamps, H.A. Teunis, M. Wessling, C.A. Smolders, Gas transport and sub-T<sub>g</sub> relaxations in unmodified and nitrated polyarylethersulfones, J. Membrane Sci., 74 (1992) 193

---

## CURRICULUM VITAE

Matthias Wessling was born on March 10, 1963 at Ahaus, Germany. He graduated at the Alexander-Hegius Gymnasium in 1982. After graduation he served in the German army. In 1983, he entered the University of Dortmund, studied at the Department of Chemical Technology and took his Diplom-Ingenieur degree in 1989.

During this time, he participated in practical traineeships at Chemicke Zavody Juraja Dimitrova, Bratislava (Czechoslovakia), National Testing Company, Dhahran (Saudi Arabia) and Procter & Gamble, Frankfurt (Germany). In 1986 he entered the group of Prof. U. Werner and worked as a student assistant on the characterization of microfiltration membranes by means fractionated retention curves. In 1988 he was sent as an exchange student to the University of Cincinnati/USA and he worked for 8 months with Prof. S.-T. Hwang on the separation of aromatic C<sub>8</sub>-isomers by means of pervaporation. This work was accepted as his diploma-thesis for the studies at the University of Dortmund.

After graduation, in July 1989, he entered the Membrane Technology Group of Prof. Smolders at the University of Twente and worked in the field of penetrant induced relaxation phenomena in dense gas separation membranes. He finishes this research period at the University of Twente with a Doctor degree on March 5, 1993. From April 1993 on, he will occupy the position of a Senior Research Scientist at Membrane Technology and Research Inc., Menlo Park/CA, USA.





